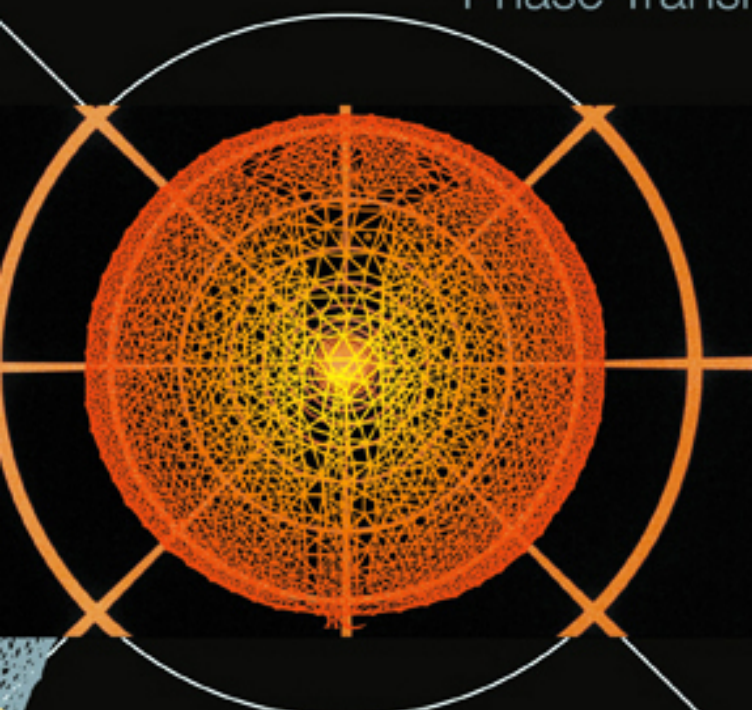


Order, Disorder and Criticality

Advanced Problems of
Phase Transition Theory



Volume 2

Editor

Yurij Holovatch

Order, Disorder and Criticality

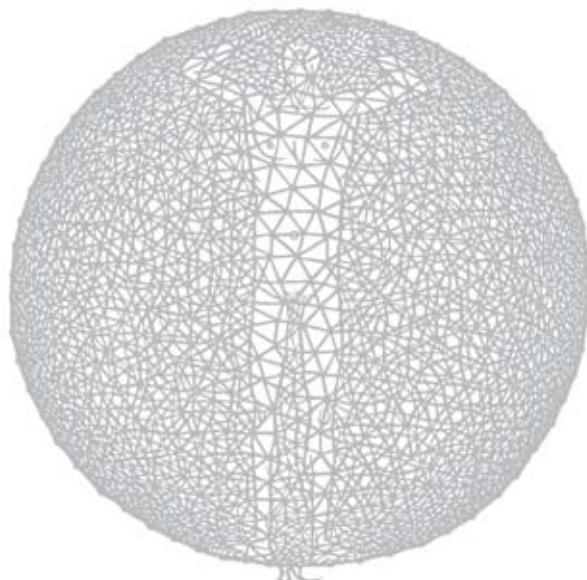
Advanced Problems of
Phase Transition Theory

Volume 2

This page intentionally left blank

Order, Disorder and Criticality

Advanced Problems of
Phase Transition Theory



Volume 2

Editor

Yurij Holovatch

National Academy of Sciences, Ukraine

 **World Scientific**

NEW JERSEY • LONDON • SINGAPORE • BEIJING • SHANGHAI • HONG KONG • TAIPEI • CHENNAI

Published by

World Scientific Publishing Co. Pte. Ltd.

5 Toh Tuck Link, Singapore 596224

USA office: 27 Warren Street, Suite 401-402, Hackensack, NJ 07601

UK office: 57 Shelton Street, Covent Garden, London WC2H 9HE

British Library Cataloguing-in-Publication Data

A catalogue record for this book is available from the British Library.

ORDER, DISORDER AND CRITICALITY — Volume II

Advanced Problems of Phase Transition Theory

Copyright © 2007 by World Scientific Publishing Co. Pte. Ltd.

All rights reserved. This book, or parts thereof, may not be reproduced in any form or by any means, electronic or mechanical, including photocopying, recording or any information storage and retrieval system now known or to be invented, without written permission from the Publisher.

For photocopying of material in this volume, please pay a copying fee through the Copyright Clearance Center, Inc., 222 Rosewood Drive, Danvers, MA 01923, USA. In this case permission to photocopy is not required from the publisher.

ISBN-13 978-981-270-767-3

ISBN-10 981-270-767-0

Printed in Singapore.

PREFACE

"Order, Disorder, and Criticality" - a book with this title appeared in the World Scientific almost three years ago.^a The aim of the volume was to review a number of problems related to phase transitions and critical phenomena that have attracted considerable attention due to essentially new contributions. More broadly, the book also aimed to demonstrate that the phase transition theory, which experienced its 'golden age' during the 1970s and 1980s, was far from over and there was still a good deal of work to be done, both on the fundamental level and in respect of applications. It is, of course, impossible to cover all recent developments on pages of a single book; moreover, new directions in research continue to appear. For this reason, the World Scientific Publishing Co. has decided to establish a series of review volumes serving this purpose.

This, the second volume in this series, consists of five chapters. The first chapter, written by Bertrand Delamotte, serves as an introduction to the non-perturbative renormalization group. In a traditional survey, an application of a renormalization group (RG) formalism in the quantitative theory of critical phenomena originates from two seminal papers by Kenneth Wilson^b relying on Kadanoff-Wilson coarse graining ideas which do not assume *per se* any perturbation expansion. However, in 1970-80s – the most advanced period for the application of the method – the term 'renormalization group' was used nearly synonymously with the perturbative field theoretical RG. The last, indeed, served as a powerful tool for giving an accurate quantitative description of criticality. As rare exceptions we can mention papers by G. R. Golner, E. K. Riedel, K. E. Newman, C. Bagnuls, C. Bervillier, G. Zumbach et al., where the non-perturbative approach was further developed and exploited. Also worthy of mention in this context is the work

^a *Order, Disorder and Criticality. Advanced Problems of Phase Transition Theory*, edited by Yu. Holovatch (World Scientific, Singapore, 2004).

^b K. G. Wilson, Phys. Rev. B **4**, 3174 (1971); *ibid.* **4**, 3184 (1971).

of I. R. Yukhnovskii and his group,^c where momentum-shell integration was used in combination with the collective variables method. We are now witnessing a certain return to the original ideas of Wilson, resulting in an increasing interest in the non-perturbative RG. In particular, the method serves as an alternative tool for tackling problems where controversial results are obtained by standard approaches based on weak coupling perturbative expansions. At the beginning of the chapter, the non-perturbative RG a la Wilson is introduced in the context of statistical field theory and compared with the perturbative RG. Basic notions of renormalization are introduced taking the 2d Ising model on the triangular lattice as an example. Thereafter two ‘modern’ non-perturbative formalisms are described: the Wilson-Polchinski and the effective average action approaches. Explaining in greater detail how the second one works, the author, at the same time, reviews main results obtained with the help of the non-perturbative RG for the Ising and $O(N)$ models.

A second chapter, written by Reinhard Folk, is devoted to critical dynamics. At the beginning of the chapter, an overview is given of the experimental situation in dynamics, with emphasis on liquids (transport coefficients, light and sound scattering), ferromagnets (neutron scattering) and the lambda transition in liquid He-4 (thermal conductivity, second sound); the van Hove theory and the concept of dynamic scaling theory are also discussed. Thereafter, the main steps of the dynamic renormalization group are explained. It is technically much more difficult to obtain dynamic RG perturbative expansions than static ones. Typically, one works within the two-loop order in dynamics (cf. with the fifth or sixth order in statics). Recently, it was recognized^d that dynamical vertex functions have a structure, allowing the singling out of genuine dynamic and static parts. This result has led to considerable progress in the quantitative description of dynamic criticality. In particular, it has allowed for the simplification of perturbation theory expansions and has made tractable the two-loop critical dynamics of the superfluid transition in He-3/He-4 mixtures, critical dynamics of model C. The rest of the review is devoted to the comparison of theoretical results with experiments. The main topic in this comparison is an explanation of observed crossover phenomena from the hydrodynamic region to the critical one.

^cI.R. Yukhnovskii. *Phase Transitions of the Second Order. Collective Variables Method* (World Scientific, Singapore, 1987).

^dR. Folk and G. Moser, Phys. Rev. Lett. **91**, 030601 (2003); *ibid* **89**, 125301 (2002); Erratum: *ibid* **93**, 229902 (2004).

The first two chapters of this book make use of the field-theoretical formalism to analyze different features of criticality. The third chapter, written by Wolfhard Janke and Adriaan Schakel, makes use of field-theoretical ideas in a rather unexpected and, as the reader will discover, very fruitful way – namely, in a similar fashion as the Feynman path integral formalism provides another view on quantum field theory, the spacetime approach, discussed in this chapter, provides one more – geometric – way to describe critical phenomena. The fact that a geometric description is inherent to criticality has already been demonstrated by the celebrated ‘polymer’ $N \rightarrow 0$ limit^e of the $O(N)$ spin model: on the one hand, it has allowed for the introduction of powerful methods, elaborated to analyze magnetic systems, in polymer physics; on the other hand, it serves as a link between criticality of thermodynamic phase transitions and purely geometrical scaling of self-avoiding walks. In the $O(N = 0)$ model, the statistics of self-avoiding walks naturally arise if one analyzes high-temperature expansion. In a more general context, the high-temperature expansion provides a geometrical description of phase transitions in spin models, as detailed in this chapter. Information about critical exponents governing temperature scaling at second-order phase transition can be recovered by an analysis of the fractal (geometrical) structure of appropriate high-temperature graphs. In particular, it is shown that the fractal dimensions of the relevant geometrical objects (Peierls domain walls in the Ising model, worldlines in Bose-Einstein condensates, vortex loops in superfluid He-4) encode the critical exponents.

In standard critical phenomena, there is a control parameter that can be varied to obtain a radical change in behaviour. Self-organized critical phenomena, by contrast, are exhibited by driven systems that reach a critical state by means of their intrinsic dynamics, independently of the value of any control parameter. Self-organized criticality offers considerable insight into various phenomena ranging from an archetypal sandpile to earthquakes and traffic jams and is the subject of the chapter by Alexander Olemskoi and Dmytro Kharchenko. After giving a short overview of different approaches to the description of self-organized critical behaviour, the authors provide new results obtained in this field. Initial models for describing self-organized critical phenomena were introduced by means of computer-aided procedures^f. Since then, computer simulations have been playing an impor-

^eP. G. de Gennes, Phys. Lett. A **38**, 339 (1972).

^fP. Bak, C. Tang, and K. Wiesenfeld, *Phys. Rev. Lett.* **59**, 381 (1987); C. Tang and P. Bak, *Phys. Rev. Lett.* **60**, 2347 (1988).

tant, if not a leading, role in this field. However, a particular feature of the review is that it is focused on an analytic perspective in the description of self-organized criticality. The authors consider self-organized criticality as an example of complexity in a system's behaviour and follow its inherent features (fractal geometry, anomalous time evolution, power-law distribution of catastrophic events – avalanches) throughout the review. Using the framework of Langevin dynamics, combined with generalized statistics, a unified picture is offered that allows for the description of both a single avalanche formation and the behaviour of an avalanche ensemble.

The last chapter, written by Ihor Stasyuk, deals with typical descriptions of phase transition problems in solid-state physics. Here, the question of principal interest is a change in the phase diagram of strongly-correlated electron systems caused by (correlation-induced) changes in their energy spectrum. A comprehensive review of a phase behaviour of a so-called pseudospin–electron model is given. The last is a generalization of a Hubbard model to account for the vibrational degrees of freedom, described as pseudospins. Recent applications of the model include high- T_c superconducting crystals, molecular and crystalline hydrogen-bonded systems, intercalated layered structures, etc. An analysis is performed in two complementary ways: the non-perturbative dynamical mean field theory approach and a generalized random phase approximation. The last relies on an elaborated diagram technique for Hubbard operators,^g which is a generalization of a corresponding technique for the spin operators. Reviewed results for thermodynamics and the energy spectrum bring about rich phase behaviour with a variety of uniform and modulated (commensurate or incommensurate) phases.

There is one more reason behind the choice of the topics for this review series. Since 1997, with the assistance of the Institute for Condensed Matter Physics of the National Academy of Sciences of Ukraine and Ivan Franko National University of Lviv (Ukraine), we have been organizing annual workshops called "The Ising Lectures". The aim of these workshops is to bring together students, as well as young and mature scientists, interested in phase transitions and critical phenomena. These workshops provide a possibility for participants to attend review lecture courses, to take part in informal discussions and to obtain information about new results directly from the principal investigators. This is the context in which the review

^gP. M. Slobodjan, I. V. Stasyuk, *Teor. Mat. Fiz.* **19**, 423 (1974) [Theor. Math. Phys. USSR **19**, 616 (1974).]

chapters of this volume were initiated.

I am deeply indebted to my colleagues, the authors of this volume, for coming to Lviv and for their devoted work, both in connection with the solving of various puzzles posed by nature and with preparing future generations for solving such puzzles. Special thanks are due to the World Scientific for their interest in getting this book published.

Yurij Holovatch

ICMP, National Academy of Sciences of Ukraine,

Lviv, Ukraine

& Johannes Kepler Universität Linz, Austria

10 August 2006

Contents of vol. 1

**Mathematical Theory of the Ising Model and its Generalizations:
an Introduction**

Yuri Kozitsky

Relaxation in Quantum Spin Chains: Free Fermionic Models

Dragi Karevski

**Quantum Phase Transitions in Alternating Transverse Ising
Chains**

Oleg Derzhko

Phase Transitions in Two-Dimensional Random Potts Models

Bertrand Berche and Christophe Chatelain

Scaling of Miktoarm Star Polymers

Christian von Ferber

Field Theoretic Approaches to the Superconducting Phase Transition

Flavio S. Nogueira and Hagen Kleinert

CONTENTS

<i>Preface</i>	v
Introduction to the Non-Perturbative Renormalization Group	1
<i>Bertrand Delamotte</i>	
Introduction to Critical Dynamics	79
<i>Reinhard Folk</i>	
Spacetime Approach to Phase Transitions	123
<i>Wolfhard Janke and Adriaan M. J. Schakel</i>	
Representations of Self-Organized Criticality	181
<i>Alexander Olemeskoi and Dmytro Kharchenko</i>	
Phase Transitions in the Pseudospin-Electron Model	231
<i>Ihor Stasyuk</i>	
<i>Index</i>	291

This page intentionally left blank

CHAPTER 1

INTRODUCTION TO THE NON-PERTURBATIVE RENORMALIZATION GROUP

Bertrand Delamotte

*Laboratoire de Physique Théorique de la Matière Condensée,
Université Paris VI, Pierre et Marie Curie, 4 Place Jussieu,
F-75252 Paris Cedex 05, France
E-mail: delamotte@lptmc.jussieu.fr*

An elementary introduction to the non-perturbative renormalization group is presented mainly in the context of statistical mechanics. No prior knowledge of field theory is necessary. The aim of this article is not to give an extensive overview of the subject but rather to focus on conceptual aspects and to explain in detail the main technical steps. It should be taken as an introduction to more advanced readings.

Contents

1	Wilson's Renormalization Group	2
1.1	Introduction	2
1.2	The Perturbative Method in Field Theory	3
1.3	Wilson's Approach to the Renormalization Group	6
2	Renormalization Group Transformations	9
2.1	Blocks of Spins	9
2.2	Two Remarks Concerning RG Transformations	15
2.3	Linear RG Transformations and Behaviour of the Correlation Length	17
3	Properties of the RG Flow: Fixed Points, Critical Surface, Relevant Directions	21
3.1	Scaling Relations – Linearization of the Flow Around the Fixed Point	23
3.2	The Correlation Length and the Spin-Spin Correlation Function	28
3.3	Scaling of the Correlation Function in the Presence of a Magnetic Field – Relation Among Exponents	29
3.4	The Example of the Two-Dimensional Ising Model on the Triangular Lattice	31
4	The Non-Perturbative Renormalization Group	32
4.1	Introduction	32
4.2	The Effective Average Action Method	38
4.3	An Integral Representation of Γ_k and the Limit $k \rightarrow \Lambda$	42
5	The Exact RG Equation and Its Properties	42
5.1	Some General Properties of the Effective Average Action Method	43

6	Approximation Procedures	46
6.1	The Green Function Approach	47
6.2	The Derivative Expansion	49
7	The Local Potential Approximation for the Ising Model	52
7.1	The Flow Equation of the Potential	52
7.2	The Scaling Form of the RG Equation of the Dimensionless Potential .	53
8	The Critical and Non-Critical Behaviour of the Ising Model within the LPA .	54
8.1	The Low and the High Temperature Phases	57
8.2	The Critical Point	58
8.3	The Critical Exponents	60
9	The $O(N)$ Models at $O(\delta^2)$ of the Derivative Expansion	62
9.1	The RG Equation for the Potential	63
9.2	The RG Equation for the Dimensionless Potential \tilde{U}_k	64
9.3	The Limits $d \rightarrow 4$, $d \rightarrow 2$ and $N \rightarrow \infty$	67
10	Conclusion	68
Appendix A.	Definitions, conventions	69
Appendix B.	The Exact RG equations	72
Appendix B.1.	RG equation for $W_k[B]$	72
Appendix B.2.	RG equation for $\Gamma_k[M]$	73
Appendix B.3.	RG equation for the effective potential	74
References	76

1. Wilson's Renormalization Group

1.1. Introduction

We give in these notes a short presentation of both the main ideas underlying Wilson's renormalization group (RG) and their concrete implementation under the form of what is now called the non-perturbative renormalization group (NPRG). Prior knowledge of perturbative field theory is not required for the understanding of the core of the article. However, some basic knowledge about phase transitions in Ising and $O(N)$ models is supposed.^{1–3} We shall mainly work in the framework of statistical field theory but when it will turn out to be illuminating we shall also use the language of particle physics.

The beginning of this article will be rather elementary and known to most physicists working in the field of critical phenomena. Nevertheless, both for completeness and to set up a language (actually a way of thinking at renormalization group) it has appeared necessary to include it. The first part of this article deals with a comparison between perturbative and Wilson's RG. Then, presented in the next part is the implementation of Kadanoff-Wilson's RG on the very peculiar case of the two-dimensional Ising model on the triangular lattice. This allows us to introduce the idea of decimation and block spins and also those of RG flow of coupling con-

stants and fixed point. The last part, which is also the core of this article, deals with the “modern” implementation of Wilson’s ideas. Both the general framework and detailed calculations for the $O(N)$ models will be given.

1.2. The Perturbative Method in Field Theory

The idea behind perturbation theory is to consider an exactly solvable model, either the Gaussian or the mean-field “model”, and to add, in a perturbation expansion, the term(s) present in the model under study and which are not taken into account in the exactly solvable model taken as a reference.^{1,4} For instance, in the “ ϕ^4 ” model (which belongs to the same universality class as the Ising model):

$$Z = \int \mathcal{D}\phi e^{-H(\phi)+\int B\phi} \quad (1)$$

with

$$H(\phi) = \int d^d x \left\{ \frac{1}{2} (\nabla\phi)^2 + \frac{1}{2} r_0 \phi^2 + \frac{1}{4!} u_0 \phi^4 \right\} \quad (2)$$

it is possible to take as a reference model the Gaussian model:

$$Z_0 = \int \mathcal{D}\phi e^{-H_0(\phi)+\int B\phi} \quad (3)$$

where

$$H_0(\phi) = \int d^d x \left(\frac{1}{2} (\nabla\phi)^2 + \frac{1}{2} r_0 \phi^2 \right). \quad (4)$$

Z is then developed as a series in u_0 around Z_0 :

$$\begin{aligned} Z = & \int \mathcal{D}\phi \left(1 - \frac{u_0}{4!} \int_{x_1} \phi^4(x_1) + \frac{1}{2} \left(\frac{u_0}{4!} \right)^2 \int_{x_1, x_2} \phi^4(x_1) \phi^4(x_2) \right. \\ & \left. + \dots \right) e^{-H_0(\phi)+\int B\phi}. \end{aligned} \quad (5)$$

This expansion leads to the series of Feynman diagrams for the Green functions.

The problem with this approach is that the “fluctuations” induced by the ϕ^4 term around the Gaussian model are large. In the perturbation expansion they lead to integrals – corresponding to the loops in the Feynman diagrams – of the form:

$$\int^\Lambda d^d q_1 \dots d^d q_L \prod_i (\text{propagator}(q_i)) \quad (6)$$

where

$$\text{propagator}(q_i) \sim \frac{1}{(q_i + Q)^2 + r_0}. \quad (7)$$

These integrals are supposed to be cut-off at the upper bound by Λ which is an ultra-violet regulator. In the following, it will be convenient to think Λ as the (analog of the) inverse of a lattice spacing, lattice that would be used to regularize the field theory. In statistical mechanics, it is actually the other way around: the microscopic model is very often a lattice model whereas the field theory is only an effective model useful to describe the long-distance physics.

If Λ were sent to infinity, the integrals in Eq. (6) would be generically divergent for d sufficiently large. This means that for Λ finite but large, the integrals are large and depend crucially on the value of Λ . This is very unpleasant for at least two reasons:

(i) This invalidates the perturbation expansion even if u_0 is small. For instance, in the ϕ^4 model and for the four-point connected correlation function $G_c^{(4)}(x_1, \dots, x_4) = \langle \phi(x_1) \dots \phi(x_4) \rangle_c$, the one-loop approximation writes in Fourier space at zero momentum:

$$G_c^{(4)} \sim u_0 + (\text{constant}).u_0^2. \int^\Lambda \frac{d^d q}{(2\pi)^d} \frac{1}{(q^2 + r_0)^2} + \dots \quad (8)$$

This integral is divergent for $d \geq 4$ in the limit $\Lambda \rightarrow \infty$.

(ii) The universal quantities (critical exponents, etc.) are expected to be independent of the underlying lattice and thus, at least for these quantities, it is paradoxical that the lattice spacing ($\sim \Lambda^{-1}$) plays such a crucial role.

Perturbative renormalization is the method that allows to reparametrize the perturbation expansion in such a way that the sensitive dependence on Λ has been eliminated.^a Then, the renormalization group allows to partially resum the perturbation expansions and thus to compute universal behaviours.^{1,3,4}

Let us now make a list of questions that are not very often addressed in the litterature. Some answers are explicitly given in this text. Some others are worth thinking over. They are mainly there to nourish the reader's imagination....

^aLet us emphasize that apart from the field renormalization, the whole renormalization process is nothing but a reparametrization.

Q1: The occurrence of ultra-violet divergences in field theory is often considered as a fundamental property of the theory. Thus, why do they play no role in the few known exact solutions of field theories or statistical models ? For instance, in Onsager's solution of the two dimensional Ising model no divergence occurs. This is also the case when Wilson's RG is implemented in field theoretical models.

Q2: Ultra-violet divergences are often said to be related to the infinite number of degrees of freedom of a field theory (the value of the field at each point). But then, why does a classical field theory that also involves an infinite number of degrees of freedom show no divergence ?

Q3: The answer to the last question often relies in the litterature on the fact that a statistical (or quantum) field theory involves fluctuations contrary to a classical field theory. Fluctuations are thus supposed to be responsible for the divergences. The computation of the contributions of the fluctuations — the Feynman diagrams — is thus often considered to be the reason why field theoretical techniques are relevant in statistical mechanics. But there always exist thermal fluctuations in a statistical system whereas field theoretical techniques are most of the time useless in statistical mechanics. Then, which types of fluctuations require field theory and which ones do not ?

Q4: Ultra-violet divergences are also often said to be related to the fact that we multiply fields at the same point (in a lagrangian) while fields are distributions the product of which is ill-defined. But what are the distributions in the case of the Ising model ? And since the interaction takes place between spins that are not on the same site but on two neighboring sites why should we take care about this difficulty ?

Q5: In the ϕ^4 theory for instance, the renormalization group flow of the coupling constant — given by the β -function — is determined (in $d = 4$) by the UV divergences. But then why is the (IR stable) zero of the β -function, that is the non-gaussian fixed point, useful to describe the infrared behavior of a field theory and in particular the critical behavior ?

Q6: Why should we bother about the continuum limit in a statistical system — its ultra-violet behavior — for which on one hand there always exist a natural ultra-violet cut-off (such as a lattice spacing or a typical range of interaction) and for which on the other hand we are interested only in its long-distance physics ?

1.3. Wilson's Approach to the Renormalization Group

There are two crucial remarks behind Wilson's method:⁵⁻⁷

- (i) in general, we cannot compute exactly the contributions of the fluctuations (otherwise we could solve exactly the model);
- (ii) the way fluctuations are summed over in perturbation theory is not appropriate since *all wavelengths* are treated *on the same footing* in Feynman diagrams. This is what produces integrals: at a given order of the perturbation expansion *all* fluctuations are summed over.^b

Wilson's idea is to organize the summation over fluctuations in a better way. Note that because of remark (i) above, “better way” means “with respect to an approximation scheme”.^c What is the idea behind Wilson's method of summation over the fluctuations? Before answering, let us notice that

- in strongly correlated systems (e.g. close to a second order phase transition) the two relevant scales are (i) the microscopic scale a – a lattice spacing, an intermolecular distance, the Planck length, etc. – , (ii) the correlation length ξ . These two scales are very different for $T \simeq T_c$ so that fluctuations exist on *all* wavelengths between a and ξ . In particle physics, ξ corresponds to the Compton wavelength of the particle $(mc/\hbar)^{-1}$ and a to the typical (inverse) energy scale of the “fundamental theory”: 10^{16} GeV for a Grand Unified Theory or 10^{19} GeV for quantum gravity.
- for the long distance physics and for universal quantities (magnetization, susceptibility, etc.) the short distance “details” of the model have been completely washed out. This means that these “details” (existence and shape of the lattice for instance) do matter for the short distance physics but that they are averaged out at large distances: there must exist *average processes* that eliminate the microscopic details as the scale at which we “observe” the system is enlarged.^d

^bIn quantum field theory, Feynman diagrams represent the summation over probability amplitudes corresponding to all possible exchanges of virtual particles compatible with a given process at a given order. Note that these integrals are cut-off in the ultraviolet by Λ and in the infrared by the “mass” r_0 (see Eq. (6)). In statistical mechanics, the mass is related to the correlation length ξ by $r_0 \sim \xi^{-2}$ (at the mean-field approximation).

^cIt is extremely rare that renormalization group enables to solve exactly a model that was not already solved by another and simpler method.

^dNote that this is true only for universal quantities. The critical temperatures for in-

Wilson's idea is therefore to build an *effective theory for the long-distance degrees of freedom* we are interested in.^{6–8} This is achieved by integrating out the short distance ones. Since, at least for universal quantities, these short distance quantities do not matter crucially, it should be possible to devise approximations that preserve the physics at long distance.

Actually, Wilson's idea is more general: it consists in saying that the “best” (approximate) way to study a subset of degrees of freedom of a system is to build an effective theory for them by integrating out the others. For instance, in molecular physics, one should build an effective Hamiltonian for the valence electrons obtained by “integrating out” the core electrons (corresponding to high energy degrees of freedom).

For the Ising model, this consists in integrating out in the partition function the “high energy modes” of the field $\phi(p)$ – those for which $p \in [\Lambda - d\Lambda, \Lambda]$ – and in computing the effective Hamiltonian for the remaining modes. By iterating this procedure down to a scale k , one should obtain an effective Hamiltonian for the “low energy modes”, those corresponding to $p < k$. The long distance physics, obtained for $p \rightarrow 0$, should then be readable on the effective Hamiltonian corresponding to $k \rightarrow 0$ since no fluctuation would remain in this limit.

Once again, let us emphasize that if we could perform exactly the integration on these “rapid” modes, we could iterate this integration and obtain the exact solution of the model. In most cases, this is impossible and the interest of this method, beyond its conceptual aspect, lies in the possibility to implement new approximation schemes better than the usual perturbation expansion.^e

Schematically, to implement Wilson's method, we divide $\phi(p)$ into two pieces: $\phi_>(p)$ that involves the rapid modes $p \in [\Lambda/s, \Lambda]$ of $\phi(p)$ and $\phi_<(p)$ that involves the slow modes $p \in [0, \Lambda/s]$:

$$Z = \int \mathcal{D}\phi e^{-H[\phi, \vec{K}, \Lambda]} = \int \mathcal{D}\phi_< \mathcal{D}\phi_> e^{-H[\phi_<, \phi_>, \vec{K}, \Lambda]}, \quad (9)$$

where $\vec{K} = (K_1, K_2, \dots)$ represents *all possible coupling constants* compatible with the symmetries of the system. Here, we have supposed that H involves all these couplings although the initial Hamiltonian (that is, at scale Λ) involves in general only a finite number of them. For instance, in

stance, which are non-universal, depend on microscopic details such as the shape of the lattice.

^eLet us already mention that if Wilson's RG equations are truncated in a perturbation expansion, all the usual perturbative results are recovered as expected.

the ϕ^4 model all (initial) couplings K_i are vanishing, but those corresponding to the terms $(\nabla\phi)^2$, ϕ^2 and ϕ^4 . The integration of the rapid modes consists in integrating out the $\phi_>$ field. In this integration, *all the couplings K_i that were initially vanishing start to grow* (this is why we have considered them from the beginning) but since we have considered the most general Hamiltonian H (compatible with the symmetries of the problem), its functional form remains unchanged. Let us call \vec{K}' the new coupling constants obtained after integrating out $\phi_>$. By definition of \vec{K}' :

$$Z = \int \mathcal{D}\phi_< e^{-H[\phi_<, \vec{K}', \Lambda/s]} \quad (10)$$

with

$$e^{-H[\phi_<, \vec{K}', \Lambda/s]} = \int \mathcal{D}\phi_> e^{-H[\phi_<, \phi_>, \vec{K}, \Lambda]} . \quad (11)$$

We thus build a series of coupling constants, each associated with a given scale:

$$\begin{aligned} \Lambda &\rightarrow \vec{K}, \\ \frac{\Lambda}{s} &\rightarrow \vec{K}', \\ \frac{\Lambda}{s^2} &\rightarrow \vec{K}'', \quad \text{etc.} \end{aligned} \quad (12)$$

This method has several advantages compared with the usual, à la Feynman, approach:

- There is no longer any summation over all length scales since the integration is performed on a momentum shell, $|q| \in [\Lambda/s, \Lambda]$. Thus, there can be no divergence and there is no need for any renormalization in the usual sense (subtraction of divergences).
- The coupling constants K_i are naturally associated with a scale whereas this comes out in the perturbative scheme as a complicated by-product of regularization and renormalization. Wilson's method by-passes completely renormalization to directly deals with renormalization group.
- The method is not linked with a particular expansion and there is therefore a hope to go beyond perturbation expansion.
- The “flow” of coupling constants $\vec{K} \rightarrow \vec{K}' \rightarrow \vec{K}'' \rightarrow \dots$ is sufficient to obtain much information on the physics of the system under

study. In particular, the notion of “fixed point” of this flow will play a particularly important role in statistical mechanics.

2. Renormalization Group Transformations

2.1. *Blocks of Spins*

As a pedagogical introduction, let us start by a simple and illuminating example of Wilson’s method implemented in x -space instead of momentum space and without having recourse to field theory.

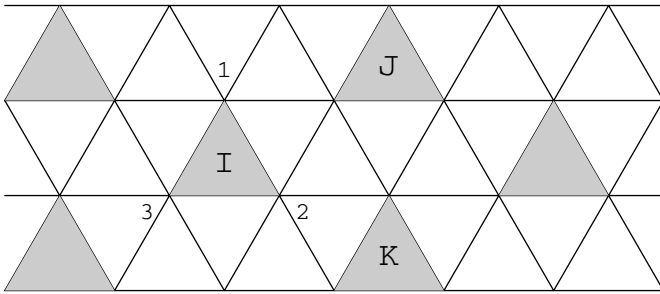


Fig. 1. Partition of the triangular lattice into plaquettes. The plaquettes are labelled by capital letters I, J, K, \dots and the spins inside the plaquettes are denoted, in obvious notations, S_i^I , $i = 1, 2, 3$. The lattice of plaquettes is again triangular with a lattice spacing $a\sqrt{3}$.

We consider a triangular lattice with Ising spins to exemplify block spin transformations:

$$H = -J \sum_{\langle ij \rangle} S_i S_j - B \sum_i S_i \quad (13)$$

where S_i are Ising spins: $S_i = 1$, the summation $\langle \dots \rangle$ runs only on nearest neighbours and B is a uniform magnetic field. The lattice is partitioned into triangular plaquettes labelled by capital letters I, J, \dots . We call S_i^I , $i = 1, 2, 3$ the spin number i of the I -th plaquette. As a first step, we separate the 8 configurations of the three spins S_i^I of plaquette I into 24 configurations of (i) the block spin $S_I = 1$ – which is chosen here to be an Ising spin – and (ii) the four configurations, called σ_I^α , corresponding to a given value of S_I either +1 or -1. We choose (and this will be modified in the following) to define S_I by a majority rule:

$$S_I = \text{sign}(S_1^I + S_2^I + S_3^I) = 1. \quad (14)$$

Thus, for the four configurations of the S_i^I compatible with $\mathcal{S}_I = +1$, we define the four variables $\sigma_I^{\alpha+}$ by:

$$\begin{aligned}\sigma_I^{1+} &\text{ corresponds to } \uparrow\uparrow\uparrow \\ \sigma_I^{2+} &\text{ corresponds to } \uparrow\uparrow\downarrow \\ \sigma_I^{3+} &\text{ corresponds to } \uparrow\downarrow\uparrow \\ \sigma_I^{4+} &\text{ corresponds to } \downarrow\uparrow\uparrow\end{aligned}. \quad (15)$$

For $\mathcal{S}_I = -1$, the $\sigma_I^{\alpha-}$ correspond to the opposite configurations of the spins. Note that it will not be necessary in the following to compute the S_i^I in terms of the σ_I^α . The sum over all spin configurations in the partition function can be written as:

$$\sum_{\{S_i\}} = \sum_{\{S_i^I\}} = \sum_{\{\mathcal{S}_I\}} \sum_{\{\sigma_I^\alpha\}}. \quad (16)$$

The partition function can thus be rewritten as

$$Z[B, T, n] = \sum_{\{\mathcal{S}_I\}} \sum_{\{\sigma_I^\alpha\}} e^{-H[\mathcal{S}_I, \sigma_I^\alpha, B, T, n, a]}, \quad (17)$$

where n is the number of lattice sites ($n \rightarrow \infty$ corresponds to the thermodynamical limit) and a is the lattice spacing. We have also chosen to redefine the coupling constant J and the magnetic field B so that the prefactor $1/k_B T$ of H in the Boltzmann weight is absorbed into the normalization of these quantities. In this example, the lattice spacing of the blocked lattice is $a\sqrt{3}$. The summation over the short distance degrees of freedom σ_I^α can be formally performed

$$Z[B, T, n] = \sum_{\{\mathcal{S}_I\}} e^{-H'[\mathcal{S}_I, B, T, n/3, a\sqrt{3}]} \quad (18)$$

with, by definition of H' :

$$e^{-H'[\mathcal{S}_I, B, T, n/3, a\sqrt{3}]} = \sum_{\{\sigma_I^\alpha\}} e^{-H[\mathcal{S}_I, \sigma_I^\alpha, B, T, n, a]}. \quad (19)$$

Let us make some remarks here.

- We have chosen the majority rule to define the block spin \mathcal{S}_I so that it is again an Ising spin. The price to pay is that relation (14) between \mathcal{S}_I and the S_i^I 's is non-linear. This is a source of many difficulties in more complicated systems than the Ising model on

the triangular lattice. Moreover, it is difficult to generalize this rule to continuous, N -component, spins.

- The explicit computation of H' , Eq. (18), shows that it involves infinitely many interaction terms, even if H involves only a nearest neighbour interaction. Thus, as it stands, the form of H is not stable under block-spin transformations.

There is a solution to both problems.

- We define \mathcal{S}_I through a linear transformation instead of the majority rule:

$$\mathcal{S}_I \propto \sum_{i \in I} S_i^I \quad (20)$$

The Ising character is lost but the relation (20) is simpler than (14) and can be generalized to other models.

- We take for H a Hamiltonian involving all possible couplings among the S_i compatible with the \mathbb{Z}_2 symmetry ($S_i \rightarrow -S_i$ for all i) of the Ising model (they will all be generated) :

$$\begin{aligned} H = & -K_1 \sum_{\langle ij \rangle} S_i S_j + K_2 \sum_{\ll ij \gg} S_i S_j \\ & + K_3 \sum_{\langle i j k l \rangle} S_i S_j S_k S_l + \dots \end{aligned} \quad (21)$$

where $\ll ij \gg$ means summation over the next nearest neighbours.

Now $H = H(\vec{K}, S_i, n)$ where $\vec{K} = (K_1, K_2, \dots)$ represents the set of all \mathbb{Z}_2 -symmetric coupling constants as well as the magnetic field if necessary. For the initial Hamiltonian: $K_{i \neq 1} = 0$. Of course, this seems extremely complicated but it is the only possibility to have a form-invariant Hamiltonian. The fact that all couplings are generated when fluctuations are integrated out simply means that even if a Hamiltonian involves a finite number of couplings, all correlation functions, involving an arbitrary number of spins, are non-trivial. We shall come back on this point later.

Let us finally remark that for $n = \infty$, $n/3 = \infty$, $n/3^2 = \infty$, etc., and the number of “spins” remains identical. However, the lattice spacing varies: $a \rightarrow \sqrt{3}a \rightarrow 3a \rightarrow \dots$. Since, we shall look for *fixed point Hamiltonians*^f

^fFixed point Hamiltonian is meant in the usual sense. If $H(\vec{K}^*, S_i)$ is a fixed point Hamiltonian this means that $\vec{K}^* \rightarrow \vec{K}^*$ by summation over the σ_I^α 's, Eq. (19). The rescaling of

in the following, it will be necessary to rescale the lattice spacing by a factor $1/\sqrt{3}$ after each summation of the rapid modes in such a way that we obtain, after summation over the σ_I^α 's, the same Hamiltonian for the same system. We shall come back on this point later.

We can now rewrite Eq. (19) for $n = \infty$ as

$$e^{-H[\vec{K}', \mathcal{S}_I, a\sqrt{3}]} = \sum_{\{\sigma_I^\alpha\}} e^{-H[\vec{K}, \mathcal{S}_I, \sigma_I^\alpha, a]}. \quad (22)$$

This transformation, together with the rescaling of the lattice spacing, is called a renormalization group transformation. Such a RG transformation

- preserves the partition function Z and thus its singularities and thus the critical behaviour; more generally, all thermodynamical quantities are preserved;^g
- maps a Hamiltonian onto another Hamiltonian (a system onto another system) in such a way that they have the *same long distance physics*;
- consists in integrating out (averaging over) short distance degrees of freedom to obtain an *effective Hamiltonian* for the long distance degrees of freedom;
- can be summarized in a change of (infinitely many) coupling constants: $\vec{K} \rightarrow \vec{K}'$.

And now, two questions:

Question 1: “Why is it interesting to integrate out the σ_I^α 's? Isn't it as complicated to integrate them out as would be the full integration over all degrees of freedom?”

It is true that integrating out *exactly* the σ_I^α 's is of the same difficulty as calculating Z completely. However,

- the complete calculation of Z contains much more information than what we want to obtain to get a satisfactory description of the critical physics. Moreover, for universal quantities, we guess that we shall be able to make rather drastic approximations as for the microscopic details of the model, that is the integration of the short

the lattice spacing, which is equivalent to measuring all dimensionful quantities in terms of the *running* lattice spacing and not in terms of the (fixed) initial lattice spacing, is a necessary step to obtain fixed point Hamiltonians.

^gIf we wanted to compute correlation functions of the original spins, we would have first to couple the system to an arbitrary magnetic field (in order to be able to compute derivatives of Z with respect to the magnetic field B_i). This is a complicated task.

distance degrees of freedom, since they probably play a minor role; this opens the possibility of new *approximation schemes*;

- the qualitative (or semi-quantitative) behaviour of the RG flow of coupling constants $\vec{K} \rightarrow \vec{K}' \rightarrow \vec{K}'' \rightarrow \dots$ is enough to predict many non-trivial behaviours occurring around a second order phase transition.

Question 2: “Why should we make a series of small block-spins (coarse-graining) instead of directly a large one?”

This question, which is not independent of the first one, is somewhat subtle and requires some developments. Once again, if we were able to perform exactly the integration over the σ_I^α 's, small or large blocks would make no difference. Thus, the problem comes from the approximations and is therefore not fully under control before precise calculations are performed. However, the general idea is not difficult to grasp.

Let us call $\vec{T}(\cdot, p)$ the function that maps $\vec{K} = \vec{K}^{(0)}$ onto $\vec{K}^{(p)}$ after p iterations of the RG transformations:

$$\vec{K}^{(p)} = \vec{T}\left(\vec{K}^{(0)}, p\right) \quad (23)$$

We, of course, have the property

$$\vec{K}^{(p)} = \vec{T}\left(\vec{K}^{(r)}, p - r\right) = \vec{T}\left(\vec{T}\left(\vec{K}^{(0)}, r\right), p - r\right) \quad (24)$$

and thus

$$\vec{T}(\cdot, p) = \vec{T}\left(\vec{T}(\cdot, r), p - r\right). \quad (25)$$

This is called a *self-similarity*⁹ property.^h If \vec{T} were exactly known, this property would be trivially verified. However, once approximations are performed, it is generically violated as is the case for instance in perturbative renormalization.

Let us illustrate the concept of self-similarity on the simple example of differential equations.¹⁰ We consider the trivial differential equation:

$$\dot{y} = -\epsilon y \quad (26)$$

^hSomething is said to be self-similar if it is everywhere the same. In our case, the self-similar character comes from the fact that the functional form of the RG flow does not depend on the initial couplings $\vec{K}^{(0)}$ since the same function \vec{T} is used to transform $\vec{K}^{(0)}$ into $\vec{K}^{(p)}$ or $\vec{K}^{(r)}$ into $\vec{K}^{(p)}$. This results in the fact that the right hand side of Eq. (25) is independent of r since the left hand side is. This independence is completely similar to the independence of the renormalized theory on the renormalization scale in perturbative renormalization. This is what allows to derive the Callan-Symanzik RG equations in the perturbative context.

with $y(t_0) = y_0$. The solution is

$$y = f(t - t_0, y_0) = y_0 e^{-\epsilon(t-t_0)}. \quad (27)$$

Of course, f obeys a self-similarity property which means that we can either (i) first integrate (26) between t_0 and τ to obtain $y(\tau) = y_\tau$ and then integrate again (26) between τ and t with y_τ as new initial condition or (ii) directly integrate (26) between t_0 and t :

$$y(t) = f(t - t_0, y_0) = f(t - \tau, f(\tau - t_0, y_0)). \quad (28)$$

This is trivially verified by the exact solution (27) since

$$f(u, v) = v e^{-\epsilon u} = v e^{-\epsilon a} e^{-\epsilon(u-a)} = f(u - a, f(a, v)). \quad (29)$$

However, this property is violated at any finite order of the perturbation expansion in ϵ of $y(t)$. Let us show this at first order in ϵ for which we, of course, obtain:

$$y(t) = y_0(1 - \epsilon(t - t_0)) + O(\epsilon^2). \quad (30)$$

This defines the approximation of order one of f :

$$f^{(1)}(t - t_0, y_0) = y_0(1 - \epsilon(t - t_0)). \quad (31)$$

We obtain at this order:

$$\begin{aligned} f^{(1)}(u - a, f^{(1)}(a, v)) &= v(1 - \epsilon a)(1 - \epsilon(u - a)) \\ &= f^{(1)}(u, v) + \epsilon^2 v a (u - a) \end{aligned} \quad (32)$$

By comparing this result with Eq. (29), we find that self-similarity is obeyed at order ϵ , as expected, but is violated at order ϵ^2 . The problem is that this violation can be arbitrarily large if u (which represents $t - t_0$) is large. Thus, even if ϵ is small, the self-similarity property is violated for large time intervals. This is true at any finite order of perturbation theory. This large violation comes ultimately from the fact that the perturbation expansion is not an expansion in ϵ but in $\epsilon(t - t_0)$. This is completely reminiscent of the perturbation expansion in field theory where the expansion is not performed in terms of u_0 but in terms of $u_0 \log \Lambda$ where u_0 is the bare coupling constant and Λ the cut-off (see Eq. (8) for the ϕ^4 theory in $d = 4$). Reciprocally, it is clear that if $u = t - t_0$ is small, so is the violation in Eq. (32) since, in this case, both a and $u - a$ are small. Thus, using perturbation expansions on small or, even better, on infinitesimal time intervals preserves self-similarity at each step. In geometrical terms, this means that we can safely use perturbation theory to compute the envelope of the curve $f(u, v)$

– the field of tangent vectors $\beta(u)$ – but not the curve itself.¹⁰ The curve $f(u, v)$ can only be obtained in a second step by integration of its envelope.

The analogue for the RG is that small blocks will be under control. Coarse graining in this case respects self-similarity even when approximations are used while large ones lead inevitably to large errors.

Before studying the structure of the RG flow, let us make two remarks about the RG transformations and their physical meaning.

2.2. Two Remarks Concerning RG Transformations

The first remark is that it is still widely believed that the correlation length $\xi(T)$ is a measure of the typical size of clusters of spins having the same orientation, that is of ordered domains (in the Ising case). As a consequence, it is believed that the divergence of ξ at T_c is a consequence of the divergence of the size of these (so-called) naive clusters. The traditional metaphor is that at T_c there would exist oceans of up spins with continents of down spins that would contain themselves lakes of up spins with islands of down spins, etc, with some kind of fractal geometry. This is wrong. It has been shown long ago that the distribution of cluster boundaries *does not scale at criticality*. Rather, at a temperature T_p well below T_c the clusters of spins having the opposite sign of the spontaneous magnetization merge into a large percolating cluster. An important point is that, strictly speaking, no phase transition occurs at T_p since no local order parameter of the Ising model can be built out the spins in order to describe this transition: there is no singularity of the partition function at T_p . In fact, it is possible to construct clusters of spins that are critical at T_c . These are the famous Fortuin and Kasteleyn clusters.¹¹ They are used in the Swendsen-Wang algorithm of Monte Carlo simulations of the Ising model since they partially defeat critical slowing down.¹²

The second remark is that the “microscope analogy” is often used to give an intuition of the physical meaning of the RG transformations. In this analogy, the coarse-graining implemented in the RG transformations would be similar to what occurs when the magnification of a microscope is decreased. Let us imagine that we look at an image made of small pixels of definite colours (say blue, green or red). At a mesoscopic scale, the pixels are no longer seen and only a smearing of the colors of blocks of pixels can be observed. As a result, the “physics” observed would depend on the scale as in the RG transformations. This analogy has several virtues but also several drawbacks. Let us mention some. First, our brain plays a crucial

role for the color vision. From the three colors blue, green and red the cones in the retina are sensitive to, our brain is smart enough to reconstruct the impression of a continuous spectrum of colors. Although the analogy leads us to believe that our perception of the colors at a mesoscopic scale is a linear combination at this scale of the elementary colors of the pixels, this is not so. Second, in a RG transformation, there are two main steps (not to mention the final change of scale to go back to the original lattice spacing). The first one is to build a stochastic variable for the block.ⁱ The second is to build an effective hamiltonian for this block variable by integration over short distance fluctuations. We can imagine that the first step is analogous to the superimposition of the electromagnetic field produced by the different pixels. But then what is the analog of the second step? The laws of classical electrodynamics for the propagation of light do not change from one scale to the other. Let us repeat here that the effective hamiltonians for the block variables in the Ising model are extremely complicated: they involve all powers of the fields and not only interactions among nearest neighbors.^j There is no analog for this step in the microscope analogy although it is the crucial one from the RG point of view. In fact, things go almost the other way around. Whereas the electromagnetic field emitted by several pixels is the linear superposition of the field produced by each of them, the β -function in quantum field theory that gives the evolution of the coupling constant with the scale is a measure of the deviation to the trivial rescaling invariance (in the case of quantum electrodynamics). Thus, although the microscope analogy can be useful it should be employed with some care (and a grain of salt).

Let us now show how linear RG transformations can be implemented. This will allow us to prove a simple relation about the behavior under RG transformations of the two-point correlation function $\langle S_i S_j \rangle$ and thus on the correlation length.^{1,7}

ⁱThis can be performed either by a majority rule as in Eq.(14) or by a linear relation as in Eq.(34).

^jOnce the continuum limit has been taken and continuous RG transformations are implemented this means that the effective hamiltonians involve all powers of the field and of its derivatives.

2.3. Linear RG Transformations and Behaviour of the Correlation Length

Instead of the majority rule, we consider a linear transformation between the spins of a plaquette and the block-spin. The simplest idea is to take a *spatial* average (not a thermodynamic one)

$$\mathcal{S}'_I = \frac{1}{s^d} \sum_{i \in I} S_i^I \quad (33)$$

where s is the “linear size” of the block, that is s^d is the number of spins per block. In our example of the triangular lattice, $d = 2$ and $s = \sqrt{3}$. As we already said, we shall also need to perform a rescaling of all dimensionful quantities (in order to find fixed points). Thus we take:

$$\mathcal{S}_I = \frac{\lambda(s)}{s^d} \sum_{i \in I} S_i^I \quad (34)$$

where $\lambda(s)$ is a function that will be determined in such a way that we find a fixed point. This relation among the stochastic variables S_i^I and \mathcal{S}_I leads to relations among their thermodynamic averages. The most important one is the two-point correlation function:

$$\begin{aligned} \langle \mathcal{S}_I \mathcal{S}_J \rangle &= \frac{1}{Z} \sum_{\{\mathcal{S}_I\}} \mathcal{S}_I \mathcal{S}_J e^{-H[\vec{K}', \mathcal{S}_L]} \\ &= \frac{1}{Z} \sum_{\{\mathcal{S}_I\}} \mathcal{S}_I \mathcal{S}_J \sum_{\{\sigma_L^\alpha\}} e^{-H[\vec{K}, \mathcal{S}_L, \sigma_L^\alpha]} \\ &= \frac{\lambda^2(s)}{s^{2d}} \frac{1}{Z} \sum_{\{\mathcal{S}_I\}} \sum_{\{\sigma_I^\alpha\}} \sum_{i \in I, j \in J} S_i^I S_j^J e^{-H[\vec{K}, S_i]} \\ &= \frac{\lambda^2(s)}{s^{2d}} \sum_{i \in I, j \in J} G^{(2)}(\vec{x}_i, \vec{x}_j) \end{aligned} \quad (35)$$

where, by definition

$$G^{(2)}(\vec{x}_i, \vec{x}_j) = G^{(2)}(r_{ij}, \vec{K}) = \langle S_i S_j \rangle \quad (36)$$

is the two-point correlation function of the spins S_i . If the correlation length is large compared to the size of the plaquettes and if we consider two plaquettes I and J such that their distance is very large compared to a : $|\vec{x}_{i \in I} - \vec{x}_{j \in J}| \gg a$, then $G^{(2)}(\vec{x}_i, \vec{x}_j)$ does not vary much for $i \in I$ and $j \in J$. Thus, in this case:

$$\sum_{i \in I, j \in J} G^{(2)}(\vec{x}_i, \vec{x}_j) \simeq s^{2d} G^{(2)}(\vec{x}_i, \vec{x}_j). \quad (37)$$

Therefore, close to the critical temperature and for distant plaquettes:

$$\langle \mathcal{S}_I \mathcal{S}_J \rangle \simeq \lambda^2(s) \langle S_i^I S_j^J \rangle. \quad (38)$$

The important point is that $\langle \mathcal{S}_I \mathcal{S}_J \rangle$ is also the two-point correlation function of a \mathbb{Z}_2 -invariant magnetic system. The only difference is that it is computed with the set of couplings \vec{K}' instead of \vec{K} . We thus obtain:

$$\langle \mathcal{S}_I \mathcal{S}_J \rangle = G^{(2)}(r_{IJ}, \vec{K}') \quad (39)$$

where $G^{(2)}$ is the same function as in Eq. (36).^k We thus deduce:

$$G^{(2)}(r_{IJ}, \vec{K}') \simeq \lambda^2(s) G^{(2)}(r_{ij}, \vec{K}) \quad (40)$$

for sufficiently distant plaquettes.

Let us now explain the precise meaning of this relation. Let us suppose that we are given a new Ising model on a triangular lattice with a set of couplings \vec{K}' . In principle, we can compute the correlation function $G^{(2)}$ of the spins of this new system. Our claim is that this correlation function is identical to the correlation function of the block-spins of the original lattice. Of course, to compare the two functions we have to say how to compare the distances r_{ij} between spins in the two lattices. Our calculation shows that what we have to do is to measure all distances in the length unit intrinsic to the system, that is in units of the lattice spacing of each system. This means that the quantities r_{ij} and r_{IJ} that appear in Eq. (40) must be *numerically different*

$$r_{IJ} = r_{ij}/s \quad (41)$$

since they correspond to the same “distance” but measured in two different units: a for the original system and $a' = a\sqrt{3}$ for the coarse-grained system. It is important to understand that measured in an extrinsic length unit, like metres, these distances are indeed the same since $r_{IJ}a' = (r_{ij}/s)(sa) = r_{ij}a$ whereas they are different when they are measured in the length unit intrinsic to each system. Put it differently, the dimensionful distances, measured in a common length unit, are equal whereas the dimensionless distances, measured in terms of the lattice spacing of each system, are different. We shall put a bar or a tilde on dimensionless quantities to distinguish them.

^kLet us point out here a subtlety. This statement is not fully rigorous since the original spins are Ising spins whereas the block spins \mathcal{S}_I are not. The correlation functions $\langle S_i^I S_j^J \rangle$ and $\langle \mathcal{S}_I \mathcal{S}_J \rangle$ are therefore not computed exactly in the same way since the summation over the configurations of S_i and of \mathcal{S}_I do not run on the same values. In fact, after several blocking iterations, the spins that are summed over become almost continuous variables and the aforementioned difficulty disappears.

Let us emphasize that the value in an extrinsic unit like metres of, say, the correlation is almost meaningless. From a physical point of view, the only relevant measure of the correlation length is in units of the lattice spacing. The difficulty in our case is two-fold. First, to write down a field theory, it is necessary to perform the continuum limit $a \rightarrow 0$. It is therefore convenient to rescale the position vectors by a factor a before performing this limit (thus, as usual, $[\vec{x}] = \text{length}$).¹ Second, since we have to consider several systems with different lattice spacings, it will be convenient to work in the continuum with lengths measured in units of the running lattice spacings.

Let us therefore define dimensionless quantities as

$$\bar{r} = \frac{r}{a} , \quad \bar{\xi} = \frac{\xi}{a} , \quad \bar{r}' = \frac{r}{sa} . \quad (43)$$

where r and ξ are the dimensionful quantities (measured in meters) that will be convenient once the continuum limit will be taken, that is in the field theory formalism. Eq. (40) that involves only dimensionless quantities can then be rewritten:

$$G^{(2)}\left(\frac{\bar{r}}{s}, \vec{K}'\right) \simeq \lambda^2(s) G^{(2)}(\bar{r}, \vec{K}). \quad (44)$$

Let us give a concrete example of the significance of this relation. In three dimensions and at large distances: $r_{ij} \gg 1$, a typical form of the two-point correlation function is:

$$\langle S_i S_j \rangle = G^{(2)}(\bar{r}, \bar{\xi}) \sim \frac{e^{-\bar{r}/\bar{\xi}}}{\bar{r}^\theta} \quad (45)$$

with $\bar{\xi}$ the correlation length in units of the lattice spacing a and $\bar{r} = \bar{r}_{ij}$. We can use the same formula as in Eq. (45) for the correlation function of

¹It will also be convenient to rescale the spin-field by the appropriate power of a : $S_i \rightarrow \phi(\vec{x})$ so that the gradient term $(\nabla\phi)^2$ comes in the Hamiltonian of the field theory with a dimensionless prefactor:

$$H = \int d^d x \left(\frac{1}{2} (\nabla\phi)^2 + U(\phi) \right) . \quad (42)$$

We find from this equation that $[\phi(x)] = [x^{-\frac{d-2}{2}}]$ so that the rescaling involves a factor $a^{-\frac{d-2}{2}}$. Note that the original variables S_i are dimensionless since $S_i = 1$. The function $G^{(2)}$ in Eq. (40) is therefore also dimensionless. This is consistent with the fact that the vectors \vec{x}_i have integer components that label the position of the sites of the lattice and are therefore also dimensionless.

the block-spin system:

$$\langle \mathcal{S}_I \mathcal{S}_J \rangle \sim \frac{e^{-\bar{r}'/\bar{\xi}'}}{\bar{r}'^\theta} . \quad (46)$$

We thus obtain

$$G^{(2)}(\bar{r}', \bar{\xi}') \sim \frac{e^{-\frac{\bar{r}'/\bar{s}}{\bar{\xi}'}}}{\bar{r}'^\theta} s^\theta \quad (47)$$

and, by comparing with Eq. (40), we find that

$$\bar{\xi}' = \frac{\bar{\xi}}{s} \quad \text{and} \quad \lambda(s) = s^{\theta/2} . \quad (48)$$

By comparing all these relations we find that

- the dimensionful correlation lengths of the original and of the block-spin systems are identical: it is a RG-invariant. Thus, the dimensionless correlation lengths decrease as the coarse graining scale s increases. This means that the coarse-grained systems are less correlated than the initial one and that the correlation length varies linearly with the scale. Since the correlation length behaves as a power law close to the critical temperature

$$\xi \sim (T - T_c)^{-\nu} \quad (49)$$

parameterizing $G^{(2)}$ in terms of the (reduced) temperature

$$t = \frac{T - T_c}{T_c} \quad (50)$$

or in terms of the correlation length is equivalent. Thus, saying that $\bar{\xi}$ decreases with the block size s is equivalent to saying that the running reduced temperature $t(s)$ increases with s : the coarse-grained system is “less critical” than the original one. We call relevant a parameter that increases with the scale s .

- the reduced temperature t is one particular coupling among all the couplings \vec{K} . We shall explain in the following why the form of $G^{(2)}$ given above and in which only the correlation length appears is valid at large distance.
- if we combine two RG transformations of scale s_1 and s_2 we must obtain the same result as a unique transformation of scale $s_1 s_2$ (this is self-similarity). This clearly implies that

$$\lambda(s_1) \lambda(s_2) = \lambda(s_1 s_2) . \quad (51)$$

It is straightforward to show that the only solution of this equation is a power law. The example above shows that the exponent of this power law is directly related to the power law behaviour of $G^{(2)}(\bar{r})$ at $T = T_c$, Eq. (48).

3. Properties of the RG Flow: Fixed Points, Critical Surface, Relevant Directions

The RG flow takes place in the space of Hamiltonians, that is in the space of coupling constants \vec{K} (see Fig. 2). We now study this flow. One of its nice properties is that, without specifying any particular statistical system, very general information on second order transitions can be obtained from it by only making very natural assumptions.

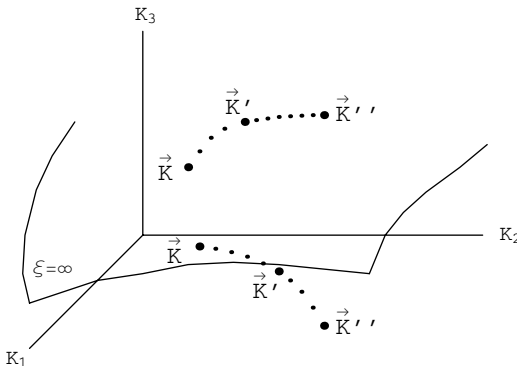


Fig. 2. Schematic representation of the RG flow in the space of couplings, K_1, K_2, \dots . This space is infinite dimensional and the critical surface, defined by the set of points for which the correlation length is infinite is of co-dimension one. Under RG transformations the critical surface is stable whereas a point away from the critical surface is mapped onto another one “further away” from it.

At T_c , $\xi = \infty$ ($\bar{\xi} = \infty$) at a second order phase transition. Thus the point $\vec{K}^{(0)}$ is mapped onto $\vec{K}^{(1)}$ for which $\bar{\xi}' = \infty$ again (the block-spin system is also critical). We define the *critical surface* as the set of points \vec{K} in the coupling constant space for which $\bar{\xi} = \infty$. For a second order phase transition only one parameter needs to be fine-tuned to make the system critical (the temperature for instance). Thus, the critical surface is of co-dimension one. It is stable under RG transformations.

If we now consider a system described by a point $\vec{K}^{(0)}$ such that $\bar{\xi} < \infty$

then $\bar{\xi}' = \bar{\xi}/s$ and the block-spin system, being “less critical”, is described by $\vec{K}^{(1)}$ which is “further away” from the critical surface than $\vec{K}^{(0)}$. If we iterate the blocking process, we obtain points $\vec{K}^{(2)}, \vec{K}^{(3)}, \dots$ that will be further and further away from the critical surface.

We shall consider in the following the continuum limit of the Ising model and this will allow us to perform continuous RG transformations. We call in this case the set of points $\vec{K}_s, s \in \mathbb{R}$ a RG trajectory. To different \vec{K}_s on the same RG trajectory correspond systems that are different microscopically (this means at the scale of their own lattice spacing) but that lead to the *same long-distance physics* since they all have the same partition function. Let us now make the fundamental hypothesis (that must be checked on each example):

Hypothesis: For points in a (finite or infinite) domain on the critical surface, the RG flow converges to a fixed point \vec{K}^* : $\vec{K}^* = \vec{T}(\vec{K}^*, s)$.

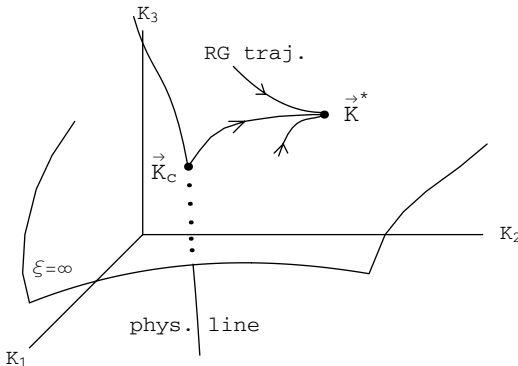


Fig. 3. Schematic representation of continuous RG trajectories on the critical surface. The flow converges to the fixed point \vec{K}^* . For a given model, the “physical line” corresponds to a change of the temperature. It is not a RG trajectory.

This domain is called the basin of attraction of the fixed point \vec{K}^* . Under this hypothesis, the typical topology of the flow on the critical surface is summarized in Fig.3. We have called “physical line” in this figure the line on which the temperature alone is varied. It is *not* a RG trajectory. Reciprocally, a RG trajectory does not, in general, correspond to any transformation doable on a physical system by a human being. It is only a mapping that preserves the partition function without any connection to a

physical transformation.

All the systems that belong to the basin of attraction of \vec{K}^* belong to the same universality class since they all have the same long-distance physics. Note that \vec{K}^* depends on the choice of RG transformations $\vec{T}(., s)$. Apart from being fixed for this particular choice of RG transformations, this point is nothing else than a particular critical point.

3.1. Scaling Relations – Linearization of the Flow Around the Fixed Point

The existence of an attractive (in the critical surface) fixed point is sufficient to explain universality since, independently of the starting point \vec{K}_c on the critical surface, all RG trajectories end at the same point \vec{K}^* . However, universality holds also for systems that are not right at T_c (which is anyway impossible to reach experimentally) but close to T_c . It is thus natural to assume that the flow is continuous in the vicinity of \vec{K}^* . In this case, starting at a point \vec{K} close to the point \vec{K}_c and on the same physical line, the RG trajectory emanating from \vec{K} remains close to the one emanating from \vec{K}_c during many steps before it diverges from the critical surface. It is easy to estimate the typical value of s for which the RG trajectory diverges from the critical surface.

As long as the running (dimensionless) correlation length $\bar{\xi}(s) = \bar{\xi}/s$ remains large, the system behaves as if it were critical and the representative point $\vec{K}(s)$ must be close to the critical surface. When the running correlation length becomes of order 1, the coarse grained system is no longer critical and $\vec{K}(s)$ must be at a distance of order 1 of the critical surface. More precisely, at the beginning of the flow, $\vec{K}(s)$ moves towards \vec{K}^* (by continuity). It remains close to it as long as $\bar{\xi}(s)$ remains large so that the memory of the initial point \vec{K} is largely lost. Finally, it departs from \vec{K}^* when $s \sim \bar{\xi}$. Another and more precise way to state the same result is to say that the running reduced temperature $t(s)$ is of order 1 when $s \sim \bar{\xi}$:

$$t(s) \sim 1 \quad \text{for } s \sim \bar{\xi}. \tag{52}$$

We shall see in the following that the hypothesis of the existence of a fixed point together with this relation are sufficient to predict the existence of power law behaviours for many thermodynamical quantities with critical exponents that are universal and that satisfy “scaling relations” *independently of any specific microscopic model*. Clearly, to obtain these relations, only the vicinity of \vec{K}^* is important since after a few RG steps, all RG

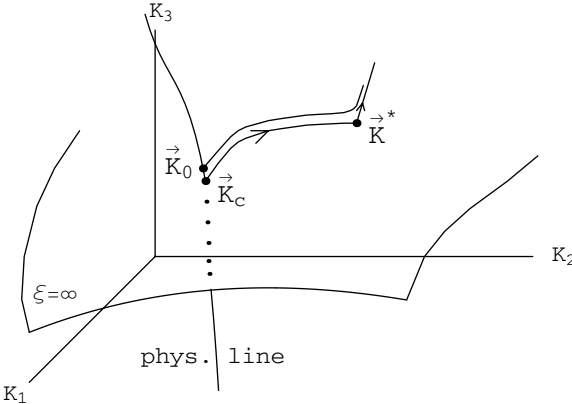


Fig. 4. Schematic representation of two continuous RG trajectories corresponding to the same model for two different temperatures. The trajectory starting at \vec{K}_c is on the critical surface ($T = T_c$) and the other, starting at \vec{K}_0 , is slightly away from it. There exists a RG trajectory emanating from the fixed point \vec{K}^* and which is not on the critical surface. It is an eigendirection of the RG flow corresponding to the relevant direction. Note that we could parametrize the coupling constant space in such a way that the axis denoted K_3 represents the temperature. It is not necessary that this axis coincides with the relevant eigendirection of the RG flow at \vec{K}^* but it is necessary that it has a non vanishing projection onto this axis since the temperature is for sure a relevant parameter. Note that this is non trivial in an infinite dimensional space.

trajectories emanating from points close to criticality are in the vicinity of this point. This will allow us to linearize the RG flow around \vec{K}^* .

For the sake of simplicity, we assume in the following that s can take continuous values (we work in the continuum, that is the continuous limit, $a \rightarrow 0$, has been taken). We also suppose that the RG transformation with $s = 1$ is the identity (no block spin) and that the composition law is such that a RG transformation of parameter s_1 followed by another one of parameter s_2 is equivalent to a transformation of parameter $s_1 s_2$.

As already emphasized, to obtain approximations of the RG flow that are under control, it is preferable to perform a series of infinitesimal RG transformations rather than directly a transformation with s large. It is thus necessary to study the differential form of these transformations. There are two ways to do so:

(i) The first way consists in comparing two RG transformations of parameters s and $s + \epsilon$ performed from an initial set of couplings \vec{K}_{in} :

$$\vec{K}_{s+\epsilon} - \vec{K}_s = \vec{T}(\vec{K}_{\text{in}}, s + \epsilon) - \vec{T}(\vec{K}_{\text{in}}, s) \quad (53)$$

and thus

$$\frac{\partial \vec{K}_s}{\partial s} = \frac{\partial \vec{T}}{\partial s}|_{(\vec{K}_{\text{in}}, s)} . \quad (54)$$

This formula is not convenient since it is expressed in terms of the initial couplings \vec{K}_{in} and, as a consequence, in terms of a parameter s that can be large (and thus for RG transformations that will not be under control once approximations will be implemented). Using approximate expressions of \vec{T} together with this expression would lead to violations of the composition law of RG transformations.

(ii) The second way consists in comparing two sets of running couplings differing by an infinitesimal RG transformation: \vec{K}_s and $\vec{K}_{s(1+\epsilon)}$ and in expressing the result as a function of \vec{K}_s :

$$\vec{K}_{s(1+\epsilon)} - \vec{K}_s = \vec{T}\left(\vec{K}_s, 1 + \epsilon\right) - \vec{T}\left(\vec{K}_s, 1\right) \quad (55)$$

and thus

$$s \frac{\partial \vec{K}_s}{\partial s} = \frac{\partial \vec{T}}{\partial s}|_{(\vec{K}_s, 1)} \quad (56)$$

It is important to notice here several things.

- The composition law of RG transformations will be automatically satisfied if $\vec{K}(s)$ is obtained by integration of this expression, even if an approximate expression of \vec{T} is used. This comes from the fact that, by construction, $\vec{K}(s')$ is computed in terms of $\vec{K}(s)$ by composing the infinitesimal group law between s and s' : this is the meaning of integrating Eq. (56).
- Eq. (56) leads naturally to the logarithmic evolution of the couplings with s , contrary to Eq. (54).
- In Eq. (54), the variations of \vec{T} had to be known for only one set of couplings \vec{K}_{in} but for all s . This was the real problem of this approach since we are interested in large values of s . In Eq. (56) only the variation of \vec{T} for $s = 1$ have to be known. The price to pay is that this must be known for all values of \vec{K}_s . In perturbation theory this is not problematic as long as the running coupling used in the perturbation expansion remains small all along the flow. Of course, if \vec{K}_s converges to \vec{K}^* such that the coupling(s) of the perturbation expansion at the fixed point is large, perturbation theory runs into trouble.

We define

$$\vec{\beta}(\vec{K}_s) = \frac{\partial \vec{T}}{\partial s}|_{(\vec{K}_s, 1)} \quad (57)$$

which gives the evolution of the couplings of the model with the scale. Note that $\vec{\beta}(\vec{K}_s)$ does not depend explicitly on s since the right hand side of Eq. (57) is evaluated at $s = 1$ and thus does not depend on this variable.^m The only dependence on s of this function is implicit and comes through the dependence of the couplings \vec{K}_s on s . By definition of the fixed point \vec{K}^* of the RG

$$\vec{\beta}(\vec{K}^*) = \vec{0}. \quad (58)$$

We thus obtain

$$s \frac{d\vec{K}_s}{ds} - s \frac{d\vec{K}^*}{ds} = \vec{\beta}(\vec{K}_s) - \vec{\beta}(\vec{K}^*) = \frac{d\vec{\beta}}{d\vec{K}_s} |_{\vec{K}^*} \cdot \delta\vec{K}_s + O(\delta\vec{K}_s^2) \quad (59)$$

where, by definition

$$\delta\vec{K}_s = \vec{K}_s - \vec{K}^* \quad (60)$$

and

$$\frac{d\vec{\beta}}{d\vec{K}_s} |_{\vec{K}^*} \quad \text{is a matrix} \quad \mathcal{M}_{ij} = \frac{d\beta_i}{dK_{s,j}} |_{\vec{K}^*}. \quad (61)$$

Thus, in the neighbourhood of \vec{K}^* :

$$s \frac{d\delta\vec{K}_s}{ds} = \mathcal{M} \delta\vec{K}_s. \quad (62)$$

\mathcal{M} is not symmetric in general. We suppose in the following that it can be diagonalized and that its eigenvalues are realⁿ (this must be checked on each example). We moreover suppose that the set of eigenvectors $\{\vec{e}_i\}$ is a complete basis:

$$\mathcal{M}\vec{e}_i = \lambda_i \vec{e}_i \quad \text{with} \quad \lambda_i \in \mathbb{R} \quad (63)$$

and

$$\delta\vec{K}_s = \sum_i v_i(s) \vec{e}_i. \quad (64)$$

^mIn perturbation theory, the fact that the β -function of the marginal coupling is cut-off independent and thus scale independent is a consequence of the renormalizability of the model.

ⁿIt can happen that some eigenvalues are complex. In this case, the RG flow around the fixed point is spiral-like (focus) in the corresponding eigendirections.

Under these hypotheses, we obtain:

$$s \frac{d\delta \vec{K}_s}{ds} = \sum_i v_i(s) \mathcal{M} \vec{e}_i = \sum_i \lambda_i v_i(s) \vec{e}_i \quad (65)$$

and thus

$$s \frac{dv_i(s)}{ds} = \lambda_i v_i(s) \quad \Rightarrow \quad v_i(s) = v_i(1) s^{\lambda_i}. \quad (66)$$

We conclude that around the fixed point, the RG flow behaves as power laws along its eigendirections (but if $\lambda_i = 0$). There are three possibilities:

- $\lambda_i > 0$ and $v_i(s) \nearrow$ when $s \nearrow$ which means that the flow in the direction \vec{e}_i goes away from \vec{K}^* . \vec{e}_i is called a relevant direction and v_i a relevant coupling. As we have already seen, the reduced temperature is relevant since the system is less and less critical along the RG flow which means that $t(s)$ increases with s .
- $\lambda_i < 0$ and $v_i(s) \searrow$ when $s \nearrow$ which means that the flow in the direction \vec{e}_i approaches \vec{K}^* . \vec{e}_i is called an irrelevant direction and v_i an irrelevant coupling.
- $\lambda_i = 0$ and v_i is said to be marginal. It is necessary to go beyond the linear approximation to know whether it is relevant or irrelevant. The flow in this direction is slow: it is logarithmic instead of being a power law. This is important since it is the case of the renormalizable couplings in the upper critical dimension (that is $d = 4$ for the Ising model).

Physically, we expect a small number of relevant directions since, clearly, there are as many such directions as there are parameters to be fine-tuned to be on the critical surface (the co-dimension of this surface). For second order phase transitions there is one coupling to be fine-tuned to make the system critical: the temperature (for instance). There is actually one more parameter which is relevant but which is also \mathbb{Z}_2 non-invariant: the magnetic field. All the other directions of the RG flow are supposed to be irrelevant (this can be checked explicitly once a specific model is given).

In the following, we shall use the language of magnetic systems although our discussion will be completely general. We shall suppose that together with the magnetic field, there is only one other relevant direction. We shall show that this implies scaling laws for all thermodynamical quantities with only two independent critical exponents.

3.2. The Correlation Length and the Spin-Spin Correlation Function

Let us start by studying the critical physics of a model at zero external magnetic field having only one relevant coupling. We call v_1 this coupling and λ_1 the eigenvalue of the flow at \vec{K}^* associated with v_1 . We order the other eigen-couplings v_2, v_3, \dots in such a way that $0 > \lambda_2 > \lambda_3 \dots$. Physically, the reduced temperature is expected to be a relevant parameter. It is not necessary that it corresponds to the relevant eigen-direction of the RG flow but it is that its projection onto this eigen-direction be non vanishing. For the sake of simplicity we ignore this subtlety that does not play any role in the following and we assume that $v_1 = t$. We have seen, Eq. (40), that for large \bar{r} :

$$G^{(2)}\left(\bar{r}, \vec{K}\right) \simeq \lambda^{-2}(s) G^{(2)}\left(\frac{\bar{r}}{s}, \vec{K}_s\right) \quad \text{with} \quad \lambda(s) = s^{\theta/2}. \quad (67)$$

From these relations we can deduce two relations, one at T_c and another one away from T_c :

- For $t = 0$ and in the neighbourhood of \vec{K}^* :

$$G^{(2)}(\bar{r}, 0, v_2, v_3, \dots) \simeq s^{-\theta} G^{(2)}\left(\frac{\bar{r}}{s}, 0, s^{\lambda_2} v_2, s^{\lambda_3} v_3, \dots\right). \quad (68)$$

Let us now suppose that we integrate out all fluctuations between scales a and r . This amounts to taking $s = \bar{r}$:

$$G^{(2)}(\bar{r}, 0, v_2, \dots) \simeq \bar{r}^{-\theta} G^{(2)}(1, 0, \bar{r}^{\lambda_2} v_2, \dots). \quad (69)$$

Since $\lambda_2 < 0$, we obtain that for \bar{r} sufficiently large: $\bar{r}^{\lambda_2} v_2 \ll 1$ and thus

$$G^{(2)}(\bar{r}, 0, v_2, \dots) \simeq \bar{r}^{-\theta} G^{(2)}(1, 0, 0, \dots). \quad (70)$$

From the definition of the anomalous dimension

$$G^{(2)}(r) \underset{T=T_c}{\simeq} \frac{1}{r^{d-2+\eta}}. \quad (71)$$

we find that

$$\theta = d - 2 + \eta. \quad (72)$$

Note that the $d - 2$ part of θ is purely dimensional: it corresponds to the engineering dimension of the spin field. The η part corresponds to a dynamical contribution. It can be proven rigorously and for many field theories (as the ϕ^4 theory) that $\eta \geq 0$. This means that the fluctuations contribute to decrease the correlations of the system with the distance.

- For $t \neq 0$, $\xi < \infty$ and we can therefore integrate all fluctuations between scales a and ξ by taking $s = \bar{\xi}$. As explained above, Eq. (52), the running temperature at this scale must be of order 1 since the coarse-grained system at this scale is no longer critical. We thus deduce

$$t(s = \bar{\xi}) = t \bar{\xi}^{\lambda_1} \sim 1 . \quad (73)$$

From the definition of the critical exponent ν :

$$\xi \sim t^{-\nu} \quad (74)$$

we find that

$$\nu = \frac{1}{\lambda_1} . \quad (75)$$

The behaviour of the correlation function close to the critical temperature follows from Eqs. (67), (73) and from $\bar{\xi} \gg 1$:

$$\begin{aligned} G^{(2)}(\bar{r}, t, v_2, \dots) &\simeq \bar{\xi}^{-\theta} G^{(2)}\left(\frac{\bar{r}}{\bar{\xi}}, t \bar{\xi}^{\lambda_1}, v_2 \bar{\xi}^{\lambda_2} \dots\right) \simeq \\ &\simeq \bar{\xi}^{-\theta} G^{(2)}\left(\frac{\bar{r}}{\bar{\xi}}, 1, 0 \dots\right) \simeq \bar{r}^{-\theta} f\left(\frac{\bar{r}}{\bar{\xi}}\right) . \end{aligned} \quad (76)$$

We can see on this relation that close to T_c and at large distance the correlation function is no longer a function of infinitely many coupling constants but of only one parameter, the correlation length. One can also see that the Yukawa-like form of the correlation function that we have considered in Eq. (45) has the right form.

3.3. Scaling of the Correlation Function in the Presence of a Magnetic Field – Relation Among Exponents

We now couple the system to a uniform magnetic field. In a RG transformation:

$$B \sum_i S_i = B \sum_I \frac{s^d}{\lambda(s)} \mathcal{S}_I \stackrel{\text{def}}{=} B_s \sum_I \mathcal{S}_I . \quad (77)$$

Thus

$$B_s = s^{d-\theta/2} B . \quad (78)$$

We call

$$\lambda_B = d - \theta/2 = \frac{d+2-\eta}{2} \quad (79)$$

the magnetic eigenvalue. Since η is always smaller than $d + 2$ (even for $d = 1$), $\lambda_B > 0$ so that the magnetic field is a relevant variable.

Relation (67) can be trivially generalized in the presence of a magnetic field and to any correlation function. We now consider the magnetization per spin which is the one-point function: $G^{(1)} = m = \langle S \rangle$. Clearly, it behaves as:

$$m(t, B, \dots) \simeq s^{-\theta/2} m(s^{\lambda_1} t, s^{\lambda_B} B, \dots). \quad (80)$$

Once again, we can obtain several relations among exponents by considering the scaling of physical quantities at and away from T_c .

- For $t = 0$ and $B \neq 0$

$$m(0, B, \dots) \simeq s^{-\theta} m(0, s^{\lambda_B} B, \dots). \quad (81)$$

and, by taking s such that $s^{\lambda_B} B \simeq 1$, we obtain

$$m(0, B, \dots) \simeq B^{\theta/2\lambda_B} m(0, 1, \dots) \sim B^{1/\delta} \quad (82)$$

by definition of the exponent δ . We thus find:

$$\delta = \frac{d+2-\eta}{d-2+\eta} \quad (83)$$

- For $t < 0$ and $B = 0$ we find:

$$m(t, 0, \dots) \simeq s^{-\theta/2} m(s^{\lambda_1} t, 0, \dots). \quad (84)$$

and by taking $s = \bar{\xi}$:

$$m(t, 0, \dots) \simeq \bar{\xi}^{-\theta/2} m(1, 0, \dots) \simeq (T_c - T)^\beta \quad (85)$$

by definition of the exponent β . Thus we find

$$\beta = \nu \frac{d-2+\eta}{2}. \quad (86)$$

- For the susceptibility $\chi = \partial m / \partial B$, at $t \neq 0$, we obtain:

$$\chi(t, B, \dots) \simeq s^{-\theta/2} \frac{\partial}{\partial B} m(s^{\lambda_1} t, s^{\lambda_B} B, \dots) \simeq s^{\lambda_B - \theta/2} \chi(s^{\lambda_1} t, s^{\lambda_B} B, \dots). \quad (87)$$

By taking $B = 0$ and $s = \bar{\xi}$, we find:

$$\chi(t, 0, \dots) \simeq \bar{\xi}^{\lambda_B - \theta/2} \chi(1, 0, \dots) \sim (T - T_c)^{-\gamma}. \quad (88)$$

Thus, by definition of γ

$$\gamma = \nu(2 - \eta). \quad (89)$$

Finally, for the exponent α of the specific heat, the calculation is subtler and requires to consider the free energy. One finds:

$$\alpha = 2 - \nu d . \quad (90)$$

To conclude, we have found that the hypothesis of the existence of a fixed point in the RG flow is sufficient to explain:

- universality since the critical exponents depend only on the RG flow around the fixed point and not on the point \vec{K}_c representing the system when it is critical;
- the scaling behaviour of the thermodynamic quantities such as the magnetization, the susceptibility, the correlation function, etc.;
- the relations existing between critical exponents;
- the irrelevance of infinitely many couplings and the fact that the scaling of the correlation length with the temperature drives the scaling of many other thermodynamic quantities.

Two remarks are in order here. First, for second order transitions, only two exponents are independent, ν and η for instance. Second, universality is a much more general concept than what we have seen here on critical exponents. It is possible to show in particular that the RG enables to understand why it is possible to keep track of only a small number of coupling constants in field theory while these theories involves infinitely many degrees of freedom and thus, *a priori*, infinitely many couplings.

3.4. *The Example of the Two-Dimensional Ising Model on the Triangular Lattice*

This model is very famous as an example where the block-spin method à la Kadanoff can be implemented rather easily. We shall not repeat the explicit calculation of the RG flow that can be found in most textbooks on this subject. We shall only give the main ideas that will be relevant for our purpose.

As already explained above, the idea is to partition the lattice in triangular plaquettes, to build an Ising block-spin S_I for each plaquette by a majority rule, Eq. (14), and to integrate out the fluctuations inside the plaquettes compatible with a given value of S_I . We have already said that the implementation of this idea imposes to take into account all possible \mathbb{Z}_2 -invariant couplings among the spins. From a practical point of view it is thus necessary to perform truncations. The approximations usually

performed consists in keeping only some couplings and projecting the RG flow onto this restricted space of couplings. We shall see that almost the same idea is used in the field theoretical implementation of non-perturbative renormalization group. The simplest truncation consists in keeping only the nearest neighbour interaction, that is K_1 , in Hamiltonian (21) as well as the magnetic field B . For concreteness, let us give here the result of the RG transformation on the triangular lattice for a small magnetic field:

$$K_{1,s} = 2K_1 \frac{e^{-K_1} + e^{3K_1}}{3e^{-K_1} + e^{3K_1}}, \quad (91)$$

$$B_s = 3B \frac{e^{-K_1} + e^{3K_1}}{3e^{-K_1} + e^{3K_1}}. \quad (92)$$

A fixed point is trivially found

$$K_1^* = 0.336, \quad (93)$$

$$B^* = 0. \quad (94)$$

The exponent ν can be computed as well as δ and we find:

$$\nu = 1.118, \quad \delta = 2.17. \quad (95)$$

All the other exponents can be found using the scaling relations among them. The exact values, given by Onsager's solution are

$$\nu = 1, \quad \delta = 15. \quad (96)$$

Let us notice that these RG results can be systematically improved by keeping more and more couplings. They drastically and rapidly improve with the next orders of approximations.

4. The Non-Perturbative Renormalization Group

4.1. Introduction

All the different implementations of the non-perturbative renormalization group (NPRG) rely on Kadanoff-Wilson's ideas of block spins, coarse graining and *effective long-distance theories*. However, they can substantially differ as for the way they are implemented. In the framework of field theory, there exists two main formulations: the Wilson (also called Wilson-Polchinski) approach^{6–8,13,14} and the “effective average action” approach.^{15–28} We shall deal with the second one which is not the best known, probably for historical reasons. Since it is nevertheless interesting to have an idea of the Wilson-Polchinski formulation, we start by this approach although we shall not study it in detail.

4.1.1. The Wilson-Polchinski Approach

We shall work in the context of statistical field theory (at equilibrium). This means that we shall not deal with a Minkowski metrics (this brings its own difficulties) and that we suppose a continuum description of the systems under study. The microscopic physics is supposed to correspond to a scale Λ in momentum space which is – up to a factor of unity – the inverse of a microscopic length (a lattice spacing, an intermolecular distance, etc.). The partition function is thus given by a functional integral:

$$Z[B] = \int d\mu_{C_\Lambda}(\phi) \exp \left(- \int V(\phi) + \int B\phi \right) \quad (97)$$

where $d\mu_{C_\Lambda}$ is a (functional) Gaussian measure with a cut-off at scale Λ :

$$d\mu_{C_\Lambda} = \mathcal{D}\phi(x) \exp \left(-\frac{1}{2} \int_{x,y} \phi(x) C_\Lambda^{-1}(x-y) \phi(y) \right) \quad (98)$$

with (in momentum space)

$$C_\Lambda(p) = (1 - \theta_\epsilon(p, \Lambda)) C(p) \quad (99)$$

and C is the usual free propagator:

$$C(p) = \frac{1}{p^2 + r} . \quad (100)$$

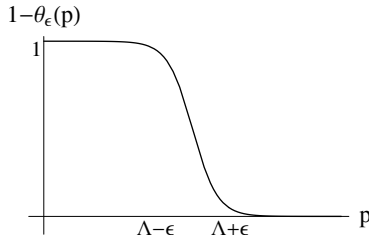


Fig. 5. A typical cut-off function in the Wilson-Polchinski approach.

The “cut-off” function θ_ϵ is a step function in p -space starting at Λ and smoothed around Λ on an interval of typical width ϵ , see Fig.5. If $\epsilon = 0$, the quadratic part of the Hamiltonian becomes the usual gradient and “mass” term, cut-off at scale Λ :

$$\frac{1}{2} \int_0^\Lambda \frac{d^d q}{(2\pi)^d} \phi(-p)(p^2 + r)\phi(p) . \quad (101)$$

The role of ϵ is to smoothen the sharp cut-off at Λ which is conceptually simple but technically unpleasant.

We want to implement the block-spin idea in our field theory framework, that is to separate $\phi_p = \phi(p)$ into “rapid” and “slow” modes (with respect to a scale k). The slow modes will play the role of block-spins while the rapid ones will correspond to fluctuations inside the blocks. It is convenient to work in Fourier space where the derivative operators are diagonalized (and the cut-off is simple).

We define

$$\phi_p = \phi_{p,<} + \phi_{p,>} \quad (102)$$

and associate

$$\phi_p \rightarrow C_\Lambda(p), \quad \phi_{p,<} \rightarrow C_k(p), \quad \phi_{p,>} \rightarrow C_\Lambda(p) - C_k(p). \quad (103)$$

It is important to notice that ϕ is the sum of $\phi_{p,<}$ and $\phi_{p,>}$ for all p : it does not coincide with $\phi_{p,<}$ on $[0, k]$ and with $\phi_{p,>}$ on $[k, \Lambda]$. The meaning of $\phi_<$ and $\phi_>$ comes from their propagator $C_k(p)$ and $C_\Lambda(p) - C_k(p)$ respectively. A beautiful identity allows us to rewrite the original partition function in terms of $\phi_<$ and $\phi_>$, $C_k(p)$ and $C_\Lambda(p) - C_k(p)$ and to perform (at least formally) the integration on the slow modes:

$$d\mu_{C_\Lambda}(\phi) = d\mu_{C_k}(\phi_<) d\mu_{C_\Lambda - C_k}(\phi_>). \quad (104)$$

Let us show it on a one-dimensional integral:

$$I = \int_{-\infty}^{+\infty} dx e^{-x^2/2\gamma}. \quad (105)$$

where x is the analogue of ϕ and γ of C_Λ . We now define

$$\begin{cases} x = y + z \\ \gamma = \alpha + \beta \end{cases} \quad (106)$$

y and z are the analogues of $\phi_>$ and $\phi_<$ respectively and α and β are the analogues of $C_\Lambda - C_k$ and of C_k . Then

$$I \propto \int_{-\infty}^{+\infty} dy dz e^{-y^2/2\alpha} e^{-z^2/2\beta}. \quad (107)$$

Demonstration.

We define:

$$J = \int_{y,z} e^{-y^2/2\alpha - z^2/2\beta} \quad (108)$$

and we rewrite the exponent

$$-\frac{y^2}{2\alpha} - \frac{z^2}{2\beta} = -\frac{1}{2} \left(\frac{1}{\alpha} + \frac{1}{\beta} \right) y^2 + \frac{xy}{\beta} - \frac{x^2}{2\beta} \quad (109)$$

$$= -\frac{1}{2} \frac{\gamma}{\alpha\beta} \left(y - \frac{\alpha}{\gamma} x \right)^2 + \frac{\alpha}{2\beta\gamma} x^2 - \frac{x^2}{2\beta}. \quad (110)$$

We now define

$$u = y - \frac{\alpha}{\gamma} x \quad (111)$$

and change variables: $(y, z) \rightarrow (u, x)$. The Jacobian is 1 and thus:

$$J = \int_{u,x} e^{-\gamma u^2/2\alpha\beta - x^2/2\gamma} = \sqrt{\frac{2\pi\alpha\beta}{\gamma}} I. \quad (112)$$

Actually, we are not only interested in Gaussian integrals and our result can be trivially generalized :

$$\int_{-\infty}^{+\infty} dx e^{-x^2/2\gamma - V(x)} \propto \int_{-\infty}^{+\infty} dy dz e^{-y^2/2\alpha - z^2/2\beta - V(y+z)}. \quad (113)$$

This result can be generalized straightforwardly to functional integrals since it is a property of the Gaussian integrals.^o It becomes

$$\int d\mu_{C_\Lambda}(\phi) e^{-\int V(\phi)} \propto \int d\mu_{C_k}(\phi_<) d\mu_{C_\Lambda - C_k}(\phi_>) e^{-\int V(\phi_< + \phi_>)}. \quad (114)$$

Thus, by performing formally the integration on $\phi_>$, we define a running “potential” V_k at scale k :

$$e^{-\int V_k(\phi_<)} = \int d\mu_{C_\Lambda - C_k}(\phi_>) e^{-\int V(\phi_< + \phi_>)} \quad (115)$$

with, by definition, $V_\Lambda = V$, the initial potential. Let us emphasize that it is called a potential because we do not have included in it the quadratic derivative term. However, generically, as soon as $k < \Lambda$, V_k involves derivative terms with, moreover, any power of the derivatives.

It is possible to write down a differential equation for the evolution of V_k with k : this is the Wilson-Polchinski equation derived in B.1.⁶⁻⁸ It is a possible starting point for a non-perturbative formulation of the RG. The one we shall use is mathematically equivalent to this one although it is more convenient in many respects when approximations are used. Before going to this second formulation, let us make some remarks here.

^oWe first consider a N -dimensional Gaussian integral and then take the limit $N \rightarrow \infty$.

- $\phi_<$ at scale k represents approximately a spatial average of ϕ over a volume of order k^{-d} . It is not a thermal average. For $k = 0$, $\phi_{p=0,<}$ would represent only what is (improperly) called the magnetization mode: $\int d^d x \phi(x)$ which is *not* the magnetization. It has a highly non-trivial probability distribution and the true magnetization is the thermal average of this mode computed with this distribution. Thus $\phi_<$ at scale $k \neq 0$ is *not a precursor* of the order parameter: it is still a stochastic variable whose physical interpretation is not so trivial.
- The flow of “potentials” $V_k(\phi_<)$ does not contain all the information on the initial theory: the correlation functions of the rapid modes cannot be computed from this flow. It is necessary to first couple the system to an arbitrary “source” $B(x)$ and to follow the flow of this term to reconstruct the correlations of the initial fields in the whole momentum range $p \in [0, \Lambda]$. Thus the information is split into two different kinds of terms: the k -dependent Hamiltonians which give rise to a flow for all the couplings involved in these Hamiltonians and the source term. Fortunately, much information about the theory (e.g. critical behaviour) can be obtained from the flow of Hamiltonians alone. It is nevertheless an open question to know if the difficulties encountered with this method are related to the fact that the information on the Green functions is not contained in the flow of Hamiltonians.
- The effective Hamiltonians V_k (and the corresponding Boltzmann weights) are highly abstract objects! One should remember in particular that the RG transformations do not correspond to any transformations that a human being can perform on the system. This is a purely theoretical idea that moreover will be useful only when approximations are used.
- The flow equation on V_k was written more than thirty years ago but was not much used in actual physical problems before the mid 90’s (for exceptions see, Golner, Newman, Riedel, Bagnuls, Bervillier, Zumbach, etc.).^{13,29–35} There are three main reasons for this strange fact. First, perturbation theory was extremely successful for $O(N)$ models (as well as in particle physics) and the need for NPRG was not obvious in many situations. Second, perturbation theory was believed to correspond to a controlled approximation whereas approximations performed in the NPRG framework seemed uncontrolled. However, this is *completely wrong*. Perturbation series are

not convergent.⁴ They are asymptotic series, at best.^P For the $O(N)$ model at l loops, the coefficient in front of u^l of a correlation function behaves at large l as $l!(-a)^l$ with a a real number. Thus, even in cases where many orders of the perturbation expansion have been computed, resummation methods of the renormalized series are required (Padé-Borel, conformal-Borel, etc.). In many cases, these resummation techniques fail to produce convergent results. As for the NPRG, there is no general theorem about the convergence of the series of approximations that are used. However, from the few results yet obtained, it seems that this method has good convergence properties.^{28,36–40} It is however too early to draw any firm conclusion on this question. Third, it seemed that the anomalous dimension was crucially depending on the choice of cut-off function θ_ϵ that separates the rapid and the slow modes whereas it should be independent on it. This was especially important when studying the $O(N)$ models in two dimensions where it seemed impossible to reproduce the perturbative results obtained from the non-linear sigma model. This difficulty is very simply overcome in the “effective average action” approach.^{28,41,42}

Let us finally mention two other “psychological” difficulties related to NPRG.

- The NPRG equation on V_k can be truncated in perturbation theory. This enables, of course, to recover the usual perturbation expansion (what else could it lead to?). However, the way it was implemented most of the time in the 70’s did not allow to retrieve the two-loop results.^q It is still widely believed for this reason, even by “specialists”, that Wilson’s method does not work at two-loop order and beyond!
- $V_k(\phi)$ involves infinitely many couplings contrary to perturbation theory that involves only the renormalizable ones. For this rea-

^PThe $O(N)$ models are completely exceptional in this respect since they are the only ones for which it has been proven that the series of the β -function is Borel-summable in $d = 3$ (in the massive scheme). In all other cases, either this is not known or it is known that the series are not Borel-summable. For QED, this is not yet a problem because the smallness of the fine structure constant ensures up to now an apparent convergence of the perturbative results.

^qThese calculations did not correspond to a series expansion of the exact NPRG equation on V_k . They enabled to retrieve the one-loop results easily but became very cumbersome beyond one-loop.

son, it is widely believed that the recourse to numerical methods is unavoidable in the NPRG approach whereas it is not in the perturbative one. This is not fully correct for two reasons. First, even in perturbation theory the RG flow cannot be integrated analytically in general. Second, even in the NPRG approach, very crude approximations, involving only very few couplings, often lead both to analytically tractable computations and to highly non-trivial non-perturbative results.²⁸

Let us now turn to the other implementation of the NPRG formalism.

4.2. The Effective Average Action Method

Many formal results about the NPRG method as well as some “physical” results have been obtained within the Wilson-Polchinski approach.^r However, the revival of Wilson’s ideas as well as their concrete implementation in the last fifteen years is largely linked with the development of an alternative, although formally equivalent, formulation.^{19–28} In practice, this has allowed to compute in a reasonable way the anomalous dimension η and, more importantly, to study the physics of the $O(N)$ models and of many others, in all dimensions, including two.^{28,42} Moreover, the whole scheme is more intuitive, allows to retrieve very easily the one-loop results in both $4 - \epsilon$ and $2 + \epsilon$ dimensions and in the large N limit. This has convinced many specialists of the subject to work with this formalism.

4.2.1. Block-Spins, Coarse Graining, Legendre Transform, etc.

The original Kadanoff-Wilson’s idea is to perform coarse graining and to map Hamiltonians onto other Hamiltonians at larger scales. The Hamiltonians thus obtained are the Hamiltonians of the modes *that have not yet been integrated out* in the partition function, that is $\phi_<$. As already emphasized, these Hamiltonians are very abstract objects.^s Instead of computing this sequence of Hamiltonians, we can compute the Gibbs free energy $\Gamma[M]$ of the rapid modes (that is $\phi_>$) that have *already been integrated out*.^t

^rSee the impressive and inspiring works of Bagnuls and Bervillier about the formal aspects of Wilson’s RG, as well as their criticisms of the perturbative approach.^{43–45}

^sIt is impossible to get easily any physical information from it apart at “mean field-like” level: a functional integral has still to be performed.

^tThe Helmholtz free energy is $F = -k_B T \log Z[B]$. It is a functional of the source $B(x)$. The Gibbs free energy is obtained by a Legendre transform from F and is a functional

Thus, the idea is to build a one-parameter family of models, indexed by a scale k such that²⁸

- when $k = \Lambda$, that is when no fluctuation has been integrated out, the Gibbs free energy $\Gamma_k[M]$ is equal to the microscopic Hamiltonian:^u

$$\Gamma_{k=\Lambda}[M] = H[\phi = M] . \quad (116)$$

- when $k = 0$, that is when all fluctuations are integrated out, $\Gamma_{k=0}$ is nothing but the Gibbs free energy of the original model:

$$\Gamma_{k=0}[M] = \Gamma[M] . \quad (117)$$

Thus, as k decreases more and more fluctuations are integrated out. The magnetization at scale k is therefore a precursor of the true magnetization (obtained at $k = 0$) and the free energy Γ_k , also called the effective average action, a precursor of the true free energy Γ (also called the effective action).

Let us notice two points. First, k plays the role of an *ultra-violet* cut-off for the slow modes $\phi_<$ in the Wilson-Polchinski formulation (analogous to Λ in the original model). It plays the role of an *infrared* cut-off in the effective average action method since Γ_k is the free energy of the rapid modes. Second, the slow modes play a fundamental role in the Wilson-Polchinski approach whereas they are absent of the effective average action method which involves only the (free energy of the) rapid modes. As a by-product, we shall see that all the information on the model (RG flow, existence of a fixed point, computations of correlation functions, etc.) are contained in a single object: $\Gamma_k[M]$. This is a rather important advantage of this method compared to the Wilson-Polchinski one.

Now the question is to build explicitly this one-parameter family of Γ_k . The idea is to decouple the slow modes of the model in the partition function. A very convenient implementation of this idea is to give them a large mass.²⁸ In the language of particle physics, a large mass corresponds to a small Compton wavelength (\hbar/mc) and thus to a small range of distances where quantum fluctuations are important. A very heavy particle decouples from the low energy (compared to its mass) physics since it can play a role at energies below its mass threshold only through virtual processes.

of the magnetization $M(x)$. It is the generating functional of the one-particle irreducible (1PI) correlation functions.

^uLet us emphasize that at the mean-field approximation, the Gibbs free energy of the system is identical to the Hamiltonian. Eq. (116) is an exact version of this statement (remember that no fluctuation is taken into account at the mean-field level).

These processes are themselves suppressed by inverse powers of the mass of the heavy particle coming from its propagator. In the language of critical phenomena, the “mass” term $r\phi^2/2$ in the Hamiltonian corresponds to the deviation to the critical temperature: $r \propto T - T_c$ (at the mean-field level, at least). Thus a large “mass” r corresponds to a theory which is far from criticality ($\xi \sim a$), that is where thermal fluctuations are small.

Therefore, the idea is to build a one-parameter family of models for which a “momentum-dependent mass term” has been added to the original Hamiltonian:²⁸

$$Z_k[B] = \int \mathcal{D}\phi(x) \exp \left(-H[\phi] - \Delta H_k[\phi] + \int B\phi \right) \quad (118)$$

with

$$\Delta H_k[\phi] = \frac{1}{2} \int_q R_k(q) \phi_q \phi_{-q} . \quad (119)$$

The function $R_k(q)$ – called the cut-off function from now on – must be chosen in such a way that

- when $k = 0$, $R_{k=0}(q) = 0$ identically ($\forall q$) so that:

$$Z_{k=0}[B] = Z[B] . \quad (120)$$

This will ensure that the original model is recovered when all fluctuations are integrated out, see Eq. (117).

- when $k = \Lambda$, all fluctuations are frozen. This will ensure that relation (116) is obeyed. Giving an infinite mass to all modes $q \in [0, \Lambda]$ freezes their propagation completely and we must therefore take

$$R_{k=\Lambda}(q) = \infty, \quad \forall q . \quad (121)$$

An approximate, but convenient way to achieve this goal is to choose a function $R_{k=\Lambda}$ not infinite but of the order of Λ^2 for all momenta.

- when $0 < k < \Lambda$, the rapid modes (those for which $|q| > k$) must be almost unaffected by $R_k(q)$ which must therefore almost vanish for these modes:

$$R_k(|q| > k) \simeq 0 . \quad (122)$$

On the contrary, the slow modes must have a mass that almost decouple them from the long distance physics.

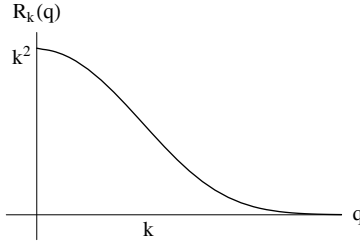


Fig. 6. A typical cut-off function in the effective average action approach.

Remembering that R_k is homogeneous to a mass square, it is not difficult to guess its generic shape, at least if we require that it is an analytic function of q^2 , see Fig.6.

We shall discuss in the following some convenient choices for R_k but let us first define precisely what Γ_k is. In principle, having defined Z_k by Eq. (118), the Legendre transform of $\log Z_k$ should be unambiguous and should lead to Γ_k . Let us follow this program and see that there is a subtlety. We thus define

$$W_k[B] = \log Z_k[B] \quad (123)$$

which is the Helmholtz free energy, up to the $-k_B T$ term that plays no role in what follows. The Legendre transform of W_k is defined by

$$\Gamma'_k[M] + W_k[B] = \int BM \quad (124)$$

where the magnetization $M(x)$ is, by definition the average of $\phi(x)$ and is therefore:

$$M(x) = \frac{\delta W_k}{\delta B(x)} . \quad (125)$$

Of course, for $k \rightarrow 0$, $R_k \rightarrow 0$, $W_k \rightarrow W$ and thus $\Gamma'_k \rightarrow \Gamma$ = Gibbs free energy of the system. However, it is easy to show that $\Gamma'_{\Lambda}[M] \neq H[M]$ contrary to what is expected, see Eq. (116). This comes from the $\Delta H_{k=\Lambda}$ term, which is large. Thus, we prefer to work with a modified free energy where the R_k term has been subtracted in Γ_k :²⁸

$$\Gamma_k[M] + W_k[B] = \int BM - \frac{1}{2} \int_q R_k(q) M_q M_{-q} . \quad (126)$$

The R_k term in Eq. (126) does not spoil the limit $k \rightarrow 0$ since in this limit it vanishes for $\forall q$. Let us now show that Eq. (126) is the correct definition of Γ_k leading to the limit $\Gamma_{k=\Lambda}[M] = H(M)$, Eq. (117).

4.3. An Integral Representation of Γ_k and the Limit $k \rightarrow \Lambda$

We start from the definition of Z_k , Eq. (118) and from the definition of Γ_k , Eq. (126). We deduce by differentiation (see, B.2):

$$B_x = \frac{\delta \Gamma_k}{\delta M_x} + \int_y R_k(x-y) M_y . \quad (127)$$

Thus, by substituting Eq. (126) and Eq. (127) into the definition of W_k we obtain:

$$e^{-\Gamma_k[M]} = \int \mathcal{D}\phi \exp \left(-H[\phi] + \int_x \frac{\delta \Gamma_k}{\delta M_x} (\phi_x - M_x) \right) \quad (128)$$

$$\exp \left(-\frac{1}{2} \int_{x,y} (\phi_x - M_x) R_k(x-y) (\phi_y - M_y) \right) . \quad (129)$$

If we choose a function $R_k(q)$ that diverges for all q as $k \rightarrow \Lambda$ then, in this limit:

$$\exp \left(-\frac{1}{2} \int_{x,y} (\phi_x - M_x) R_k(x-y) (\phi_y - M_y) \right) \sim \delta(\phi - M) \quad (130)$$

that is, it behaves as a functional Dirac delta. Therefore,

$$\Gamma_k[M] \rightarrow H[\phi = M] \quad \text{as } k \rightarrow \Lambda \quad (131)$$

if the cut-off R_k is such that it diverges in this limit. If R_k does not diverge and is only very large,

$$\Gamma_{k=\Lambda} \sim H . \quad (132)$$

5. The Exact RG Equation and Its Properties

The RG equation on Γ_k , that is the differential equation $\partial_k \Gamma_k = f(\Gamma_k)$ is derived in detail in B.2. The strategy is to obtain first an evolution equation for Z_k , then to deduce the equation on Γ_k . It writes

$$\partial_k \Gamma_k = \frac{1}{2} \int_q \partial_k R_k(q) \left(\Gamma_k^{(2)}[M] + \mathcal{R}_k \right)_{q,-q}^{-1} \quad (133)$$

where $\mathcal{R}_k(x, y) = R_k(x-y)$. The inverse $\left(\Gamma_k^{(2)}[M] + \mathcal{R}_k \right)_{q,-q}^{-1}$ has to be understood in the operator sense. It is convenient in practice to rewrite Eq. (133) as²⁸

$$\partial_k \Gamma_k = \frac{1}{2} \tilde{\partial}_k \operatorname{Tr} \log \left(\Gamma_k^{(2)} + R_k \right) \quad (134)$$

where $\tilde{\partial}_k$ acts only on the k -dependence of R_k and not on $\Gamma_k^{(2)}$ as:

$$\tilde{\partial}_k = \frac{\partial R_k}{\partial k} \frac{\partial}{\partial R_k} \quad (135)$$

and the trace means integral over q .

5.1. Some General Properties of the Effective Average Action Method

Let us mention some important properties of Γ_k .

- If the microscopic Hamiltonian H and the functional measure are symmetric under a group G and if there exists a cut-off function R_k such that the mass term ΔH_k respects this symmetry, then Γ_k is symmetric under G for all k and thus so is $\Gamma = \Gamma_{k=0}$. It can happen that there is no mass-like term that respects the symmetry whereas the theory, that is Γ is invariant under G . This means that the symmetry is broken for all finite k and that the symmetry is recovered only for $k \rightarrow 0$. This is the case of gauge symmetry. This symmetry breaking term can be controlled by modified Ward identities that become, in the limit $k \rightarrow 0$, the true Ward identities. It remains nevertheless difficult up to now to compute RG flows in a completely controlled way in gauge theories.
- An exact RG equation for theories involving fermions can also be derived along the same line.
- Eq. (134) looks very much like a one-loop result. At one-loop:

$$\Gamma_k = H + \frac{1}{2} \text{Tr} \log \left(H^{(2)} + R_k \right) . \quad (136)$$

Thus, substituting $H^{(2)}$ by the full $\Gamma_k^{(2)}[M]$ function changes the one-loop result into an exact one! There exists a diagrammatic representation of the RG equation written as in Eq. (133) and that emphasizes its one-loop structure, see Figs.7 and 8.

We define

$$G_k[M] = \left(\Gamma_k^{(2)}[M] + \mathcal{R}_k \right)^{-1} , \quad (137)$$

which is the “full”, that is M -dependent, propagator, see Fig.7.

- This one-loop structure has a very important practical consequence: only one integral has to be computed and thanks to rotational invariance, it is one-dimensional. This is very different from

$$G_{k,q,-q'} = q \xrightarrow{\quad} -q'$$

Fig. 7. Diagrammatic representation of the “full” propagator that is the M -dependent function $G_k[M] = \left(\Gamma_k^{(2)}[M] + \mathcal{R}_k \right)^{-1}_{q,-q}$.

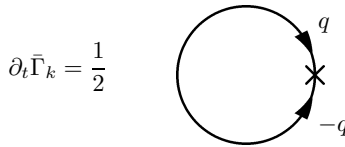


Fig. 8. Diagrammatic representation of the RG equation on the effective average action. The line represents the “full” propagator, Fig.7 and the cross $\partial_k R_k(q)$ and the loop, the integral over q .

perturbation theory where l loop-diagrams require l d -dimensional integrals. This is a tremendous simplification of the NPRG method compared to perturbation theory.

- The perturbation expansion can be retrieved from the NPRG equation (and the all-order proof of renormalizability can be simpler in this formalism).
- Because of the term $\partial_k R_k$ in the NPRG equation, only momenta q^2 of the order of k^2 or less contribute to the flow at scale k (we come back in detail to this point in the following). Thus the RG flow is regular both in the ultra-violet and in the infra-red. All the divergences of perturbation theory are avoided: we compute directly the RG flow and not first the relationship between bare and renormalized quantities from which is computed, in a second step, the RG flow.
- k acts as an infrared regulator (for $k \neq 0$) somewhat similar to a box of finite size $\sim k^{-1}$. Thus, for $k > 0$, there is no phase transition and thus no singularity in the free energy $\alpha \Gamma_k$. At finite k , everything is regular and can be power-expanded safely. We can therefore conclude that

- (i) the singularities of Γ_k build up as k is lowered and are thus smoothed by k ,
- (ii) the precursor of the critical behaviour should already show up at finite k for $|q| \gg k$.
- An important consequence of the regularity of Γ_k at $k > 0$ is that it can be expanded in a power series of $\nabla M(x)$. For slowly varying fields $M(x)$ this expansion is expected to be well-behaved. This is the basis of the *derivative expansion* that consists in proposing an *ansatz* for Γ_k involving only a finite number of derivatives of the field.²⁸ Two of the most used approximations, based on the derivative expansion, are

$$\Gamma_k = \int d^d x \left(U_k(M(x)) + \frac{1}{2} (\nabla M)^2 \right) \quad (138)$$

called the local potential approximation (LPA) since no field renormalization in front of the derivative term is included and

$$\Gamma_k = \int d^d x \left(U_k(M(x)) + \frac{1}{2} Z_k(M) (\nabla M)^2 \right) \quad (139)$$

often called the $O(\partial^2)$ approximation or the leading approximation.^v Of course, in principle, Γ_k involves all powers of ∇M compatible with rotational and \mathbb{Z}_2 invariance. We shall come back in detail to these approximations in the following.

- We shall see in the following that by working with dimensionless (and renormalized) quantities, the NPRG equation can be rewritten in a way that makes no explicit reference to the scales k and Λ . This will allow us to find fixed points from which quantities like critical exponents can be computed. The fact that Λ disappears from the flow equation also ensures that the “group law” of composition of RG transformations is obeyed. This self-similarity property of the flow will be automatic even if Γ_k is truncated (as in Eqs. (138), (139) for instance). This is a major advantage of this method compared to many others where renormalizability, that is self-similarity, is spoiled by approximations (Schwinger-Dyson approximations for instance).
- A property that follows from the last point is the decoupling of massive modes. Let us consider a theory with one very massive

^vThe function $Z_k(M)$ has, of course, nothing to do with the partition function $Z_k[B]$ introduced in Eq. (118) although it is customary to use the same symbol.

mode (m_1) and another one with a lower mass (m_2). Since only the modes $|q| \leq k$ contribute to the flow of Γ_k , once $k \ll m_1$, the massive mode does (almost) no longer contribute to the flow: it decouples. This means that it contributes to the flow when k is between Λ and m_1 (or, in real space, when the running lattice spacing is between a and its correlation length m_1^{-1}) and almost not below m_1 . This also means that if we are given a model at a scale $k_0 \ll m_1$, we cannot know whether the underlying “fundamental theory” (at scales larger than m_1) involves or not a massive particle since there is no longer any signal of the presence of this mode in the theory (that is, in the RG flow).

- Self-similarity and decoupling of massive modes will have universality (in the vicinity of a second order transition) as a consequence. We shall see that universality is not just the consequence of the existence of a fixed point. It is the consequence of a very peculiar geometry of the RG flow.^{44,46}

6. Approximation Procedures

The NPRG equation is an extremely complicated equation. It is a functional partial differential equation since it involves the functionals $\Gamma_k[M]$ and $\Gamma_k^{(2)}[M]$. Needless to say that we do not know how to solve it in general. Some approximations are thus required. Two main kinds of approximations are usually considered: the Green function approach and the derivative expansion. In both cases, the strategy consists in solving the RG equation in a *restricted functional space* and not as a series expansion in a small parameter. This is why we can hope to obtain non-perturbative results. Both methods need to project consistently the exact RG equation in the functional space that has been chosen. Of course, the quality of the result will depend crucially on the choice of space in which we search a solution. Depending on the problem, one choice can be drastically better than another. In all cases, it is impossible to know whether we have missed some physically crucial ingredient by making one choice rather than another one. But this problem is not specific to NPRG. It is generic in physics...

Let us review briefly the Green function approach and then explain in some details the derivative expansion which is the most employed method in statistical mechanics.

6.1. The Green Function Approach

From Eq. (133) we can deduce the infinite hierarchy of RG equations for the correlations functions defined by

$$\bar{\Gamma}_{k,p_1 \dots p_n}^{(n)} = \frac{\delta^n \Gamma_k}{\delta M_{p_1} \dots \delta M_{p_n}} \quad (140)$$

taken in a particular field configuration (the zero and the uniform field configurations being the most studied). We define $t = \log k/\Lambda$ which is often called the RG “time”. From Eq. (133), we obtain

$$\partial_t \frac{\delta \Gamma_k}{\delta M_p} = -\frac{1}{2} \int_{q_1, q_2, q_3} \partial_t R_k(q_1) G_{k q_1, -q_2} \frac{\delta \Gamma_k^{(2)}}{\delta M_p} G_{k q_3, -q_1} . \quad (141)$$

Therefore, setting $\dot{R}_k = \partial_t R_k = k \partial_k R_k$ we obtain

$$\begin{aligned} \partial_t \frac{\delta^2 \Gamma_k}{\delta M_p \delta M_{p'}} &= \int_{\{q_i\}} \dot{R}_{k, q_1} G_{k q_1, -q_2} \Gamma_{k p, q_2, -q_3}^{(3)} G_{k q_3, -q_4} \Gamma_{k q_4, -q_5, p'}^{(3)} \\ &G_{k q_5, -q_1} - \frac{1}{2} \int_{\{q_i\}} \dot{R}_{k, q_1} G_{k q_1, -q_2} \Gamma_{k q_2, -q_3, p, p'}^{(4)} G_{k q_3, -q_1} \end{aligned} \quad (142)$$

where both the left and the right hand sides are functions of M_q since they have not yet been evaluated in a particular configuration. These equations look terrible but in fact they are not since there exists a diagrammatic way to obtain them automatically. We represent $\Gamma_{k p_1, p_2, p_3}^{(3)}$ as in Fig.9. We

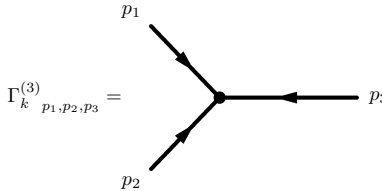
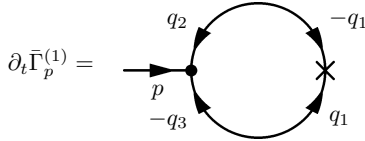
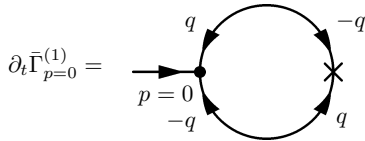
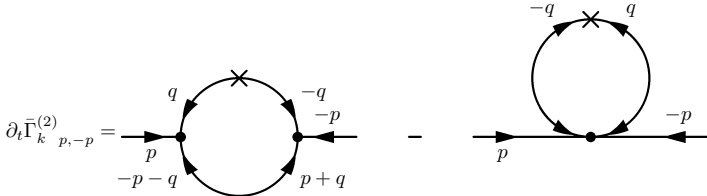


Fig. 9. Diagrammatic representation of $\Gamma_{k p_1, p_2, p_3}^{(3)}[M]$.

obtain for $\partial_t \Gamma_k^{(1)}$ the graph in Fig.10. Of course, if we evaluate $\partial_t \Gamma_k^{(1)}$ in a uniform field configuration, the momentum is conserved at each vertex and for each “propagator”. The function is thus non-vanishing only at zero momentum and we obtain the equation in Fig.11. It is clear on the diagrammatic representation that only one momentum integral remains. The RG equation for $\partial_t \Gamma_k^{(2)}$ evaluated in a uniform field configuration is given

Fig. 10. Diagrammatic representation of $\partial_t \bar{\Gamma}_k^{(1)}$.Fig. 11. Diagrammatic representation of $\partial_t \bar{\Gamma}_k^{(1)}$ evaluated in a uniform field configuration.Fig. 12. Diagrammatic representation of $\partial_t \bar{\Gamma}_k^{(2)}$ evaluated in a uniform field configuration. Note that the factor $\frac{1}{2}$ has not been represented on the figure for the tadpole (contrary to what we did for the other figures) because it can be retrieved from the topology of the graph itself (in fact the minus sign can also be retrieved from the graph).

in Fig.12. It is clear from these diagrammatic representations that $\partial_t \bar{\Gamma}_k^{(n)}$ involves $\bar{\Gamma}_k^{(n+1)}$ and $\bar{\Gamma}_k^{(n+2)}$. If we want to solve this infinite tower of equations, we have to truncate it. A possible truncation consists, for instance, in keeping $\bar{\Gamma}_k^{(2)}$ and $\bar{\Gamma}_k^{(4)}$ evaluated at $M = 0$ and to neglect the contribution of $\bar{\Gamma}_k^{(6)}$ in the equation on $\partial_t \bar{\Gamma}_k^{(4)}$ ($\bar{\Gamma}_k^{(3)}[M = 0] = 0$ in a \mathbb{Z}_2 -invariant model). A better method is to find an ansatz for $\bar{\Gamma}_k^{(6)}$ in terms of $\bar{\Gamma}_k^{(2)}$ and $\bar{\Gamma}_k^{(4)}$. In both cases, the system of equations becomes closed and can, at least in principle, be solved. Let us finally notice that this method consists in truncating the field-dependence of $\bar{\Gamma}_k[M]$ while keeping the momentum dependence of $\bar{\Gamma}_k^{(2)}$

and $\Gamma_k^{(4)}$. Tremendous improvements of this type of approximation has been performed these last years.^{47–49}

We now study another truncation method which is somewhat the reverse.

6.2. The Derivative Expansion

The principle of this approximation has already been introduced previously, see Eqs. (138), (139). The underlying idea is that we are mostly interested (for the study of critical phenomena) in the long distance physics, that is the $|q| \rightarrow 0$ region of the correlation functions.^w Thus, we keep only the lowest orders of the expansion of Γ_k in ∇M while we keep all orders in the fields M

$$\Gamma_k = \int d^d x \left(U_k(M(x)) + \frac{1}{2} Z_k(M) (\nabla M)^2 \right) + O(\nabla^4). \quad (143)$$

This approximation is based on a somewhat opposite philosophy as the one that prevailed in the Green function approach. However, it should be clear that for statistical mechanics, the most important information – e.g. the equation of state – is hidden in the effective potential $U_{k=0}$ of the theory that, therefore, needs to be computed as accurately as possible (see however Ref. [48]).

It is in fact remarkable that we can combine both methods by making a field expansion of U_k, Z_k, \dots on top of the derivative expansion while preserving many non-trivial results. The simplest such truncation consists in using the LPA and in keeping only the first two terms of the expansion of U_k in powers of M :^x

$$\Gamma_k[M] = \int d^d x (g_{2,k} M^2 + g_{4,k} M^4 + \frac{1}{2} (\nabla M)^2) \quad (144)$$

With this kind of ansatz, the RG equation on Γ_k becomes a set of ordinary differential equations for the couplings retained in the *ansatz*:

$$\partial_t g_{n,k} = \beta_n (\{g_{p,k}\}) . \quad (145)$$

^wThe computation of quantities like the total magnetization or the susceptibilities require only the knowledge of the spin-spin correlation function at zero momentum. The same thing holds for the correlation length.

^xLet us notice that if the k -dependence of the couplings were neglected, this ansatz would exactly coincide with the *ansatz* chosen by Landau to study second order phase transitions. We know that it would lead to the mean field approximation. It is remarkable that keeping the scale dependence of the couplings and substituting precisely this *ansatz* into the RG equation of Γ_k is sufficient to capture almost all the qualitative features of the critical physics of the Ising and $O(N)$ models in all dimensions (see the following).

For instance, if the truncation above is considered we find (see section 9.2 for the derivation of these equations)

$$\partial_t \kappa_k = -(d-2)\kappa_k + 6v_d l_1^d(2\kappa_k \lambda_k) \quad (146)$$

$$\partial_t \lambda_k = (d-4)\lambda_k + 6v_d \lambda_k^2 l_2^d(2\kappa_k \lambda_k) \quad (147)$$

where l_1^d , l_2^d are defined in the Appendix, Eq.(A.13). These equations are already non perturbative since the functions l_1^d , l_2^d are non polynomial. If U_k, Z_k, \dots are not truncated in a field expansion, the RG equation on Γ_k becomes a set of coupled partial differential equations for these functions. The initial condition at scale Λ is given by the Hamiltonian of the model. Before studying in detail this approximation method let us make an important remark.

Contrary to perturbation theory where only the renormalizable couplings are retained in the renormalized action, all powers of the fields appear in the ansatz of Eq. (143). There is no longer any distinction – at this level at least – between the two kinds of couplings, renormalizable and non-renormalizable. Although we shall not enter into any detail, let us comment briefly on this difference between the perturbative and non-perturbative approaches.^{8,44,46}

To understand the origin of this difference, it is necessary to remember that in perturbative field theory, the action (bare or renormalized) is *not* a physical quantity. It is only the “object” that generates the vertices of the theory from which Feynman diagrams are computed. As for the Feynman diagrams they are physical objects in the sense they are the building blocks of the Green functions that are physical (in particle physics, the S -matrix is physical). The effective action $\Gamma[M]$ is also physical. The action of perturbative field theory can well be polynomial and involve only a few couplings, $\Gamma[M]$ always involve all powers of the field in a non-trivial manner. In the particle physics language, this means that $\Gamma^{(n)}$ with $n = 6, 8, \dots$, corresponding to the scattering of n particles, cannot, in general, be factorized trivially into products of $\Gamma^{(p)}$ with $p < n$ corresponding to the scattering of fewer particles. Thus all couplings are non-trivial, even those corresponding to an arbitrarily large number of fields. They all have a non-trivial RG evolution that, *a priori*, needs to be taken into account into the flow of Γ_k . This is the reason why we must keep a complete function of M for U_k and not just the first terms of its expansion in M .

This is paradoxical because it seems in conflict with what we know from perturbation theory where only the marginal couplings drive the whole RG flow. In fact, it can be shown that at sufficiently long distance, that is

for sufficiently small k , all RG trajectories – that belong to an infinite dimensional space – are attracted towards a submanifold of dimension the number of renormalizable couplings (including the masses). This is particularly clear, and has been studied in detail by Bagnuls and Bervillier, for the critical theories of the \mathbb{Z}_2 -invariant theories in $d = 3$.^{44,46} In this case, the trajectories belong to the critical surface. For all of them, after a transient regime, they (almost) collapse on a line joining the Gaussian fixed point to the non-trivial fixed point describing the phase transition of the Ising model (called the Wilson-Fisher fixed point). Thus, if one is only interested in the long-distance physics compared to Λ^{-1} , the RG flow behaves as if it were driven by a unique coupling. As long as the projection of this line on the axis corresponding to the ϕ^4 -coupling is non-singular, it is possible to describe the flow along this line by the flow of the ϕ^4 -coupling alone. This is what perturbation theory does. Of course, this flow is universal: it depends only on the flow between the Gaussian and the Wilson-Fisher fixed point. It is therefore impossible to get any non-universal information on a given system from this RG trajectory alone because once we focus on this particular RG trajectory, it is impossible to reverse the flow (in the ultra-violet direction) to go back to the microscopic system we started with. Bagnuls and Bervillier have used the following metaphor:^{44,46} the RG trajectories on the critical surface are like rivers in the mountains. In the valley, there is a large river along which the flow is slow. Many small rivers, coming from the mountains, flow very rapidly into the large one. Once in the large river, it is almost impossible to know where the water came from. The large river has its source at the Gaussian fixed point and stops at the Wilson-Fisher fixed point. Perturbation theory can only focus on the large river whereas NPRG, because it is functional in essence, can follow any RG trajectory. Of course, the “continuum limit”, $\Lambda \rightarrow \infty$, (at fixed large distance physics) can only be taken on a trajectory where this limit is defined. There is only one such trajectory: the large river joining the Gaussian to the Wilson-Fisher fixed point. On this trajectory, the RG flow does not blow up at infinity in the continuum limit since the trajectory has a fixed point – the Gaussian – at its source. This theory is asymptotically free in the ultra-violet. Let us emphasize that the continuum limit is probably irrelevant from a physical viewpoint: who cares about the physics at asymptotically small distances or, in particle physics, at asymptotically large energies?

7. The Local Potential Approximation for the Ising Model

7.1. The Flow Equation of the Potential

We now consider the *ansatz* Eq. (138) for a \mathbb{Z}_2 symmetric theory. As already mentioned, the problem is to project the RG equation (133) on the potential U_k . This is naturally performed by *defining* the potential as Γ_k computed for *uniform* field configurations:

$$U_k(M_{\text{unif.}}) = \frac{1}{\Omega} \Gamma_k[M_{\text{unif.}}] \quad (148)$$

where Ω is the volume of the system. To compute the RG flow of U_k we act on both sides of this equation with ∂_t and we evaluate the right hand side thanks to Eq. (133). The only “difficulty” of this calculation is to invert $\Gamma_k^{(2)}[M] + R_k$ for uniform field configurations using the LPA *ansatz* to compute $\Gamma_k^{(2)}[M]$. This is performed in detail in B.3. The final result reads:

$$\partial_k U_k(\rho) = \frac{1}{2} \int_q \frac{\partial_k R_k(q)}{q^2 + R_k(q) + U'_k(\rho) + 2\rho U''_k(\rho)}, \quad (149)$$

where

$$\rho = \frac{1}{2} M^2 \quad (150)$$

is the \mathbb{Z}_2 -invariant and $U'_k(\rho)$ and $U''_k(\rho)$ are derivatives of U_k with respect to ρ . An important remark is in order here. Once the angular integral has been performed, the integrand of Eq. (149) is (up to a constant factor)

$$f(q^2, w) = |q|^{d-1} \frac{\partial_k R_k(q^2)}{q^2 + R_k(q^2) + w}. \quad (151)$$

Let us consider a typical cut-off function:

$$R_k(q^2) = \frac{q^2}{e^{q^2/k^2} - 1}. \quad (152)$$

Then, for generic values of w , the typical shape of f at fixed k is given in Fig.13 (for $d > 1$). As expected, only a window of momenta around k contributes to the flow at scale k . We see in particular that the rapid modes are efficiently integrated out by this kind of cut-off function. This explains the decoupling of massive modes already discussed section 5.1. The cut-off function (152) has been used many times in the literature but it turns out that another one is convenient because it allows to perform analytically the integral in Eq. (149). It writes⁵⁰

$$R_k(q^2) = (k^2 - q^2) \theta(k^2 - q^2). \quad (153)$$

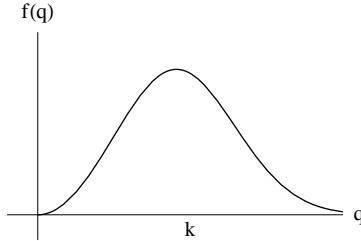


Fig. 13. The typical shape of the integrand $f(q)$.

With this choice of R_k we easily find for the RG flow of U_k

$$\partial_t U_k(\rho) = \frac{4v_d}{d} \frac{k^{d+2}}{k^2 + U'_k(\rho) + 2\rho U''_k(\rho)} \quad (154)$$

where v_d is defined in Eq. (A.3). All we can learn about the model at this approximation is contained in the solution of this equation. We can already see that, as expected, this equation does not admit a fixed point U^* . We have already seen that it is necessary to go first to the dimensionless variables to find a fixed point. This is what we now do.

7.2. The Scaling Form of the RG Equation of the Dimensionless Potential

We have already emphasized when studying block-spins that it is necessary to measure all lengths in units of the running lattice spacing to find a fixed point of the RG flow. Looking for a fixed point is a convenient method to study the critical behaviour of a model and we shall now spend some time deriving the RG equation for the dimensionless potential.

In our formalism, k is the analogue of the running lattice spacing and we must therefore “de-dimension” all dimensionful quantities thanks to k to find a fixed point. We have

$$[\Gamma_k] = k^0 \implies [M] = k^{\frac{d-2}{2}} \quad \text{and} \quad [U_k] = k^d. \quad (155)$$

We define the dimensionless variables by

$$y = \frac{q^2}{k^2}, \quad (156)$$

$$R_k(q^2) = q^2 r(y) = k^2 y r(y), \quad (157)$$

$$\tilde{x} = k x, \quad (158)$$

$$\tilde{M}(\tilde{x}) = k^{\frac{2-d}{2}} M(x), \quad (159)$$

$$\tilde{U}_t(\tilde{M}(\tilde{x})) = k^{-d} U_k(M(x)) . \quad (160)$$

To derive the RG equation for \tilde{U}_t we must keep in mind that the ∂_t in Eq. (154) is taken at fixed ρ whereas we want now to take it at fixed $\tilde{\rho}$. The detailed calculation is performed in the Appendix and the result is:

$$\partial_t \tilde{U}_t = -d\tilde{U}_t + (d-2)\tilde{\rho}\tilde{U}'_t - 2v_d \int_0^\infty dy y^{d/2+1} \frac{r'(y)}{y(1+r(y)) + \tilde{U}'_t + 2\tilde{\rho}\tilde{U}''_t} . \quad (161)$$

Once again, with the cut-off (153) the integral can be performed analytically and we find

$$\partial_t \tilde{U}_t = -d\tilde{U}_t + (d-2)\tilde{\rho}\tilde{U}'_t + \frac{4v_d}{d} \frac{1}{1 + \tilde{U}'_t + 2\tilde{\rho}\tilde{U}''_t} . \quad (162)$$

We clearly see on this equation that the flow of \tilde{U}_t has two parts, one that comes from the dimensions of U_k and ρ and one that comes from the dynamics of the model. This RG equation on \tilde{U}_t is a rather simple partial differential equation that can be easily integrated numerically. We are thus in a position to discuss the critical behaviour of the Ising model and to look for fixed points.²⁸

8. The Critical and Non-Critical Behaviour of the Ising Model within the LPA

Having derived the RG flow of the potential, we can relate a “microscopic” model defined at scale Λ by an Hamiltonian (or directly by Γ_Λ) with the free energy $\Gamma = \Gamma_{k=0}$. Let us emphasize that there is no reason why the Hamiltonian H should involve only ϕ^2 and ϕ^4 terms and not ϕ^6 , ϕ^8 , ... terms. In fact, the Hubbard-Stratonovich transformation enables us to obtain the exact potential at the scale of the lattice spacing of a magnetic system. In the Ising case, the potential thus obtained is

$$U_\Lambda(\phi) \propto \log \cosh \phi \quad (163)$$

and is thus non-polynomial. In the NPRG framework this is not a problem since, even if it were a polynomial at scale Λ , it would become non-polynomial *at any other scale*.

Let us anyway, for the sake of simplicity, consider a dimensionless potential at scale Λ of the form:

$$\tilde{U}_\Lambda(\tilde{\rho}) = \frac{\lambda_\Lambda}{2}(\tilde{\rho} - \kappa_\Lambda)^2 \quad (164)$$

with $\kappa_\Lambda > 0$. At the mean-field level, $\Gamma^{\text{MF}} = \Omega U_\Lambda$ and we would deduce at this approximation that the system is in its broken phase with a spontaneous magnetization per unit volume $M_{\text{sp}} = \Lambda^{\frac{d-2}{2}} \sqrt{2\kappa_\Lambda}$.^y However, the integration of the fluctuations can drastically change this picture: the minimum of the potential has a non-trivial RG flow that can drive it to 0. If this happens, the system is in fact in its symmetric (high temperature) phase.

Let us call $\kappa(k)$ the running minimum of the dimensionless potential at scale k (more appropriately at “time” $t = \log k/\Lambda$):

$$\partial_{\tilde{\rho}} \tilde{U}_k|_{\kappa_k} = 0. \quad (165)$$

It is physically clear, and this can be checked on the flow of U_k , that the spontaneous magnetization decreases because of the fluctuations. This means that the true spontaneous magnetization is always less than the mean-field spontaneous magnetization $\Lambda^{\frac{d-2}{2}} \sqrt{2\kappa_\Lambda}$. There are thus three possibilities.

(i) The system is in its broken phase (low temperature), the spontaneous magnetization is given by

$$M_{\text{sp}} = \sqrt{2\rho_0(k=0)} \quad (166)$$

where $\rho_0(k)$ is the location of the minimum of the (dimensionful) potential $U_k(\rho)$.^z The relation between $\kappa(k)$ and $\rho_0(k)$ is

$$\rho_0(k) = k^{d-2}\kappa(k) \quad (167)$$

from Eq. (159). Thus, if $\rho_0(k) \rightarrow M_{\text{sp}}^2/2$ when $k \rightarrow 0$, $\kappa(k)$ flows to infinity (for $d > 2$) as k^{2-d} in the same limit.

(ii) The system is in the high temperature phase, the spontaneous magnetization is vanishing. Thus, as k decreases the minimum $\kappa(k)$ must decrease and, at a finite scale k_s , hit the origin. It is easy to guess that k_s must be of the order of the inverse correlation length since as long as $k^{-1} \ll \xi$ the coarse-grained system remains strongly correlated and still behaves as if it were critical. It is only when $k^{-1} \sim \xi$ that “the system can realize” that

^yAt vanishing external magnetic field, the magnetization is given by $B = 0 = \partial U / \partial M$ and corresponds therefore to the location of the minimum of the potential.

^zWe shall see in the following that there is a subtlety here because of the convexity of the potential in the limit $k \rightarrow 0$.

its correlation length is finite and that its magnetization is vanishing. Thus $k_s \simeq \xi^{-1}$.

(iii) The system is critical. The spontaneous magnetization is vanishing which means that $\rho_0(k) = k^{d-2}\kappa(k) \rightarrow 0$ as $k \rightarrow 0$. Note that this does not require that $\kappa(0) = 0$ since $\kappa(k)$ is multiplied by a positive power of k , at least for $d > 2$. In fact, $\kappa(k)$ reaches a finite fixed point value κ^* . Note that for $d < 2$ it is necessary to take into account the field renormalization, that is the anomalous dimension, to obtain a coherent picture of the physics. This requires to go beyond the LPA (see section 9).

We can summarize the three cases in Fig.14. κ_c is the critical initial value

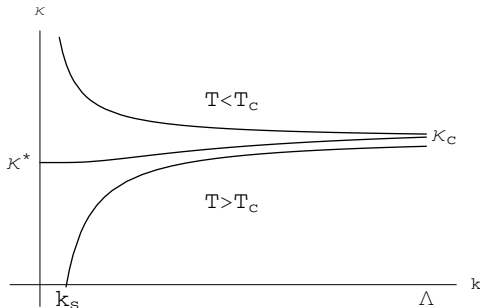


Fig. 14. Behavior of the running minimum $\kappa(k)$ of the dimensionless potential. From top to bottom: $T < T_c$, $T = T_c$ and $T > T_c$. κ_c is the critical initial value of κ_Λ for which the system is critical. This value should not be confused with κ^* which is the fixed point value of $\kappa(k)$. In the low temperature phase the dimensionless running minimum diverges whereas the dimensionful minimum converges to the value of the spontaneous magnetization since it is multiplied by a positive power of the scale k that compensates exactly the divergence of $\kappa(k)$. For the high temperature phase $k_s \simeq \xi^{-1}$.

of κ_Λ for which the system is critical. This value should not be confused with κ^* . For a generic initial potential

$$\tilde{U}_\Lambda(M) = \frac{\lambda_\Lambda}{2}(\tilde{\rho} - \kappa_\Lambda)^2 + \frac{u_{3,\Lambda}}{3!}(\tilde{\rho} - \kappa_\Lambda)^3 + \dots \quad (168)$$

the critical value κ_c of κ_Λ is a function of all the other couplings $\lambda_\Lambda, u_{3,\Lambda}, \dots$. This means that in the space of dimensionless coupling constants there exists a “critical hypersurface” of co-dimension 1 that corresponds to systems that are critical. Generically, κ_Λ is a regular function of the temperature around T_c and at first order we can assume that

$$\kappa_\Lambda - \kappa_c \propto T_c - T . \quad (169)$$

This allows us to relate the coefficients of the microscopic Hamiltonian to the temperature. Note that contrary to the mean-field analysis for which criticality is reached when the coefficient r_0 of the quadratic term of the potential (that is $r_0\phi^2/2$) is vanishing: $r_0 \propto T - T_c$, this is not true here since criticality does not correspond to the vanishing of the bare mass term. The mean-field analysis is wrong in this respect.

Let us now show what we expect for $U = U_{k=0}$ and $\tilde{U}_{k=0}$.

8.1. The Low and the High Temperature Phases

In the low temperature phase, we expect to have a spontaneous magnetization, either up or down. More precisely, the equation

$$B = \frac{\partial U}{\partial M} \quad (170)$$

is expected to have a solution $+M_{sp}$ for $B \rightarrow 0^+$ and $-M_{sp}$ for $B \rightarrow 0^-$. Moreover, U must be a convex function of M since it is obtained from a Legendre transform. Thus, U must have a very peculiar shape since it must have two minima at M_{sp} and no maximum in between (otherwise it should not be convex). The only possibility is that it is flat in between $-M_{sp}$ and $+M_{sp}$.

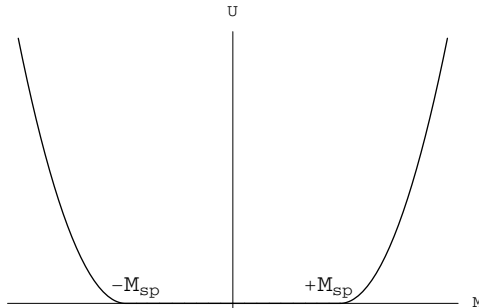


Fig. 15. Shape of the effective potential $U = U_{k=0}$ for $T < T_c$.

The convexity of the effective potential is not preserved by perturbation theory: the convex envelop has to be taken by hand. In fact, it is notoriously difficult to compute “safely” a convex effective potential and this is a property that is reproduced by NPRG already at the LPA. Note that this is no longer the case if a field expansion of the potential is performed (a polynomial can never be flat on a whole interval). In fact, starting with a potential

U_Λ showing a double-well structure and with parameters $\kappa_\Lambda, \lambda_\Lambda, \dots$ such that the system is in its low temperature phase, the RG flow of U_k is such that as k is lowered²⁸

- the minimum $\rho_0(k)$ moves towards the origin and eventually reaches a limit equal to the spontaneous magnetization M_{sp} ;
- the maximum of the potential located between the two minima decreases and goes to 0 as $k \rightarrow 0$ (the “inner part” of the potential flattens). At $k = 0$, $U_{k=0}$ looks like the potential of Fig.15.

As $T \rightarrow T_c$, that is as $\kappa_\Lambda \rightarrow \kappa_c$, M_{sp} moves towards the origin and at $T = T_c$ coincides exactly (by definition of T_c) with the origin. In the high temperature phase, that is $\kappa_\Lambda < \kappa_c$, the spontaneous magnetization vanishes. Thus U has a single minimum at the origin in this case.

Let us finally notice that when $k \neq 0$, U_k is not convex in general. This is normal since Γ_k is not the Legendre transform of W_k (W_k is convex) because of the term $1/2 \int R_k M M$ that has been subtracted.

8.2. The Critical Point

For $\kappa_\Lambda = \kappa_c$, the minimum of the potential U_k (or \tilde{U}_k) for $k > 0$ is non vanishing. It is only for $k \rightarrow 0$ that the minimum $\rho_0(k)$ reaches the origin.

To characterize the critical point it is interesting to work with \tilde{U}_k instead of U_k since, at this point, the long distance physics (compared with Λ^{-1}) is scaleless. This means that the potential, properly rescaled thanks to k , should be k -independent at $T = T_c$ and for sufficiently small k . It must be a fixed potential $\tilde{U}^*(\tilde{\rho})$

$$\partial_t \tilde{U}^*(\tilde{\rho}) = 0 . \quad (171)$$

We deduce from this equation and from Eq. (154) that $\tilde{U}^*(\tilde{\rho})$ is a solution of

$$0 = -d \tilde{U}^* + (d-2)\tilde{\rho} \tilde{U}^{*\prime} + \frac{4v_d}{d} \frac{1}{1 + \tilde{U}^{*\prime} + 2\tilde{\rho} \tilde{U}^{*\prime\prime}} . \quad (172)$$

At first sight, the situation looks paradoxical since this is a second order differential equation that should admit infinitely many solutions indexed by two numbers whereas we expect only one fixed point in $d = 3$ corresponding to the universality class of the Ising model. In fact, it can be shown that among all these solutions, *only one* is well defined for all $\tilde{\rho} \in [0, \infty]$.¹⁴

An easy way to show this is the “shooting method”. We first write down the fixed point equation for $\tilde{U}^{*\prime\prime}(\tilde{M})$ analogous to Eq. (172) and which is

more convenient. Then, one initial condition is given by the \mathbb{Z}_2 symmetry: $\tilde{U}^*(\tilde{M} = 0) = 0$. The other initial condition: $\tilde{U}^{**}(\tilde{M} = 0)$ is then adjusted so that $\tilde{U}^*(\tilde{M})$ exists for all \tilde{M} . For a generic $\tilde{U}^{**}(\tilde{M} = 0)$ this is not the case: at finite \tilde{M} , \tilde{U}^* either blows up at $+\infty$ or at $-\infty$. By dichotomy, the value $\tilde{U}^{**}(\tilde{M} = 0)$ can be fine-tuned so that this occurs for larger and larger \tilde{M} . The fixed point potential thus obtained is shown in Fig.16.

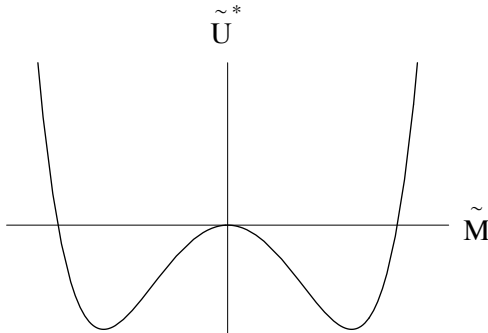


Fig. 16. Dimensionless fixed point potential of the Ising model at $d = 3$. The minima of this potential are located at $\sqrt{2\kappa^*}$. The spontaneous magnetization is vanishing although $\kappa^* \neq 0$ (see the text).

The same fixed point potential can be found “dynamically” by integrating the RG flow and by fine-tuning the value of κ_Λ to get closer and closer to κ_c . We find that for an initial κ_Λ very close to κ_c , the potential \tilde{U}_t spends a very long RG time close to \tilde{U}^* before either departing in the high or low temperature phase. Thus, all couplings reach a plateau before blowing up. On this plateau, we obtain a very good approximation of $\tilde{U}^*(\tilde{M})$ very close to the one found by the shooting method. For $\kappa(k)$ very close to κ_c this is represented in Fig.17.

One can observe that during a transient regime, $\kappa(k)$ for $k \simeq \Lambda$ is not stationary even at the critical temperature. This regime simply corresponds to the RG “time” necessary to approach the fixed point. It is non-universal since it depends on the starting point κ_c on the critical surface.

Let us finally point out a subtlety. When $k > 0$, it is possible to reconstruct $U_k(M)$ from $\tilde{U}_k(\tilde{M})$ by a somewhat trivial rescaling:

$$U_k(M) = k^d \tilde{U}_k \left(k^{-\frac{d-2}{2}} M \right) . \quad (173)$$

The k factor acts as a magnification scale when we go from M to \tilde{M} (at

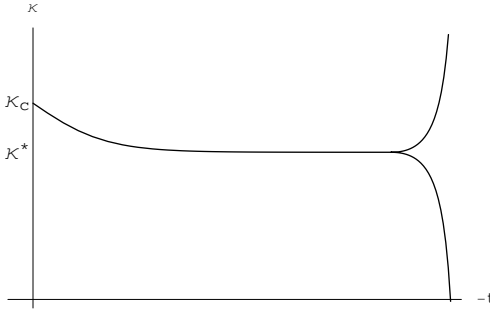


Fig. 17. Behavior of $\kappa(k)$ very close to κ_c . During the transient regime at small $-t$ the representative point of the system approaches the fixed point. Then, this point remains close to the fixed point and κ remains almost constant and very close to its fixed point value κ^* . Then, if the initial condition of the RG flow was not right on the critical surface, it departs either in the low or in the high temperature phase where κ either blows up or goes to 0.

least for $d > 2$). For $k \rightarrow 0$ an infinitesimal range of M around the origin is mapped onto a finite range of \tilde{M} . It is therefore possible – and this is what indeed occurs at $T = T_c$ – that $U_{k=0}$ has a trivial shape around $M = 0$ showing a minimum only at 0, see Fig.15 for $M_{sp} \rightarrow 0$, while $\tilde{U}_{k=0}$ shows a double-well structure!

8.3. The Critical Exponents

Within the LPA, there is no possibility to modify the mean-field like q^2 -dependence of $\Gamma_k^{(2)}(q)$ (evaluated at $M = 0$) since there is no renormalization of the derivative term. The exponent η is therefore vanishing at this order of the derivative expansion (see Eq. (71) and $\Gamma^{(2)}(q) = 1/G^{(2)}(q)$):

$$\eta^{\text{LPA}} = 0. \quad (174)$$

The exponent β defined in Eq. (85) can be calculated directly by fitting the behaviour of M_{sp} defined in Fig.15 as a function of $\kappa_\Lambda - \kappa_c$ which is itself proportional to $T_c - T$. Of course, this is not very convenient although feasible.

As for the exponent ν , we have seen that it is related to the behaviour of the RG flow around the fixed point, Eq. (75) and, more precisely, is the inverse of the positive eigenvalue of the flow at the fixed point. This means that very close to the fixed point and away from the critical surface, the

potential is such that

$$\tilde{U}(\tilde{M}, t) = \tilde{U}^*(\tilde{M}) + \epsilon e^{-t/\nu} u(\tilde{M}) . \quad (175)$$

It can be shown that $u(\tilde{M})$ must behave as a power law at large \tilde{M} and that this ensures that there is a unique value of ν such that Eq. (175) holds. Note that Eq.(175) is not general since if we choose a point on the critical surface, the corresponding potential is attracted towards $\tilde{U}^*(\tilde{M})$. This approach is governed by the so-called critical exponent ω corresponding to correction to scaling. Thus, in general, infinitesimally close to the fixed point, the evolution of the potential is given by the sum of two terms, one describing the approach to \tilde{U}^* on the critical surface and one describing the way the RG flow escapes the fixed point if one starts close but away from the critical surface. With the θ -cut-off function, Eq. (153), one finds at $d = 3$:^{28,38,39}

$$\nu^{\text{LPA}} = 0.65 \quad (176)$$

to be compared with $\nu = 0.6297(5)$ obtained by Monte Carlo simulations.

Several remarks are in order here.

- In principle, from ν and η all the other critical exponents can be calculated thanks to the scaling relations derived in section 3.3. It is interesting to verify that these relations are not spoiled by the LPA. Indeed, by computing separately all the exponents, it is found that the scaling relations among them are very well satisfied.
- In the exact theory, no physical result should depend on the choice of cut-off function R_k . However, once approximations are performed a spurious dependence on the choice of R_k is observed. As a consequence, the whole scheme makes sense only if this dependence is smooth. It is of course very difficult to obtain general results on this point since the space of cut-off functions is infinite dimensional and that we cannot sample it efficiently. In practice, we should choose a space of “reasonable” cut-off functions and study the variations of physical quantities like critical exponents in this space. This has been done in some details and it is observed that the dependence of ν on R_k is rather mild.^{38–40} Let us emphasize that this problem is not specific to NRG. Even in the perturbative schemes the critical exponents acquire a spurious dependence on several choices made during their calculations.
- The LPA is certainly not appropriate for the computation of critical exponents in $d = 2$. We have seen several times that this dimension plays a special role in the formalism although nothing spectacular

is expected in $d = 2$ for the critical behaviour, at least for the Ising model. This comes from the fact that $\eta = 0$ starts to be a bad approximation at and below $d = 2$ for this model (it is worse for the $O(N)$ models with $N \geq 2$). The exact value of η is known in $d = 2$ from Onsager's solution of the Ising model: $\eta = 0.25$. Going to the next order of the derivative expansion cures most of the problems encountered at the level of the LPA at low dimensions.^{28,51}

- As explained in the following for the $O(N)$ models, it is possible to go beyond the LPA and to compute with greater accuracy the critical exponents, η in particular. This kind of calculations has been performed by several authors⁵² at order $O(\partial^2)$ of the derivative expansion for the Ising and $O(N)$ models in $d = 3$ and $d = 2$ ⁵³ and also at $O(\partial^4)$ for the Ising model in $d = 3$. Let us quote the best results obtained for the Ising model in $d = 3$:

order	ν	η
∂^0	0.6506	0
∂^2	0.6281	0.044
∂^4	0.632	0.033
7-loops	0.6304(13)	0.0335(25)

where the $O(\partial^4)$ results come from⁴⁰ and the 7-loops results from.⁴

Let us now study the $O(N)$ models at order $O(\partial^2)$ of the derivative expansion.

9. The $O(N)$ Models at $O(\partial^2)$ of the Derivative Expansion

Although the Ising and $O(N)$ models have much in common, there are several non-trivial points specific to the $O(N)$ models that are worth studying. Among them is the presence of Goldstone modes in the low temperature phase, the Mermin-Wagner theorem in $d = 2$ and the Kosterlitz-Thouless transition for $N = 2$ in $d = 2$. We shall use again the derivative expansion that writes at $O(\partial^2)$:

$$\Gamma_k = \int d^d x \left(U_k(\vec{M}^2(x)) + \frac{1}{2} Z_k(\vec{M}^2) (\nabla M)^2 + \frac{1}{4} Y_k(\vec{M}^2) (\vec{M} \cdot \nabla \vec{M})^2 \right) \quad (177)$$

where \vec{M} is a N -component vector. In fact, we shall mainly study the LPA' that consists in neglecting $Y_k(\vec{M}^2)$ and keeping only the first term of the field-expansion of $Z_k(\vec{M}^2)$ that we call Z_k :

$$\Gamma_k = \int d^d x \left(U_k(\vec{M}^2(x)) + \frac{1}{2} Z_k (\nabla M)^2 \right). \quad (178)$$

The RG equation on Γ_k is obtained along the same line as in the Ising case. We start by constructing the partition function $Z_k[\vec{B}]$

$$Z_k[\vec{B}] = \int \mathcal{D}\vec{\phi}(x) \exp \left(-H[\vec{\phi}] - \Delta H_k[\vec{\phi}] + \int \vec{B} \cdot \vec{\phi} \right) \quad (179)$$

with

$$\Delta H_k[\vec{\phi}] = \frac{1}{2} \int_q R_k(q) \vec{\phi}_q \cdot \vec{\phi}_{-q}. \quad (180)$$

Since $\Gamma_k[\vec{M}]$ is a $O(N)$ -scalar, the RG equation involves now a trace on the $O(N)$ indices

$$\partial_k \Gamma_k = \frac{1}{2} \text{Tr} \int_{x,y} \partial_k R_k(x-y) W_k^{(2)}(x,y) \quad (181)$$

where $W_k^{(2)}(x,y)$ is now a NN matrix:

$$W_{k,ij}^{(2)}(x,y) = \frac{\delta^2 W_k}{\delta B_i(x) \delta B_j(y)}. \quad (182)$$

$\Gamma_k^{(2)} + \mathcal{R}_k$ is again the inverse of $W_k^{(2)}$

$$\delta(x-z) \delta_{ik} = \int_y W_{k,ij}^{(2)}(x,y) \left(\Gamma_k^{(2)} + \mathcal{R}_k \right)_{jk} (y,z). \quad (183)$$

where the summation over repeated indices is understood (Einstein's convention). Thus the RG equation writes:

$$\partial_k \Gamma_k = \frac{1}{2} \text{Tr} \int_{x,y} \partial_k R_k(x-y) \left(\Gamma_k^{(2)} + \mathcal{R}_k \right)_{x,y}^{-1}. \quad (184)$$

9.1. The RG Equation for the Potential

Once again we define the potential as $\Gamma_k[\vec{M}]$ evaluated in a uniform field configuration \vec{M} . By symmetry, we can choose any direction we want for \vec{M} . We take

$$\vec{M} = \begin{pmatrix} M \\ 0 \\ \vdots \\ 0 \end{pmatrix}. \quad (185)$$

The RG equation for the potential writes

$$\partial_k U_k = \frac{1}{2} \text{Tr} \int_q \left(\partial_k R_k(q) \left(\frac{\partial^2 U_k}{\partial M_i \partial M_j} + (Z_k q^2 + R_k) \delta_{ij} \right)^{-1} \right). \quad (186)$$

Since

$$\frac{\partial^2 U_k}{\partial M_i \partial M_j} = \frac{\partial U_k}{\partial \rho} \delta_{ij} + \frac{\partial^2 U_k}{\partial \rho^2} M_i M_j \quad (187)$$

where $\rho = 1/2\vec{M}^2$, we obtain

$$\frac{\partial^2 U_k}{\partial M_i \partial M_j} + (Z_k q^2 + R_k) \delta_{ij} = \begin{pmatrix} Z_k q^2 + R_k + U'_k + 2\rho U''_k & & & \\ & Z_k q^2 + R_k + U'_k & & \\ & & \ddots & \\ & & & Z_k q^2 + R_k + U'_k \end{pmatrix}. \quad (188)$$

It is trivial to invert this matrix and to compute the trace. We find:

$$\partial_k U_k = \frac{1}{2} \int_q \partial_k R_k(q) \left(\frac{1}{Z_k q^2 + R_k + U'_k + 2\rho U''_k} + \frac{N-1}{Z_k q^2 + R_k + U'_k} \right). \quad (189)$$

We can see two differences with what we have done in the Ising case within the LPA:

- Since we were working within the LPA we did not have previously a “field renormalization” Z_k in front of the q^2 term. Its presence will have important consequences both from the technical and physical point of view.
- There is a new term proportional to $N - 1$ in Eq. (189). It will take care of the physics of the Goldstone bosons in the low temperature phase.

9.2. The RG Equation for the Dimensionless Potential \tilde{U}_k

Once again, Eq. (189) is not well suited for the search of a fixed point since k appears explicitly in the right hand side. We have to go to dimensionless quantities. But now, even the change of variables to dimensionless quantities, Eq. (159) is not sufficient to get rid of the k -dependence since Z_k depends on k . It can be shown that in the scaling regime⁴⁷

$$Z_{k \rightarrow 0} \sim \left(\frac{k}{\Lambda} \right)^{-\eta}. \quad (190)$$

Z_k never reach a fixed point value and it is therefore necessary to get rid of it to obtain the fixed point. We introduce therefore dimensionless and

“renormalized” quantities defined by

$$y = \frac{q^2}{k^2}, \quad (191)$$

$$R_k(q^2) = Z_k q^2 r(y) = Z_k k^2 y r(y), \quad (192)$$

$$\tilde{x} = k x, \quad (193)$$

$$\tilde{M}(\tilde{x}) = \sqrt{Z_k} k^{\frac{2-d}{2}} M(x), \quad (194)$$

$$\tilde{U}_t(\tilde{M}(\tilde{x})) = k^{-d} U_k(M(x)). \quad (195)$$

Note that a Z_k has been included in R_k . We can now repeat all the different steps leading to the RG equation on \tilde{U}_k . It is useful to define first

$$k \partial_k Z_k = -\eta_k Z_k \quad (196)$$

which we could call a “running” anomalous dimension. Because of the behaviour of Z_k , Eq. (190), η_k will reach a fixed point value (the anomalous dimension) whereas Z_k does not. From Eqs. (191)-(195) we deduce that $Z_k q^2 + R_k + U'_k + 2\rho U''_k$ becomes proportional to $Z_k k^2$ as $\partial_t R_k(q^2)$ which is at the numerator. Thus, with this rescaling, the explicit k - and Z_k -dependencies will disappear in the equation on \tilde{U}_k (in this sense, working with the dimensionless and renormalized quantities consists in going to the “co-moving frame”). The RG equation on \tilde{U}_k writes:²⁸

$$\begin{aligned} \partial_t \tilde{U}_t &= -d \tilde{U}_t + (d-2+\eta_k) \tilde{\rho} \tilde{U}'_t - v_d \int_0^\infty dy y^{d/2} (\eta_k r(y) + 2 y r'(y)) \\ &\quad \left(\frac{1}{y(1+r(y)) + \tilde{U}'_t + 2\tilde{\rho}\tilde{U}''_t} + \frac{N-1}{y(1+r(y)) + \tilde{U}'_t} \right). \end{aligned} \quad (197)$$

We shall see in the following that it is sometimes convenient to consider the field-expansion of \tilde{U}_t and the RG flow of the couplings appearing in this expansion. It is a non-trivial question to know around which field configuration one should perform the expansion. Of course, if we do not truncate this expansion and if the expansion has an infinite radius of convergence, the point around which the expansion is performed does not matter. However, the radius of convergence is not infinite and we shall be of course interested in truncating the series expansion at orders as low as possible. The rule of thumb is that each time a field-expansion has to be performed, the best

choice is to do it around the minimum of the (dimensionless) potential κ_k , Eq. (165):

$$\vec{M}_{|_{\text{Min}}} = \begin{pmatrix} \sqrt{2\kappa_k} \\ 0 \\ \vdots \\ 0 \end{pmatrix} \quad (198)$$

with

$$\tilde{U}_k = \frac{\lambda_k}{2}(\tilde{\rho} - \kappa_k)^2 + \frac{u_{3,k}}{3!}(\tilde{\rho} - \kappa_k)^3 + \dots \quad (199)$$

Let us notice that this equation is not sufficient to define completely κ_k , λ_k , $u_{3,k}$, etc. It is necessary to define them as

$$\frac{\partial \tilde{U}_k}{\partial \tilde{\rho}}|_{\tilde{\rho}=\kappa_k} = 0, \quad (200)$$

$$\frac{\partial^2 \tilde{U}_k}{\partial \tilde{\rho}^2}|_{\tilde{\rho}=\kappa_k} = \lambda_k, \quad (201)$$

$$\begin{matrix} \vdots \\ \frac{\partial^n \tilde{U}_k}{\partial \tilde{\rho}^n}|_{\tilde{\rho}=\kappa_k} = u_{n,k}. \end{matrix} \quad (202)$$

Note that Eq. (200) makes sense only if $\kappa_k \neq 0$ (for the search of the fixed point, this is not a problem since $\kappa^* \neq 0$).

The flow of all these coupling constants can be obtained trivially by acting on both sides of these equations with ∂_t and using Eq. (197). We find for instance

$$\begin{aligned} \partial_t \kappa_k &= -(d-2+\eta_k)\kappa_k + 2v_d \left(3 + 2\frac{\kappa_k u_{3,k}}{\lambda_k} \right) l_1^d(2\kappa_k \lambda_k) \\ &\quad + 2v_d(N-1)l_1^d(0), \end{aligned} \quad (203)$$

$$\begin{aligned} \partial_t \lambda_k &= (d-4+2\eta_k)\lambda_k + 2v_d(N-1)\lambda_k^2 l_2^d(0) \\ &\quad + 2v_d(3\lambda_k + 2\kappa_k u_{3,k})^2 l_2^d(2\kappa_k \lambda_k) \\ &\quad - 2v_d \left(2u_{3,k} + 2\kappa_k u_{4,k} - 2\frac{\kappa_k u_{3,k}^2}{\lambda_k} \right) l_1^d(2\kappa_k \lambda_k) \end{aligned} \quad (204)$$

where the threshold functions l_n^d have been defined in A.13. One remarks that the flow of λ_k involves $u_{3,k}$ and $u_{4,k}$. This is a general rule: the flow of $u_{n,k}$ involves $u_{n+1,k}$ and $u_{n+2,k}$. The non-perturbative character of these

flows comes from the non-polynomial character of the threshold functions l_n^d . This, in turn, implies that the right hand side of Eqs.(203,204) are not series expansions in the coupling constant λ_k .

The computation of the anomalous dimension η_k requires the computation of the flow of Z_k . As we did for the potential this is possible after a definition of Z_k in terms of Γ_k has been found. It is clear that Z_k corresponds to the term in Γ_k which is quadratic in M and in q . In fact, this definition is not sufficient to completely characterize Z_k since it is the first term in the expansion of the function $Z_k(\tilde{\rho})$ and it is necessary to specify around which value of $\tilde{\rho}$ the expansion is performed. Here again, we choose the minimum κ_k of the potential, Eqs. (198)-(200).

A precise calculation shows that

$$Z_k = \frac{(2\pi)^d}{\delta(p=0)} \lim_{p^2 \rightarrow 0} \frac{d}{dp^2} \left(\bar{\Gamma}_{(2,p),(2,-p)}^{(2)}|_{\text{Min}} \right) \quad (205)$$

where $\bar{\Gamma}_{(2,p),(2,-p)}^{(2)}$ is the second derivative of Γ_k with respect to $M_2(p)$ and $M_2(-p)$. The flow of Z_k is now obtained by acting on both sides of Eq. (205) with ∂_t . After a straightforward although somewhat tedious calculation we obtain:

$$\eta_k = \frac{16v_d}{d} \kappa_k \lambda_k^2 m_{2,2}^d(2\kappa_k \lambda_k) \quad (206)$$

where $m_{2,2}^d$ is a threshold function defined in (A.16). We thus find that η_k is *not an independent quantity*. It is entirely determined by the other couplings.

9.3. The Limits $d \rightarrow 4$, $d \rightarrow 2$ and $N \rightarrow \infty$

A very nice feature of the effective average action formalism is that the one-loop results obtained in $d = 4 - \epsilon$ (with the ϕ^4 theory) and $d = 2 + \epsilon$ (with the non-linear sigma model for $N \geq 3$) are retrieved very simply while keeping in the *ansatz* for Γ_k only κ_k , λ_k and Z_k , Eqs. (203), (204), (206).^{28,42} The large N limit is also retrieved at leading order with the same *ansatz*. This is a very interesting property since it indicates that the same calculation leads to controlled results both in the upper and lower critical dimensions and at $N = \infty$. Needless to say that this is completely out of reach of the perturbative expansion.

It has also been shown – with the same *ansatz* – that the Kosterlitz-Thouless transition is qualitatively well reproduced. With the complete $O(\partial^2)$ approximation, a fairly good quantitative agreement is obtained.⁵²

The remarkable point here is that these results have been obtained without introducing by hand the vortices as is usually done otherwise.

Morris has also shown that the infinite sequence of multicritical fixed points of the Ising model in $d = 2$ can be retrieved. This is also a non-trivial result since it would be very complicated to obtain them perturbatively.⁵¹

10. Conclusion

In this introduction to the NPRG we have focused on its application to statistical mechanics and on some of its relations with perturbative renormalization. We have seen three important points.

First, at a conceptual level, the NPRG enables to understand how microphysics can be continuously related to macrophysics, something that is not possible in general within perturbative field theory. As a by-product, one can solve this way the paradox that a field theory involving infinitely many *interacting* degrees of freedom can be described in the infrared regime with only a finite (and small) number of coupling constants, precisely those that are called renormalizable within perturbation theory. This comes from the attractive character of the submanifold spanned by the renormalizable couplings in the space of coupling constants (the large river effect) and is the very meaning of universality.

Second, we have seen that contrary to common belief, it is possible to obtain qualitatively good results about the long distance physics with NPRG techniques from very short ansätze and even results that reproduce one-loop results around the upper and the lower critical dimensions and at large N . This is probably why the NPRG results obtained at finite N and for dimensions in between the upper and the lower critical dimension are reliable.

Third, the series obtained from the derivative expansion seem to converge rapidly, at least in dimension three for the Ising model. This makes the NPRG a quantitative tool for studying strongly correlated systems and not only, as often claimed, a qualitative one. Of course, this claim should be substantiated by calculations performed beyond the $O(\partial^4)$ and also in dimension two. It is nevertheless encouraging to see that critical exponents already converge at this order to the best known values without any resummation and that non universal quantities can be accurately computed.

Let us finally mention that a crucial drawback of the derivative expansion is its inadequacy to the calculation of the momentum dependence of the correlation functions. In fact, it can be shown that the derivative ex-

pansion makes sense only when the external momenta of the correlation functions are less than the running scale k . Thus, when $k \rightarrow 0$ only the infrared physics can be computed with the derivative expansion. Crucial improvements in the computation of the momentum dependence of $\Gamma^{(2)}$ and $\Gamma^{(4)}$ has been performed these last years^{47–49} and there is no doubt that if this method works it will be a new step in our possibility of computing new non perturbative phenomena in field theory.

Acknowledgements

I want first to thank D. Mouhanna without whom the little group in Paris (with an antenna in Grenoble) working on the NPRG would have never existed. I owe my understanding of this subject to many discussions and common works with him. I also thank M. Tissier with whom I collaborated and from whom I have learned a lot. It is also a great pleasure to thank L. Canet and H. Chaté with whom I have collaborated and discussed many aspects of statistical mechanics and renormalization. I also thank I. Doronic and J. Vidal with whom I collaborated and G. Tarjus, J. Berges, C. Bervillier and C. Wetterich for many discussions about the NPRG. More recently, discussions with R. Mendez-Galain and N. Wschebor on their own version of the NPRG have greatly improved my understanding of this subject and I want to thank them for that. I also thank J-M. Caillol for several discussions. Finally, I thank Yu. Holovatch who encouraged me to write down my lecture notes, the students who helped me to improve them (P. Hosteins and G. Gurtner in particular) and A. Schwenk and J.-P. Blaizot who invited me in Trento to give a set of lectures on the NPRG.

Appendix A. Definitions, conventions

- *Integrals in x and q spaces*

In real and Fourier spaces we define

$$\int_x = \int d^d x \quad , \quad \int_q = \int \frac{d^d q}{(2\pi)^d} \quad (\text{A.1})$$

- *Fourier transform*

$$f(x) = \int_q \tilde{f}(q) e^{iqx} \quad , \quad \tilde{f}(q) = \int_x f(x) e^{-iqx} . \quad (\text{A.2})$$

Depending on the context, we omit or not the tilde on the Fourier transform.

- Definition of v_d

$$\int_q f(q^2) = 2v_d \int_0^\infty dx x^{d/2-1} f(x) \quad \text{with} \quad v_d = \frac{1}{2^{d+1}\pi^{d/2}\Gamma(\frac{d}{2})}. \quad (\text{A.3})$$

- Functional derivatives

$$\frac{\delta}{\delta\tilde{\phi}_q} = \int_x \frac{\delta\phi(x)}{\delta\tilde{\phi}(q)} \frac{\delta}{\delta\phi(x)} = \int_x \frac{e^{iqx}}{(2\pi)^d} \frac{\delta}{\delta\phi_x}. \quad (\text{A.4})$$

- Correlation functions

$\Gamma[M]$ is a functional of $M(x)$. We define the 1PI correlation functions by

$$\Gamma^{(n)}[M(x), x_1, \dots, x_n] = \frac{\delta^n \Gamma[M]}{\delta M_{x_1} \dots \delta M_{x_n}} \quad (\text{A.5})$$

We also define the Fourier transform of $\Gamma^{(n)}$ by

$$\tilde{\Gamma}^{(n)}[M(x), q_1, \dots, q_n] = \int_{x_1 \dots x_n} e^{-i(q_1 x_1 + \dots + q_n x_n)} \Gamma^{(n)}[M(x), x_1, \dots, x_n] \quad (\text{A.6})$$

and

$$\bar{\Gamma}^{(n)}[M(x), q_1, \dots, q_n] = \frac{\delta^n \Gamma}{\delta \tilde{M}_{q_1} \dots \delta \tilde{M}_{q_n}}. \quad (\text{A.7})$$

The relation between $\tilde{\Gamma}^{(n)}$ and $\bar{\Gamma}^{(n)}$ follows from Eq. (A.4) :

$$\tilde{\Gamma}^{(n)}[M(x), q_1, \dots, q_n] = (2\pi)^{-nd} \bar{\Gamma}^{(n)}[M(x), q_1, \dots, q_n]. \quad (\text{A.8})$$

- Cut-off function in x and q spaces

$$\Delta H_k[\phi] = -\frac{1}{2} \int_q \tilde{\phi}_q \tilde{\phi}_{-q} \tilde{R}_k(q^2) = -\frac{1}{2} \int_x \phi(x) R_k(x-y) \phi(y). \quad (\text{A.9})$$

One should be careful about the fact that R_k is sometimes considered as a function of q and sometimes as a function of q^2 . It can be convenient to define a cut-off function with two entries by

$$\mathcal{R}_k(x, y) = R_k(x-y). \quad (\text{A.10})$$

Then

$$\tilde{\mathcal{R}}_k(q, q') = (2\pi)^d \delta^d(q + q') \tilde{R}_k(q) \quad (\text{A.11})$$

- k -dependent anomalous dimension

By definition:

$$k \partial_k Z_k = -\eta_k Z_k . \quad (\text{A.12})$$

- Threshold functions l_n^d

$$l_n^d(w, \eta) = \frac{n + \delta_{n,0}}{2} \int_0^\infty dy y^{d/2-1} \frac{s(y)}{(y(1+r(y)) + w)^{n+1}} \quad (\text{A.13})$$

where

$$R_k(q^2) = Z_k q^2 r(y) \quad \text{with} \quad y = \frac{q^2}{k^2} \quad (\text{A.14})$$

and, by definition of $s(y)$

$$\begin{aligned} k \partial_k R_k(q^2) &= k \partial_k \left(Z_k q^2 r\left(\frac{q^2}{k^2}\right) \right) \\ &= Z_k k^2 (-\eta_k y r(y) - 2y^2 r'(y)) = Z_k k^2 s(y) . \end{aligned} \quad (\text{A.15})$$

- Threshold functions m_{n_1, n_2}^d

$$m_{n_1, n_2}^d(w) = -\frac{1}{2} Z_k^{-1} k^{d-6} \int_0^\infty dx x^{d/2} \tilde{\partial}_t \frac{(\partial_x P)^2(x, 0)}{P^{n_1}(x, 0) P^{n_2}(x, w)} \quad (\text{A.16})$$

with

$$P(x, w) = Z_k x + R_k(x) + w. \quad (\text{A.17})$$

- Universal value of $l_n^{2n}(0, 0)$ for $n > 0$

For $n > 0$ and independently of the choice of cut-off function R_k :

$$l_n^{2n}(0, 0) = \frac{n}{2} \int_0^\infty dy (-2) \frac{r'(y)}{(1+r(y))^{n+1}} = 1 . \quad (\text{A.18})$$

- Derivative of l_n^d

$$\partial_w l_n^d(w, \eta) = -(n + \delta_{n,0}) l_{n+1}^d(w, \eta) . \quad (\text{A.19})$$

- θ -cut-off

A convenient cut-off function R_k that allows to compute analytically some threshold functions is

$$R_k(q) = Z_k (k^2 - q^2) \theta\left(1 - \frac{q^2}{k^2}\right) . \quad (\text{A.20})$$

With this cut-off we find

$$r(y) = \frac{1-y}{y} \theta(1-y) . \quad (\text{A.21})$$

- Threshold functions l_n^d with the θ -cut-off

With the cut-off function, Eq. (A.20), the l_n^d threshold functions can be computed analytically

$$l_n^d(w, \eta) = \frac{2}{d}(n + \delta_{n,0}) \left(1 - \frac{\eta_k}{d+2}\right) \frac{1}{(1+w)^{n+1}}. \quad (\text{A.22})$$

- Threshold functions $m_{2,2}^d$ with the θ -cut-off

$$m_{2,2}^d(w) = \frac{1}{(1+w)^2}. \quad (\text{A.23})$$

Appendix B. The Exact RG equations

For the sake of simplicity, we consider a scalar theory (e.g. Ising). We have by definition

$$Z_k[B] = \int \mathcal{D}\phi(x) \exp \left(-H[\phi] - \frac{1}{2} \int_q R_k(q) \phi_q \phi_{-q} + \int B\phi \right), \quad (\text{B.24})$$

$$W_k[B] = \log Z_k[B], \quad (\text{B.25})$$

$$\Gamma_k[M] + W_k[B] = \int_x BM - \frac{1}{2} \int_{x,y} M(x) R_k(x-y) M(y) \quad (\text{B.26})$$

with, by definition of $M(x)$:

$$\frac{\delta W_k}{\delta B(x)} = M(x) = \langle \phi(x) \rangle. \quad (\text{B.27})$$

When $B(x)$ is taken k -independent (as in $Z_k[B]$) then $M(x)$ computed from W_k is k -dependent. Reciprocally, if $M(x)$ is taken fixed (as in $\Gamma_k[M]$), then $B(x)$ computed from Eq. (B.31) becomes k -dependent.

Appendix B.1. RG equation for $W_k[B]$

$$\begin{aligned} \partial_k e^{W_k[B]} &= -\frac{1}{2} \int \mathcal{D}\phi \left(\int_{x,y} \phi_x R_k(x-y) \phi_y \right) \\ &\quad \exp \left(-H[\phi] - \frac{1}{2} \int_q R_k(q) \phi_q \phi_{-q} + \int B\phi \right) = \end{aligned}$$

$$\begin{aligned}
&= \left(-\frac{1}{2} \int_{x,y} \partial_k R_k(x-y) \frac{\delta}{\delta B_x} \frac{\delta}{\delta B_y} \right) e^{W_k[B]} \\
&= -\frac{1}{2} \int_{x,y} \partial_k R_k(x-y) \left(\frac{\delta^2 W_k}{\delta B_x \delta B_y} + \frac{\delta W_k}{\delta B_x} \frac{\delta W_k}{\delta B_y} \right) e^{W_k[B]}. \quad (\text{B.28})
\end{aligned}$$

We therefore obtain for W_k :

$$\partial_k W_k[B] = -\frac{1}{2} \int_{x,y} \partial_k R_k(x-y) \left(\frac{\delta^2 W_k}{\delta B_x \delta B_y} + \frac{\delta W_k}{\delta B_x} \frac{\delta W_k}{\delta B_y} \right) \quad (\text{B.29})$$

which is the Polchinski equation.

Appendix B.2. RG equation for $\Gamma_k[M]$

We first derive the reciprocal relation of Eq. (B.27). The Legendre transform is symmetric with respect to the two functions that are transformed. Here the Legendre transform of W_k is $\Gamma_k + 1/2 \int R_k M M$. Thus

$$\frac{\delta}{\delta M_x} \left(\Gamma_k + \frac{1}{2} \int_{x,y} M_x R_k(x-y) M_y \right) = B_x \quad (\text{B.30})$$

and then

$$\frac{\delta \Gamma_k}{\delta M_x} = B_x - \int_y R_k(x-y) M_y. \quad (\text{B.31})$$

In the Polchinski equation (B.29), the k -derivative is taken at fixed B_x . We must convert it to a derivative at fixed M :

$$\partial_k|_B = \partial_k|_M + \int_x \partial_k M_x|_B \frac{\delta}{\delta M_x}. \quad (\text{B.32})$$

Acting on Eq. (B.26) with $\partial_k|_B$, we obtain:

$$\begin{aligned}
\partial_k \Gamma_k[M]|_B + \partial_k W_k[B]|_B &= \int_x B \partial_k M|_B - \frac{1}{2} \int_{x,y} \partial_k R_k(x-y) M_x M_y \\
&\quad - \int_{x,y} R_k(x-y) M_x \partial_k M_y|_B. \quad (\text{B.33})
\end{aligned}$$

Substituting Eqs. (B.31), (B.29), (B.32) into this equation we finally obtain

$$\partial_k \Gamma_k[M] = \frac{1}{2} \int_{x,y} \partial_k R_k(x-y) \frac{\delta^2 W_k}{\delta B_x \delta B_y}. \quad (\text{B.34})$$

The last step consists in rewriting the right hand side of this equation in terms of Γ_k only. We start from (B.27) and act on it with $\delta/\delta M_z$:

$$\delta(x-z) = \frac{\delta^2 W_k}{\delta B_x \delta M_z} = \int_y \frac{\delta^2 W_k}{\delta B_x \delta B_y} \frac{\delta B_y}{\delta M_z}. \quad (\text{B.35})$$

Now, using (B.31), we obtain

$$\delta(x - z) = \int_y \frac{\delta^2 W_k}{\delta B_x \delta B_y} \left(\frac{\delta^2 \Gamma_k}{\delta M_y \delta M_z} + R_k(y - z) \right). \quad (\text{B.36})$$

We define

$$W_k^{(2)}(x, y) = \frac{\delta^2 W_k}{\delta B_x \delta B_y} \quad (\text{B.37})$$

and thus

$$\delta(x - z) = \int_y W_k^{(2)}(x, y) \left(\Gamma_k^{(2)} + \mathcal{R}_k \right)(y, z). \quad (\text{B.38})$$

$\Gamma_k^{(2)} + \mathcal{R}_k$ is therefore the inverse of $W_k^{(2)}$ in the operator sense. Note that this relation is valid for arbitrary M . The RG equation (B.34) can now be written in terms of Γ_k only:

$$\partial_k \Gamma_k[M] = \frac{1}{2} \int_{x,y} \partial_k R_k(x - y) \left(\Gamma_k^{(2)} + \mathcal{R}_k \right)^{-1}(x, y). \quad (\text{B.39})$$

In Fourier space this equation becomes:

$$\partial_k \Gamma_k[M] = \frac{1}{2} \int_q \partial_k \tilde{R}_k(q) \left(\tilde{\Gamma}_k^{(2)} + \tilde{\mathcal{R}}_k \right)_{q,-q}^{-1}. \quad (\text{B.40})$$

Appendix B.3. RG equation for the effective potential

The derivative expansion consists in expanding Γ_k as

$$\Gamma_k[M(x)] = \int_x \left(U_k(M^2(x)) + \frac{1}{2} Z_k(M^2(x)) (\nabla M)^2 + \dots \right) \quad (\text{B.41})$$

where we have supposed that the theory is \mathbb{Z}_2 symmetric so that U_k, Z_k, \dots are functions of M^2 only. To compute the flow of these functions it is necessary to define them from Γ_k . The effective potential U_k coincides with Γ_k when it is evaluated for uniform field configurations $M_{\text{unif.}}$:

$$\Gamma_k[M_{\text{unif.}}] = \Omega U_k(M_{\text{unif.}}^2) \quad (\text{B.42})$$

where Ω is the volume of the system. It is easy to derive an RG equation from this definition of U_k if we use the local potential approximation (LPA) that consists in truncating Γ_k as in (B.41) with $Z_k(M) = 1$:

$$\Gamma_k^{\text{LPA}}[M(x)] = \int_x \left(U_k(M^2(x)) + \frac{1}{2} (\nabla M)^2 \right). \quad (\text{B.43})$$

By acting on Eq. (B.42) with ∂_k we obtain:

$$\partial_k U_k(M) = \frac{1}{2\Omega} \int_q \partial_k R_k(q) \left(\Gamma_k^{(2)}|_{M_{\text{unif.}}} + R_k \right)^{-1}_{q,-q} . \quad (\text{B.44})$$

Thus, we have to invert $\Gamma_k^{(2)} + R_k$ for a uniform field configuration and within the LPA. From now on, we omit the superscript LPA on Γ_k . An elementary calculation leads to

$$\bar{\Gamma}_{k,q,q'}|_{M_{\text{unif.}}} = \left(\frac{\partial^2 U_k}{\partial M^2} + q^2 \right) (2\pi)^{-d} \delta(q+q') . \quad (\text{B.45})$$

Using $\delta(q=0) = \Omega(2\pi)^{-d}$ we find

$$\partial_k U_k = \frac{1}{2} \int_q \frac{\partial_k R_k(q)}{q^2 + R_k(q) + \frac{\partial^2 U_k}{\partial M^2}} . \quad (\text{B.46})$$

It is convenient to re-express this equation in terms of

$$\rho = \frac{1}{2} M^2 \quad (\text{B.47})$$

which is the \mathbb{Z}_2 -invariant.

$$\partial_k U_k(\rho) = \frac{1}{2} \int_q \frac{\partial_k R_k(q)}{q^2 + R_k(q) + U'_k(\rho) + 2\rho U''_k(\rho)} \quad (\text{B.48})$$

where $U'_k(\rho)$ and $U''_k(\rho)$ are derivatives of U_k with respect to ρ .

To obtain the RG equation for the dimensionless potential we have to perform the change of variables of Eq.160. We find

$$\partial_{t|_\rho} = \partial_{t|_{\tilde{\rho}}} + (2-d-\eta)\tilde{\rho} \frac{\partial}{\partial \tilde{\rho}} \quad (\text{B.49})$$

and

$$\partial_{t|_{q^2}} = \partial_{t|_y} - 2y\partial_y . \quad (\text{B.50})$$

Inserting these relations together with Eq.(160) and with

$$\partial_t R_k(q^2) = -y(\eta_k r(y) + y r'(y)) Z_k k^2 \quad (\text{B.51})$$

in Eq.(B.48) leads to the RG equation on \tilde{U}_t , Eq.(161).

References

1. M. Le Bellac, *Quantum and Statistical Field Theory* (Clarendon Press, Oxford, 1991).
2. J. J. Binney, N. J. Dowrick, A. J. Fisher, and M.E.J. Newman, *The Theory of Critical Phenomena: an Introduction to the Renormalization Group* (Oxford University Press, Oxford, 1992).
3. N. Goldenfeld, *Lectures on Phase Transitions and the Renormalization Group* (Addison-Wesley, Reading, 1992).
4. J. Zinn-Justin, *Quantum Field Theory and Critical Phenomena* (Oxford University Press, New York, 1989).
5. L. P. Kadanoff, Physics **2**, 263 (1966).
6. F. J. Wegner and A. Houghton, Phys. Rev. A **8**, 401 (1973).
7. K. G. Wilson and J. Kogut, Phys. Rep. **12C**, 75 (1974).
8. J. Polchinski, Nucl. Phys. B **231**, 269 (1984).
9. D. V. Shirkov and V. F. Kovalev, Phys. Rep. **352**, 219 (2001).
10. B. Delamotte, Am. J. Phys. **72**, 170 (2004).
11. C.M. Fortuin and P.W Kasteleyn, Physica, **57**, 536 (1972).
12. R.H. Swendsen and J.S. Wang, Phys. Rev. Lett. **58**, 86 (1987).
13. G. R. Golner and E. K. Riedel, Phys. Rev. Lett. **34**, 856 (1975).
14. A. Hasenfratz and P. Hasenfratz, Nucl. Phys. B [FS] **270**, 687 (1986).
15. J. F. Nicoll, T. S. Chang, and H. E. Stanley, Phys. Rev. Lett. **33**, 540 (1974); erratum: *ibid.* **33** 1525 (1974).
16. J. F. Nicoll, T. S. Chang, and H. E. Stanley, Phys. Lett. **57A**, 7 (1976).
17. J. F. Nicoll and T. S. Chang, Phys. Lett. **62A**, 287 (1977).
18. A. Ringwald and C. Wetterich, Nucl. Phys. **334**, 506 (1990).
19. C. Wetterich, Nucl. Phys. B **352** 529 (1991).
20. N. Tetradis and C. Wetterich, Nucl. Phys. B **383**, 197 (1992).
21. C. Wetterich, Phys. Lett. B **301**, 90 (1993).
22. U. Ellwanger, Z. Phys. C **58**, 619 (1993).
23. U. Ellwanger, Z. Phys. C **62**, 503 (1993).
24. N. Tetradis and C. Wetterich, Nucl. Phys. B [FS] **422**, 541 (1994).
25. U. Ellwanger, Phys. Lett. B **335**, 364 (1994).
26. T. R. Morris, Int. J. Mod. Phys. A **9**, 2411 (1994).
27. T. R. Morris, Phys. Lett. B **329**, 241 (1994).
28. J. Berges, N. Tetradis, and C. Wetterich, Phys. Rep., **363**, 223 (2002).
29. K. E. Newman and E. K. Riedel, Phys. Rev. B **30**, 6615 (1984).
30. K. E. Newman, E. K. Riedel, and S. Muto, Phys. Rev. B **29**, 302 (1984).
31. C. Bervillier, Phys. Lett. A **331**, 110 (2004).
32. H. Kunz and G. Zumbach, J. Phys. A **26**, 3121 (1993).
33. G. Zumbach, Phys. Rev. Lett. **71**, 2421 (1993).
34. G. Zumbach, Nucl. Phys. B **413**, 754 (1994).
35. G. Zumbach, Phys. Lett. A **190**, 225 (1994).
36. S. Liao, J. Polonyi, and M. Strickland, Nucl. Phys. B **567**, 493 (2000).
37. D. Litim, J. High Energy Phys. **0111**, 059 (2001).
38. D. F. Litim, Nucl. Phys. B **631**, 128 (2002).

39. L. Canet, B. Delamotte, D. Mouhanna, and J. Vidal, Phys. Rev. D **67**, 065004 (2003).
40. L. Canet, B. Delamotte, D. Mouhanna, and J. Vidal, Phys. Rev. B **68**, 064421 (2003).
41. M. Tissier, B. Delamotte, and D. Mouhanna, Phys. Rev. Lett. **84**, 5208 (2000).
42. B. Delamotte, D. Mouhanna, and M. Tissier, Phys. Rev. B **69**, 134413 (2004).
43. C. Bagnuls and C. Bervillier, Phys. Rev. B **41**, 402 (1990).
44. C. Bagnuls and C. Bervillier, Phys. Rep. **348**, 91 (2001).
45. C. Bervillier, J. Phys.: Condens. Matter **17**, S1929 (2005).
46. C. Bagnuls and C. Bervillier, Int. J. Mod. Phys. A **16**, 1825 (2001).
47. J.-P. Blaizot, R. Mendez-Galain, and N. Wschebor, *preprint hep-th/0512317* (2005).
48. J.-P. Blaizot, R. Mendez-Galain, and N. Wschebor, Phys. Lett. B **632**, 571 (2006).
49. J.-P. Blaizot, R. Mendez-Galain, and N. Wschebor, *preprint hep-th/0603163* (2006).
50. D. Litim, Int. J. Mod. Phys. A **16**, 2081 (2001).
51. T. R. Morris, Phys. Lett. B **345**, 139 (1995).
52. G. v. Gersdorff and C. Wetterich, Phys. Rev. B **64**, 054513 (2001).
53. H. Ballhausen, J. Berges, and C. Wetterich, Phys. Lett. B, **582**, 144 (2004).

CHAPTER 2

INTRODUCTION TO CRITICAL DYNAMICS

Reinhard Folk

*Institute for Theoretical Physics, University of Linz,
Altenbergerstrasse 69, A-4040 Linz, Austria
E-mail: reinhard.folk@jku.at*

An introduction to the field of critical dynamics is given and recent progress made is presented. Comparison of experiments in fluids, ferromagnets and superfluid helium with field theoretical calculations is performed.

Contents

1	Introduction	80
2	Experimental Evidence	81
2.1	Fluids	81
2.2	Light Scattering	84
2.3	Ferromagnets	85
2.4	Superfluid ^4He	85
3	Van Hove Theory	87
4	Dynamical Scaling	90
4.1	Scaling Form of the Dynamic Susceptibility	90
4.2	Finding the Dynamical Exponent z by Scaling Relations	92
5	From Dynamic Equations to a Lagrangian	94
5.1	Static Functional	95
5.2	Dynamic Equations	98
5.3	Dynamic Functional	101
5.4	Renormalization	105
6	Renormalization and the Dynamical Exponent	107
6.1	Structure and Renormalization	107
6.2	Calculating the Dynamical Exponent	108
7	Comparison with Experiment	113
7.1	General Procedure	113
7.2	Fluids: The Linewidth in Light Scattering	114
7.3	Ferromagnets: The Shape Function	117
7.4	Superfluid Transition: The Thermal Conductivity	118

References	120
----------------------	-----

1. Introduction

Critical phenomena are an everyday life experience, mostly we are confronted with first-order phase transitions, like the liquid-solid transition. However under certain circumstances we may observe second-order phase transitions. An example is the gas-liquid critical point in a fluid terminating the first order gas-liquid phase transition line. Near this special point we observe a spectacular behaviour of physical quantities, most prominent examples are the divergence of the specific heat and critical opalescence. We also say the system undergoes a continuous phase transition.

The experimental study of second-order phase transition behaviour started in the middle of the 19th century.¹ Theoretical explanations developed: van der Waals theory for fluids, mean field theory for magnets and the more general Landau-Ginzburg theory. Already in 1896 Verschafelt² recognized differences between the predictions of mean field theory and experiments in fluids. Later on Onsager solved the two-dimensional Ising model proving the mean field theory to be inadequate to calculate e.g. critical exponents.

Finally, critical behaviour could be explained by renormalization group (RG) theory formulated 1971 by Wilson,³ which proved already developed concepts like scaling⁴ and universality for the exponents and amplitude ratios in the power laws for the temperature dependence of physical quantities near a second-order transition. Moreover the concept of scaling naturally arises due to the divergence of the correlation length and the invariance of the relevant model parameters with respect to RG transformations. The RG theory connects a specific critical behaviour to the existence of a fixed point, and to the critical dimension of such a fixed point. The RG transformation leads to a 'flow' of the model parameters to this fixed point.

More complicated and more realistic situations could be explained by the existence of additional fixed points and a crossover from unstable fixed points to a stable fixed point.⁵ The knowledge in this field - static critical behaviour - is collected already in several textbooks and I mention just a couple of them⁶ (restricted to those containing field theoretic methods).

Dynamical critical behaviour was less well understood but the phenomenon of critical slowing down was recognized (the characteristic relaxational time τ_c for dynamical phenomena diverges when one approaches the critical point), and Van Hove theory⁷ could give an explanation although it assumes

that transport coefficients and/or kinetic coefficients remain non-critical. However the important point was that within dynamics a separation of time scales was recognized to be important. Slow variables were recognized to be important for the description of dynamical critical behaviour, but it was not understood how the diverging correlations of the static fluctuations affect the transport coefficients. In the sixties scaling ideas were applied to dynamical phenomena too, and parallel to mode-coupling theory, dynamical scaling theory⁸ evolved into the formulation of dynamical renormalization group theory by De Dominicis, Brezin and Zinn-Justin^{9,10} and by Bausch, Janssen, and Wagner.¹¹ The development up to 1977 is summarized in the review of Halperin and Hohenberg.¹²

Although dynamical phenomena are more complicated than static ones, all the concepts known in statics can also be found in dynamics. These are: (i) universality (power laws with universal exponents and universal amplitude ratios in the asymptotics), (ii) scaling properties (in the asymptotics), (iii) crossover phenomena. In defining certain dynamical universality classes an important role however is played by the conservation properties of the order parameter (OP), and the static and dynamical coupling of the OP to other slow conserved densities. Thus models described by the same static functional and belonging to the same static universality class may be in different dynamical universality classes. For example the dynamical critical behaviour of a Heisenberg magnet differs if it is described by a simple diffusive model or a model containing Larmor precession terms. Although there is no textbook directly devoted solely to dynamical critical theory, larger sections on dynamics can be found in several textbooks.¹³ One may also find useful and short summaries in contributions to encyclopedias.¹⁴

2. Experimental Evidence

In this section, I collect some experimental examples of dynamical critical behaviour that are the subject also of *quantitative* theoretical calculations within dynamical renormalization group theory. It is a personal selection and mainly reflects research in which I collaborated with others. The experimental results are in most cases the most recent ones presenting the state of the art.

2.1. Fluids

In fluids two transport coefficients are of primary interest: the shear viscosity and the thermal conductivity. They are directly connected to the model

describing the dynamical critical behaviour. However there are other transport coefficients which show critical behaviour but they are not included when defining the dynamic universality class. An example is the sound mode, where the sound velocity and the sound absorption show critical behaviour. Although the sound mode couples to the OP of the gas-liquid

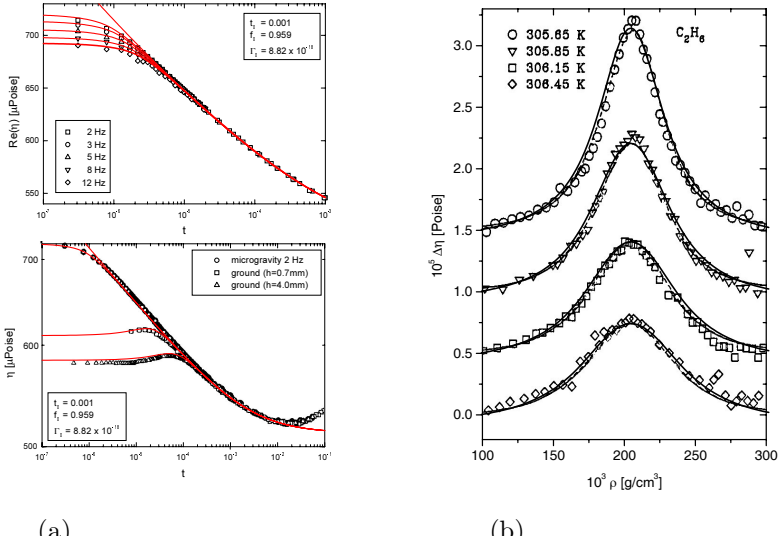


Fig. 1. (a) Temperature dependence ($t = (T - T_c)/T_c$) of the shear viscosity of Xenon with and without gravity for different frequencies.^{15,16} In the case of the microgravity experiment different frequencies, in the earth-bound experiment different cell heights are shown. Taken from Ref. [18]. (b) Density dependence of the shear viscosity of C_2H_6 for different temperatures.¹⁷ The curves were shifted for better clearness. Taken from Ref. [19].

transition this coupling is not relevant for the genuine critical behaviour of the thermal conductivity and the shear viscosity. This holds for both the asymptotic critical behaviour as well as for the non-asymptotic behaviour further away from the critical point.

Let us first look at experimental results for the shear viscosity of Xenon (see Fig. 1). The temperature dependence has been measured on earth¹⁵ and in space (reduced gravity).¹⁶ On earth the shear viscosity reaches a finite value at the phase transition temperature. This is due to the earth's gravity which couples to the density. In the specific measurements of the shear viscosity with oscillating discs within cells of a certain height, gravity produces a density distribution around the critical density ρ_c in the middle

of the cell. Thus one has to take into account that the disks measure a value of the shear viscosity densities larger or smaller than the critical density. This makes the shear viscosity at T_c finite (and the finite value depends on the height of the cell).

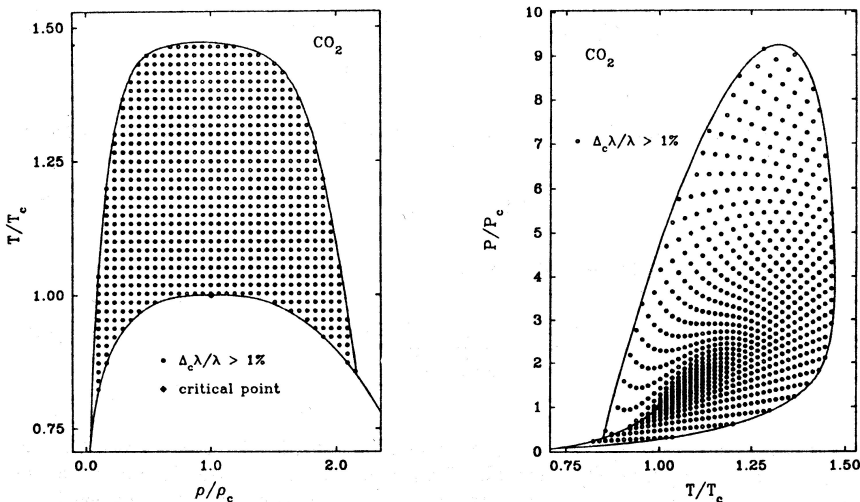


Fig. 2. Region for CO_2 of more than 1% enhancement to the thermal conductivity due to fluctuations in the temperature-density plane and the pressure-temperature plane. Taken from Ref. [20].

Fig. 1(b) shows the shear viscosity of methane as a function of density around the critical density for different temperatures.¹⁷ A peak is seen at the critical density but a possible divergence of the shear viscosity with a power law at T_c may only be observed by reducing the gravitational effects, e.g. by going to space. Experimental results in microgravity are shown in the upper figure of Fig. 1(a). The lower Fig. 1(b) shows the microgravity data at the lowest frequency together with those on earth in cells with different heights. Although the evolution of a power law is recognized, finally near T_c again a finite value is reached. This is due to the small but finite frequency at which the experiment is performed. Again the experiment is not *at* criticality which is defined by $T = T_c$ and $\rho = \rho_c$ (or equivalent $\xi(T_c, \rho_c) = \infty$) but also the modulus k of the wave vector and the frequency ω involved in the experimental setup have to be zero.

The thermal conductivity is also strongly enhanced when approaching

the critical point and a power law divergence can be observed. The region where fluctuations, which lead to the divergence, contribute is shown in Fig. 2.

2.2. Light Scattering

Another method to investigate dynamical critical phenomena are light scattering experiments. In statics (measurements at frequency $\omega = 0$) one observes critical opalescence. In dynamics from the width at half height of the frequency dependent scattering intensity at different wave vector modulus k and a certain temperature distance from T_c (or correlation length ξ) one deduces the critical dispersion $\omega(k, \xi)$. If $k\xi < 1$ one is in the hydrody-

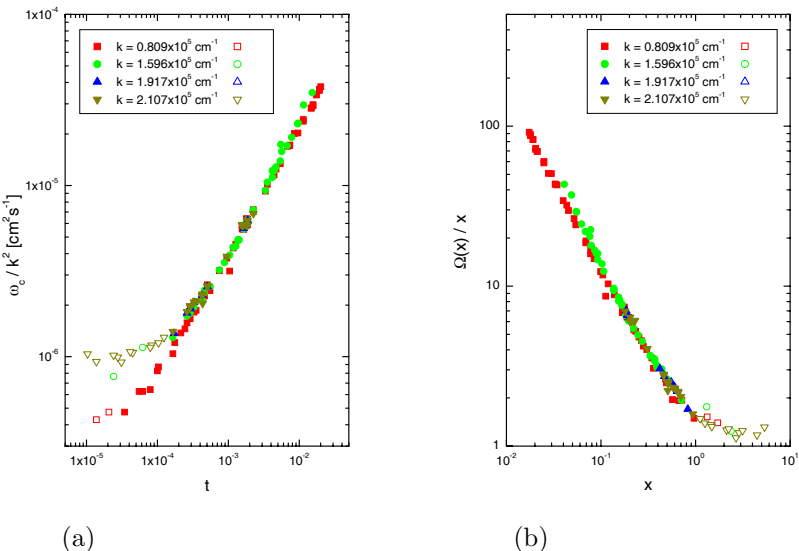


Fig. 3. (a) Linewidth data of light scattering intensity in Xenon,²¹ (b) the same in scaling variables (see Eq. (20) in section 4)

namic region and one may get the temperature dependence of transport coefficients e.g. of the diffusion coefficient $D(\xi)$ from the dispersion

$$\omega(k, \xi) = D(\xi)k^2. \quad (1)$$

Examples are the thermal diffusion coefficient in a pure liquid or the mass diffusion coefficient in a mixture. At T_c the critical dispersion is for very small wave vector modulus k given by a power law

$$\omega(k, \xi^{-1} = 0) \sim k^z, \quad (2)$$

with the dynamic critical exponent z which has been found to be a little bit larger than three. At a finite distance from criticality one may test scaling by introducing scaling variables, which contain powers e.g. of the correlation length $\xi = \xi_0 t^{-\nu}$. For correct exponents the data collapse to one curve. This is demonstrated again for Xenon near its gas-liquid critical point in Fig. 3. The data as a function of relative temperature distance from T_c ($t = (T - T_c)/T_c$) at different wave vector modulus k can be scaled on one curve connecting the asymptotic hydrodynamic region at small values of $x = k\xi$ to the asymptotic critical region at large values of x . The dispersion has been scaled as

$$\Omega(k\xi) = \frac{\omega(k, \xi)\xi^{z-2}}{k^2\Gamma^{as}}. \quad (3)$$

Indeed for $x \gg 1$ according to Eq. (2) one has $\Omega(x) \rightarrow x^{z-2}$ which goes roughly^a as x , whereas for $x \ll 1$ according to Eq. (1) one has $\Omega(x) \sim \text{constant}$ since $D(\xi)$ goes roughly as ξ^{-1} . The collapse of the data is only reached if the dynamic exponent z is chosen properly.

2.3. Ferromagnets

Neutron scattering is the main technique to study magnetic critical phenomena. However this is a little bit more complicated than what we have discussed so far since the dynamical susceptibility taken from theory has to be folded with a resolution function characteristic for the experimental setup.

In this way one may look at the shape and the width of the scattering function (intensity) in an experimental setup where either the wave vector is kept constant during the measurement or the energy transfer. Let us consider the shape of the scattering function at T_c . In Fig. 4 the intensity is compared with a Lorentzian and a non-Lorentzian shape function. It is clearly demonstrated that the shape is non-Lorentzian and this is attributed to dynamical fluctuation effects. At T_c the width at half height as a function of the wave vector (see Eq. (2)) shows a power law with an exponent of roughly $z = 2.5$.

2.4. Superfluid ${}^4\text{He}$

The superfluid transition is an exceptional example of a second-order phase transition since the symmetry breaking is exact (another system is the

^aRoughly means neglecting $x_\eta \sim 0.065$, then $z = 3$.

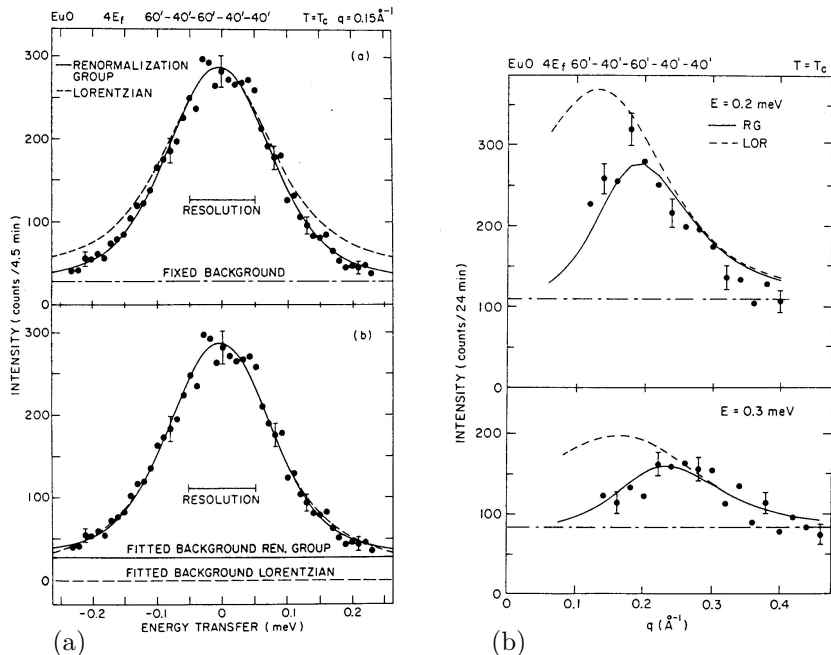


Fig. 4. (a) Constant wave vector scans in EuO. (b) Constant energy scans in EuO. Both demonstrate deviations from a Lorentzian shape function (dashed curve). Taken from Ref. [22].

antiferromagnet). No physical field exists that is conjugate to the order parameter. It is also exceptional with respect to the existence of a whole line of phase transitions as a function of pressure. This makes it an ideal system for testing universality.

The thermal transport properties are of main interest. This transport is diffusive above T_λ and propagating (second sound) below T_λ . We show the thermal conductivity λ for different pressures as a function of temperature. A power law divergence seems to be observable, but looking closer at the data by extracting the universal amplitude^b $R_\lambda^{\exp 25}$

$$R_\lambda^{\exp} = \frac{\lambda}{g_0 \sqrt{\xi C_p}} \quad (4)$$

involving the specific heat C_p , the correlation length ξ and a constant g_0 , it

^bThere are other dynamic amplitude ratios defined for the superfluid transition and for other physical systems; an overview can be found in Ref. [24].

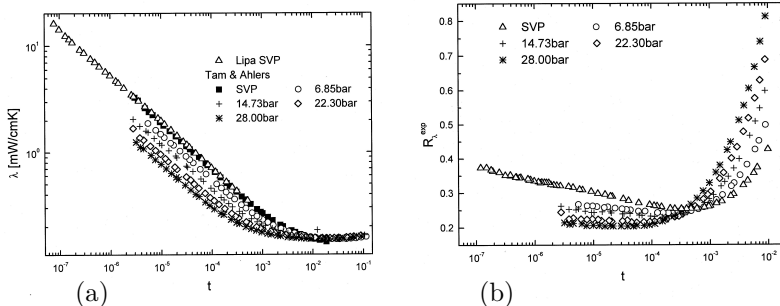


Fig. 5. (a) Temperature dependence of the thermal conductivity of ${}^4\text{He}$ for different pressures near the superfluid transition.^{23,26} (b) The same for the amplitude ratio, which should be universal and was expected to be temperature and pressure independent.

turns out that R_λ^{exp} remains temperature and pressure dependent even in the range of relative temperature distances as 10^{-6} and 10^{-7} . There it was expected that the amplitude has already reached its universal asymptotic value (see Fig. 5). Even for the superfluid transition it is necessary to go to reduced gravity in order to get reliable data in this region nearest to T_λ . In statics one reaches fantastic values of $t = 10^{-10}$ for specific heat measurements in microgravity.²⁶

3. Van Hove Theory

Let us consider a model described by the simplest dynamical equation, which might be suitable for a one-component order parameter (OP) ψ_k . One may have in mind the magnetization then the equation of motion describes simply the relaxation or diffusion mode present in this system

$$\frac{\partial \psi_k(t)}{\partial t} = -\Gamma k^a(r + k^2)\psi_k(t) + \zeta_k(t), \quad (5)$$

where Γ is the kinetic coefficient and $a = 0$ or $a = 2$ has to be taken for a non-conserved or a conserved OP respectively (the equation without the stochastic force is known as time-dependent Ginzburg-Landau equation in the theory of superconductivity). The OP is a slow variable, all other variables are assumed to be fast and represented in the dynamical equation by Gaussian distributed fluctuating forces. In order to reach in equilibrium the correct statics the Einstein relation

$$\langle \zeta_k(t)\zeta_{k'}(t') \rangle = 2\Gamma k^a \delta_{k-k'} \delta(t-t') \quad (6)$$

has to be fulfilled by the stochastic forces. From equation (5) the dynamic susceptibility

$$\langle \psi(\vec{x}, t)\psi(\vec{x}', t') \rangle_\zeta = \chi_{dyn}(\vec{x} - \vec{x}', t - t') \quad (7)$$

and its Fourier transform

$$\chi_{dyn}(\vec{k}, \omega) = \langle \psi(\vec{k}, \omega)\psi(-\vec{k}, -\omega) \rangle_\zeta \quad (8)$$

are easily calculated by performing the averaging over the stochastic force. The solution of the equation of motion reads

$$\psi_{k,\omega} = \frac{\zeta_{k,\omega}}{-i\omega + \Gamma k^a(r + k^2)} \quad (9)$$

and using Eq. (6) leads to the **dynamic susceptibility**

$$\chi_{dyn}(k, \omega) = \frac{2\Gamma k^a}{\omega^2 + \{\Gamma k^a(r + k^2)\}^2}. \quad (10)$$

Integration over ω gives the **static susceptibility**

$$\chi_{st}(k, \xi) = \frac{1}{r + k^2}, \quad r = \xi^{-2}. \quad (11)$$

A **characteristic frequency** may be defined by the **half width at half height**

$$\omega_c(k, \xi) = \Gamma k^a(\xi^{-2} + k^2), \quad (12)$$

and with these definitions the result for the dynamic susceptibility can be cast into the **scaling form**

$$\chi_{dyn}(k, \omega, \xi) = \frac{\chi_{st}(k, \xi)}{\omega_c(k, \xi)} F\left(\frac{\omega}{\omega_c(k, \xi)}, k\xi\right) \quad (13)$$

defining the **shape function** $F(y, x)$ with $x = k\xi$ and $y = \omega/\omega_c(k, \xi)$.

The characteristic frequency may also be written in scaling form

$$\omega_c(k, \xi) = Ak^z\Omega(x) \quad (14)$$

defining the **dynamical critical exponent**

$$z = 2 + a \quad (15)$$

and the scaling function

$$\Omega(x) = \left(\frac{1}{x^2} + 1 \right). \quad (16)$$

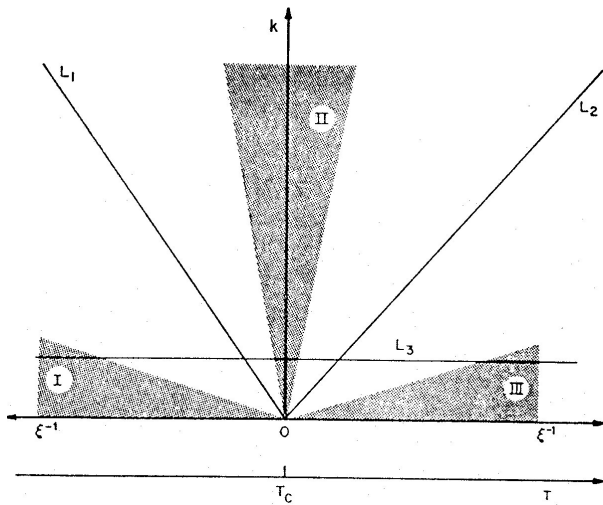


Fig. 6. I: hydrodynamic region below T_c , II: critical region below and above T_c and III: hydrodynamic region above T_c .

This function has in the critical region and in the hydrodynamic region where

$$\omega_c = \begin{cases} Ak^z & k\xi \gg 1 \\ Ak^{z-2}\xi^{-2} & k\xi \ll 1 \end{cases} \quad (17)$$

the limiting behaviour

$$\lim_{x \rightarrow \infty} \Omega(x) = 1 \quad \text{and} \quad \lim_{x \rightarrow 0} \Omega(x) \sim x^{-2}. \quad (18)$$

The shape function is given by a Lorentzian independent from x

$$F(y, x) = \frac{2}{y^2 + 1} \quad y = \frac{\omega}{\omega_c}. \quad (19)$$

That means the shape is the same in the critical and in the hydrodynamic region.

Although the Van Hove model⁷ captures some features observed in experiments qualitatively (e.g. behaviour of the characteristic frequency) it fails quantitatively. One also sees from the calculation that the behaviour of the characteristic frequency is just a consequence of the critical behaviour of the static susceptibility. No genuine 'dynamical' critical contribution is present. Especially the **critical slowing down** characterizing the approach to equilibrium by the typical relaxation time $\tau(k, \xi) \sim \omega^{-1}(k, \xi) \sim \xi^z$ (at

$k = 0$ for $a = 0$) is only induced by the appearance of the static susceptibility in the characteristic frequency. It reflects the fact that due to the divergence of the correlation length the region of deviation from equilibrium by a fluctuation becomes larger and larger approaching the critical point, correspondingly it takes longer and longer to relax to equilibrium. One task of dynamical critical theory is to calculate the critical behaviour of the kinetic coefficient Γ . Depending on the structure of the dynamical model to be used (see below) the dynamical critical exponent might be *increased* (in models without mode coupling terms, Γ goes to zero at criticality) or *decreased* (in models with mode coupling terms, Γ diverges at criticality). In any case a slowing down of the order parameter dynamics remains.

4. Dynamical Scaling

We now generalize the scaling laws found in Van Hove theory by assuming that scaling holds but with different values for the exponents and different form of the scaling functions.⁸ In this way already an analysis of experiments can be performed and exponents and scaling functions can be extracted. This however relies on the assumption that the system has reached with all its variables already the asymptotic region ($\xi \rightarrow \infty$, $k \rightarrow 0$, $\omega \rightarrow 0$). As an example already shown in Fig. 3 the linewidth of Xenon as a function of temperature for different wave vectors was considered. Introducing the scaling variables

$$\xi = \xi_0 t^{-\nu}, \quad x_\eta \sim 0.04, \quad x = k\xi, \quad \frac{\omega_c \xi^{1+x_\eta}}{k^2 \Gamma_{as}} = \Omega(x), \quad (20)$$

the data at different wave vectors k of Fig. 3(a) collapse almost on one curve - the scaling function - shown in Fig. 3(b). However a warning should be expressed at this place because non-asymptotic effects may be less visible in such a scaling plot. From the scaling according to Van Hove theory instead of the exponent $1 - x_\eta = z - 2$ (compare Eq. (3)), $z = 3 - x_\eta$ one would have expected $z_{Van\;Hove} = 4$ meaning an exponent of 2 for $z - 2$.

4.1. Scaling Form of the Dynamic Susceptibility

The scaling form of the dynamic susceptibility χ_{dyn} of the OP reads

$$\chi_{dyn}(\xi, k, \omega) = \frac{\chi_{st}(\xi, k)}{\omega_c(\xi, k)} F \left(\frac{\omega}{\omega_c(\xi, k)}, k\xi \right). \quad (21)$$

As well as the characteristic frequency ω_c (width at half height, Eq. (14)) the static correlation function χ_{st}

$$\chi_{st}(\xi, k) = k^{-2+\eta} g(k\xi) \quad (22)$$

can be written in scaling form. This leads to the dynamic shape function $F(y, x)$ which fulfills

$$\int dy F(y, x) = 2\pi \quad \text{and} \quad F(1, x) = \frac{1}{2} F(0, x) \quad (23)$$

since ω_c is the half width at half height.

As a consequence of the validity of scaling one obtains a **crossover in the shape** changing from the hydrodynamic to the critical region. In the hydrodynamic region $k\xi \ll 1$, the characteristic frequency is given by the hydrodynamic mode (we think of a conserved OP as for the case of a ferromagnet) $\omega_c = Dk^2$ and the static susceptibility reads $\chi \sim \xi^{\gamma/\nu}$. In consequence we find the temperature dependence of the diffusion coefficient

$$D(\xi) = \Gamma(\xi)/\chi_{st}(\xi, 0) \sim \xi^{2-z} \quad \text{and} \quad \Gamma(\xi) \sim \xi^{2-z+\frac{\gamma}{\nu}} \quad (24)$$

for the OP Onsager coefficient Γ . Note that in Van Hove theory one immediately obtains $z = 4 - \eta$ since $\gamma/\nu = 2 - \eta$ in order to have a non-critical transport coefficient (in mean field theory $\eta = 0$ and one recovers $z = 4$). The shape function calculated within hydrodynamics has a Lorentzian shape

$$F(y, x \ll 1) = \frac{1}{y^2 + 1}. \quad (25)$$

In the critical region, $k\xi \gg 1$ and at $T = T_c$, the characteristic frequency and the static susceptibility are given by $\omega_c \sim k^z$ and $\chi \sim k^{-2+\eta}$ respectively and the dynamic susceptibility scales as

$$\chi_{dyn}(k, \omega) \sim k^{-z-2+\eta} F(y, \infty). \quad (26)$$

We now make use of the conservation property of the OP which demands for $k \rightarrow 0$ and $\omega \rightarrow 0$ that $\chi_{dyn} \sim k^2$. This leads to the following y dependence for small and large arguments

$$\begin{aligned} F(y, \infty) &\sim \text{const.} & \text{for} & \quad y \rightarrow 0, \\ F(y, \infty) &\sim y^{-\frac{z+4-\eta}{z}} & \text{for} & \quad y \rightarrow \infty. \end{aligned}$$

Thus if $z \neq 4$ and $\eta \neq 0$ one recognizes that the decay of the shape function for large scaling argument is non-Lorentzian. Taking the value $z \sim 2.5$ valid for the ferromagnet this decay would be

$$F \sim y^{-2.6} \quad \text{instead of} \quad F \sim y^{-2}. \quad (27)$$

4.2. Finding the Dynamical Exponent z by Scaling Relations

4.2.1. Ferromagnet

Let us consider a ferromagnet below T_c . Due to the breaking of the continuous symmetry (in OP-space) by the non-zero OP a symmetry restoring propagating mode (Goldstone mode) is present - the spin wave mode. Its dispersion (undamped) in the hydrodynamic region is given by ($d = 3$)

$$\omega_c^- = v k^2, \quad v \sim \frac{\rho_{stiff}}{M} \sim \xi^{-1+\beta/\nu}. \quad (28)$$

The 'spin wave velocity' v is a static quantity and can be expressed²⁷ by the transverse correlation length ξ , via the so called stiffness constant^c ρ_{stiff} and the magnetization M (M is the OP). On the other hand it defines a characteristic frequency fulfilling dynamical scaling (note that we are below the phase transition temperature and the scaling functions are different above and below as is already known from statics. This is indicated by the superscript '−')

$$\omega_c^- \sim k^z \Omega^-(k\xi) \sim \xi^{2-z} k^2. \quad (29)$$

Comparing with the dispersion

$$2 - z = -1 + \beta/\nu \quad \rightarrow \quad z = 3 - \beta/\nu = (5 - \eta)/2 \quad (30)$$

leads to the value of the dynamical exponent. Use has been made of static scaling laws $2\beta + \gamma = 2 - \alpha = 3\nu$ at $d = 3$ and $\gamma/\nu = 2 - \eta$ leading to $\beta/\nu + 1 - \eta/2 = 3/2$.

Since z is now known, we can make predictions on the temperature dependence of the spin diffusion constant in the hydrodynamic region above T_c

$$\omega_c^+ = D k^2 \sim k^z \Omega^+(k\xi), \quad D \sim \xi^{2-z} \sim \xi^{(-1+\eta)/2} \quad (31)$$

in agreement with the experiment mentioned above.

^cA term in the free energy below T_c containing the stiffness constant is due to the invariance of the energy with respect to uniform rotations of the OP. It is a consequence of the spontaneous symmetry breaking in systems with a *continuous* symmetry and connected to the transverse (transverse to the OP) correlations (see e.g. Goldenfeld, chapter 11.1.3 in Ref. [13]). A similar expression appears at the superfluid phase in ⁴He, see below.

4.2.2. Fluids

In the liquid the thermal transport below and above T_c is diffusive and nothing can be gained at the moment.

4.2.3. Superfluid Transition

Similar to the ferromagnet also in superfluid ^4He below T_λ one has a propagating mode - the second sound mode, which is the corresponding Goldstone mode. Its dispersion (undamped) in the hydrodynamic region ($d = 3$) reads

$$\omega_c^- = v k, \quad v \sim \left(\frac{\rho_{stiff}}{C_p} \right)^{1/2} \sim \xi^{-1/2+\alpha/2\nu}. \quad (32)$$

The second sound velocity v is a static quantity and is expressed by $\rho_{stiff} \sim \rho_s$ with ρ_s the superfluid density, $\rho_s \sim \xi^{-1}$, and the specific heat $c_p \sim \xi^{\alpha/\nu}$ (if it is diverging, i.e. $\alpha > 0$). Comparing with the dynamical scaling law

$$\omega_c^- \sim k^z \Omega^-(k\xi) \sim \xi^{1-z} k \quad (33)$$

one finds again the critical dynamical exponent

$$1 - z = -1/2 + \alpha/2\nu \quad \rightarrow \quad z = 3/2 - \alpha/2\nu. \quad (34)$$

This derivation assumed $\alpha > 0$, however experimentally it turned out to be smaller than zero. Then one has to set^d α to zero and one gets $z = 3/2$.

We now know the dynamical critical exponent z and therefore we can make predictions on the temperature dependence of the thermal diffusion constant in the hydrodynamic region above T_c

$$\omega_c^+ = D k^2 \sim k^z \Omega(k\xi), \quad D \sim \xi^{2-z} \sim \xi^{1/2}. \quad (35)$$

Table 1 lists different physical systems with their names according to Hohenberg and Halperin and defining the dynamic universality class. It also summarizes some concrete physical examples and the theoretical dynamical critical exponents for the different universality classes. One observes that in some cases the dynamical critical exponent could be expressed by static ones (model B,C,E,F,G,J), in other cases (model A,H) this is not the case.

^dWhen $\alpha < 0$ the static coupling of the order parameter to entropy density goes to zero at the fixed point. This changes the second relation in (32).

Table 1. Different dynamic models with their name and the reference where the model was set up, some examples for which the models apply, the respective Goldstone mode and the dynamical critical exponent.

model	name	system	Goldstone mode	dyn. exp.
relaxation	A ²⁸	FeF ₂	-	$2 + c\eta \sim 2$
diffusion	B ²⁹		-	$4 - \eta \sim 4$
relaxation	C ²⁹		-	$2 + \alpha/\nu$ ($n = 1$)
relaxation	C ²⁹		-	$2 + c\eta$ ($n \geq 2$)
symm. planar m.	E ²⁵	XY Magnet	spin wave	3/2
asymm. planar m.	F ²⁵	⁴ He	2nd sound	3/2
antiferromagnet	G ²⁹	RbMgF ₃	spin wave	3/2
fluid	H ²⁵	Xenon	-	$3 + x_\eta \sim 3$
ferromagnet	J ³⁰	Fe	spin wave	$1/2(5 - \eta) \sim 5/2$

5. From Dynamic Equations to a Lagrangian

The steps to set up a model for the critical dynamics follow a systematic procedure. The time scale is set by the OP and the fact that one observes critical slowing down. Therefore one has to consider besides the OP (conserved or not) the slow densities in the system, which are the densities of the conserved quantities. Thus the set of densities to be considered is enlarged in comparison to statics. In a first step one has to reconsider the static functional including the additional densities.

In the second step one has to find out the equations of motion for these slow variables. The fast variables are included as stochastic forces in the equations of motion for the slow variables. The fast variables are also related to damping effects. The form of the equations of motion is known in general and fulfills the following conditions: (i) the system reaches - due to irreversible terms in the dynamic equations - the statics described by the static functional (derived in the first step), (ii) in the hydrodynamic limit the system reproduces the known hydrodynamic equations leading to the reversible terms given by Poisson brackets. In order to fulfill (i) the Gaussian distributed stochastic forces have to obey Einstein relations. The Poisson brackets may be derived using certain symmetry groups inherent in the given problem.³¹ These symmetry group properties leading to the Poisson brackets are equivalent to the symmetries considered to derive Ward identities. They play an important role to find out the renormalization of the dynamic mode coupling and lead to the dynamic scaling relations expressing the dynamical exponent z already found by connecting the characteristic frequency above and below T_c in systems with a propagating mode in the condensed phase.

In the following the different steps are shown for the case of a pure fluid already contained in the appendices of Ref. [32]. The sound mode is included although this is not necessary in defining the dynamical universality class - model H - for the critical point in a fluid.

5.1. Static Functional

Let us briefly sketch the derivation of a static functional for pure liquids. The starting point is a local equilibrium distribution function

$$w_{loc} = \frac{1}{\mathcal{N}} e^{-\int_V d^d x \frac{\Omega(x)}{k_B T(x)}} \quad (36)$$

with the normalization factor \mathcal{N} and temperature $T(x)$. $\Omega(x)$ is the corresponding local thermodynamic potential

$$\Omega(x) = e(x) + e_k(x) - T(x)s(x) - \mu(x)\rho(x) - \mathbf{v}(x)\mathbf{j}'(x), \quad (37)$$

in which $e(x)$ is the internal energy density, $e_k(x) = \mathbf{j}'(x)^2/2\rho(x)$ is the kinetic energy density, $\mathbf{j}'(x)$ the momentum density and $s(x)$ the entropy density. The chemical potential $\mu(x)$ and velocity $\mathbf{v}(x)$ are external fields. Assuming that the densities are fluctuating about their thermodynamic average values, one can write

$$\begin{aligned} e(x) &= e + \Delta e(x), & e_k(x) &= e_k + \Delta e_k(x), \\ s(x) &= s + \Delta s(x), & \rho(x) &= \rho + \Delta \rho(x), \\ \mathbf{j}'(x) &= \mathbf{j}' + \Delta \mathbf{j}'(x). \end{aligned} \quad (38)$$

Additionally we allow small variations of the conjugate external fields

$$\begin{aligned} T(x) &= T + \delta T(x), & \mu(x) &= \mu + \delta \mu(x), \\ \mathbf{v}(x) &= \mathbf{v} + \delta \mathbf{v}(x). \end{aligned} \quad (39)$$

Inserting (38) and (39) in (37) the local thermodynamic potential can be split into three parts

$$\frac{\Omega(x)}{k_B T} = \frac{\Omega^{(0)}}{k_B T} + \mathcal{H}(x) - \delta \mathcal{H}(x). \quad (40)$$

The first part represents the thermodynamic average and contains the Gibbs free energy $\Omega^{(0)} = e + e_k - Ts - \mu\rho - \mathbf{v}\mathbf{j}'$. The second part involves the fluctuation contributions of the densities and is given by

$$\mathcal{H}(x) = \frac{1}{k_B T} (\Delta e(x) + \Delta e_k(x) - T \Delta s(x) - \mu \Delta \rho(x) - \mathbf{v} \Delta \mathbf{j}'(x)). \quad (41)$$

The third part consists of the first order contributions due to the external field variation

$$\begin{aligned}\delta\mathcal{H}(x) = & \frac{e(x) + e_k(x) - \mu\rho(x) - \mathbf{v}\mathbf{j}'(x)}{k_B T} \frac{\delta T(x)}{T} \\ & + \frac{\rho(x)\delta\mu(x)}{k_B T} + \frac{\mathbf{j}'(x)\delta\mathbf{v}(x)}{k_B T}.\end{aligned}\quad (42)$$

Inserting (40) into the local distribution function (36) and expanding in first order of the external field variations, we get analogous to Ref. [33] for the correlation functions:

$$\langle s \ s \rangle_c = k_B T \left(\frac{\partial s}{\partial T} \right)_\mu, \quad \langle \rho \ \rho \rangle_c = k_B T \left(\frac{\partial \rho}{\partial \mu} \right)_T, \quad (43)$$

$$\langle s \ \rho \rangle_c = k_B T \left(\frac{\partial \rho}{\partial T} \right)_\mu = k_B T \left(\frac{\partial s}{\partial \mu} \right)_T. \quad (44)$$

From (43) and (44) one can see that the thermodynamic derivatives involve the chemical potential μ . Experimentally the pressure P is accessible and therefore for a comparison with experimentally measured quantities the local thermodynamic potential (40) has to be expressed in densities, which correspond to external fields T and P instead of T and μ . This can be obtained by changing from entropy density per volume $s(x)$ to entropy density per mass $\sigma(x) = s(x)/\rho(x)$. The corresponding fluctuations then transform

$$\Delta s(x) = \rho \Delta \sigma(x) + \sigma \Delta \rho(x). \quad (45)$$

The correlation functions (43) and (44) change to

$$\langle \sigma \ \sigma \rangle_c = \frac{k_B T}{\rho} \left(\frac{\partial \sigma}{\partial T} \right)_P, \quad \langle \rho \ \rho \rangle_c = \rho k_B T \left(\frac{\partial \rho}{\partial P} \right)_T, \quad (46)$$

$$\langle \sigma \ \rho \rangle_c = \frac{k_B T}{\rho} \left(\frac{\partial \rho}{\partial T} \right)_P = \rho k_B T \left(\frac{\partial \sigma}{\partial P} \right)_T. \quad (47)$$

Expanding the Hamiltonian (41) in powers of the fluctuations of the entropy per mass, the mass density and the momentum density we obtain (this expanded \mathcal{H} is now named H ; it appears in the dynamic equations in the

next section)

$$H = \int d^d x \left\{ \frac{1}{2} a_{\sigma\sigma} (\Delta\sigma(x))^2 + \frac{1}{2} c_{\sigma\sigma} (\nabla \Delta\sigma(x))^2 + \frac{1}{2} a_{\rho\rho} (\Delta\rho(x))^2 \right. \\ \left. + a_{\sigma\rho} \Delta\sigma(x) \Delta\rho(x) + + \frac{1}{2} a'_j (\Delta\mathbf{j}'(x))^2 \right. \\ \left. + \frac{1}{3!} v_\sigma (\Delta\sigma(x))^3 + \frac{1}{4!} u_\sigma (\Delta\sigma(x))^4 + \frac{1}{2} \gamma_\rho \Delta\rho(x) (\Delta\sigma(x))^2 \right\}. \quad (48)$$

The coefficients of the different terms in H are defined by the corresponding (thermodynamic) expansion coefficients. For dynamic calculations it is convenient^e to choose the entropy density fluctuations as OP. With regard to this we have expanded in (48) the entropy density fluctuations up to fourth order, while the mass density and momentum density fluctuations, considered as secondary densities, only need to be expanded up to quadratic order. This takes into account all terms in the Hamiltonian that are relevant for the critical theory. The Gaussian part of (48) is non-diagonal and contains terms which are not invariant against order parameter inversion. These terms proportional to $\Delta\rho\Delta\sigma$ and $(\Delta\sigma)^3$ can be removed by introducing a shifted order parameter $\phi_0(x)$ and a transformed secondary density $q_0(x)$ like

$$\phi_0(x) = \sqrt{N_A} (\Delta\sigma(x) - \langle \Delta\sigma(x) \rangle), \quad (49)$$

$$q_0(x) = \sqrt{N_A} \left[\Delta\rho(x) - \left(\frac{\partial\rho}{\partial\sigma} \right)_P (\Delta\sigma(x) - \langle \Delta\sigma(x) \rangle) \right]. \quad (50)$$

N_A has been introduced for convenience to obtain the appearance of the gas constant R instead of the Boltzmann constant k_B in the equations and parameter definitions. Introducing a rescaled momentum density $\mathbf{j} = \mathbf{j}_l + \mathbf{j}_t = \sqrt{N_A} \Delta\mathbf{j}'$, one ends up with the final expression for the static functional^f

$$H = \int d^d x \left\{ \frac{1}{2} \overset{o}{\tau} \phi_0^2(x) + \frac{1}{2} (\nabla \phi_0(x))^2 + \frac{\overset{o}{\tilde{u}}}{4!} \phi_0^4(x) + \frac{1}{2} a_q q_0^2(x) \right. \\ \left. + \frac{1}{2} \overset{o}{\gamma}_q q_0(x) \phi_0^2(x) + \frac{1}{2} a_j \mathbf{j}_t^2(x) + \frac{1}{2} a_j \mathbf{j}_l^2(x) - \overset{o}{h}_q q_0(x) \right\}, \quad (51)$$

The coefficients are related to those of (48).

^eThe light scattering structure factor contains the Rayleigh peak centred at frequency zero, whose width is related to thermal diffusion and the Brillouin peaks centred at finite frequencies given by the sound mode. The diffusive mode dominates the spectrum near T_c (C_v/C_p goes to zero).

^f Regarding the notation we name the unrenormalized quantities by \circ and/or the subscript 0. Later on we introduce the renormalized counterparts.

5.2. Dynamic Equations

Due to the critical slowing down the dynamics of critical phenomena is explicitly influenced mainly by slow processes. The influence of variables which vary on short time scales may be considered stochastically. Thus only projections of the dynamic variables into a subspace of slowly varying variables need to be considered.^{34,35} Let $\psi_i(x, t)$ be a set of slow variables, then the corresponding dynamic equations can be written as^{36–39}

$$\frac{\delta\psi_i(x, t)}{\delta t} = V_i\{\psi(x, t)\} - \sum_j \Lambda_{ij}(x) \frac{\delta H\{\psi(x, t)\}}{\delta\psi_j(x, t)} + \Theta_i(x, t). \quad (52)$$

$\Theta_i(x, t)$ are fluctuating forces which fulfill the Einstein relations^g

$$\langle \Theta_i(x, t) \Theta_j(x', t') \rangle = 2\Lambda_{ij}(x)\delta(t - t')\delta(x - x') \quad (53)$$

when Markovian processes are assumed. $\Lambda_{ij}(x)$ are the kinetic coefficients, which are constants $\Lambda_{ij}(x) = \Lambda_{ij}$ in the case of non conserved densities $\psi(x, t)$ and are given by $\Lambda_{ij}(x) = -\Lambda_{ij}\nabla^2$ in the case of conserved densities. The reversible contributions $V_i\{\psi(x, t)\}$ of the dynamic equations can be written as^h

$$V_i\{\psi(x, t)\} = \sum_j \int dx' dt' \left[\frac{\delta Q_{ij}(x, t; x', t')}{\delta\psi_j(x', t')} - Q_{ij}(x, t; x', t') \frac{\delta H\{\psi(x, t)\}}{\delta\psi_j(x', t')} \right]. \quad (54)$$

The quantities $Q_{ij}(x, t; x', t')$ are related to the Poisson brackets of the densities

$$Q_{ij}(x, t; x', t') = k_B T \{ \psi_i(x, t), \psi_j(x', t') \}. \quad (55)$$

For simple liquids the slowly varying densities $\psi_i(x)$ correspond to the volume densities $s(x)$, $\rho(x)$ and $\mathbf{j}'(x)$. Generalized Poisson brackets for hydrodynamic densities may be derived from infinitesimal displacements.³¹ The

^gThe Einstein relation together with the form of the relaxing or damping terms guarantees that the dynamical system reaches the proper equilibrium described by the static functional H .

^hThe presence of reversible terms leads to organized motion. One of the simplest examples to imagine is the harmonic oscillator without damping, where the time derivative of the elongation couples to the momentum and the time derivative of the momentum to the elongation. This leads to an oscillatory motion. Similarly in magnets the reversible coupling leads to the Larmor precession below T_c , in liquids to sound waves, in superfluid ^4He (below T_λ) to second sound.

resulting Poisson brackets are

$$\begin{aligned}\{\mathbf{j}'(x, t), s(x', t')\} &= s(x, t) \nabla \delta(x - x') \delta(t - t') , \\ \{\mathbf{j}'(x, t), \rho(x', t')\} &= \rho(x, t) \nabla \delta(x - x') \delta(t - t') , \\ \{j'_k(x, t), j'_l(x', t')\} &= [j'_l(x, t) \nabla_k \delta(x - x') - j'_k(x', t') \nabla_l \delta(x - x')] \delta(t - t') .\end{aligned}\quad (56)$$

All other Poisson brackets are zero. The reversible terms (54) of the dynamic equations turn with (56) to be (we omit the explicit indication of space and time dependence in the following)

$$V_s = -k_B T \nabla \left(s \frac{\delta H}{\delta \mathbf{j}'} \right) , \quad (57)$$

$$V_\rho = -k_B T \nabla \left(\rho \frac{\delta H}{\delta \mathbf{j}'} \right) , \quad (58)$$

$$V_j = -k_B T \left[s \nabla \frac{\delta H}{\delta s} + \rho \nabla \frac{\delta H}{\delta \rho} \right] - k_B T \sum_k \left[j'_k \nabla \frac{\delta H}{\delta j'_k} - \nabla_k \mathbf{j}' \frac{\delta H}{\delta j'_k} \right] . \quad (59)$$

The matrix Λ_{ij} is determined by the dissipation processes in hydrodynamics. For a liquid at rest ($\mathbf{v} = 0$) the hydrodynamic equation for the entropy density reads

$$T \frac{\partial s}{\partial t} = -\nabla \cdot \mathbf{q} , \quad \mathbf{q} = -\kappa_T^{(0)} \nabla T , \quad (60)$$

in which $\kappa_T^{(0)}$ is the thermal conductivity in the background. Expanding the functional H in (41) in powers of the fluctuations $\Delta s(x)$, $\Delta \rho(x)$ and $\Delta \mathbf{j}'(x)$, a comparison of the coefficients in quadratic order with thermodynamic relations shows that we can write $\nabla^2 T = k_B T \delta H / \delta s$. Thus the hydrodynamic equation (60) can be written as

$$\frac{\partial s}{\partial t} = k_B \kappa_T^{(0)} \nabla^2 \frac{\delta H}{\delta s} . \quad (61)$$

From the above equation it follows that in the dynamic equation (52) for the entropy density the only non-vanishing kinetic coefficient is $\Lambda_{ss} = -k_B \kappa_T^{(0)} \nabla^2$. With (57) we obtain

$$\frac{\partial s}{\partial t} = k_B \kappa_T^{(0)} \nabla^2 \frac{\delta H}{\delta s} - k_B T \nabla \left(s \frac{\delta H}{\delta \mathbf{j}'} \right) + \Theta_s \quad (62)$$

for the non-linear entropy density equation. Due to mass conservation no dissipative contributions appear in the dynamic equation for the mass density. With (58) we simply get

$$\frac{\partial \rho}{\partial t} = -k_B T \nabla \left(\rho \frac{\delta H}{\delta \mathbf{j}'} \right) . \quad (63)$$

The conservation of mass is an exact relation, therefore Eq.(63) contains no stochastic force. Linearizing the hydrodynamic equation for the momentum density in the velocity, the equation reads

$$\frac{\partial \mathbf{j}'}{\partial t} = (\zeta^{(0)} + \frac{\bar{\eta}^{(0)}}{3}) \nabla(\nabla \mathbf{v}) + \bar{\eta}^{(0)} \nabla^2 \mathbf{v}, \quad (64)$$

$\zeta^{(0)}$ and $\bar{\eta}^{(0)}$ are the bulk viscosity and the shear viscosity in the non-critical background. Eq.(64) may be separated in an equation for the longitudinal and transverse part of the momentum density according to $\mathbf{j}' = \mathbf{j}'_l + \mathbf{j}'_t$ with $\nabla \times \mathbf{j}'_l = 0$ and $\nabla \mathbf{j}'_t = 0$

$$\frac{\partial \mathbf{j}'_l}{\partial t} = (\zeta^{(0)} + \frac{4}{3} \bar{\eta}^{(0)}) \nabla^2 \mathbf{v}_l, \quad \frac{\partial \mathbf{j}'_t}{\partial t} = \bar{\eta}^{(0)} \nabla^2 \mathbf{v}_t. \quad (65)$$

From the kinetic energy in the static functional (41) it follows that the longitudinal and transverse velocity in (65) can be written as $\mathbf{v}_i = k_B T \delta H / \delta \mathbf{j}'_i$ ($i = l, t$). With the reversible term (59) we get for the non-linear dynamic equation

$$\begin{aligned} \frac{\partial \mathbf{j}'}{\partial t} &= k_B T (\zeta^{(0)} + \frac{4}{3} \bar{\eta}^{(0)}) \nabla^2 \frac{\delta H}{\delta \mathbf{j}'_l} + k_B T \bar{\eta}^{(0)} \nabla^2 \frac{\delta H}{\delta \mathbf{j}'_t} \\ &- k_B T \left[s \nabla \frac{\delta H}{\delta s} + \rho \nabla \frac{\delta H}{\delta \rho} \right] - k_B T \sum_k \left[j'_k \nabla \frac{\delta H}{\delta j'_k} - \nabla_k \mathbf{j}' \frac{\delta H}{\delta j'_k} \right] + \Theta_{j'}. \end{aligned} \quad (66)$$

Changing from entropy per volume to entropy per mass $\sigma(x) = s(x)/\rho(x)$, analogous to statics, Eq.(62) turns into

$$\frac{\partial \sigma}{\partial t} = \frac{k_B \kappa_T^{(0)}}{\rho^2} \nabla^2 \frac{\delta H}{\delta \sigma} - k_B T (\nabla \sigma) \frac{\delta H}{\delta \mathbf{j}'} + \Theta_\sigma. \quad (67)$$

From (66) we get the corresponding equation for the momentum density

$$\begin{aligned} \frac{\partial \mathbf{j}'}{\partial t} &= k_B T (\zeta^{(0)} + \frac{4}{3} \bar{\eta}^{(0)}) \nabla^2 \frac{\delta H}{\delta \mathbf{j}'_l} + k_B T \bar{\eta}^{(0)} \nabla^2 \frac{\delta H}{\delta \mathbf{j}'_t} \\ &- k_B T \left[\rho \nabla \frac{\delta H}{\delta \rho} - (\nabla \sigma) \frac{\delta H}{\delta \sigma} \right] - k_B T \sum_k \left[j'_k \nabla \frac{\delta H}{\delta j'_k} - \nabla_k \mathbf{j}' \frac{\delta H}{\delta j'_k} \right] + \Theta_{j'}. \end{aligned} \quad (68)$$

The equation for the mass density (63) remains unchanged. Eqs.(63), (67) and (68) constitute a set of non-linear equations which describe the dynamics of fluctuations in liquids. The equationsⁱ

$$\frac{\partial \phi_0}{\partial t} = \overset{o}{\Gamma} \nabla^2 \frac{\delta H}{\delta \phi_0} + \overset{o}{L}_\phi \nabla^2 \frac{\delta H}{\delta q_0} - \overset{o}{g} (\nabla \phi_0) \frac{\delta H}{\delta \mathbf{j}'} + \Theta_\phi, \quad (69)$$

ⁱSee footnote f.

$$\begin{aligned} \frac{\partial q_0}{\partial t} &= \overset{o}{L}_\phi \nabla^2 \frac{\delta H}{\delta \phi_0} + \overset{o}{\lambda} \nabla^2 \frac{\delta H}{\delta q_0} - \overset{o}{c} \nabla \frac{\delta H}{\delta \mathbf{j}_l} - \overset{o}{g} \nabla \left(q_0 \frac{\delta H}{\delta \mathbf{j}} \right) \\ &\quad - \overset{o}{g}_l \phi_0 \nabla \frac{\delta H}{\delta \mathbf{j}_l} + \Theta_q , \end{aligned} \quad (70)$$

$$\begin{aligned} \frac{\partial \mathbf{j}_l}{\partial t} &= \overset{o}{\lambda}_l \nabla^2 \frac{\delta H}{\delta \mathbf{j}_l} - \overset{o}{c} \nabla \frac{\delta H}{\delta q_0} - \overset{o}{g}_l \nabla \left(\phi_0 \frac{\delta H}{\delta q_0} \right) \\ &\quad + \overset{o}{g} (1 - T) \left\{ (\nabla \phi_0) \frac{\delta H}{\delta \phi_0} + q_0 \nabla \frac{\delta H}{\delta q_0} \right\} \\ &\quad - \overset{o}{g} (1 - T) \left\{ \sum_k \left[j_k \nabla \frac{\delta H}{\delta j_k} - \nabla_k \mathbf{j} \frac{\delta H}{\delta j_k} \right] \right\} + \Theta_l , \end{aligned} \quad (71)$$

$$\begin{aligned} \frac{\partial \mathbf{j}_t}{\partial t} &= \overset{o}{\lambda}_t \nabla^2 \frac{\delta H}{\delta \mathbf{j}_t} + \overset{o}{g} T \left\{ (\nabla \phi_0) \frac{\delta H}{\delta \phi_0} + q_0 \nabla \frac{\delta H}{\delta q_0} \right\} \\ &\quad - \overset{o}{g} T \left\{ \sum_k \left[j_k \nabla \frac{\delta H}{\delta j_k} - \nabla_k \mathbf{j} \frac{\delta H}{\delta j_k} \right] \right\} + \Theta_t \end{aligned} \quad (72)$$

are obtained by introducing the fields ϕ_0 and q_0 from (49) and (50) and by splitting the momentum density equation into a longitudinal and transverse part (this is done by the operator T which projects onto the transverse components).

5.3. Dynamic Functional

In order to calculate the dynamic correlation functions in a perturbation expansion we need a generating dynamic functional (see Ref. [11]). Considering the dynamic equations (67) to (68), we write the equations which contain stochastic forces in a short notation

$$\partial_t \vec{\alpha} = \vec{V} + \vec{\Theta} \quad \text{with} \quad \vec{\alpha} = \begin{pmatrix} \sigma \\ \mathbf{j}'_l \\ \mathbf{j}'_t \end{pmatrix} , \quad \vec{\Theta} = \begin{pmatrix} \Theta_\sigma \\ \Theta'_l \\ \Theta'_t \end{pmatrix} . \quad (73)$$

The vector \vec{V} contains the rest of Eqs.(67) and (68). The fluctuating forces $\vec{\Theta}$ fulfill Einstein relations (Gaussian distributed stochastic force) with correlation given by the coefficient matrix

$$\mathbf{L}' = \begin{pmatrix} -(k_B \kappa_T^{(0)} / \rho^2) \nabla^2 & 0 & 0 \\ 0 & -k_B T (\zeta^{(0)} + \frac{4}{3} \bar{\eta}^{(0)}) \nabla^2 & 0 \\ 0 & 0 & -k_B T \bar{\eta}^{(0)} \nabla^2 \end{pmatrix} . \quad (74)$$

Additionally we have the exact continuity equation (63) in the short form

$$\partial_t \rho = V_\rho \quad (75)$$

which may be considered as a constraint for the generating functional. The stochastic forces fluctuate in such a way that (75) always is fulfilled. Thus the generating functional (Onsager-Machlup functional) can be written as

$$Z_d = \int \mathcal{D}(\vec{\Theta}) \mathcal{D}(F) \delta(F) \exp \left[-\frac{1}{4} \int dt dx \vec{\Theta}^T \mathbf{L}'^{-1} \vec{\Theta} \right], \quad (76)$$

where $F = \partial_t \rho - V_\rho$ and the superscript T denotes the transposed vector. \mathcal{D} refers to a suitable integration measure. Inserting (73) and changing the integration variables leads to

$$\begin{aligned} Z_d &= \int \mathcal{D}(\vec{\alpha}, \rho) \delta(\partial_t \rho - V_\rho) \\ &\times \exp \left[-\frac{1}{4} \int dt \int dx \left([\partial_t \vec{\alpha} - \vec{V}]^T \mathbf{L}'^{-1} [\partial_t \vec{\alpha} - \vec{V}] + 2 \sum_i \frac{\delta V_i}{\delta \alpha_i} + 2 \frac{\delta V_\rho}{\delta \rho} \right) \right]. \end{aligned} \quad (77)$$

The delta function may be expressed by an exponential function

$$\delta(\partial_t \rho - V_\rho) = \int \mathcal{D}(i\tilde{\rho}) \exp \left[- \int dx \int dt \tilde{\rho} (\partial_t \rho - V_\rho) \right]. \quad (78)$$

Introducing auxiliary fields^j $i\vec{\alpha}$ and $i\tilde{\rho}$ in performing a Gaussian transformation (77) turns into

$$Z_d = \int \mathcal{D}(\vec{\alpha}, \rho, i\vec{\alpha}, i\tilde{\rho}) e^{-J} \quad (79)$$

with the Janssen-DeDominicis functional

$$\begin{aligned} J &= \int dt \int dx \left(-\vec{\alpha}^T \mathbf{L}' \vec{\alpha} + \vec{\alpha}^T (\partial_t \vec{\alpha} - \vec{V}) \right. \\ &\quad \left. + \tilde{\rho} (\partial_t \rho - V_\rho) + \frac{1}{2} \sum_i \frac{\delta V_i}{\delta \alpha_i} + \frac{1}{2} \frac{\delta V_\rho}{\delta \rho} \right). \end{aligned} \quad (80)$$

Introducing the order parameter (49) and the secondary density (50) in (80) the dynamic functional reads

$$J = \int dt \int dx \left(-\vec{\beta}^T \mathbf{L} \vec{\beta} + \vec{\beta}^T (\partial_t \vec{\beta} - \vec{V}) + \frac{1}{2} \sum_i \frac{\delta V_i}{\delta \beta_i} \right), \quad (81)$$

^jThey are introduced in order to lower the powers of the densities appearing in the exponent of the functional.

where the densities are $\vec{\beta}^T = (\phi_0, q_0, \mathbf{j}_l, \mathbf{j}_t)$ and \mathbf{L} is the coefficient matrix^k

$$[L_{ij}] = \begin{pmatrix} -\frac{o}{\Gamma} \nabla^2 & -\frac{o}{L_\phi} \nabla^2 & 0 & 0 \\ -\frac{o}{L_\phi} \nabla^2 & -\frac{o}{\lambda} \nabla^2 & 0 & 0 \\ 0 & 0 & -\frac{o}{\lambda_l} \nabla^2 & 0 \\ 0 & 0 & 0 & -\frac{o}{\lambda_t} \nabla^2 \end{pmatrix}. \quad (82)$$

The conjugate densities $\vec{\tilde{\beta}}$ are defined accordingly. An explicit expression for (81) is obtained by inserting the dynamic equations (69)-(72). The Fourier transformed Gaussian part can be written as

$$J^{(0)} = \frac{1}{2} \int_{k,\omega} (\vec{\beta}^T(k, \omega), \vec{\tilde{\beta}}^T(k, \omega)) \mathbf{\Gamma}^{(0)}(k, \omega) \begin{pmatrix} \vec{\beta}(-k, -\omega) \\ \vec{\tilde{\beta}}(-k, -\omega) \end{pmatrix}. \quad (83)$$

The integration is defined as $\int_{k,\omega} = \int \frac{d^d k}{(2\pi)^d} \int \frac{d\omega}{2\pi}$. The elements of the matrix $\mathbf{\Gamma}^{(0)}(k, \omega)$ are the dynamic vertex functions in lowest order perturbation theory. They are explicitly given by

$$\mathbf{\Gamma}^{(0)}(k, \omega) = \begin{pmatrix} \mathbf{0} & -i\omega \mathbf{1} + \mathbf{L}(k) \\ i\omega \mathbf{1} + \mathbf{L}^\dagger(k) & -2\lambda(k) \end{pmatrix}, \quad (84)$$

where $\mathbf{1}$ denotes the unit matrix and the superscript \dagger the adjoint matrix. In the present case the submatrices are

$$\mathbf{L}(k) = \begin{pmatrix} \frac{o}{\Gamma} k^2 (\frac{o}{\Gamma} + k^2) & \frac{o}{L_\phi} k^2 (\frac{o}{\Gamma} + k^2) & -ik \frac{o}{g_l} \frac{o}{h_q} & 0 \\ a_q \frac{o}{L_\phi} k^2 & a_q \frac{o}{\lambda} k^2 & ika_q \frac{o}{c} & 0 \\ 0 & ika_j \frac{o}{c} & a_j \frac{o}{\lambda_l} k^2 & 0 \\ 0 & 0 & 0 & a_j \frac{o}{\lambda_t} k^2 \end{pmatrix}, \quad (85)$$

$$\lambda(k) = \begin{pmatrix} \frac{o}{\Gamma} k^2 & \frac{o}{L_\phi} k^2 & 0 & 0 \\ \frac{o}{L_\phi} k^2 & \frac{o}{\lambda} k^2 & 0 & 0 \\ 0 & 0 & \frac{o}{\lambda_l} k^2 & 0 \\ 0 & 0 & 0 & \frac{o}{\lambda_t} k^2 \end{pmatrix}. \quad (86)$$

The interaction terms in the Hamiltonian (51) and the mode coupling terms in the dynamic equation modify the matrix (84) and may be calculated in a

^kNot all coefficients are independent: the coefficients $\frac{o}{L_\phi}$ and $\frac{o}{\lambda}$ are proportional to $\frac{o}{\Gamma}$ (see Ref. [32]).

perturbation expansion. The dynamic two-point vertex functions are given by

$$\Gamma(k, \omega) = \Gamma^{(0)}(k, \omega) - \Sigma(k, \omega), \quad (87)$$

where $\Sigma(k, \omega)$ contains 1-irreducible diagrams with two external legs. The matrix $\Gamma(k, \omega)$ of the vertex functions has the structure

$$\Gamma(k, \omega) = \begin{pmatrix} [0] & [\Gamma_{\alpha, \tilde{\beta}}](k, \omega) \\ [\Gamma_{\tilde{\alpha}, \beta}](k, \omega) & [\Gamma_{\tilde{\alpha}, \tilde{\beta}}](k, \omega) \end{pmatrix} \quad (88)$$

with the submatrix

$$[\Gamma_{\alpha, \tilde{\beta}}] = \begin{pmatrix} \overset{o}{\Gamma}_{\phi\tilde{\phi}} & \overset{o}{\Gamma}_{\phi\tilde{q}} & \overset{o}{\Gamma}_{\phi\tilde{l}} & 0 \\ \overset{o}{\Gamma}_{q\tilde{\phi}} & \overset{o}{\Gamma}_{q\tilde{q}} & \overset{o}{\Gamma}_{q\tilde{l}} & 0 \\ \overset{o}{\Gamma}_{l\tilde{\phi}} & \overset{o}{\Gamma}_{l\tilde{q}} & \overset{o}{\Gamma}_{q\tilde{l}} & 0 \\ 0 & 0 & 0 & \overset{o}{\Gamma}_{t\tilde{t}} \end{pmatrix}. \quad (89)$$

The submatrices $[\Gamma_{\tilde{\alpha}, \beta}]$ and $[\Gamma_{\tilde{\alpha}, \tilde{\beta}}]$ are defined accordingly. Then the propagators of the model are determined by the elements of the inverted matrix (84). In the limit $\overset{o}{c} \rightarrow \infty$ (which is in fact the time scale separation between primary densities - model defining - and secondary ones influenced by the critical behaviour of the primary densities) the propagators of order $(\overset{o}{c})^0$ are identical to the known model H propagators. One gets the response propagators

$$\langle \phi_0(k, \omega) \tilde{\phi}_0(-k, -\omega) \rangle_0 = \frac{1}{-i\omega + \overset{o}{\Gamma} k^2 (\overset{o}{\tau} + k^2)}, \quad (90)$$

$$\langle \mathbf{j}_t(k, \omega) \otimes \tilde{\mathbf{j}}_t(-k, -\omega) \rangle_0 = \frac{1}{-i\omega + a_j \overset{o}{\lambda}_t k^2} \mathbf{1}_t, \quad (91)$$

and the correlation propagators

$$\langle \phi_0(k, \omega) \phi_0(-k, -\omega) \rangle_0 = \frac{2 \overset{o}{\Gamma} k^2}{\left| -i\omega + \overset{o}{\Gamma} k^2 (\overset{o}{\tau} + k^2) \right|^2}, \quad (92)$$

$$\langle \mathbf{j}_t(k, \omega) \otimes \mathbf{j}_t(-k, -\omega) \rangle_0 = \frac{2 \overset{o}{\lambda}_t k^2}{\left| -i\omega + a_j \overset{o}{\lambda}_t k^2 \right|^2} \mathbf{1}_t. \quad (93)$$

There $\mathbf{1}_t$ contains the projection into the transverse subspace due to the presence of the projector \mathcal{T} in the equations of motion. In the extended model additional propagators of order $(\overset{o}{c})^{-1}$ arise, which contribute in the

limit $\overset{o}{c} \rightarrow \infty$ in diagrams with vertices of order $\overset{o}{c}$ to the vertex functions. They read

$$\langle \phi_0(k, \omega) \tilde{\mathbf{j}}_l(-k, -\omega) \rangle_0 = -\frac{\overset{o}{L}_\phi \mathbf{k}}{i \overset{o}{c} \left(-i\omega + \frac{\overset{o}{\Gamma}}{\overset{o}{\Gamma}} k^2 (\overset{o}{\tau} + k^2) \right)}, \quad (94)$$

$$\langle \mathbf{j}_l(k, \omega) \tilde{\phi}_0(-k, -\omega) \rangle_0 = -\frac{\overset{o}{L}_\phi (\overset{o}{\tau} + k^2) \mathbf{k}}{ia_j \overset{o}{c} \left(-i\omega + \frac{\overset{o}{\Gamma}}{\overset{o}{\Gamma}} k^2 (\overset{o}{\tau} + k^2) \right)}, \quad (95)$$

$$\langle q_0(k, \omega) \tilde{\phi}(-k, -\omega) \rangle_0 = -\frac{\overset{o}{g}_l \overset{o}{h}_q}{ia_q \overset{o}{c} \left(-i\omega + \frac{\overset{o}{\Gamma}}{\overset{o}{\Gamma}} k^2 (\overset{o}{\tau} + k^2) \right)}, \quad (96)$$

$$\langle q_0(k, \omega) \tilde{\mathbf{j}}_l(-k, -\omega) \rangle_0 = \frac{\mathbf{k}}{ia_q \overset{o}{c} k^2}, \quad (97)$$

$$\langle \mathbf{j}_l(k, \omega) \tilde{q}_0(-k, -\omega) \rangle_0 = \frac{\mathbf{k}}{ia_j \overset{o}{c} k^2}, \quad (98)$$

$$\langle \phi_0(k, \omega) q_0(-k, -\omega) \rangle_0 = \frac{2 \frac{\overset{o}{\Gamma}}{\overset{o}{\Gamma}} k^2 \overset{o}{g}_l \overset{o}{h}_q}{a_q \overset{o}{c} \left| -i\omega + \frac{\overset{o}{\Gamma}}{\overset{o}{\Gamma}} k^2 (\overset{o}{\tau} + k^2) \right|^2}, \quad (99)$$

$$\langle \phi_0(k, \omega) \mathbf{j}_l(-k, -\omega) \rangle_0 = -\frac{2 \overset{o}{L}_\phi \mathbf{k} \omega}{a_j \overset{o}{c} \left| -i\omega + \frac{\overset{o}{\Gamma}}{\overset{o}{\Gamma}} k^2 (\overset{o}{\tau} + k^2) \right|^2}. \quad (100)$$

The steps presented here follow quite closely the Lagrangian theory developed by Bausch, Janssen and Wagner 1976.¹¹ The Lagrangian obtained is the starting point for the field theoretic version of the dynamic renormalization group theory. As it has been described here it treats the model of a pure fluid including the sound mode. The primary critical modes are the thermal mode of heat diffusion and the shear mode. As already mentioned the dynamical equations for these modes alone define the universality class of model H. The sound mode is a secondary mode, which does not influence the critical properties of model H including non-asymptotic properties. However the coupling of the secondary mode to the primary densities leads to critical effects in the sound mode not considered here (for more details see Ref. [32]).

5.4. Renormalization

We are now in the position to perform the calculation of the relevant vertex functions. It turns out that these functions have singularities and within the

Table 2. References to the papers where the of field theoretic dynamical RG calculations are presented, i.e where the ζ -functions can be found.

model	references	calculation in
A	Antonov, Vasil'ev 1984, Ref. [40]	three loops
C	Folk, Moser 2002, Ref. [41]	two loops
E	Dohm 1978, Ref. [42]	two loops
F	Folk, Moser 2004, Ref. [43]	two loops
E'	Dohm, Folk 1983, Ref. [45]	two loops
F'	Folk, Moser 2004, Ref. [43]	two loops
G	de Dominicis, Peliti 1978, Ref. [46]	two loops
H	Adzhemyan et al. 1999, Ref. [47]	two loops
H'	Folk, Moser 1995, Ref. [48]	one loop
J	Dohm 1976, Ref. [49]	one loop

concept of RG theory these singularities are shifted into renormalization constants.¹¹ The renormalization of the kinetic coefficients and the static and dynamical couplings are of special interest. The kinetic coefficients allow to define a set of time scale ratios which are introduced in the set of dynamical parameters. E.g. for model H not considering the sound mode one has only the dynamical mode coupling as dynamical parameter¹ defined as

$$f = \frac{g}{\sqrt{\Gamma \lambda_t}}. \quad (101)$$

From the renormalization constants one finds the ζ -functions (defining the asymptotic values of exponents) and these lead to β -functions for the static and dynamic couplings and time ratios. The fixed point values of these parameters are found by the zeros of the β -functions. Let us write

$$\ell \frac{df}{d\ell} = \beta_f(\{f\}), \quad (102)$$

where we consider f now as one out of the set of all renormalizing model parameters. Usually for ℓ going to zero the flow comes to rest (then the left hand side and the right hand side of Eq. (102), the β -function is zero^m) and the parameters $\{f\}$ reach some values called fixed point values $\{f^*\}$. The

¹The time scale ratios $\hat{w}_{t,l} = \hat{\omega}_t / (a_j \hat{\lambda}_{t,l})$ are strongly irrelevant and have to be set to zero.⁴⁶

^mThere may (i) be several regions attracted to different fixed points. (ii) These regions might be zero, then the fixed point is called unstable. However an unstable fixed point may first attract the flow but finally repel it. This leads to the phenomenon of crossover between different types of critical behaviour.

region where this happens is called the asymptotic region. Inserting fixed point values into the ζ -functions leads to the universal values of the critical exponents. The physical expressions calculated from vertex functions are functions of the model parameters and choosing the fixed point values for them may lead to universal amplitude ratios.

One sees that there is more to calculate than the fixed points. It is already clear that one is also interested in the flow properties of the parameters described by the flow equations given by the β functions. Effective exponents and amplitude ratios can then be calculated and compared with experiments. An overview on the status of the field theoretic calculations is given in Table 2.

6. Renormalization and the Dynamical Exponent

An important point in the theoretical calculations is the structure of perturbation theory. It turns out that a reduction of graphical contributions is reached by introducing the T_c -shift and the correlation length (note that the correlation length does not renormalize) within the perturbational expansion. This is already known from statics.⁴⁴

6.1. Structure and Renormalization

More important for dynamics is to recognize that the dynamical OP vertex function can be quite generally split into different parts

$$\overset{o}{\Gamma}_{\phi\tilde{\phi}}(\xi, k, \omega) = -i\omega \overset{o}{\Omega}_{\phi\tilde{\phi}}(\xi, k, \omega) + \overset{o(st)}{\Gamma}_{\phi\phi}(\xi, k) \overset{o}{\Gamma}^a k^a \overset{o(d)}{\Gamma}_{\phi\tilde{\phi}}(\xi, k, \omega). \quad (103)$$

In this way (i) a separation of genuine dynamic and static parts and (ii) a separation of perturbational contributions with different couplings as prefactors take place. The perturbational loop-wise contributions to $\overset{o}{\Omega}_{\phi\tilde{\phi}+}$ have static couplings, the static fourth order coupling $\overset{o}{u}$ and the static couplings $\overset{o}{\gamma}$ of the OP to the conserved densities, as prefactors, if the OP is non-conserved

$$\overset{o}{\Omega}_{\phi\tilde{\phi}+}(\xi, \overset{o}{u}, \overset{o}{\gamma}, \overset{o}{g}) = 1 + \overset{o}{u}^2 \overset{o(A)}{\omega}_{\phi\tilde{\phi}+}(\xi, \overset{o}{u}) + \overset{o}{\gamma} \overset{o}{\omega}_{\phi\tilde{\phi}+}(\xi, \overset{o}{u}, \overset{o}{\gamma}, \overset{o}{g}). \quad (104)$$

The perturbational terms depend of course on the mode coupling $\overset{o}{g}$. If the OP is conserved there is no contribution to $\overset{o}{\Omega}_{\phi\tilde{\phi}+}$. The prefactors of $\overset{o(d)}{\Gamma}_{\phi\tilde{\phi}+}$ are given by the mode couplings

$$\overset{o(d)}{\Gamma}_{\phi\tilde{\phi}+}(\xi, \overset{o}{u}, \overset{o}{\gamma}, \overset{o}{g}) = 2 \left[\overset{o}{\Gamma} k^2 + \overset{o}{g} \overset{o}{G}_{\phi\tilde{\phi}+}(\xi, \overset{o}{u}, \overset{o}{\gamma}, \overset{o}{g}) \right]. \quad (105)$$

The renormalization follows the usual lines known from statics (see e.g. Ref. [6]) where the following Z -factors have to be introduced besides those for $\overset{o}{u}$, $\overset{o}{\gamma}$, and $\overset{o}{g}$

$$\overset{o}{\Gamma}_{\phi\tilde{\phi}} = Z_{\phi}^{-1/2} Z_{\tilde{\phi}}^{-1/2} \Gamma_{\phi\tilde{\phi}}, \quad \overset{o}{\Gamma}_{\phi\phi}^{(st)} = Z_{\phi}^{-1} \Gamma_{\phi\phi}^{(st)}, \quad \overset{o}{\Gamma} = Z_{\Gamma} \Gamma, \quad (106)$$

and

$$\overset{o}{\Omega}_{\phi\tilde{\phi}} = Z_{\Omega_{\phi\tilde{\phi}}} \Omega_{\phi\tilde{\phi}}, \quad \overset{o}{\Gamma}_{\phi\tilde{\phi}}^{(d)} = Z_{\Gamma_{\phi\tilde{\phi}}}^{(d)} \Gamma_{\phi\tilde{\phi}}^{(d)}. \quad (107)$$

The renormalized vertex function leads to certain relations for the corresponding ζ -functions defined as logarithmic derivatives of the Z -factors. From Eq. (106) one finds the finite renormalized vertex function

$$\Gamma_{\phi\tilde{\phi}} = -i\omega Z_{\phi}^{1/2} Z_{\tilde{\phi}}^{1/2} Z_{\Omega_{\phi\tilde{\phi}}} \Omega_{\phi\tilde{\phi}} + Z_{\phi}^{1/2} Z_{\tilde{\phi}}^{1/2} Z_{\phi}^{-1} \Gamma_{\phi\phi}^{(st)} Z_{\Gamma} \Gamma k^a Z_{\Gamma_{\phi\tilde{\phi}}}^{(d)} \Gamma_{\phi\tilde{\phi}}^{(d)} \quad (108)$$

given by two finite parts. Since the poles are completely removed in both parts one obtains two relations for the corresponding ζ -functions. Taking the ζ -functions at the stable fixed point one finds

$$-\zeta_{\phi\tilde{\phi}}^* = \frac{1}{2} \zeta_{\phi}^* + \frac{1}{2} \zeta_{\tilde{\phi}}^*, \quad \zeta_{\phi}^* - \zeta_{\Gamma}^* - \zeta_{\Gamma_{\phi\tilde{\phi}}}^{(d)*} = \frac{1}{2} \zeta_{\phi}^* + \frac{1}{2} \zeta_{\tilde{\phi}}^*. \quad (109)$$

Solving for ζ_{Γ}^* it follows

$$\zeta_{\Gamma}^* = -\zeta_{\Gamma_{\phi\tilde{\phi}}}^{(d)*} + \frac{1}{2} \zeta_{\phi}^* - \frac{1}{2} \zeta_{\tilde{\phi}}^* = -\zeta_{\Gamma_{\phi\tilde{\phi}}}^{(d)*} + \zeta_{\Omega_{\phi\tilde{\phi}}}^* + \zeta_{\phi}^*. \quad (110)$$

This allows one to express the ζ -function for the OP Onsager coefficient by the ζ -functions of the two dynamical parts $\Omega_{\phi\tilde{\phi}}$ and $\Gamma_{\phi\tilde{\phi}}^{(d)}$. Similar relations are found for the conserved density m with a kinetic coefficient λ coupled to the OP (an example may be the energy or entropy density)

$$\overset{o}{\Gamma}_{m\tilde{m}}(\xi, k, \omega) = -i\omega \overset{o}{\Omega}_{m\tilde{m}}(\xi, k, \omega) + \overset{o}{\Gamma}_{mm}(\xi, k) \overset{o}{\Gamma} k^a \overset{o}{\Gamma}_{m\tilde{m}}^{(d)}(\xi, k, \omega), \quad (111)$$

$$\zeta_{\lambda}^* = -\zeta_{\Gamma_{m\tilde{m}}}^{(d)*} + \zeta_{\Omega_{m\tilde{m}}}^* + \zeta_m^*. \quad (112)$$

6.2. Calculating the Dynamical Exponent

The characteristic frequency of the OP susceptibility at T_c as a function of the wave vector is given by a power law and defines the dynamical exponent z :

$$\omega_c(T_c, k) = A k^z. \quad (113)$$

On the other hand a characteristic frequency can be written as

$$\omega_c = \Gamma(\ell) k^{2+a}, \quad \ell = \xi_0 k \quad (114)$$

and the asymptotic solution of the flow equation for $\Gamma(\ell)$ reads

$$\Gamma(\ell) \sim \ell^{\zeta_\Gamma^*}. \quad (115)$$

Taking everything together one finds the dynamical exponent as

$$z_\phi = a + 2 + \zeta_\Gamma^*. \quad (116)$$

Inserting for ζ_Γ^* the relation found from the vertex function structure (110) one obtains

$$z_\phi = 2 + a + \zeta_\phi^* + \zeta_{\Omega_{\phi\bar{\phi}}}^* - \zeta_{\Gamma_{\phi\bar{\phi}}}^{(d)*}. \quad (117)$$

For a conserved density coupled to the OP one always has $\zeta_{\Omega_{m\bar{m}}}^* = 0$ and therefore the corresponding dynamical exponent reads

$$z_m = 2 + \zeta_m^* - \zeta_{\Gamma_{m\bar{m}}}^{(d)*}. \quad (118)$$

Strong dynamical scaling states that there is only one dynamic exponent z and in all vertex functions (of the OP and the other slow densities) the time scales with this z . Therefore one has the relation between the different defined exponents $z_\phi = z_m$. Weak dynamic scaling allows different time scales for the OP and the other conserved densities. Thus one has in this case at least two different dynamic exponents z .

From statics it is already known that

$$\zeta_\phi^* = -\eta, \quad \zeta_m^* = \frac{\alpha}{\nu} \quad (119)$$

with α the positive specific heat exponent.ⁿ

6.2.1. Models without Mode Coupling Terms

In the relaxational model ($a = 0$; model A)

$$\zeta_{\Gamma_{\phi\bar{\phi}}}^{(d)*} = 0 \quad (120)$$

as in all the following models in this subsection. Since there are no mode couplings present, z is written

$$z_\phi = 2 + c\eta, \quad (121)$$

where c is a dynamical coefficient calculated loopwise from $\zeta_{\Omega_{\phi\bar{\phi}}}^*$.

ⁿNote that for a non-divergent specific heat α is set to zero (see remark after Eq. (34)). Then the second relation of Eq. (119) reads $\zeta_m^* = 0$.

When the OP is conserved as in model B ($a = 2$) in addition to Eq. (120)

$$\zeta_{\Omega_{\phi\tilde{\phi}}}^* = 0 \quad (122)$$

holds. This shows the absence of a genuine dynamic renormalization and according to (110) and (119)

$$z_\phi = 4 - \eta. \quad (123)$$

A more complicated situation is found in model C ($a = 0$) where a non-conserved OP is coupled in the static functional to a conserved density (energy). Let us assume that the specific heat is diverging (finite value of γ^*) and the fixed point value of time ratio $w = \Gamma/\lambda$ is finite and nonzero. According to the assumption the equation for the fixed point values reads

$$0 = \beta_w = w^*(\zeta_\phi^* + \zeta_{\Omega_{\phi\tilde{\phi}}}^* - \zeta_m^*) \quad \text{or} \quad \zeta_\phi^* + \zeta_{\Omega_{\phi\tilde{\phi}}}^* = \frac{\alpha}{\nu}. \quad (124)$$

For the OP we have

$$\zeta_{\Gamma_{\phi\tilde{\phi}}}^{(d)*} = 0. \quad (125)$$

The secondary density is conserved and the genuine dynamic ζ -functions are zero as in model B. Thus one has

$$z_\phi = 2 + \zeta_\phi^* + \zeta_{\Omega_{\phi\tilde{\phi}}}^* = 2 + \frac{\alpha}{\nu} = z_m, \quad (126)$$

where the last equality holds according to (112), which means that strong scaling holds. Note that this equality becomes possible since the value of $\zeta_{\Omega_{\phi\tilde{\phi}}}^*$ depends on the value of w^* . There may be another fixed point with $w^* = 0$, the weak scaling fixed point, that is stable. For this fixed point nothing can be concluded from (124) and the characteristic frequency of the OP scales differently from that for the conserved density. One obtains for the respective dynamic exponents $z_\phi = 2 + c\eta$ and $z_\alpha = 2 + \alpha/\nu$.⁴³

6.2.2. Models with Mode Coupling Terms

Ward identities play an important role in critical dynamics since the symmetry properties on which they base determine the Poisson brackets. Moreover since the structure of the renormalized models is the same as that of the unrenormalized ones the renormalization of the Poisson brackets can be used to find the renormalization factor Z_g of the mode coupling g_0 (of course the mode couplings have naive dimensions which determine the upper dynamical critical dimension above which the mode couplings are irrelevant).

Ward identities make use of symmetries in dimensional space (translation, rotation etc.) or in OP-space (rotation etc.). Let us discuss an example from statics and consider rotation of the OP ($n = 2$). The rotation matrix R may be written

$$R = \begin{pmatrix} 1 & -\alpha \\ \alpha & 1 \end{pmatrix}. \quad (127)$$

The invariance of the partition function

$$Z(R\vec{H}) = Z(\vec{H}) \quad (128)$$

leads to the Ward identity (the terms proportional to α should be zero)

$$H_1 \frac{\delta Z}{\delta H_2} - H_2 \frac{\delta Z}{\delta H_1} = 0. \quad (129)$$

Similar relations can be derived for vertex functions via Legendre transformations. From such relations, which hold also for the renormalized quantities, relations between the Z -factors (the ζ -functions) can be derived. Another example is the gauge transformation in superconductors which leads to an expression for the renormalization of the coupling to the gauge field.

Now coming back to dynamics the important observation for model E, F, G and J is that the second conserved density m (besides the conserved or non-conserved OP) is the generator of rotations in OP-space. This is reflected by the Poisson bracket (and the renormalized version) between the OP = ϕ and m

$$\{\phi, m\} = g\phi, \quad m = \phi \quad \text{for model J.} \quad (130)$$

This leads to the relation

$$Z_g = Z_m^{1/2} = 1 \quad \text{and for model J} \quad Z_g = Z_\phi^{1/2}. \quad (131)$$

In the case of model H the Galilean invariance is used to calculate the Poisson bracket between the OP and the mass current, which is the generator of movements. This leads to $Z_g=1$.

Knowing the renormalization of the mode coupling g and its naive dimension (easily seen by comparing terms in the Lagrangian) we find additional relations by the conditions of finite fixed point values for the time ratio w and the mode coupling f .

In model E ($a = 0$) with finite fixed point value of $w = \Gamma/\lambda$

$$0 = \beta_w = w^*(\zeta_\phi^* + \zeta_{\Omega_{\phi\tilde{\phi}}}^* - \zeta_{\Gamma_{\phi\tilde{\phi}}}^{(d)*} - \zeta_\lambda^{(d)*}) \quad (132)$$

and finite fixed point value of $f = g/\sqrt{\Gamma\lambda}$

$$0 = \beta_f = \frac{1}{2} f^* (4 - d + \zeta_\phi^* + \zeta_{\Omega_{\phi\tilde{\phi}}}^* - \zeta_{\Gamma_{\phi\tilde{\phi}}}^{(d)*} + \zeta_\lambda^{(d)*}) \quad (133)$$

one concludes

$$\zeta_\phi^* + \zeta_{\Omega_{\phi\tilde{\phi}}}^* - \zeta_{\Gamma_{\phi\tilde{\phi}}}^{(d)*} = \frac{d-4}{2} \quad (134)$$

and inserting into (117) one obtains the exact expression for the dynamic critical exponent

$$z_\phi = \frac{d}{2} \quad (135)$$

in spatial dimension d . Moreover one concludes that strong scaling holds since according to (132)

$$z_m = 2 + \zeta_\lambda^* = 2 + \zeta_\Gamma^* = z_\phi. \quad (136)$$

The same value of the dynamical critical exponent may be derived in model G. There exists also a fixed point with $w^* = 0$. Then nothing can be concluded from (132) for ζ_λ^* and the dynamical correction exponent appears in the dynamic critical exponent (see Ref. [52]).

In model H ($a = 2$) the OP and the secondary density scale differently, both are densities of conserved quantities. Defining the mode coupling as $f = g/\sqrt{\Gamma\lambda_t}$ from its finite fixed point value follows

$$0 = \beta_f = \frac{1}{2} f^* (4 - d + \zeta_\phi^* + \zeta_{\Gamma_{\phi\tilde{\phi}}}^{(d)*} + \zeta_{\lambda_t}^{(d)*}). \quad (137)$$

This leads to a relation between the two dynamical exponents - for the two kinetic coefficients, shear viscosity and thermal conductivity. At $d = 3$ it reads

$$\zeta_{\Gamma_{\phi\tilde{\phi}}}^{(d)*} + \zeta_{\lambda_t}^{(d)*} = 1 - \eta. \quad (138)$$

Thus z has to be calculated explicitly from one dynamic ζ -function.

In Model J ($a = 2$, OP conserved) the finite fixed point value of the mode coupling $f = g/\Gamma$ with (130) leads to

$$0 = \beta_f = f^* \left(\frac{6-d}{2} + \frac{1}{2} \zeta_\phi^* - \zeta_{\Gamma_{\phi\tilde{\phi}}}^{(d)*} \right) \quad (139)$$

and according to (117)

$$z_\phi = 4 + \zeta_\phi^* - \zeta_{\Gamma_{\phi\tilde{\phi}}}^{(d)*} = 4 - \frac{6-d}{2} + \frac{1}{2} \zeta_\phi^* \quad (140)$$

which finally gives the dynamic critical exponent

$$z_\phi = \frac{2+d-\eta}{2}. \quad (141)$$

Note that in all cases the naive dimension of the mode coupling g is $(4-d)/2$ except that of model J where it is $(6-d)/2$. Thus the static upper borderline dimension for the irrelevance of the static coupling u is different from that for the irrelevance of the mode coupling g in model J.

We may conclude that in many cases the asymptotic dynamical power laws can be found without explicit perturbational calculations, which are necessary for the relaxational model A, the liquid-gas critical point model H and for the superfluid transition described by model E or F if the weak scaling fixed point is stable (what seems to be the case). As we shall see below perturbational calculations are necessary anyway for calculating dynamical correlation functions or the crossover from background behaviour to the asymptotic behaviour of transport coefficients.

7. Comparison with Experiment

7.1. General Procedure

We are not only interested in the asymptotic region where the coupling parameters of the model (static and dynamic) as well as the time scale ratios take on their fixed point values but in the comparison with experiments in the non-asymptotic region. This involves the change of the model parameters described by the flow equations as already mentioned. The general form of these equations is e.g. for the fluid without coupling to the sound mode (model H in one loop order)

$$\ell \frac{d\Gamma}{d\ell} = -\frac{3}{4}\Gamma f^2, \quad (142)$$

$$\ell \frac{df}{d\ell} = -\frac{1}{2}f(1 - \frac{19}{24}f^2). \quad (143)$$

In order to get the dependence of the parameters on the physical quantities such as the relative temperature distance from the phase transition temperature (or on the correlation length), the wave vector and the frequency we have to connect the so far arbitrary flow parameter ℓ to these variables. This is achieved by formulating a suitable matching condition usually found by the condition that certain logarithmic terms in the calculated vertex functions are zero. This also guarantees that the vertex functions are properly defined in all the limits one may consider. E.g. for fluids one chooses for the

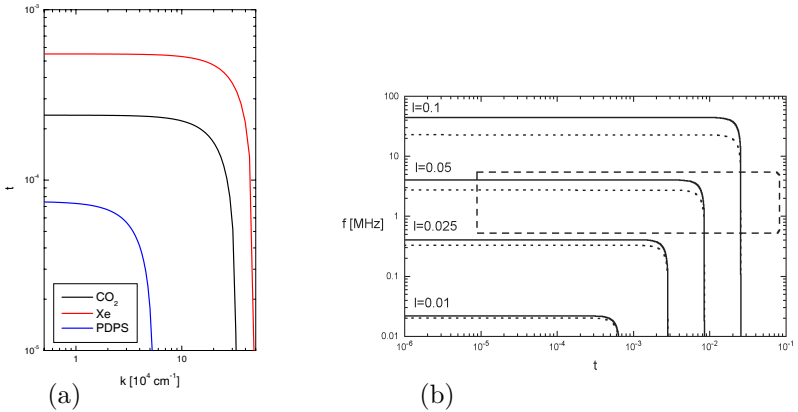


Fig. 7. (a) Comparison of the matching condition Eq. (142) at zero frequency for different fluids and (b) comparison at zero wave vector of asymptotic matching lines (dotted curves) with non-asymptotic lines in one fluid (see Eq. (143)). The dashed frame gives the region where sound experiments are made.

cases when vertex functions are calculated at zero frequency or zero wave vector (see Fig. 7)

$$\ell^2 = \left(\frac{\xi_0}{\xi(t)} \right)^2 + (\xi_0 k)^2, \quad \text{or} \quad (144)$$

$$\ell^8 = \left(\frac{\xi_0}{\xi(t, \Delta\rho)} \right)^8 + \left(\frac{2\omega}{\Gamma(\ell)} \right)^2 \quad (145)$$

respectively. Note that the matching condition contains non-universal parameters^o like ξ_0 or $\Gamma(\ell = 10^{-1})$. It may not be solvable explicitly for ℓ as in the more general second case and it needs the solution of the flow equations.

7.2. Fluids: The Linewidth in Light Scattering

7.2.1. Theoretical Result in One Loop Order

Calculating the dynamic susceptibility in one loop order leads to a Lorentzian shape function

$$\chi_{dyn}(k, \xi, \omega) = \frac{\chi_{st}(k, \xi)}{\omega_c(k, \xi)} \frac{2}{1 + y^2}, \quad y = \omega/\omega_c \quad (146)$$

^oThe nonuniversal parameters are amplitudes like ξ_0 or the background values of the renormalized parameters like $\Gamma(\ell = 10^{-1})$ (initial values of the flow equations which appears in the solution $\Gamma(\ell)$).

and to a half width at half height¹⁸

$$\omega_c(k, \xi) = \Gamma(\ell) k^2 (\xi^{-2} + k^2) \left\{ 1 - \frac{f_t^2(\ell)}{16} [-5 + 6 (k\xi)^{-2} \ln(1 + (k\xi)^2)] \right\}. \quad (147)$$

The flow parameter ℓ has to be replaced by the matching condition (see Eqs. (144), (145), and the functions of the mode coupling $f(\ell)$ and $\Gamma(\ell)$ have to be replaced by the solutions of the corresponding flow equations. In one loop order this can be done analytically to give

$$\omega_c(k, x) = \Gamma_{as} k^z c_{na}(k, x)^{x_\lambda} f(k, x) \left(\frac{1+x^2}{x^2} \right)^{1-x_\lambda/2}, \quad (148)$$

$$c_{na}(k, x) = \left[1 + \frac{k}{k_0} \sqrt{\frac{1+x^2}{x^2}} \right], \quad f^* = \sqrt{\frac{24}{19}}, \quad x_\lambda = \frac{18}{19}, \quad (149)$$

$$f(k, x) = 1 - \frac{f^{*2}}{16 c_{na}(k, x)} [-5 + 6 x^{-2} \ln(1 + x^2)], \quad (150)$$

$$x = k\xi(t), \quad \Gamma_{as} = \Gamma_0 \left(\frac{19}{24} \frac{f_0^2 \ell_0}{\xi_0} \right)^{x_\lambda}, \quad k_0^{-1} = \left(\frac{24}{19 f_0^2} - 1 \right) \frac{\xi_0}{\ell_0}. \quad (151)$$

We are now in the position to discuss all the different limits of the expression (148) for the characteristic frequency:^P the asymptotic, the non-asymptotic limit and within these limits the crossover from the hydrodynamic to the critical region.

7.2.2. Limiting behaviour

Depending on the region in the ξ^{-1} - k -plane (see Fig. 6) where one performs an experiment one may simplify the expression for the characteristic frequency.

In the asymptotic region the mode coupling reaches its fixed point value thus $f_0 \rightarrow f^* = \sqrt{24/19}$ that means $k_0 \rightarrow \infty$. Thus starting from the beginning with the fixed point value we have

$$\omega_c(k, x) = \Gamma_0 k^4 (k\xi_0/\ell_0)^{-x_\lambda} \left(\frac{1+x^2}{x^2} \right)^{1-x_\lambda/2} f(k, x) \quad (152)$$

^PNote that the expression (148) is not a scaling function since it is also valid in the non-asymptotic region. Therefore it contains non-universal parameters.

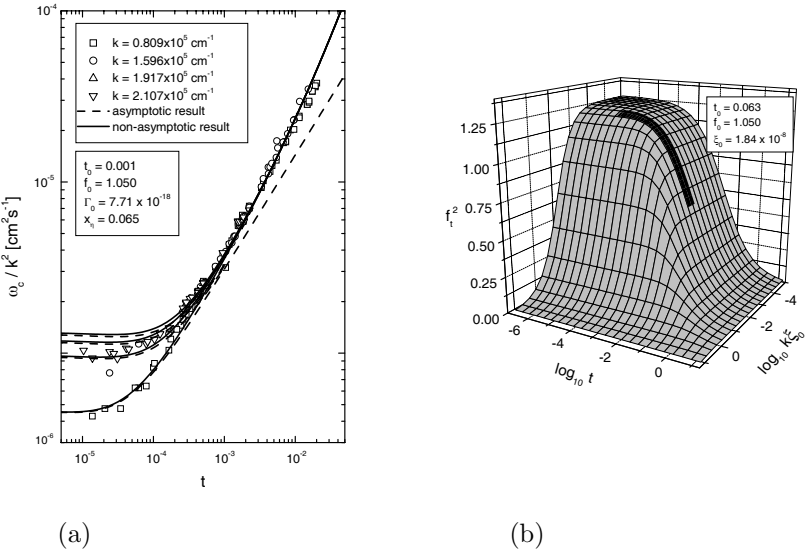


Fig. 8. (a) Asymptotic (dashed) and non-asymptotic expressions (full) for the characteristic frequency ω_c Eq. (148) calculated in ε -expansion. f_0 is a parameter, Γ_0 is taken from the shear viscosity. (b) 'Mountain' of mode coupling f with the 'plateau' where the mode coupling has reached its fixed point value. The black region is the experimental region and it can be seen that it lies to a large extent not on the 'plateau' but on the 'slope' of the crossover region. Taken from Ref. [54].

with

$$f(k, x) = 1 - \frac{f^{*2}}{16} \left[-5 + 6x^{-2} \ln(1 + x^2) \right]. \quad (153)$$

In the 'opposite' (background) limit the mode coupling goes to zero $f_0 \rightarrow 0$ that means $k_0 \rightarrow 0$ and $f(k, x) \rightarrow 1$ and the Van Hove scaling function is recovered

$$\omega_c(k, x) = \Gamma_0 k^4 \left(\frac{1}{x^2} + 1 \right). \quad (154)$$

In the hydrodynamic limit (asymptotic or non-asymptotic) ($k\xi \rightarrow 0$) the characteristic frequency depends quadratically on the wave vector

$$\omega_c(k, \xi) = \Gamma_{as} k^2 \xi^{-2+x_\lambda} \left[1 + \frac{1}{\xi k_0} \right]^{x_\lambda} \left\{ 1 - \frac{f^{*2}}{16} \left[1 + \frac{1}{\xi k_0} \right]^{-1} \right\}. \quad (155)$$

The temperature dependence shows the crossover from the Van Hove behaviour $D \sim \xi^{-2}$ to the asymptotic behaviour $D \sim \xi^{-2+x_\lambda}$.

In the critical limit ($k\xi \rightarrow \infty$, $z = 4 - x_\lambda$) we find

$$\omega_c(k) = \Gamma_{as} k^z \left[1 + \frac{k}{k_0} \right]^{x_\lambda} \left\{ 1 + \frac{5f^{*2}}{16} \left[1 + \frac{k}{k_0} \right]^{-1} \right\}. \quad (156)$$

Again a crossover from the asymptotic regime ($D \sim k^z$) to the Van Hove regime ($D \sim k^4$) at larger values of k takes place.

In Fig. 8(a) we compare our result with experiments in Xenon. The crossover from the non-asymptotic regime (solid curve) to the asymptotic regime (dashed curves asymptotic result $f_0 = f^*$) is seen. This is more explicitly shown in Fig. 8(b) where we have plotted the value of the mode coupling as a function of the wave vector and temperature. The black region is the region of the experiments. The plot is obtained from the solution of the flow equations with the initial conditions found in the comparison with the experiment in Xe, using the matching condition (144) and for the correlation length $\xi = \xi_0 t^{-\nu}$.

7.2.3. Remarks on the Shear Viscosity

A similar analysis at $k = 0$ but $\omega \neq 0$ has been performed for the shear viscosity leading to the solid curves in Fig. 1. The experiments on earth take into account gravity and demonstrate for Xe (Fig. 1(a)) that the effect of the frequency dependence is superimposed by the gravity effect. It should however be noted that agreement with the frequency dependence in microgravity can only be reached by adjusting the frequency scale by a parameter $A \neq 1$. This parameter is introduced to simulate the effects of two loop order terms. Such a two loop calculation has not been done so far. The density dependence which is used in the calculation of gravity effects is well represented by the results of RG theory (Fig. 1(b)).

7.3. Ferromagnets: The Shape Function

The complete scattering function in the asymptotic region for the ferromagnet in one loop order has been calculated but with another method than field theory.⁵⁵ The expression allows to discuss the already mentioned shape crossover between the hydrodynamic and critical region. The comparison at T_c demonstrates agreement with the critical shape (see the solid lines in Fig. 4). This shape may be approximated by (such a form has been suggested earlier in Ref. [56])

$$F(y, \infty) = \Re \frac{1}{iy + (a + iby)^{\frac{z-4}{z}}}, \quad (157)$$

where the parameters $a = 1.51$ and $b = 0.89$ are determined by RG theory.

The peak position in the constant energy scans depends on the shape and the changes when crossing over from the critical to the hydrodynamic regime. Satisfactory agreement in Ni, Ref. [57], has been reached by changing the parameters appearing in the complete result.⁵⁵ The decay of the shape function has been also measured (in a region 100 times larger than the half width) and a decay exponent of 2.3 (the RG prediction is 2.6) has been found.

The comparison of predictions of RG theory is complicated by the fact that besides the Heisenberg interaction in most cases also dipolar forces are present. This complicates the analysis since the dipolar critical behaviour is the asymptotic behaviour and one may observe crossover behaviour. This makes important computer simulations which simulate 'ideal' Heisenberg ferromagnets, however other problems arise like finite size scaling and time problems due to critical slowing down. Nevertheless for some aspects agreement with RG theory has been found in Ref. [58].

7.4. Superfluid Transition: The Thermal Conductivity

Within model F one needs for a comparison with experiment the theoretical expression for the amplitude function of the thermal conductivity and the flow equations for the coupling parameters of the model. The most difficult quantity to calculate is the ζ -function of the OP kinetic coefficient Γ . This has been achieved recently⁴³

$$\zeta_\Gamma = \mathcal{F}^2 + \frac{u^2}{9} \left(L_0 + x_1 L_1 - \frac{1}{2} \right) - \frac{2}{3} u \mathcal{F} a - \frac{1}{2} \mathcal{F}^2 b, \quad (158)$$

$$\zeta_\lambda = \gamma^2 - \frac{F^2}{2w'} \left(1 + \frac{1}{2} \Re[Q] \right), \quad (159)$$

where $\mathcal{F} = \mathcal{C} - i\mathcal{E}$, $\mathcal{C} = \sqrt{\frac{w}{1+w}}$, $\mathcal{E} = \frac{F}{\sqrt{w(1+w)}}$, $\Gamma = \Gamma' + i\Gamma''$, $w = \Gamma/\lambda$, $F = g/\lambda$, $f = F^2/w'$ and the other quantities not mentioned are functions of F and w . With this result we have reanalysed along the lines presented in Ref. [59] the effective amplitude (M are the two loop contributions⁶⁰).

$$R_\lambda^{eff} = \frac{1 - f/4 + fM(w, F, \gamma, u)}{2\sqrt{\pi f w' (1 + \gamma^2 F_+(u))}}. \quad (160)$$

Parameters in the fits of the effective amplitude (see Fig. 9) are the background values of f and w . The main result of the correction of the earlier result for ζ_Γ is the background value found for the imaginary part w'' . The

unrenormalized value was predicted⁶¹ to be $w_0'' = 0.21$ at saturated vapour pressure (SVP) and the renormalized background value found is $w'' = 0.3$ instead of $w'' = 0.8$ found earlier⁵⁹ (see also Ref. [62] for a complete analysis of the data with the correct ζ -function.).

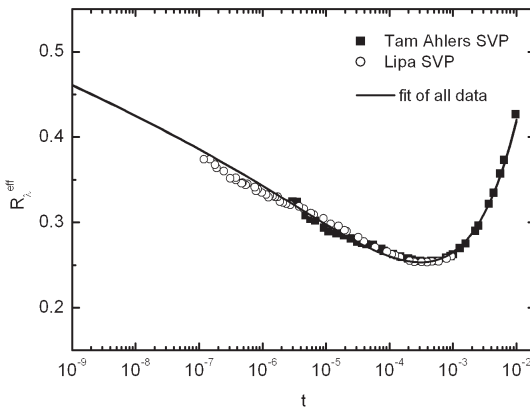


Fig. 9. Amplitude ratio for the thermal conductivity in ${}^4\text{He}$ at saturated vapour pressure.

The reason for the dominance of the non-asymptotic behaviour lies in the circumstance that the dynamical fixed point (w^*, f^*) lies near a stability border line where the scaling fixed point $(w'^* \neq 0, w''^* = 0, f^* \neq 0, z_\phi = z_\alpha)$ changes its stability with the weak scaling fixed point $(w^* = 0, w''^* = 0, f^* \neq 0, z_\phi \neq z_m)$ and w' appears in the denominator of R_λ^{eff} . Near a stability border line at least one transient exponent goes to zero and the value of $w'^* \sim 0$. It turns out that it depends on the fixed point value w^* which of the dynamic fixed points is stable,^a but this is only of little relevance in the physically accessible region.

^aIt turns out that the stability border line between the strong and the weak scaling fixed point depends on the fixed point value of the static coupling u^* . This value is found by sophisticated field theoretic treatment and depends on the order of the loop expansion. The value in $d = 3$ has been taken to be $u^* = 0.0362$ ⁵⁹ with the consequence that the weak-scaling fixed point $w^* = 0$ is the stable fixed point. Although the stable dynamic fixed point is of principal interest it is of less relevance for the analysis in the experimentally accessible region since the non-asymptotic behaviour dominates anyway.

One may find much more material on critical dynamics in the recent review Ref. [63].

Acknowledgements

I want to thank G. Moser for the long lasting cooperation in this field. The progress made in the last years is based on work done with him. I also thank all those with whom I worked together in this field and those which were interested in the results. They all stimulated me to stay within the field of critical dynamics over such a long time. This work was supported by FWF project P15247.

References

1. C. Domb, *The Critical Point* (Taylor and Francis, London, 1996).
2. J. E. Verschaffelt, Versl. Kon. Akad. Werensch. Amsterdam **5**, 94 (1896).
3. K. G. Wilson, Phys. Rev. B **4**, 3174; *ibid.* **4**, 3184 (1971); K. G. Wilson and J. Kogut, Phys. Rep. **12 C**, 75 (1974) (classical papers on application of RG to critical phenomena).
4. L. P. Kadanoff, W. Götze, D. Hamblen, R. Hecht, E. A. S. Lewis, V. V. Palciauskas, M. Rayl, J. Swift, D. Aspnes, and J. Kane, Rev. Mod. Phys. **39**, 395 (1967) (static scaling); B. I. Halperin and P. C. Hohenberg, Phys. Rev. **177**, 952 (1969) (dynamic scaling).
5. M.E. Fisher, Rev. Mod. Phys. **46**, 597 (1974).
6. D. J. Amit, *Field Theory, the Renormalization Group, and Critical Phenomena* (World Scientific, Singapore, 1989) 2nd edition; M. Le Bellac, *Quantum and Statistical Field Theory* (Clarendon Press, Oxford, 1991); J.J. Binney, N. J. Dowrick, A. J. Fisher, and M. E. J. Newman, *The Theory of Critical Phenomena. An Introduction to the Renormalization Group* (Clarendon Press, Oxford, 1992); J. Zinn-Justin, *Quantum Field Theory and Critical Phenomena* (Clarendon Press, Oxford, 1996) 3rd edition; H. Kleinert and Verena Schulte Frohlinde, *Critical Properties of Φ^4 -Theory* (World Scientific, Singapore, 2001);
7. L. Van Hove, Phys. Rev. **93**, 268 (1954); *ibid.* **95**, 249 (1954); *ibid.* **95**, 1374 (1954).
8. R. A. Ferrell, N. Menyhard, H. Schmidt, F. Schwabl, and P. Szepfalusy, Phys. Rev. Lett. **18**, 891 (1967); Phys. Lett. **24A**, 493; Ann. Phys. (NY) **47**, 565 (1968) (classical paper on dynamic scaling).
9. C. De Dominicis, E. Brezin, and J. Zinn-Justin, Phys. Rev. B **12**, 4945 (1975) (model A).
10. P. C. Martin, E. D. Siggia, and H. A. Rose, Phys. Rev. A **8**, 423 (1973).
11. R. Bausch, H. K. Janssen, and H. Wagner, Z.Phys.B **24**, 113 (1976) (classical paper on field theoretic method applied to dynamics).
12. P. C. Hohenberg and B. I. Halperin, Rev.Mod.Phys. **49**, 435 (1977).

13. H. E. Stanley, *Introduction to Phase Transitions and Critical Phenomena* (Clarendon Press, Oxford, 1971) (part VI); J. Cardy, *Scaling and Renormalization in Statistical Physics* (Cambridge University Press, Cambridge, 1996) (chapter 10); N. Goldenfeld, *Lectures on Phase Transitions and the Renormalization Group* (Addison Wesley, 1992); A. N. Vasil'ev, *The Field Theoretic Renormalization Group in Critical Behaviour Theory and Stochastic Dynamics* (Chapman & Hall/CRC, 2004) (chapter 5).
14. F. Schwabl and U. C. Täuber, Phase Transitions: Renormalization and Scaling, in: *Encyclopedia of Applied Physics* (VCH, New York, 13, 343 (1995)); V. Dohm, Phase Transitions, in: *Encyclopedia of Physics*, edited by R.G. Lerner and G.L. Trigg (VCH Publ., New York), 3rd edition, to be published.
15. R. F. Berg and M. R. Moldover, *J. Chem. Phys.* **93**, 1926 (1990).
16. R. F. Berg, M. R. Moldover, and G. A. Zimmerli, *Phys. Rev. Lett.* **82**, 920 (1999); *Phys. Rev. E* **60**, 4079 (1999).
17. H. Iwasaki and M. Takahashi, *J. Chem. Phys.* **74**, 1930 (1981).
18. G. Flossmann and R. Folk, *Phys. Rev. E* **62**, 2460 (2000).
19. G. Flossmann, R. Folk, and G. Moser, *Phys. Rev. E* **60**, 779 (1999).
20. Jan V. Sengers, in: *Supercritical Fluids*, edited by Kiran and J. M. H. Levelt Sengers (Kluwer Academic Publishers, 1994) pages 231-271.
21. H. L. Swinney and D. L. Henry, *Phys. Rev. A* **8**, 2586 (1973).
22. P. Böni, M. E. Chem, and G. Shirane, *Phys. Rev. B* **35**, 8449 (1987).
23. W. Y. Tam and G. Ahlers, *Phys. Rev. B* **33**, 133 (1986).
24. V. Privman, P. C. Hohenberg, and A. Aharony, in: *Phase Transitions and Critical Phenomena*, vol. 14, edited by C. Domb and J. L. Lebowitz (Academic Press, London, 1991).
25. B. I. Halperin, P. C. Hohenberg, and E. D. Siggia, *Phys. Rev. B* **13**, 1299 (1976); *ibid.* **21** 2044(E) (1980) (model E, F, H).
26. Q. Li, PhD Thesis, Stanford University (1991); J. A. Lipa and Q. Li, *Czech. J. Phys.* **46**, 185 (1996).
27. B. I. Halperin and P. C. Hohenberg, *Phys. Rev.* **188**, 898 (1969).
28. B. I. Halperin, P. C. Hohenberg, and S.-k. Ma, *Phys. Rev. Lett.* **29**, 1548 (1972) (model A).
29. B. I. Halperin, P. C. Hohenberg, and S.-k. Ma, *Phys. Rev. B* **10**, 139 (1974) (model C).
30. S.-k. Ma and G. F. Mazenko, *Phys. Rev. B* **11**, 4077 (1975).
31. I. E. Dzyaloshinskii, G. E. Volovick, *Ann. Phys. (N. Y.)* **125**, 67 (1980).
32. R. Folk and G. Moser, *Phys. Rev. E* **57**, 683 (1998).
33. A. Onuki, *J. Low Temp. Phys.* **53**, 1 (1983).
34. M. S. Green, *J. Chem. Phys.* **20**, 1281 (1952).
35. R. W. Zwanzig, *J. Chem. Phys.* **33**, 1338 (1960); *Phys. Rev.* **124**, 983 (1961).
36. H. Mori and H. Fujisaka, *Prog. Theor. Phys.* **49**, 764 (1973).
37. H. Mori, H. Fujisaka, and H. Shigematsu, *Prog. Theor. Phys.* **51**, 109 (1974).
38. K. Kawasaki, in: *Phase Transitions and Critical Phenomena*, vol. 5a, edited by C. Domb and M. S. Green (Academic Press, London, 1975).
39. H. K. Janssen, in: *Lecture Notes in Physics*, vol 104 (Springer Verlag, Berlin, 1979).

40. N.V. Antonov and N.Vasil'ev, Theor. Mat. Fiz., **60**, 59 (1984) (model A).
41. R. Folk and G. Moser, acta physica slovaca **52**, 285 (2002); Phys. Rev. Lett. **91**, 030601 (2003).
42. V. Dohm, Z. Phys. B **31**, 327 (1978).
43. R. Folk and G. Moser, Phys. Rev. Lett. **89**, 125301 (2002); Erratum: Phys. Rev. Lett. **93**, 229902 (2004). The quantity x_0 in the Erratum is identical to x_- in the letter. (model F' (for the superfluid transition in ^3He - ^4He mixtures) contains model F).
44. R. Schloms and V. Dohm, Nucl. Phys. B **328** (1989).
45. V. Dohm and R. Folk, Phys. Rev. B **28**, 1332 (1983).
46. C. De Dominicis and L. Peliti, Phys. Rev. B **18**, 353 (1978) (model E,F, H, G).
47. L. Ts. Adzhemyan, A. N. Vasil'ev, Yu. S. Kabrits, and M. V. Kompaniets, Theor. Math. Phys. **119**, 454 (1999) (model H).
48. R. Folk and G. Moser, Phys. Rev. Lett. **75** 2706 (1995), (model H and H'). and Phys. Rev. E **58**, 6246 (1998) (model H' (for mixtures) contains model H).
49. V. Dohm, Solid State Comm. **20**, 657 (1976).
50. E. Brezin and C. De Dominicis, Phys. Rev. B **12**, 4954 (1975) (model C).
51. V. Dohm, Z. Phys. B **33**, 79 (1979).
52. C. De Dominicis and L. Peliti, Phys. Rev. Lett. **38**, 505 (1977).
53. V. Dohm and R. A. Ferrell, Phys. Lett. **67A**, 387 (1978).
54. G. Flossmann and R. Folk, Int. J. Thermophys. **22** 1099 (2001).
55. H. Iro, Z. Phys. B **68**, 485 (1987); Journal de Physique, **49** C8 - 1563 (1988); J. Magn. Mat Mater. **73**, 175 (1988).
56. K. Bhattacharjee and R. A. Ferrell, Phys. Rev. B **24**, 6480 (1981).
57. P. Böni, H. A. Mook, J. L. Martinez and G. Shirane, Phys. Rev. B **47**, 3171 (1993).
58. K. Chen and D. P. Landau, Phys. Rev. B **49**, 3266 (1994).
59. V. Dohm, Phys. Rev. B **44**, 2697 (1991); *ibid.* **73**, 099901 (E) (2006) (ζ -functions).
60. V. Dohm, Z. Phys. B **61**, 193 (1985) (amplitude function for the thermal conductivity).
61. V. Dohm, Phys. Rev. B **29**, 1497 (1984).
62. V. Dohm, Phys. Rev. B **73**, 092503 (2006).
63. R. Folk and G. Moser, J. Phys. A: Math. Gen. **39**, R207-R313 (2006).

CHAPTER 3

SPACETIME APPROACH TO PHASE TRANSITIONS

Wolfhard Janke

*Institut für Theoretische Physik, Universität Leipzig, Augustusplatz 10/11,
D-04109 Leipzig, Germany*
E-mail: Wolfhard.Janke@itp.uni-leipzig.de

Adriaan M. J. Schakel

*Institut für Theoretische Physik, Freie Universität Berlin, Arnimallee 14,
D-14195 Berlin, Germany*
E-mail: schakel@physik.fu-berlin.de

In these notes, the application of Feynman's sum-over-paths approach to thermal phase transitions is discussed. The paradigm of such a spacetime approach to critical phenomena is provided by the high-temperature expansion of spin models. This expansion, known as the hopping expansion in the context of lattice field theory, yields a geometric description of the phase transition in these models, with the thermal critical exponents being determined by the fractal structure of the high-temperature graphs. The graphs percolate at the thermal critical point and can be studied using purely geometrical observables known from percolation theory. Besides the phase transition in spin models and in the closely related ϕ^4 theory, other transitions discussed from this perspective include Bose-Einstein condensation, and the transitions in the Higgs model and the pure U(1) gauge theory.

Contents

1	Introduction	124
2	Lattice Field Theory	126
2.1	Noninteracting Theory	128
2.2	Loop Gas	134
2.3	$ \phi ^4$ Field Theory	138
2.4	O(N) Spin Model	142
2.5	Ising Model	146

2.6	Summary	148
3	Critical Properties	148
3.1	Fractal Structure	149
3.2	Loop Proliferation	150
3.3	Critical Exponents	152
3.4	Self-Avoiding Random Walks	153
3.5	$O(N)$ Models	154
3.6	Summary	156
4	Monte Carlo Simulations	156
4.1	Plaquette Update	157
4.2	Numerical Results	158
4.3	Summary	163
5	Further Applications	163
5.1	Higgs Model	164
5.2	Bose-Einstein Condensation	166
5.3	Summary	172
6	Dual Theories	172
6.1	Peierls Domain Walls	172
6.2	Vortex Lines	173
6.3	Monopole Loops	176
6.4	Summary	177
	References	177

1. Introduction

Feynman's spacetime approach to quantum mechanics provides a marvelously intuitive, yet computationally powerful entry to the quantum world.¹ In this sum-over-paths approach, transition amplitudes are computed by summing over all possible trajectories a particle can take. Although it is most extensively applied to nonrelativistic quantum mechanics,² for which it was originally designed, the worldline approach also found applications in the context of relativistic systems.^{3,4} (For overviews and references to a host of applications in high energy physics, see Refs. [5–8].) In these notes, we explore its use in the theory of critical phenomena.

The possibility to adapt Feynman's sum-over-paths approach to describe phase transitions derives from particle-field duality. Featuring the particle content of the system, the spacetime approach provides a completely equivalent alternative to the quantum field theoretic description. Although by no means the only successful method,⁹ field theory is frequently used to describe critical phenomena,^{10–12} whether the fluctuations are thermal as in phase transitions taking place at finite temperature, or quantum as in zero-temperature transitions. Particle-field duality then opens the possibility for a spacetime approach to critical phenomena. In the context of classical critical phenomena, the line objects described by the field theory are current

lines.

Though not formulated as such, the high-temperature expansion of spin models^{6,13} probably provides the first example of the spacetime approach to critical phenomena (see below). A particular intuitive example is offered by the nonlinear $O(N)$ spin model defined on a lattice in the limit $N \rightarrow 0$, where the high-temperature graphs form random self-avoiding walks.¹⁴ In the early 1950ies, Feynman¹⁵ applied his approach to the superfluid phase transition in liquid ^4He , and showed that, in this picture, Bose-Einstein condensation arises when the worldlines of individual particles combine to form large lines threading the entire system. In the late 1970ies,^{16–20} the approach was applied to phase transitions in relativistic lattice models possessing line-like topological defects, thus mapping these models onto the statistical mechanics problem of random loop configurations. The line defects were pictured as forming a grand canonical ensemble of fluctuation loops of arbitrary shape and length—a so-called *loop gas*. In the 1980ies, the statistical properties of such loop gases were further investigated in the context of cosmic strings and their role in phase transitions in the early universe, with the loop distribution given a central position,^{21,22} as well as in the context of deconfinement phase transitions, where percolation observables were introduced to characterize them.^{23,24} More recently, these ideas were pursued further with the goal to arrive at a complete quantitative understanding of phase transitions in terms of the geometrical properties of the loop gas under consideration.^{25–32} The resulting geometric description of critical phenomena ties together various strains of theoretical physics: statistical mechanics, quantum field theory, polymer physics, and percolation theory—all to be discussed below.

The plan of these notes is as follows. In Sec. 2, the particle content of the linear $O(N)$ symmetric quantum field theory, defined on a hypercubic lattice, is studied in the spirit of Feynman’s sum-over-paths approach, starting from the noninteracting theory in Secs. 2.1 and 2.2. Interactions are perturbatively included in Sec. 2.3, where also the spacetime interpretation of Feynman diagrams is pursued. In Sec. 2.4, the strong-coupling limit, where the field theory reduces to the nonlinear $O(N)$ spin model, is considered. The high-temperature representation of the nonlinear model is shown to provide a purely geometric representation, directly connected to Feynman’s spacetime approach for the linear model. As a case study, the high-temperature representation of the Ising model, corresponding to $N = 1$, on a square lattice is detailed in Sec. 2.5.

In Sec. 3, the critical properties of the $O(N)$ universality class are ex-

amined from the perspective of particle trajectories or high-temperature graphs. In Sec. 3.1, their fractal structure is investigated, while in Sec. 3.2, the proliferation of these lines is shown to drive the $O(N)$ phase transition. In Sec. 3.3, the fractal structure of the worldlines or high-temperature graphs is related to the critical behaviour. The general relations are first applied to self-avoiding random walks, corresponding to the $N \rightarrow 0$ limit, in two dimensions (Sec. 3.4), and to arbitrary $-2 \leq N \leq 2$ (Sec. 3.5) also in two dimensions, where many exact results are available for comparison.

In Sec. 4, the high-temperature representation of the Ising model is investigated by means of Monte Carlo simulations. The Metropolis update used to generate the high-temperature graphs is introduced in Sec. 4.1, while the numerical results are summarized in Sec. 4.2.

In Sec. 5, the conclusions for the $O(N)$ universality class are extended to charged systems (Sec. 5.1) and to Bose-Einstein condensation (Sec. 5.2) to demonstrate the generality of the spacetime approach to phase transitions.

Finally, in Sec. 6, the worldlines or high-temperature graphs are reinterpreted as line defects in two (Sec. 6.1), three (Sec. 6.2), and four (Sec. 6.3) dimensions, respectively, and the so-called dual field theories, which feature these line-like configurations as topological defects, briefly discussed.

2. Lattice Field Theory

Central to our discussion is the $O(N)$ symmetric relativistic quantum field theory formulated on a hypercubic lattice in d Euclidean spacetime dimensions, with the time coordinate analytically continued to the imaginary axis τ . As an illustration, the cubic lattice in Fig. 1 represents discretized spacetime in one time and two space dimensions x_1 and x_2 . The theory,

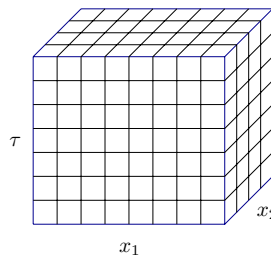


Fig. 1. Cubic lattice representing three-dimensional discretized spacetime.

describing self-interacting scalar particles of mass m , is specified by the

(Euclidean) partition function

$$Z = \text{Tr } e^{-S}, \quad (1)$$

where S is the lattice action

$$S = a^d \sum_x \left[\frac{1}{2a^2} \sum_{\mu} (\varphi_{x+a\hat{\mu}} - \varphi_x)^2 + \frac{m^2}{2} \varphi_x^2 + \frac{g}{4!} \varphi_x^4 \right], \quad (2)$$

with g the coupling constant and a the lattice spacing. The real scalar field φ_x defined on each lattice site x of the spacetime box has N components $\varphi_x = \varphi_x^\alpha = (\varphi_x^1, \varphi_x^2, \dots, \varphi_x^N)$, with the index $\alpha = 1, 2, \dots, N$ labelling the field components and $\varphi_x^4 \equiv (\varphi_x \cdot \varphi_x)^2$, where the dot product implies a summation over the field components $\varphi_x \cdot \varphi_x = \sum_{\alpha=1}^N \varphi_x^\alpha \varphi_x^\alpha$. Lattice coordinates, representing discretized spacetime, are specified by $x = x_\mu = (x_1, x_2, \dots, x_d)$, with $\mu = 1, 2, \dots, d$ and $x_d = \tau$ denoting the imaginary time coordinate, while $\hat{\mu}$ denotes the unit vector pointing in the μ -direction. In the continuum limit $a \rightarrow 0$, the lattice action reduces to

$$S = \int d^d x \left\{ \frac{1}{2} [\partial_\mu \varphi(x)]^2 + \frac{m^2}{2} \varphi^2(x) + \frac{g}{4!} \varphi^4(x) \right\}, \quad (3)$$

where $\varphi(x)$ stands for the field defined in continuous spacetime. Unless otherwise indicated, natural units $\hbar = c = 1$ are adopted throughout. The trace Tr in Eq. (1) stands for the sum or integral over all possible field configurations:

$$\text{Tr} = \prod_x \int d\varphi_x. \quad (4)$$

In the continuum limit, where the lattice spacing is taken to zero $a \rightarrow 0$, the right hand defines the *functional* measure denoted by $\int D\varphi$.

For numerical simulations, a more convenient form of the lattice action is obtained by casting Eq. (2) in terms of dimensionless fields and parameters defined via³³

$$a^{d-2} \varphi_x^2 = 2K \phi_n^2, \quad (5)$$

$$a^{4-d} g = 6 \frac{\lambda}{K^2}, \quad (6)$$

$$m^2 a^2 = \frac{1 - 2\lambda N}{K} - 2d. \quad (7)$$

The action then takes the form of an $O(N)$ spin model

$$S = -K \sum_{\langle n, n' \rangle} \phi_n \cdot \phi_{n'} + \sum_n \phi_n^2 + \lambda \sum_n (\phi_n^2 - N)^2. \quad (8)$$

Each site on the hypercubic spacetime lattice is now specified by the vector $n = n_\mu = (n_1, n_2, \dots, n_d)$ with integer components $n_\mu = x_\mu/a$ and the sum $\sum_{\langle n, n' \rangle}$ extends over all nearest neighbour pairs. In terms of these new dimensionless variables, the action is independent of the lattice spacing a . The partition function Z now reads

$$Z = \int D\mu(\phi) \exp \left(K \sum_{\langle n, n' \rangle} \phi_n \cdot \phi_{n'} \right), \quad (9)$$

with the on-site measure

$$\int D\mu(\phi) = \int \prod_n d\phi_n e^{-\phi_n^2 - \lambda(\phi_n^2 - N)^2}. \quad (10)$$

In the limit $\lambda \rightarrow \infty$, the field theory reduces to the standard $O(N)$ spin model, with a “spin” variable ϕ_n of fixed length, $\phi_n^2 = N$, located at each site of the spacetime lattice.

2.1. Noninteracting Theory

We first consider the limit $\lambda \rightarrow 0$ in Eq. (8), corresponding to the noninteracting field theory. The rescaling factor K introduced in Eqs. (5)-(7) then becomes

$$K = \frac{1}{2d + m^2 a^2} \quad (11)$$

and the action reduces to the quadratic form

$$S_0 = \sum_{n, n'} \phi_n \cdot \Lambda_{n, n'} \phi_{n'}, \quad (12)$$

with

$$\Lambda_{n, n'} = \delta_{n, n'} - K \sum_{\pm \mu} \delta_{n, n' + \hat{\mu}} \quad (13)$$

where the sum $\sum_{\pm \mu}$ extends over the positive as well as the negative directions. In matrix notation

$$\Lambda = I - K H, \quad (14)$$

where I is the identity matrix and H denotes the so-called hopping matrix whose elements $H_{n, n'}$ are unity if the two lattice sites n and n' are nearest neighbours, and zero otherwise. Physically, H describes the hopping, or propagation of a particle from one lattice site, representing a spacetime cell, to an adjacent one, with each hop carrying a weight K . Since the

theory is noninteracting, a particle is free to hop at random to any of its nearest neighbours without restriction. It can and will in general revisit sites previously visited and can even hop onto a site already occupied by another particle. The particle trajectories are therefore *phantom* worldlines that can freely intersect and share bonds of the lattice without energy penalty.

The inverse of Λ determines the lattice correlation function:

$$\langle \phi_n^\alpha \phi_{n'}^\beta \rangle = \frac{1}{2} \delta_{\alpha,\beta} \Lambda_{n,n'}^{-1} = \frac{1}{2} \delta_{\alpha,\beta} \sum_{b=0}^{\infty} H_{n,n'}^b K^b, \quad (15)$$

as can be read off from the action (12). From the definition of the hopping matrix H it follows that $H_{n,n'}$ raised to the power b gives the number of paths $z_b(n, n')$ of b steps starting at site n and ending at site n' . In this so-called *hopping expansion*,³⁴ the correlation function is therefore obtained by summing over all possible worldlines of arbitrary many steps joining the endpoints n and n' :³⁵

$$\langle \phi_n^\alpha \phi_{n'}^\beta \rangle = \frac{1}{2} \delta_{\alpha,\beta} \sum_{b=0}^{\infty} z_b(n, n') K^b = \frac{1}{2} \delta_{\alpha,\beta} \sum_{\text{worldlines}} K^b. \quad (16)$$

Each path carries a weight K^b according to the number of steps b taken. This geometric representation of the correlation function as a sum over worldlines constitutes Feynman's spacetime approach¹ to fluctuating fields on the lattice. The equivalence of the two approaches is known as *particle-field duality*.

Because of translational invariance, the number of particle trajectories $z_b(n, n')$ depends only on the relative coordinate $z_b(n, n') = z_b(n - n')$. It satisfies the recurrence relation

$$z_{b+1}(n) = \sum_{\pm \mu} z_b(n + \hat{\mu}), \quad (17)$$

with the initial condition $z_0(n) = \delta_{0,n}$. This relation is easily solved by going over to Fourier space

$$z_b(n - n') = \int_{-\pi}^{\pi} \frac{d^d q}{(2\pi)^d} e^{iq \cdot (n - n')} z_b(q), \quad (18)$$

with $q \cdot n = q_\mu n_\mu = q_1 n_1 + \cdots + q_d n_d$ and q_μ the dimensionless momentum variable, yielding

$$z_{b+1}(q) = \sum_{\mu} \cos(q_\mu) z_b(q). \quad (19)$$

With $z_0(q) = 1$ as initial condition, this gives for $z_b(n - n')$

$$z_b(n - n') = \int_{-\pi}^{\pi} \frac{d^d q}{(2\pi)^d} e^{iq \cdot (n - n')} \left[2 \sum_{\mu} \cos(q_{\mu}) \right]^b. \quad (20)$$

In the limit where the lattice spacing a is small but still finite, so that the particles still take discrete steps, we have

$$\begin{aligned} \left[2K \sum_{\mu} \cos(q_{\mu}) \right]^b &\rightarrow \left(\frac{1 - q^2/2d}{1 + m^2 a^2/2d} \right)^b \\ &\rightarrow \exp [-(q^2 + m^2 a^2)b/2d]. \end{aligned} \quad (21)$$

The lattice correlation function (16) then becomes

$$\begin{aligned} \langle \phi_n^{\alpha} \phi_{n'}^{\beta} \rangle &\rightarrow \delta_{\alpha, \beta} \frac{1}{2} \sum_{b=0}^{\infty} \int_{-\pi}^{\pi} \frac{d^d q}{(2\pi)^d} e^{iq \cdot (n - n')} e^{-(q^2 + m^2 a^2)b/2d} \\ &\rightarrow \delta_{\alpha, \beta} \frac{1}{2} \sum_{b=1}^{\infty} \left(\frac{d}{2\pi b} \right)^{d/2} \exp \left[-\frac{d}{2} \frac{(n - n')^2}{b} \right] e^{-m^2 a^2 b/2d}, \end{aligned} \quad (22)$$

showing that the end-to-end vector $n - n'$ is Gaussian distributed with an extra Boltzmann weight $\exp(-m^2 a^2/2d)$ associated with each step taken. Because of this bond fugacity, long worldlines are exponentially suppressed as long as the mass term in the action is positive, $m^2 > 0$. Notice that in the last line of Eq. (22), the lower bound on the summation is replaced by $b = 1$. This is justified because the $b = 0$ term always vanishes for $n \neq n'$.

A more familiar expression for the correlation function is obtained from Eq. (16) by first summing over the length b of the particle trajectories. With $z_b(n, n')$ given in Eq. (20), this leads to

$$\begin{aligned} \langle \phi_n^{\alpha} \phi_{n'}^{\beta} \rangle &= \delta_{\alpha, \beta} \frac{1}{2} \int_{-\pi}^{\pi} \frac{d^d q}{(2\pi)^d} \frac{e^{iq \cdot (n - n')}}{1 - 2K \sum_{\mu} \cos(q_{\mu})} \\ &= \delta_{\alpha, \beta} \frac{1}{2K} \int_{-\pi}^{\pi} \frac{d^d q}{(2\pi)^d} \frac{e^{iq \cdot (n - n')}}{2 \sum_{\mu} [1 - \cos(q_{\mu})] + m^2 a^2}. \end{aligned} \quad (23)$$

For the original fields φ_x , which are connected to the rescaled fields ϕ_n through Eq. (5), this translates into the standard form of the correlation function of a free field theory on a hypercubic lattice,

$$\langle \varphi_x^{\alpha} \varphi_{x'}^{\beta} \rangle = \delta_{\alpha, \beta} a^2 \int_{-\pi/a}^{\pi/a} \frac{d^d k}{(2\pi)^d} \frac{e^{ik \cdot (x - x')}}{2 \sum_{\mu} [1 - \cos(k_{\mu} a)] + m^2 a^2}, \quad (24)$$

where the lattice sites are now labelled again by $x_\mu = n_\mu a$, and $k_\mu = q_\mu/a$ is the momentum variable.

In the limit $a \rightarrow 0$, the correlation function (24) reduces to the standard continuum expression

$$\langle \varphi_x^\alpha \varphi_{x'}^\beta \rangle = \delta_{\alpha,\beta} \int_{-\infty}^{\infty} \frac{d^d k}{(2\pi)^d} \frac{e^{ik \cdot (x-x')}}{k^2 + m^2}. \quad (25)$$

The momentum integral can be easily carried out by introducing the Schwinger proper time representation⁴ of the integrand, which is based on Euler's form

$$\frac{1}{A^z} = \frac{1}{\Gamma(z)} \int_0^{\infty} \frac{ds}{s} s^z e^{-sA}, \quad (26)$$

where $\Gamma(z)$ is the Euler gamma function. Specifically,

$$\begin{aligned} \langle \varphi_x^\alpha \varphi_{x'}^\beta \rangle &= \delta_{\alpha,\beta} \int_0^{\infty} ds \int \frac{d^d k}{(2\pi)^d} e^{ik \cdot (x-x')} e^{-s(k^2+m^2)} \\ &= \delta_{\alpha,\beta} \int_0^{\infty} ds \left(\frac{1}{4\pi s} \right)^{d/2} e^{-(x-x')^2/4s} e^{-sm^2} \\ &= \delta_{\alpha,\beta} \frac{1}{(2\pi)^{d/2}} \left(\frac{m}{|x-x'|} \right)^{d/2-1} K_{d/2-1}(m|x-x'|), \end{aligned} \quad (27)$$

with $K_{d/2-1}$ a modified Bessel function. The integral in the second line is the continuum limit of the lattice expression (22), with the sum over the number of steps b taken by the particle replaced by an integral over the Schwinger proper time parameter s , with the identification

$$ba^2/2d \equiv s. \quad (28)$$

The parameter s is related to the proper time τ_p of the trajectory traced out by the point particle, for which

$$\left(\frac{dx_\mu(\tau_p)}{d\tau_p} \right)^2 = 1. \quad (29)$$

To make this evident, we write the integrand in the second line of Eq. (27) as a Feynman path integral¹⁹

$$\begin{aligned} &\left(\frac{1}{4\pi s} \right)^{d/2} e^{-(x-x')^2/4s} e^{-sm^2} \\ &= \int_{x(0)=x}^{x(s)=x'} Dx(s') \exp \left\{ - \int_0^s ds' \left[\frac{1}{4} \dot{x}^2(s') + m^2 \right] \right\}, \end{aligned} \quad (30)$$

where the so-called Wiener measure is defined by

$$\int_{x(0)=x}^{x(s)=x'} \mathrm{D}x(s') \equiv \lim_{b \rightarrow \infty} A^b \prod_{i=1}^{b-1} \int_{-\infty}^{\infty} \mathrm{d}x_i, \quad (31)$$

with the normalization factor

$$A = \left(\frac{d}{2\pi a^2} \right)^{d/2}. \quad (32)$$

Here, it is understood that the limit $b \rightarrow \infty$ is taken concurrently with the continuum limit $a \rightarrow 0$ in a way such that $ba^2 \rightarrow \text{const}$. The classical action of the point particle in Eq. (30), tracing out its trajectory in spacetime is the continuum limit of the lattice action present in Eq. (22):

$$\begin{aligned} W_0 &= \frac{d}{2} \sum_{i=1}^b \left(\frac{x_{i-1} - x_i}{a} \right)^2 + \frac{m^2 a^2 b}{2d} \\ &= \sum_{i=1}^b \frac{a^2}{2d} \left[\frac{1}{4} \left(\frac{x_{i-1} - x_i}{a^2/2d} \right)^2 + m^2 \right] \\ &\rightarrow \int_0^s \mathrm{d}s' \left[\frac{1}{4} \dot{x}^2(s') + m^2 \right], \end{aligned} \quad (33)$$

where in the last step the identification (28) is used. Written as a path integral, the correlation function (27) thus reads

$$\langle \varphi_x^\alpha \varphi_{x'}^\beta \rangle = \delta_{\alpha,\beta} \int_0^\infty \mathrm{d}s \int_{x(0)=x}^{x(s)=x'} \mathrm{D}x(s') e^{-W_0}. \quad (34)$$

It forms the continuum limit of the sum over all possible particle trajectories on the spacetime lattice in Eq. (16). Note that the proper time parameter s can take any positive value, in agreement with the lattice representation (16) of the correlation function where the worldlines can be arbitrarily long. The Boltzmann factor $\exp(-sm^2)$ exponentially suppresses, however, large proper times as long as $m^2 > 0$. When we set

$$s \equiv \tau_p/2m, \quad (35)$$

the continuum action (33) yields m times the arc length of the path,

$$\int_0^s \mathrm{d}s' \left[\frac{1}{4} \dot{x}^2(s') + m^2 \right] = m\tau_p, \quad (36)$$

which is the standard form of the classical action of a relativistic free scalar particle of mass m . This demonstrates that s can indeed be thought of as the proper time.

For later use, we record the second line in Eq. (27) with Planck's constant and the speed of light reinstated:

$$\langle \varphi_x^\alpha \varphi_0^\beta \rangle = \delta_{\alpha,\beta} c \int_0^\infty ds \left(\frac{1}{4\pi\hbar s} \right)^{d/2} e^{-(c^2\tau^2 + \mathbf{x}^2)/4\hbar s} e^{-sm^2c^2/\hbar}, \quad (37)$$

while the continuum action (3) becomes

$$S_0 = \int d\tau d^{d-1}x \varphi \left(-\hbar^2 \frac{\partial^2}{c^2 \partial \tau^2} - \hbar^2 \nabla^2 + m^2 c^2 \right) \varphi, \quad (38)$$

where now the spacetime coordinates are denoted by $x_\mu = (\mathbf{x}, c\tau)$, with τ the imaginary time and $\mathbf{x} = (x_1, \dots, x_{d-1})$ the spatial coordinates.

Besides the number of worldlines $z_b(n, n')$ on the spacetime lattice connecting the lattice sites n and n' in b steps, also the probability $P_b(n, n')$ for a particle to move from n to n' in b steps will become important below. The probability is given by the ratio

$$P_b(n, n') = z_b(n, n')/z_b \quad (39)$$

of $z_b(n, n')$ and the number of paths of b steps starting at n and ending at an arbitrary lattice site,

$$z_b \equiv \sum_{n'} z_b(n, n'). \quad (40)$$

The denominator in Eq. (39) is included so that P_b is a genuine probability, taking values between 0 and 1. To evaluate it, imagine the particle taking a first step to one of its nearest neighbours $n \pm \hat{\mu}$. It then has only $n-1$ steps still available to reach the final destination n' with probability $P_{b-1}(n \pm \hat{\mu}, n')$. That is, P_b satisfies the recurrence relation:

$$P_b(n, n') = \frac{1}{2d} \sum_{\pm\mu} P_{b-1}(n + \hat{\mu}, n') \quad (41)$$

where the factor $2d$ denotes the number of nearest neighbours on a d -dimensional square lattice. When $P_{b-1}(n, n')$ is subtracted from both sides of Eq. (41), the difference equation

$$P_b(n, n') - P_{b-1}(n, n') = \frac{1}{2d} \sum_{\pm\mu} [P_{b-1}(n + \hat{\mu}, n') - P_{b-1}(n, n')] \quad (42)$$

follows, with the boundary condition $P_0(n, n') = \delta_{n,n'}$. As before, the continuum limit is taken by simultaneously letting $a \rightarrow 0$ and $b \rightarrow \infty$, such

that $ba^2 \rightarrow \text{const}$. The difference equation then turns into the differential equation

$$\partial_b P_b(n, n') = \frac{a^2}{2d} \nabla^2 P_b(n, n'), \quad (43)$$

with the celebrated solution

$$P_b(n, n') = \left(\frac{d}{2\pi b} \right)^{d/2} \exp \left[-\frac{d}{2} \frac{(n - n')^2}{b} \right]. \quad (44)$$

For the probability density $p_b(x, x') \equiv P_b(n, n')/a^d$ this gives the Gaussian distribution

$$p_b(x, x') = \left(\frac{d}{2\pi b a^2} \right)^{d/2} \exp \left[-\frac{d}{2} \frac{(x - x')^2}{ba^2} \right]. \quad (45)$$

Each dimension the particle is free to roam contributes a factor $\sqrt{d/2\pi b a^2}$ to the prefactor.

2.2. Loop Gas

A similar geometric representation in terms of particle trajectories as found for the correlation function can be given for the partition function. Consider the partition function of the free theory:

$$Z_0 = \prod_n \int d\phi_n e^{-S_0}, \quad (46)$$

with the lattice action S_0 given by Eq. (12). This integral generalizes the standard Gaussian integral

$$\int \prod_{i=1}^n dx_i \exp \left(-\frac{1}{2} \sum_{i,j=1}^n x_i M_{ij} x_j \right) = (2\pi)^{n/2} \det^{-1/2}(M), \quad (47)$$

with M a symmetric positive-definite $n \times n$ matrix, and $\det(M)$ its determinant. It can therefore be evaluated exactly, with the result

$$\ln Z_0 = \ln \text{Det}^{-N/2}(\Lambda) = -\frac{N}{2} \text{Tr} \ln \Lambda, \quad (48)$$

where Tr denotes the functional trace. In deriving this, irrelevant prefactors are ignored and use is made of the identity

$$\ln \text{Det}(A) = \text{Tr} \ln A, \quad (49)$$

relating the determinant and trace of an Hermitian operator A . The relation can be easily checked explicitly for a $n \times n$ matrix. With $\Lambda = I - KH$ as before, $\ln Z_0$ can be expanded in the hopping parameter K as

$$\ln Z_0 = \frac{N}{2} L^d \sum_{b=1}^{\infty} \frac{1}{b} z_b(a) K^b \quad (50)$$

where $z_b(a)$ denotes the number of worldlines of b steps, starting at a given lattice site n and returning to one of its nearest neighbour sites $n \pm \hat{\mu}$ after b steps (see Fig. 2). The lattice spacing a serves here as a microscopic cutoff, so that $z_b(a)$ rather than $z_b(0)$ appears when closing open paths. Since a worldline can start at any site on the spacetime lattice, the right hand contains a factor L^d , denoting the total number of lattice sites, and $\ln Z_0$ is extensive. The factor $1/2b$ appearing in Eq. (50) reflects the possibility to

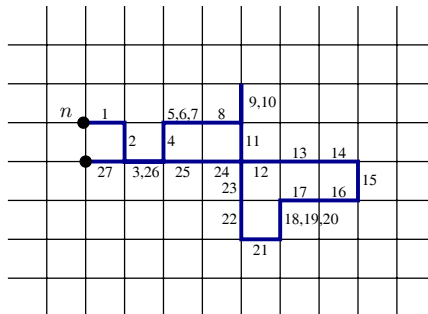


Fig. 2. A Brownian random walk on a square lattice returning to a site adjacent to its starting position n . As indicated, the particle took 27 steps in total. Observe that various bonds are traversed more than once.

trace out a closed path starting from any site along the path and going in either direction round it. The factor N reflects the degeneracy associated with a closed worldline. Written as a sum over *single* loops of arbitrary length and shape, Eq. (50) reads

$$\ln Z_0 = N \sum_{\text{single loops}} K^b, \quad (51)$$

where the loops are considered to have no orientation, whence the absence of the factor $\frac{1}{2}$, and no longer rooted, whence the absence of the factor L^d .

For a noninteracting theory, $z_b(a)$ can be obtained simply from Eq. (20) by putting the end-to-end vector $n - n'$ to zero there. Equation (50) then

reads explicitly

$$\ln Z_0 = \frac{N}{2} L^d \int_{-\pi}^{\pi} \frac{d^d q}{(2\pi)^d} \sum_{b=1}^{\infty} \frac{1}{b} \left[2K \sum_{\mu} \cos(q_{\mu}) \right]^b. \quad (52)$$

Repeating the same steps leading to Eq. (22), one finds

$$\begin{aligned} \ln Z_0 &= \frac{N}{2} L^d \sum_{b=1}^{\infty} \int_{-\pi}^{\pi} \frac{d^d q}{(2\pi)^d} \frac{1}{b} e^{-(q^2 + m^2 a^2)b/2d} \\ &= \frac{N}{2} L^d \sum_{b=1}^{\infty} \frac{1}{b} \left(\frac{d}{2\pi b} \right)^{d/2} e^{-m^2 a^2 b/2d}. \end{aligned} \quad (53)$$

It follows that the logarithm of the partition function has the form^{21,22}

$$\ln Z_0 / L^d \sim \sum_b \ell_b, \quad (54)$$

with the loop distribution

$$\ell_b \sim b^{-\tau} e^{-\theta b}, \quad (55)$$

denoting the average number (per lattice site) of times a closed worldline of b steps occurs on the lattice. The parameter $\theta \propto m^2$ physically determines the line tension of the loops, while the algebraic factor in the loop distribution, characterized by the exponent $\tau = d/2 + 1$, is an entropy factor, giving a measure of the number of ways a loop of b steps can be embedded in the lattice.

A more familiar expression for $\ln Z_0$ is obtained by again first carrying out the sum over the loop length b in Eq. (52):

$$\begin{aligned} \ln Z_0 &= -\frac{N}{2} L^d \int_{-\pi}^{\pi} \frac{d^d q}{(2\pi)^d} \ln \left[1 - 2K \sum_{\mu} \cos(q_{\mu}) \right] \\ &= -\frac{N}{2} \Omega \int_{-\pi/a}^{\pi/a} \frac{d^d k}{(2\pi)^d} \ln \left\{ 2 \sum_{\mu} [1 - \cos(k_{\mu} a)] + m^2 a^2 \right\}, \end{aligned} \quad (56)$$

where in the last step an irrelevant additive factor is ignored and $\Omega = (La)^d$ is the volume of the spacetime box. This is the standard representation of the logarithm of the partition function describing a free field theory on a hypercubic lattice. In the continuum limit $a \rightarrow 0$, the momentum integral can again best be carried out by using the Schwinger proper time representation this time of the logarithm,

$$\ln(a) = \lim_{z \rightarrow 0} \frac{1}{z} - \int_0^{\infty} \frac{ds}{s} e^{-sa}, \quad (57)$$

where the first term is an irrelevant diverging contribution. Apart from further irrelevant additive constants this leads to

$$\begin{aligned}\ln Z_0 &= \ln \text{Det}^{-N/2} (-\partial_\mu^2 + m^2) \\ &= -\frac{N}{2} \Omega \int_{-\infty}^{\infty} \frac{d^d k}{(2\pi)^d} \ln (k^2 + m^2) \\ &= \frac{N}{2} \Omega \int_0^\infty \frac{ds}{s} \left(\frac{1}{4\pi s} \right)^{d/2} e^{-sm^2},\end{aligned}\quad (58)$$

where the operator $-\partial_\mu^2 + m^2$ is the continuum limit of Λ introduced in Eq. (13). The right hand of Eq. (58) forms the continuum limit of the lattice expression in the last line of Eq. (53) with the number of steps b taken by the particle assuming the role of the Schwinger proper time parameter s : $ba^2/2d \equiv s$ as in Eq. (28).

On account of the path integral (30) with $x = x'$, the last two factors in the integrand at the right hand of Eq. (58) can be written as a path integral over *closed* worldlines

$$e^{-sm^2} \left(\frac{1}{4\pi s} \right)^{d/2} = \oint Dx(s') \exp \left\{ - \int_0^s ds' [\frac{1}{4}\dot{x}^2(s') + m^2] \right\}, \quad (59)$$

where the notation $\oint Dx(s')$ refers to closed paths. In this way, $\ln Z_0$ expressed as a path integral reads¹⁹

$$\begin{aligned}\ln Z_0 &= \ln \text{Det}^{-N/2} (-\partial_\mu^2 + m^2) \\ &= \frac{N}{2} \Omega \int_0^\infty \frac{ds}{s} \oint Dx(s') \exp \left\{ - \int_0^s ds' [\frac{1}{4}\dot{x}^2(s') + m^2] \right\},\end{aligned}\quad (60)$$

where the argument of the exponential function is given by (minus) the classical action (33) of the point particle tracing out its trajectories in spacetime. An easy mnemonic for remembering the main ingredients of this formula is to interpret $-\partial_\mu^2 + m^2$ as the Hamilton operator describing the motion of a *nonrelativistic* particle of mass $M = \frac{1}{2}$ in a constant potential $V = m^2$ in d dimensions. With the Schwinger proper time s interpreted as Newtonian time, W_0 is the corresponding nonrelativistic action, where it is recalled that in natural units $\hbar = 1$.

The first line in Eq. (58) is sometimes represented by the one-loop Feynman diagram

$$\ln Z_0 = \bigcirc. \quad (61)$$

In the spacetime approach, this diagram stands for all the terms in the sum (50), each consisting of a *single* worldline starting and ending at a given site

n . That is, the Feynman diagram at the same time denotes the topology of the particle trajectories contributing to $\ln Z_0$.³⁴

The partition function, obtained by exponentiating Eq. (50), can be written in terms of Feynman diagrams as

$$Z_0 = 1 + \bigcirc + \frac{1}{2!} \bigcirc \bigcirc + \frac{1}{3!} \bigcirc \bigcirc \bigcirc + \dots \quad (62)$$

Each diagram involves a separate integration over loop momentum k_μ . With the right hand of Eq. (62) taken as picturing the topology of the particle trajectories contributing to the partition function, it follows that Z_0 describes a loop gas – a grand canonical ensemble of fluctuation loops of arbitrary shape and length.²⁰ Being a noninteracting theory, the closed worldlines can freely intersect themselves or other worldlines and even share bonds. On the spacetime lattice, the loop gas (62) can be expressed as a sum over all possible tangles of closed paths

$$Z_0 = \sum_{\text{loops}} K^b N^l, \quad (63)$$

with b and l denoting the total number of occupied bonds and separate loops forming a given tangle. In Eq. (63), the loops are no longer considered to be rooted, i.e., they can start and end at any spacetime coordinate in the system. In comparison with rooted closed paths, i.e., closed paths all starting at a given spacetime coordinate, this yields a spacetime volume factor Ω . In the continuum, Eq. (63) translates into the path integral representation

$$Z_0 = \sum_{l=0}^{\infty} \frac{1}{l!} \left(\frac{N}{2} \right)^l \prod_{r=1}^l \left[\Omega \int_0^\infty \frac{ds_r}{s_r} \oint Dx_r(s'_r) \right] e^{-W_0^{(l)}}, \quad (64)$$

as follows from Eq. (60). Here, $W_0^{(l)}$ denotes the extension of the single particle action (33) to l particles:

$$W_0^{(l)} = \sum_{r=1}^l \int_0^{s_r} ds'_r \left[\frac{1}{4} \dot{x}_r^2(s'_r) + m^2 \right]. \quad (65)$$

2.3. $|\phi|^4$ Field Theory

We next perturbatively include the interaction in the theory (2). At the level of the partition function (1), this boils down to expanding the interaction term of the action in a Taylor series

$$e^{-(g/4!)a^d \sum_x \varphi_x^4} = 1 - \frac{g}{4!} a^d \sum_x \varphi_x^4 + \frac{1}{2!} \left(\frac{g}{4!} \right)^2 a^{2d} \sum_{x,x'} \varphi_x^4 \varphi_{x'}^4 + \dots \quad (66)$$

The terms in this expansion can all be represented by Feynman diagrams.^{10,12} Figure 3 shows the 2- and 3-loop diagrams contributing to $\ln Z$ as an example. Each loop, considered to have no orientation, carries a factor of N . The contact interaction is represented by a dashed line for convenience, each carrying a weight $\propto g$. In the equivalent spacetime approach, Feynman diagrams are understood as spacetime diagrams. Each loop of a Feynman diagram is expressed in a hopping expansion as in the noninteracting theory, with the interaction standing for an intersection between different worldlines or between different parts of a single worldline (self-intersection). In addition to the ones indicated, a worldline contributing to a given Feynman diagram may have further intersections, but these are treated as in the noninteracting case, i.e., as nonexistent. Put differently, apart from the intersections explicitly indicated, the particle trajectories still behave as phantom paths.

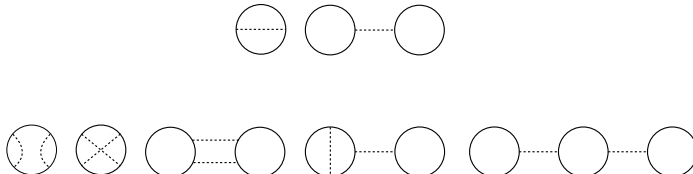


Fig. 3. Two- and 3-loop Feynman diagrams contributing to $\ln Z$ of the $|\varphi|^4$ theory.

Picturing the topology of closed worldlines, the first Feynman diagram ($\propto N$) of the 2-loop contributions ($\propto g^2$) in Fig. 3 represents single closed particle trajectories of arbitrary length and shape with one self-intersection carrying a factor of g . The second Feynman diagram ($\propto N^2$) represents two intersecting closed worldlines. The 3-loop contributions ($\propto g^3$) represent single closed worldlines with two self-intersections (1st and 2nd diagram $\propto N$), two closed worldlines intersecting twice (3rd diagram $\propto N^2$), two closed worldlines intersecting once with one of the two having in addition one self-intersection (4th diagram $\propto N^2$), and finally three closed worldlines (last diagram $\propto N^3$) connected by two intersections.

Similarly, the n th order contributions to $\ln Z$, corresponding to the $(n-1)$ th term ($\propto g^{n-1}$) in the Taylor expansion (66), all involve a total of $n-1$ intersections (including self-intersections) and up to n separate loops. The resulting loop gas is similar to that of the free theory, but the random loops are no longer phantom loops as the intersections explicitly indicated

carry a weight $\propto g$. In the path integral formulation, this is reflected by an additional steric repulsion in the worldline action,

$$W^{(l)} = \sum_{r=1}^l \int_0^{s_r} ds'_r [\frac{1}{4}\dot{x}_r^2(s'_r) + m^2] + \frac{g}{6} \sum_{r,r'=1}^l \int_0^{s_r} ds'_r \int_0^{s_{r'}} ds'_{r'} \delta [x_r(s'_r) - x_{r'}(s'_{r'})], \quad (67)$$

where the sums \sum_r and $\sum_{r'}$ extend over the l particle trajectories assumed to be present. The net result is that (self-)intersections are suppressed and the random loops tend to become mutually and self-avoiding. The more so, the larger the coupling constant g becomes. Turning on the interaction thus changes the typical form of the random loops and in particular their fractal structure.

To derive Eq. (67), we follow Symanzik³⁶ and write the interaction term in the action (2) in the continuum limit as a functional integral over an auxiliary field σ

$$\exp\left(-\frac{g}{4!} \int d^d x \varphi^4\right) = \int D\sigma \exp\left[-\int d^d x \left(\frac{6}{g}\sigma^2 - i\sigma\varphi^2\right)\right], \quad (68)$$

up to an irrelevant prefactor. The partition function (1) then becomes in the continuum limit

$$\begin{aligned} Z &= \int D\varphi D\sigma \exp\left\{-\int d^d x \left[\frac{1}{2}(\partial_\mu\varphi)^2 + \frac{m^2}{2}\varphi^2 - i\sigma\varphi^2 + \frac{6}{g}\sigma^2\right]\right\} \\ &= \int D\sigma \text{Det}^{-N/2}(-\partial_\mu^2 + m^2 - 2i\sigma) \exp\left(-\frac{6}{g} \int d^d x \sigma^2\right) \\ &= \int D\sigma \sum_{l=0}^{\infty} \frac{1}{l!} \left(\frac{N}{2}\right)^l \prod_{r=1}^l \left[\Omega \int_0^\infty \frac{ds_r}{s_r} \oint Dx_r(s'_r)\right] \exp\left(-\frac{6}{g} \int d^d x \sigma^2\right) \\ &\quad \times \exp\left(-\sum_{r=1}^l \int_0^{s_r} ds'_r \left\{\frac{1}{4}\dot{x}_r^2(s'_r) + m^2 - 2i\sigma[x_r(s'_r)]\right\}\right) \end{aligned} \quad (69)$$

where the last equality follows from the previous result (64). The auxiliary field σ is a function of the coordinates along the particle trajectories, $\sigma =$

$\sigma[x_r(s'_r)]$. A simple Gaussian integration yields

$$\begin{aligned} \int D\sigma \exp \left\{ -\frac{6}{g} \int d^d x \sigma^2 + 2i \sum_{r=1}^l \int_0^{s_r} ds'_r \sigma [x_r(s'_r)] \right\} \\ = \exp \left\{ -\frac{g}{6} \sum_{r,r'=1}^l \int_0^{s_r} ds'_r \int_0^{s_{r'}} ds'_{r'} \delta [x(s'_r) - x(s'_{r'})] \right\}, \quad (70) \end{aligned}$$

again up to an irrelevant prefactor. Using this in the last expression for Z , we obtain the spacetime representation of the partition function of the φ^4 theory

$$Z = \sum_{l=0}^{\infty} \frac{1}{l!} \left(\frac{N}{2} \right)^l \prod_{r=1}^l \left[\Omega \int_0^{\infty} \frac{ds_r}{s_r} \oint Dx_r(s'_r) \right] e^{-W^{(l)}}, \quad (71)$$

with the classical action $W^{(l)}$ of the point particles tracing out their world-lines given in Eq. (67). The l th term in this sum describes a tangle of l loops. Since the number of loops can be arbitrary large, Eq. (71) denotes the partition function of a grand canonical ensemble of fluctuation loops, each of arbitrary length and shape, with steric repulsion.

Surprisingly, as was first pointed out by Balian and Toulouse,³⁷ the non-interacting theory can be recovered from the interacting theory by taking the number of field components $N \rightarrow -2$. Consider a contribution to the partition function involving the first vertex in Fig. 4. Assume that leg 1 is connected through the rest of the Feynman diagram to leg 2. Both legs carry the same spin index α , which after taking the sum yields a factor of N . Legs 3 and 4 are necessarily also connected through the rest of the Feynman diagram. They carry the same spin index β , say, which after taking the sum also yields a factor of N . Replacing the first vertex with the second or third vertex in Fig. 4 yields identical contributions save for a change in topology regarding the routings of the spin indices. Specifically, the graph with the first vertex involves two different sets of spin indices: α and β , whereas the graphs with the second or third vertex involve only a single set of spin indices as $\alpha = \beta$. Since the first graph carries an extra factor of $N = -2$ (the loop fugacity) after the sum over the spin index is taken, the three graphs cancel. All other graphs involving vertices cancel in the same fashion three by three. What remains are phantom loops of a noninteracting theory.

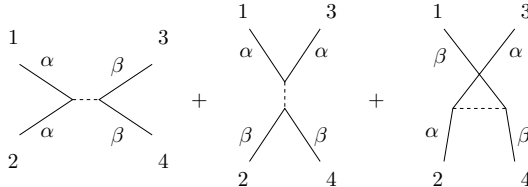


Fig. 4. The representation of the vertex of the φ^4 theory by a dashed line makes the routings of the field components, labelled by α and β , explicit.

2.4. $O(N)$ Spin Model

Whereas the free theory discussed in Sec. 2.1 corresponds to taking the coupling constant $\lambda \rightarrow 0$ in the action (8), the $O(N)$ spin model corresponds to taking the opposite limit, $\lambda \rightarrow \infty$. As for $\lambda \rightarrow 0$, the theory becomes quadratic also in this limit of infinite repulsion. The theory is nevertheless nontrivial because of the fixed-length constraint $\phi_n^2 = N$ at each lattice site. Instead of considering the conventional Boltzmann weight $\exp(K\phi_n \cdot \phi_{n'})$, often a simplified representative of the $O(N)$ universality class is studied, obtained by truncating that weight³⁸

$$Z = \text{Tr} \prod_{\langle n, n' \rangle} (1 + K\phi_n \cdot \phi_{n'}). \quad (72)$$

The product is restricted to nearest neighbour pairs. The remaining factor in the on-site measure (10) becomes trivial in this limit and has been ignored. The main difference with the original spin model is that in the truncated model bonds cannot be multiply occupied. It is generally accepted that this simplification does not change the universal properties of the theory.

The hopping expansion is usually referred to the *high-temperature expansion* in the context of spin models. Also for the truncated model, it corresponds to expanding the partition function in terms of the parameter K . The contributions to Z can again be visualized by graphs on the lattice.¹³ As will be detailed below for the Ising model, only closed graphs with an even number of occupied bonds connecting each vertex yield nonzero contributions. The virtue of the truncated model is that bonds cannot be multiply occupied. In contrast, no restriction on multiple occupancies exists in the representation with the usual Boltzmann weight. When formulated on a two-dimensional honeycomb lattice, which has coordination number $z = 3$, the high-temperature graphs of the truncated model are automatically mutually and self-avoiding;³⁸ a given lattice site is either empty or has one bond entering and one leaving the site (see Fig. 5).

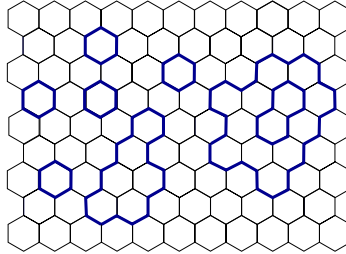


Fig. 5. Closed high-temperature graphs on a honeycomb lattice automatically form mutually and self-avoiding loops.

The partition function can then be written geometrically as a sum over all possible mutually and self-avoiding (MSA) loops,³⁸

$$Z = \sum_{\substack{\text{MSA} \\ \text{loops}}} N^l K^b, \quad (73)$$

with b and l the number of occupied bonds and separate loops forming the graph. Equation (73) constitutes the high-temperature representation of the partition function. As for the noninteracting field theory (63), each occupied bond carries a weight K (bond fugacity) and each loop carries a weight N (loop fugacity). Whereas the random loops of the noninteracting field theory are phantom loops that can freely intersect and share bonds, here they are mutually and self-avoiding. As before, they physically denote the worldlines of the particles described by the quantum field theory.

The $O(N)$ spin-spin correlation function

$$\langle \phi_n^\alpha \phi_{n'}^\beta \rangle = \frac{1}{Z} \prod_m \int d\phi_m \phi_n^\alpha \phi_{n'}^\beta \exp \left(K \sum_{\langle m, m' \rangle} \phi_m \cdot \phi_{m'} \right), \quad (74)$$

is represented diagrammatically by a modified partition function, obtained by requiring that the two sites n and n' are connected by an open high-temperature graph.¹³ On a honeycomb lattice, the scaling part of the correlation function is given by the connected graphs

$$\langle \phi_n^\alpha \phi_{n'}^\beta \rangle \sim \frac{1}{2} \delta_{\alpha, \beta} \sum_{\text{graphs}} K^b = \frac{1}{2} \delta_{\alpha, \beta} \sum_b z_b(n, n') K^b, \quad (75)$$

where $z_b(n, n')$ is the number of (open) mutually and self-avoiding graphs along b bonds connecting the lattice sites n and n' . Strictly speaking, $\langle \phi_n^\alpha \phi_{n'}^\beta \rangle < \frac{1}{2} \delta_{\alpha, \beta} \sum_{\text{graphs}} K^b$ as the cancellation of the disconnected graphs

in the numerator and Z in the denominator, required for an equality, is not complete: For a given open graph, certain loops present in Z are forbidden in the modified partition function as they would intersect the open graph, or occupy bonds belonging to it, which is not allowed. In other words, the presence of an open graph influences the loop gas and *vice versa*. Since each loop carries a factor N , the loop gas is absent in the limit $N \rightarrow 0$, pioneered by de Gennes.¹⁴ The inequality in Eq. (75) becomes an equality in this limit, and the open graphs become ordinary self-avoiding random walks on a honeycomb lattice. These walks physically describe polymers in good solvents at sufficiently high temperatures so that the van der Waals attraction between monomers is irrelevant. For the noninteracting theory, where the worldlines are phantom trajectories, the loops cancel, so that the corresponding correlation function is exactly given by the open trajectories connecting the endpoints [see Eq. (16)].

For a d -dimensional hypercubic lattice, the coordination number is $z = 2d$, so that intersections are now possible. Although the bonds of the truncated model (72) can by construction still not be multiply occupied, the high-temperature graphs are no longer mutually and self-avoiding. After rescaling the bond fugacity $K \rightarrow K/N$, the partition function (72) can be written as⁴⁰

$$Z = \sum_{\text{loops}} \nu_2^{m_2} \nu_4^{m_4} \cdots \nu_{2d}^{m_{2d}} N^l \left(\frac{K}{N} \right)^b, \quad (76)$$

where m_2, \dots, m_{2d} indicate the number of intersections of $2k$ bonds ($k = 1, \dots, d$) forming a given tangle of b bonds and l loops. An intersection of $2k$ bonds carries the weight⁴¹

$$\nu_{2k} = \frac{N^k \Gamma(N/2)}{2^k \Gamma(k + N/2)} = \frac{N^k}{N(N+2)\cdots(N+2k-2)}. \quad (77)$$

Due to the rescaling of the bond fugacity, $\nu_2 = 1$ for all N . In the limit $N \rightarrow 0$, only the weight ν_2 survives as $\nu_{2k} \rightarrow 0$ for $k > 1$, implying that even on a hypercubic lattice, intersections are completely suppressed and the high-temperature graphs reduce to self-avoiding walks.

In the opposite limit, $N \rightarrow \infty$, all the vertex weights become unity $\nu_{2k} \rightarrow 1$, and the partition function (76) takes the noninteracting form (63) after undoing the rescaling of the bond fugacity. The only difference with the noninteracting theory is that for a given number of set bonds b , only the graph with the highest number of loops needs to be included as it dominates all other graphs. This limit corresponds to the so-called spherical model.^{13,39}

The loop representation (76), featuring colourless loops, obtains by resolving a vertex where $2k$ bonds of an high-temperature graph meet into all possible routings of the paths (see Figs. 6 and 7). The number of rout-

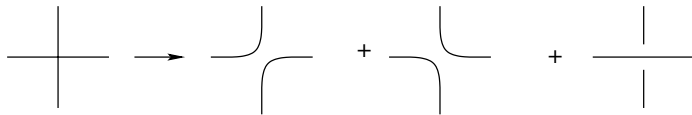


Fig. 6. A vertex with four bonds ($k = 2$) resolved into three possible routings of the paths.

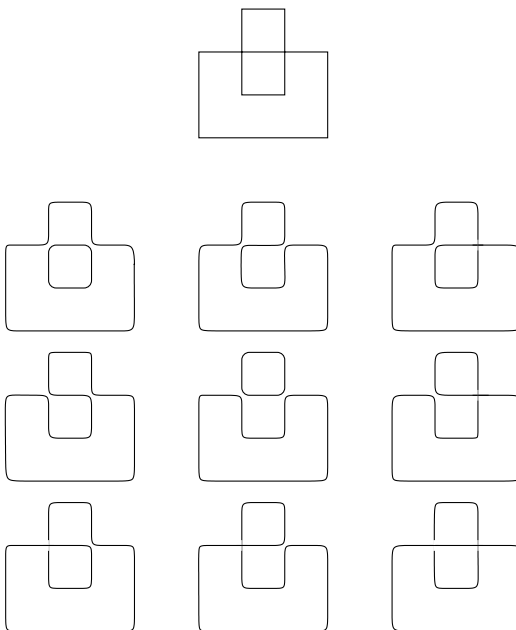


Fig. 7. A graph (top panel) involving two vertices with four bonds ($k = 2$) is resolved into 9 different loop configurations according to the rule displayed in Fig. 6.

ings equals the number of ways $2k$ objects can be divided into k distinct pairs, i.e., $(2k - 1)!!$. Each of the routings carries the same weight. A given high-temperature graph is thus resolved into loop configurations, and the partition function (76) describes a loop gas, as does Eq. (73). The loops

physically represent worldlines that can now intersect. Although loops on a honeycomb lattice cannot do so, for both the honeycomb and square lattice the same large-scale behaviour is obtained. This implies that the operator which introduces intersections is an irrelevant perturbation at the critical point.⁴²

It is worth pointing out that in the high-temperature representation, the observation that $N = -2$ describes phantom loops is far from obvious. On a square lattice, for example, a graph of b bonds and one vertex where four bonds meet contributes the following term to the partition function,

$$\lim_{N \rightarrow -2} \nu_4 N(N+2) \left(\frac{K}{N} \right)^b = (-2)^2 \left(-\frac{K}{2} \right)^b, \quad (78)$$

which is finite because the weight factor ν_4 given in Eq. (77) diverges in the limit $N \rightarrow -2$. The diagrams no longer cancel three by three as they did in Sec. 2.3

2.5. Ising Model

As an explicit example, we consider the simplest $O(N)$ model, viz. the Ising model ($N = 1$) on a square lattice. The model is defined by the Hamiltonian

$$H = -J \sum_{\langle nn' \rangle} \phi_n \phi_{n'}, \quad (79)$$

where the spins can take only two values $\phi_n = \pm 1$, and the interaction parameter J is taken to be unity. The standard partition function reads

$$Z = \text{Tr } e^{-\beta H} = \text{Tr} \prod_{\langle nn' \rangle} e^{\beta \phi_n \phi_{n'}}, \quad (80)$$

with the trace Tr denoting the sum over all possible spin configurations. In the context of statistical physics, β denotes the inverse temperature $\beta = 1/k_B T$, with k_B Boltzmann's constant. In the present context, we regard β as coupling constant. Because of the identity

$$e^{\beta \phi_n \phi_{n'}} = \cosh \beta (1 + K \phi_n \phi_{n'}), \quad (81)$$

with $K = \tanh \beta$, the standard representation can be rewritten in the truncated form (72) as:

$$Z = (\cosh \beta)^{2N} \text{Tr} \prod_{\langle nn' \rangle} (1 + K \phi_n \phi_{n'}) \quad (82)$$

up to an irrelevant prefactor. Here, $2N$ denotes the total number of bonds on a square lattice with N sites and periodic boundary conditions. The right

hand contains a total of $2N$ factors, one for each bond, and therefore a total of 2^{2N} terms when multiplied out. Each term can be visualized by a graph along the bonds on the lattice, with each bond representing a pair of adjacent spins. Because of the trace in the definition of the partition function, a graph having a loose end does not contribute to Z . Indeed, let the spin at the loose end be ϕ_n then the sum over its possible configurations yields zero, $\sum_{\phi_n=\pm 1} \phi_n = 0$. As a result, only *closed* graphs contribute. Similarly, only those closed graphs with an even number of bonds, i.e., two or four for a square lattice, connecting each vertex of the graph yield nonzero contributions. Such a vertex contributes a factor of two as $\sum_{\phi_n=\pm 1} \phi_n^m = 2$ for m even. The high-temperature representation of the Ising model therefore involves a sum over all possible closed graphs that can be drawn on the lattice:

$$Z = (\cosh \beta)^{2N} 2^N \sum_{\substack{\text{closed} \\ \text{graphs}}} K^b. \quad (83)$$

A graph of b bonds can be built from various disconnected closed subgraphs. The high-temperature representation is to be compared with the loop representation (76), which reduces to

$$Z = \sum_{\text{loops}} \left(\frac{1}{3}\right)^m K^b, \quad (84)$$

for $N = 1$ on a square lattice, with m denoting the number of vertices with four bonds. Remembering that the loop representation is obtained by resolving each of these vertices according to the rule given in Fig. 6, we see that apart from an irrelevant prefactor the two expressions coincide. The Ising model ($N = 1$) is special as the loop fugacity is unity, so that the contribution of a closed graph depends only on the number of bonds it occupies.

The correlation function of the Ising model,

$$\begin{aligned} \langle \phi_n \phi_{n'} \rangle &= \frac{1}{Z} \text{Tr} \phi_n \phi_{n'} \prod_{\langle mm' \rangle} e^{\beta \phi_m \phi_{m'}}, \\ &= \frac{1}{Z} (\cosh \beta)^{2N} \text{Tr} \phi_n \phi_{n'} \prod_{\langle mm' \rangle} (1 + K \phi_m \phi_{m'}), \end{aligned} \quad (85)$$

can similarly be visualized by graphs on the lattice. Each graph now contains a subgraph connecting the lattice sites n and n' . All other subgraphs must be closed and, except for the endpoints, all vertices must be even as

before. In terms of these graphs,

$$\langle \phi_n \phi_{n'} \rangle = \frac{1}{Z} (\cosh \beta)^{2N} 2^N \sum_{\text{graphs}} K^b. \quad (86)$$

2.6. Summary

In the spacetime approach to quantum field theory on a lattice, which is geometric in nature, the partition function and the correlation function are calculated in a hopping expansion, thus reducing the problem to counting paths on the lattice. Physically, the paths represent the worldlines traced out by the particles when hopping from one lattice site, representing a spacetime cell, to an adjacent site. The noninteracting lattice field theory features phantom worldlines that can freely intersect and share bonds. When the self-interaction is turned on, by taking the coupling constant $\lambda > 0$, intersections carry an energy penalty. This has the effect to suppress such configurations and as a result the particle trajectories tend to avoid themselves. In the limit of infinite repulsion $\lambda \rightarrow \infty$, the ϕ^4 lattice field theory reduces to the $O(N)$ spin model. The hopping expansion, known in this context as the high-temperature expansion, takes a particular simple form when the truncated $O(N)$ model (72) is implemented on a honeycomb lattice. The worldlines are then by construction mutually and self-avoiding. Since the large-scale behaviour of this representative of the $O(N)$ universality class on the honeycomb lattice is the same as for the generic ϕ^4 field theory defined on a square lattice, both multiply occupancy of bonds and intersections are irrelevant. At large scales, both loop gases have the same fractal structure. Even when considering weak repulsion by taking λ small, after coarse-graining the fractal structure of the loops appears the same as in the limit $\lambda \rightarrow \infty$. This limit therefore governs the large-scale behaviour.

3. Critical Properties

In this section, the critical properties of the $O(N)$ universality class are discussed from the perspective of worldlines. In particular, the fractal structure of the loop gas featuring in the spacetime approach to fluctuating fields close to the critical point is studied. It is shown how the critical exponents characterizing the phase transition can be obtained from the fractal structure of these geometrical objects. The discussion is geared after percolation theory, which is purely geometric in nature.⁴³

3.1. Fractal Structure

Consider the $O(N)$ theory close to the point where it undergoes a continuous phase transition to the ferromagnetic state, where the spins prefer to point in one direction in spin space. This phase transition is associated with the spontaneous breaking of the $O(N)$ symmetry to the subgroup $O(N-1)$ which includes rotations about the preferred spin direction. The logarithm of the partition function of the interacting theory can in the vicinity of this critical point be written in a form similar to the one found in Eq. (54) for the noninteracting theory as

$$\ln Z/\Omega \sim \sum_b \ell_b. \quad (87)$$

The worldline loop distribution ℓ_b asymptotically splits into two factors as it did for the phantom loops in Eq. (55):

$$\ell_b \sim b^{-\tau} e^{-\theta b}, \quad (88)$$

with τ an exponent characterizing the interacting theory. The value $\tau = d/2 + 1$ found for phantom loops is typical for a noninteracting theory where the loops are simple closed Brownian trajectories. Formally, Eq. (87) is the same as for clusters in percolation theory close to the percolation threshold. As in that context,⁴³ τ can be related to the fractal dimension of the loops. Consider the square radius of gyration R_b^2 of a loop of b steps

$$R_b^2 = \frac{1}{b} \sum_{i=1}^b (n_i - \bar{n})^2 = \frac{1}{2b^2} \sum_{i,j=1}^b (n_i - n_j)^2, \quad (89)$$

with n_i denoting the lattice sites visited by the particle while tracing out its worldline on the spacetime lattice, and $\bar{n} = (1/b) \sum_{i=1}^b n_i$ the centre of mass of the loop. Asymptotically, the average $\langle R_b^2 \rangle$ scales with the number of steps b taken as

$$\langle R_b^2 \rangle \sim b^{2/D}, \quad (90)$$

which defines the Hausdorff, or fractal dimension D . This average yields the typical linear size of a loop of b steps. Specifically, such a loop is distributed over a volume of typical linear size $\langle R_b^2 \rangle^{1/2}$. Given the definition of the loop distribution ℓ_b as the average number (per lattice site) of loops of b steps present, it follows that $b\ell_b$ is the probability that a randomly chosen lattice site belongs to such a loop, and

$$b\ell_b \sim 1/\langle R_b^2 \rangle^{d/2}, \quad (91)$$

with d the dimension of the spacetime box. This leads to the relation

$$\tau = \frac{d}{D} + 1, \quad (92)$$

which is formally the same as in percolation theory.⁴³

3.2. Loop Proliferation

The Boltzmann factor in the loop distribution (88) exponentially suppresses long loops as long as the line tension θ is finite. Upon approaching the critical point, the line tension vanishes as a power law,

$$\theta \sim (K_c - K)^{1/\sigma}, \quad (93)$$

with σ a second exponent characterizing the loop distribution. When this happens, the loops can grow arbitrarily long at no cost and the entire system becomes⁴⁴ “pierced through and through with” worldlines. It is through this *loop proliferation*²⁰ that a phase transition manifests itself in the spacetime approach. The phenomenon is completely analogous to the sudden appearance at the percolation threshold of a cluster spanning the infinite lattice in percolation phenomena.

In the field theoretic approach, the phase transition manifests itself through a nonzero vacuum expectation value of the field ϕ_n^α , where the component α indicates the preferred spin direction spontaneously chosen by the system. Since all possible directions are equivalent, the system can choose any of these. On a finite lattice, the system can easily change its preferred direction. This is in particular the case for Monte Carlo simulations using a nonlocal update, such as the Swendsen-Wang,⁴⁵ or Wolff⁴⁶ algorithm, in which not individual spins are updated, but entire clusters. For this reason, the following order parameter is frequently used in lattice simulations:⁴⁷

$$\mathcal{O} = \frac{1}{L^d} \left[\sum_\alpha \left(\sum_n \phi_n^\alpha \right)^2 \right]^{1/2}. \quad (94)$$

With this choice of the order parameter, all possible directions are treated equally. In the normal phase, the expectation value of this operator vanishes. At the critical point, a condensate forms and a nonzero expectation value develops,

$$\langle \mathcal{O} \rangle \neq 0, \quad (95)$$

typical for the ferromagnetic state with the spins pointing in a preferred direction in spin space. Those particles tracing out long worldlines all belong to the condensate.

The loop distribution (88) is related to the number of paths $z_b(a)$ of b steps returning to a site adjacent to the initial position through

$$\ell_b = \frac{1}{b} z_b(a) K^b. \quad (96)$$

Because $z_b(a)$ refers to closed worldlines, the factor $1/b$ is included to prevent overcounting as a given loop can be traced out starting at any lattice site along that loop. It should be noted that in Eq. (96) rooted loops are considered, i.e., all loops run through an arbitrary but fixed lattice site n . The relation (96) implies that $z_b(a)$ scales as

$$z_b(a) K^b \sim b^{-d/D} e^{-\theta b}. \quad (97)$$

Similarly, the number of paths z_b of b steps starting at n and ending at an arbitrary lattice site defined in Eq. (40) scales as

$$z_b K^b \sim b^{\vartheta/D} e^{-\theta b}, \quad (98)$$

with ϑ a new exponent, characterizing the number of ways an open path of b steps can be embedded in the lattice. It is worth pointing out that in contrast to the loop exponents τ and σ , this third exponent refers to open paths. Its value is expected to be positive because the number of possible rooted open paths with no constraint on their endpoints increases with the number of steps b . This is in contrast to the loop distribution (88), where the algebraic factor decreases with increasing b , reflecting the increasing difficulty for a path to close. According to Eq. (39), the ratio of $z_b(n, n')$ and z_b defines the probability $P_b(n, n')$ for a particle to move from the lattice site n on the spacetime lattice to n' in b steps. On general grounds, it scales at criticality as:

$$P_b(n, n') \sim b^{-d/D} P(|n - n'|/b^{1/D}), \quad (99)$$

with P a scaling function. This generalizes the Gaussian distribution (44) found for the noninteracting theory. Consistency of the three scaling formulas (97), (98), and (99), requires, as was first shown by McKenzie and Moore⁴⁸ for self-avoiding random walks, that the scaling function $P(t)$ must vanish for $t \rightarrow 0$ as a power law,

$$P(t) \approx t^\vartheta, \quad (100)$$

with the same exponent governing the *asymptotic* behaviour (98) of the number z_b of open paths at the critical point ($\theta = 0$).

3.3. Critical Exponents

As in percolation theory, the loop exponent σ is related to the exponent ν , which specifies how the correlation length ξ diverges at the critical point,

$$\xi \sim |K - K_c|^{-\nu}. \quad (101)$$

Physically, ξ indicates the typical length scale in the system. The radius of gyration – a second typical length scale – can be written in terms of ξ as

$$\langle R_b \rangle = \xi R(b\theta), \quad (102)$$

where R is a scaling function and θ is the same parameter as in the loop distribution (88). From the asymptotic behaviour (90), the divergence of the correlation length, and the vanishing (93) of the line tension θ as K_c is approached, the relation³¹

$$\nu = \frac{1}{\sigma D}, \quad (103)$$

or

$$\nu = \frac{\tau - 1}{d\sigma} \quad (104)$$

follows. These relations are formally identical to those in percolation theory.

The rest of the thermal critical exponents can be equally well expressed in terms of the loop exponents and ϑ . To derive these expressions, we write the correlation function in terms of $z_b(n, n')$ as on the honeycomb lattice [see Eq. (75)]

$$\left\langle \phi_n^\alpha \phi_{n'}^\beta \right\rangle \sim \frac{1}{2} \delta_{\alpha, \beta} \sum_b z_b(n, n') K^b = \frac{1}{2} \delta_{\alpha, \beta} \sum_b z_b P_b(n, n') K^b. \quad (105)$$

When evaluated at criticality, where

$$\left\langle \phi_n^\alpha \phi_{n'}^\beta \right\rangle \sim \delta_{\alpha, \beta} / |n - n'|^{d-2+\eta}, \quad (106)$$

Eq. (105) gives

$$\eta = 2 - D - \vartheta. \quad (107)$$

This relation, with ϑ defined by Eq. (100), was recently proposed for the three-dimensional XY, i.e., O(2) model in Ref. [49]. This model describes the superfluid phase transition in ${}^4\text{He}$.

Finally, using the definition of the magnetic susceptibility χ ,

$$\chi = \sum_{n'} \langle \phi_n \cdot \phi_{n'} \rangle \sim \sum_b z_b K^b, \quad (108)$$

which diverges as $\chi \sim |K - K_c|^{-\gamma}$, we find

$$\gamma = \frac{1}{\sigma} \left(1 + \frac{\vartheta}{D} \right). \quad (109)$$

The explicit expressions given for ν , η , and γ satisfy Fisher's scaling relation, $\gamma/\nu = 2 - \eta$, and

$$\frac{\gamma}{\nu} = D + \vartheta. \quad (110)$$

With $\nu = (\tau - 1)/d\sigma$, Eq. (54) yields the scaling relation $d\nu = 2 - \alpha$, where α determines the scaling behaviour of the free energy close to the critical point,

$$\ln Z/\Omega \sim |K - K_c|^{2-\alpha}. \quad (111)$$

The expressions for the other exponents follow by using the remaining scaling relations. We thus have shown that all the thermal critical exponents are determined by the configurational entropy exponents for closed and open particle trajectories, τ and ϑ , respectively, and by σ .

It is worth noting that the thermal critical exponents depend on only *two* independent variables, viz. $D + \vartheta$ and σD . Their significance in field theory is that they determine the anomalous scaling dimensions of the φ and φ^2 fields

$$d_\varphi = \frac{1}{2}(d - D - \vartheta), \quad d_{\varphi^2} = d - \sigma D, \quad (112)$$

respectively.

3.4. Self-Avoiding Random Walks

Before applying the results of the previous section to the two-dimensional $O(N)$ spin model with arbitrary $-2 \leq N \leq 2$, let us first verify that these general results are consistent with the results known in the polymer limit $N \rightarrow 0$,¹⁴ where, as we saw below Eq. (77), the high-temperature graphs reduce to self-avoiding walks. Through the exact enumeration and analysis of the number of self-avoiding loops on a square lattice up to length 110, the value $\tau = 5/2$ for the loop exponent τ has been established to very high precision.⁵⁰ According to Eq. (92), this corresponds to the fractal dimension $D = 4/3$ – a value that has been independently established to high precision in that same study by determining the average square radius of gyration $\langle R_b^2 \rangle$ of the loops. In a related study,⁵¹ where the number z_b of self-avoiding walks on a square lattice up to length 71 has been enumerated and analysed, the value of the exponent ϑ , characterizing the open trajectories has been

established. Specifically, the value $\vartheta/D = 11/32$ was found to high precision, yielding $\vartheta = 11/24$.

In most studies on self-avoiding walks, the fractal dimension of the walks is simply equated to the inverse correlation length. As follows from Eq. (103), this corresponds to setting $\sigma = 1$. A closer inspection of de Gennes' original work on the $N \rightarrow 0$ limit reveals that there indeed $\sigma = 1$.

To sum up, the two configurational entropy exponents τ (loops) and ϑ (open paths), and σ for a self-avoiding walk in two dimensions are given by

$$\tau = 5/2, \quad \vartheta = 11/24, \quad \sigma = 1. \quad (113)$$

With these values, all the critical exponents of the two-dimensional $O(N \rightarrow 0)$ model can be found through the relations of the previous subsection and standard scaling relations.

3.5. $O(N)$ Models

The class of two-dimensional $O(N)$ models for $-2 \leq N \leq 2$ can be parameterized as

$$N = -2 \cos\left(\frac{\pi}{\bar{\kappa}}\right), \quad (114)$$

with $\frac{1}{2} \leq \bar{\kappa} \leq 1$. The fractal dimension D of the high-temperature loops is known exactly⁵²

$$D = 1 + \frac{\bar{\kappa}}{2}, \quad (115)$$

leading to $\tau = (6 + \bar{\kappa})/(2 + \bar{\kappa})$. The observable whose scaling dimension is given by this fractal dimension consists of two spins in different spin states placed at the same site: $\phi_n^\alpha \phi_n^\beta$, with $\alpha \neq \beta$.³⁸ It physically measures the tendency of spins to align, as becomes intuitively clear by remembering that the spins connected by a high-temperature graph are all in the same spin state.

While the fractal dimension of the high-temperature loops is known exactly in two dimensions, the value of the entropy exponent ϑ for open paths has to our knowledge not been directly established for $N \neq 0$. In two dimensions, it can be established indirectly³² by considering the Potts model – a closely related spin model.

That model was reformulated by Fortuin and Kasteleyn⁵³ in a purely geometric fashion in terms of suitably defined spin clusters. The thermal phase transition is marked by a proliferation of these clusters, which moreover have the thermal critical exponents encoded in their fractal structure.

Percolation observables such as the average cluster size and the percolation strength, defined as the probability that a randomly chosen site belongs to the percolating cluster, serve as improved estimators for the magnetic susceptibility and the magnetization, respectively. In other words, the thermal critical exponents of the Potts model can be determined by studying the fractal structure of these so-called Fortuin-Kasteleyn clusters, with the exponents defined as in percolation theory. In two dimensions, the fractal dimension D_C of the Fortuin-Kasteleyn clusters is known exactly⁵⁴

$$D_C = 1 + \frac{\bar{\kappa}}{2} + \frac{3}{8} \frac{1}{\bar{\kappa}}, \quad (116)$$

where the Q -state Potts models are parameterized in terms of the same parameter $\bar{\kappa}$ parameterizing the $O(N)$ models as

$$\sqrt{Q} = -2 \cos(\pi \bar{\kappa}), \quad (117)$$

with $\frac{1}{2} \leq \bar{\kappa} \leq 1$, so that $0 \leq Q \leq 4$. The $Q \rightarrow 0$ Potts model ($\bar{\kappa} = \frac{1}{2}$) describes standard percolation theory. Surprisingly, the external perimeters of the Fortuin-Kasteleyn clusters have the same fractal dimension D as the $O(N)$ loops.⁵⁵ For example, the external perimeters of clusters in standard percolation theory have the dimension $\frac{4}{3}$ as have self-avoiding random walks ($\bar{\kappa} = \frac{2}{3}$). It can be shown that the entropy exponent ϑ for open trajectories and the two Potts dimensions satisfy the sum rule³²

$$d = 2D_C - D - \vartheta, \quad (118)$$

with $d = 2$ the dimension of the spacetime box. With D and D_C known exactly, the expression for ϑ follows.

Finally, the expression for the exponent σ can be inferred from the values $\sigma = 1$ for $N \rightarrow 0$ ($\bar{\kappa} = \frac{2}{3}$) and $\sigma = 0$ for $N = 2$ ($\bar{\kappa} = 1$). This last value reflects the special status of the XY model, undergoing a phase transition of the Berezinskii-Kosterlitz-Thouless type characterized by algebraic long-range order.^{56,57} Assuming, as is the case for Fortuin-Kasteleyn clusters, that both τ and σ have a similar dependence on $\bar{\kappa}$, we deduce that $\sigma = 8(1 - \bar{\kappa})/(2 + \bar{\kappa})$.

To sum up this subsection, the two configurational entropy exponents τ (loops) and ϑ (open worldlines), and σ for the $O(N)$ model with $-2 \leq N \leq 2$ are given in terms of $\bar{\kappa}$ by

$$\tau = \frac{6 + \bar{\kappa}}{2 + \bar{\kappa}}, \quad \vartheta = -1 + \frac{\bar{\kappa}}{2} + \frac{3}{4} \frac{1}{\bar{\kappa}}, \quad \sigma = 8 \frac{1 - \bar{\kappa}}{2 + \bar{\kappa}}. \quad (119)$$

Table 1 collects the resulting values for the various two-dimensional $O(N)$ models together with the corresponding thermal critical exponents. It is

worth pointing out that for $N = -2$ indeed Gaussian exponents are obtained, but that the fractal dimension of the high-temperature graphs is not given by that of a Brownian random walk, which has $D = 2$. Also note that with increasing N , the exponent ϑ decreases, while at the same time the fractal dimension D increases. The ratio ϑ/D appearing in the scaling relation (98) thus decreases with increasing N , implying that the number of possible rooted open paths with no constraint on their endpoints increases less rapidly with the number of steps b for larger N .

Table 1. Critical exponents together with the exponents characterizing the high-temperature graphs (worldlines) of various two-dimensional $O(N)$ models.

Model	N	$\bar{\kappa}$	α	β	γ	η	ν	D	τ	ϑ	σ
Gaussian	-2	$\frac{1}{2}$	1	0	1	0	$\frac{1}{2}$	$\frac{5}{4}$	$\frac{13}{5}$	$\frac{3}{4}$	$\frac{8}{5}$
SAW	0	$\frac{2}{3}$	$\frac{1}{2}$	$\frac{5}{64}$	$\frac{43}{32}$	$\frac{5}{24}$	$\frac{3}{4}$	$\frac{4}{3}$	$\frac{5}{2}$	$\frac{11}{24}$	1
Ising	1	$\frac{3}{4}$	0	$\frac{1}{8}$	$\frac{7}{4}$	$\frac{1}{4}$	1	$\frac{11}{8}$	$\frac{27}{11}$	$\frac{3}{8}$	$\frac{8}{11}$
XY	2	1	$-\infty$	∞	∞	$\frac{1}{4}$	∞	$\frac{3}{2}$	$\frac{7}{3}$	$\frac{1}{4}$	0

3.6. Summary

It was shown that the worldlines or high-temperature graphs of the $O(N)$ theory proliferate right at the thermal critical point, and that the entire set of critical exponents can be retrieved from the fractal structure of these line objects. In this way, a purely geometric description of the phase transition in these systems was arrived at.

4. Monte Carlo Simulations

We next discuss a Monte Carlo study of the Ising model on a square lattice we carried out³⁰ to support the above findings (for a summary of that study, see Ref. [58]). We consider not the original spin formulation of the model, but the high-temperature representation detailed in Sec. 2.5 instead, and examine whether the fractal structure of the high-temperature graphs indeed encodes the thermal critical behaviour. We focus exclusively on the graph configurations and use percolation observables to study the fractal properties of the graphs.

Traditionally, high-temperature expansions are carried out exactly up to a given order by enumerating all possible ways graphs up to an order

that can be embedded in the lattice.³⁴ We take a different approach and study the high-temperature graphs by means of Monte Carlo methods. The Metropolis algorithm⁵⁹ we use involves a local update and for that reason suffers from critical slowing down close the transition temperature. We have intentionally chosen the local update as it allows for a particular clean implementation of our ideas. The price we pay for this is that we cannot study too large spacetime boxes. The largest lattice we can reasonably study is of linear size $L = 256$.

4.1. Plaquette Update

The update algorithm we use in our purely geometric approach of the Ising model directly generates the high-temperature graphs that contribute to the partition function. Specifically, the closed graphs are generated by means of a Metropolis *plaquette* algorithm. A proposed plaquette update resulting in b' occupied bonds is accepted with probability

$$p_{\text{HT}} = \begin{cases} K^{b'-b} & \text{if } b' > b \\ 1 & \text{else} \end{cases}, \quad (120)$$

where b denotes the number of occupied bonds before the update.⁵⁹ In the entire temperature range $0 \leq \beta \leq \infty$, $K = \tanh \beta \leq 1$. Reflecting the Z_2 symmetry of the model, all bonds of an accepted plaquette are changed, i.e., those that were occupied become unoccupied and *vice versa* (see Fig. 8). With b_{\square} denoting the number of bonds on the proposed plaquette already

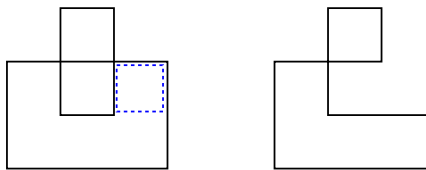


Fig. 8. Plaquette update: An existing high-temperature graph with the plaquette proposed for updating indicated by the broken square (left panel) and the new graph after the proposal is accepted (right panel).

occupied, it follows that

$$b' = b + 4 - 2b_{\square}. \quad (121)$$

The prescription (120) immediately follows from the high-temperature representation (83) of the Ising model. In equilibrium, the probability distri-

bution $P(G)$ for a given graph configuration G involving b occupied bonds reads

$$P(G) = \frac{1}{Z} (\cosh \beta)^{2N} 2^N K^b. \quad (122)$$

Such a configuration can be reached after $t + 1$ iterations from the configuration present after t iterations in the following fashion

$$P(G, t+1) = P(G, t) + \sum_{G'} [P(G', t)W(G' \rightarrow G) - P(G, t)W(G \rightarrow G')], \quad (123)$$

where $W(G \rightarrow G')$ is the probability for the system to move from the graph configuration G with b occupied bonds to the graph configuration G' with b' occupied bonds. In equilibrium, $P(G, t+1) = P(G, t) = P(G)$, and the system satisfies detailed balance

$$P(G')W(G' \rightarrow G) = P(G)W(G \rightarrow G'), \quad (124)$$

or

$$\frac{W(G \rightarrow G')}{W(G' \rightarrow G)} = \frac{P(G')}{P(G)} = \frac{K^{b'}}{K^b}. \quad (125)$$

To maximize the acceptance rate of proposed updates, the largest of the two transition probabilities $W(G \rightarrow G')$ and $W(G' \rightarrow G)$ appearing in the ratio should be given the largest possible value, i.e., one. Thus, if the number of bonds b' in the proposed configuration is larger than the number of bonds b in the present configuration, so that $K^{b'}/K^b < 1$, $W(G' \rightarrow G) = 1$, then $W(G \rightarrow G') = p_{HT}$. On the other hand, if $b' < b$, the proposed configuration carries a larger weight than the present one and will be accepted unconditionally.

By taking plaquettes, i.e., elementary loops on the spacetime lattice as building blocks, the resulting high-temperature graphs are automatically closed (see Fig. 9 for snapshots at three different temperatures).

4.2. Numerical Results

The data was collected on lattices varying in linear size from $L = 16$ to 256 in 3.3×10^5 Monte Carlo sweeps of the lattice close to the critical point and 1.1×10^5 sweeps outside the critical region. About 10% of the sweeps were used for equilibration. After each sweep, the resulting graph configuration was analysed. Statistical errors were estimated by means of binning.

We first determine whether the high-temperature graphs proliferate precisely at the inverse critical temperature $\beta_c = \ln(1 + \sqrt{2})/2 = 0.440686 \dots$

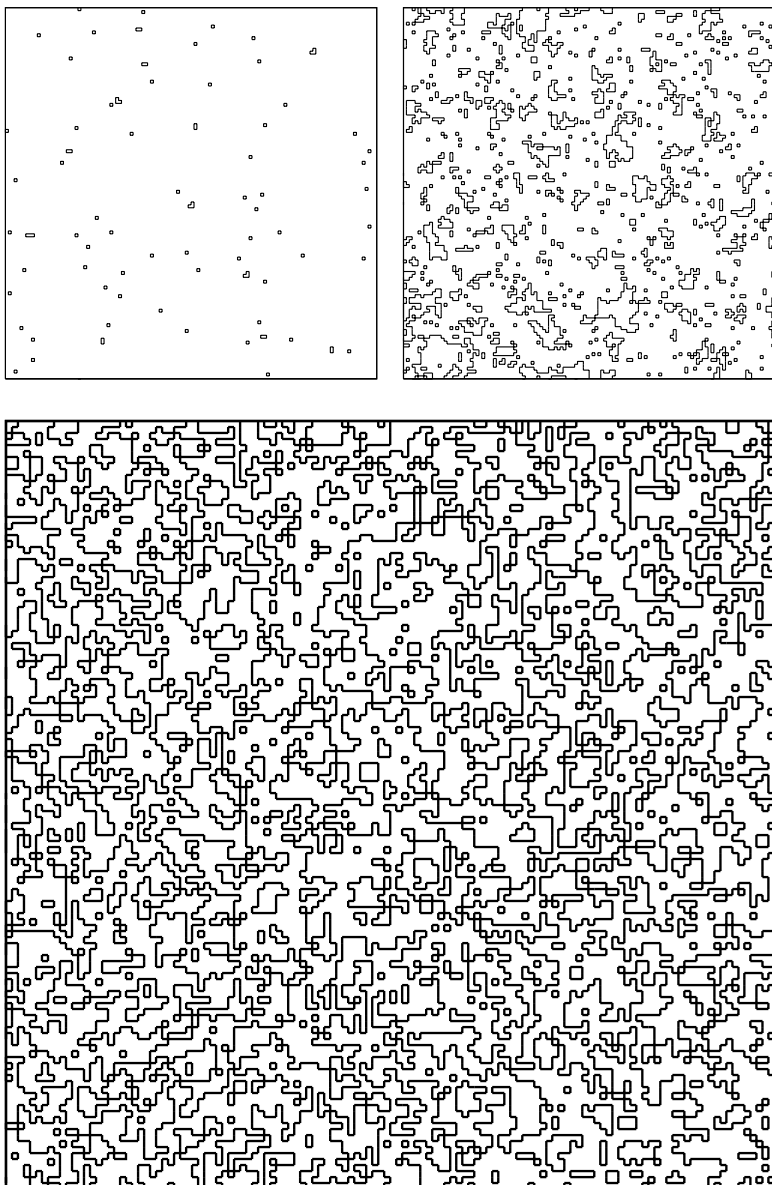


Fig. 9. Snapshots of high-temperature graphs of the Ising model on a square lattice with linear size $L = 128$ and periodic boundary conditions in the normal phase at $\beta = 0.6\beta_c$ (top left panel), at the critical point $\beta = \beta_c$ (top right panel), and in the condensed phase at $\beta = 1.4\beta_c$ (bottom panel). Because of its richer structure, the last snapshot is enlarged relative to the first two snapshots.

Remember that the inverse temperature is related to the tuning parameter K via $K = \tanh \beta$. To this end, we measure the so-called spanning probability P_S as a function of β for different lattice sizes. Giving the probability for the presence of a graph spanning the lattice, P_S tends to zero for small β , while it tends to unity for large β . This observable has no scaling dimension and plays the role of the Binder cumulant in standard thermodynamic studies. When plotted as a function of β , the curves $P_S(\beta)$ obtained for different lattice sizes should all intersect in one point. Being independent of the lattice size, this common point marks the proliferation temperature of the *infinite* system. Within the achieved accuracy, we observe that all the measured curves cross at the thermal critical point, implying that the high-temperature graphs loose their line tension θ and proliferate precisely at the Curie point (see Fig. 10).

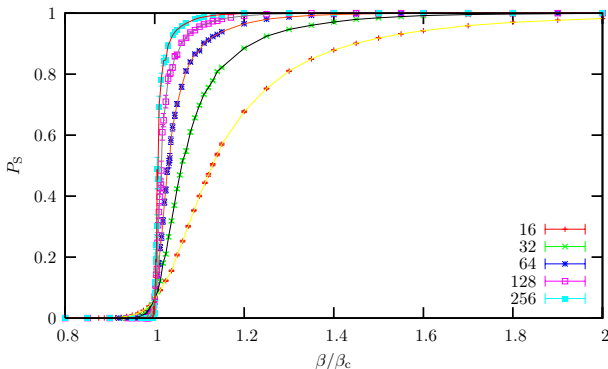


Fig. 10. Probability P_S for the presence of a spanning graph as function of the inverse temperature β measured for lattice sizes $L = 16, 32, 64, 128, 256$. Within the achieved accuracy, the curves cross at the thermal critical point $\beta = \beta_c$.

According to standard finite-size scaling, this observable obeys the scaling law⁶⁰

$$P_S(\beta, L) = P_S(L/\xi), \quad (126)$$

where P_S is a scaling function and ξ the correlation length whose divergence at criticality is governed by the exponent ν . The data gathered on lattices of different sizes is therefore a function not of β and L separately, but only of the ratio of the lattice size and the correlation length. All the data should therefore collapse onto a single curve when plotted as a function of

$(\beta/\beta_c - 1)L^{1/\nu}$. With ν given the Ising value $\nu = 1$, this is indeed what we find (see Fig. 11).

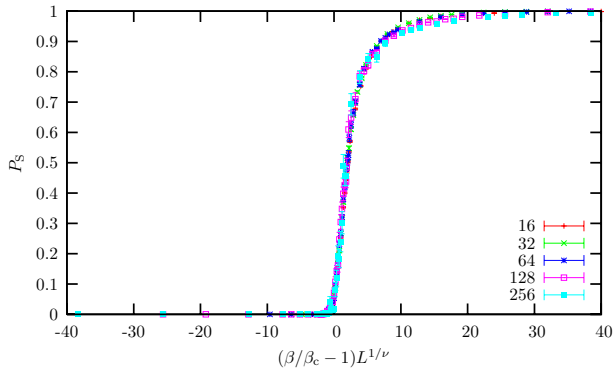


Fig. 11. Raw data of Fig. 10 replotted as a function of $(\beta/\beta_c - 1)L^{1/\nu}$, with the Ising choice $\nu = 1$. The data collapse is satisfactory over the entire temperature range.

The fractal dimension of the high-temperature graphs is best determined by following standard percolation theory⁴³ and measuring the percolation strength P_∞^G , defined as the fraction of bonds in the largest graph, and the average graph size χ_G (see Figs. 13 and 12). The percolation strength,

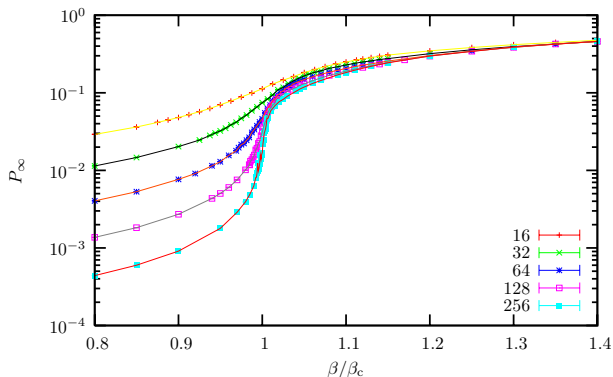


Fig. 12. Percolation strength as a function of the inverse temperature β measured on lattices of linear size $L = 16, 32, 64, 128, 256$. Note the logarithmic scale on the vertical axis.

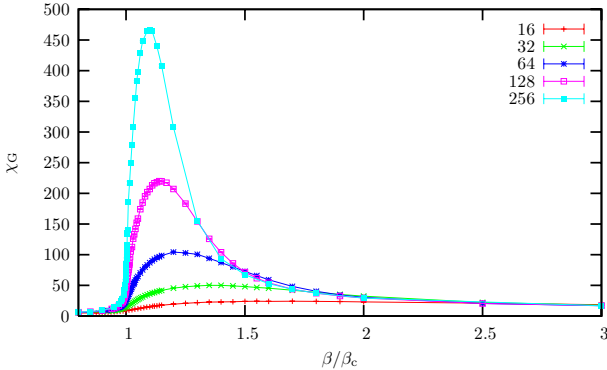


Fig. 13. Average cluster size χ_G , excluding the largest cluster, as a function of the inverse temperature measured on lattices of linear size $L = 16, 32, 64, 128, 256$.

which is finite in the low-temperature phase ($\beta > \beta_c$), vanishes as a power law when the percolation threshold is approached,

$$P_\infty^G \sim (\beta - \beta_c)^{\beta_G}. \quad (127)$$

At the same time, the average cluster size diverges,

$$\chi_G \sim |\beta - \beta_c|^{-\gamma_G}. \quad (128)$$

Here, β_G and γ_G are two percolation exponents which should not be confused with the thermal critical exponents. The ratios β_G/ν and γ_G/ν are expressed in terms of the entropy exponent τ of the graph distribution as in percolation theory⁴³

$$\frac{\beta_G}{\nu} = d \frac{\tau - 2}{\tau - 1}, \quad \frac{\gamma_G}{\nu} = d \frac{3 - \tau}{\tau - 1}, \quad (129)$$

with d the dimensionality of the lattice. According to Table 1, $\tau = 27/11 = 2.4546\dots$ for the two-dimensional Ising model. Since $D = d/(\tau - 1)$, the fractal dimension is related to these percolation exponents via

$$D = d - \frac{\beta_G}{\nu} = \frac{1}{2} \left(d + \frac{\gamma_G}{\nu} \right), \quad (130)$$

again as in percolation theory.⁴³ Close to the percolation threshold, the percolation strength and average graph size obey the finite-size scaling laws

$$P_\infty^G = L^{-\beta_G/\nu} P_\infty^G(L/\xi), \quad \chi_G = L^{\gamma_G/\nu} \chi_G(L/\xi), \quad (131)$$

so that the exponent ratios and thus D can be determined by considering the system at criticality, where these scaling relations imply an algebraic dependence on the system size L .

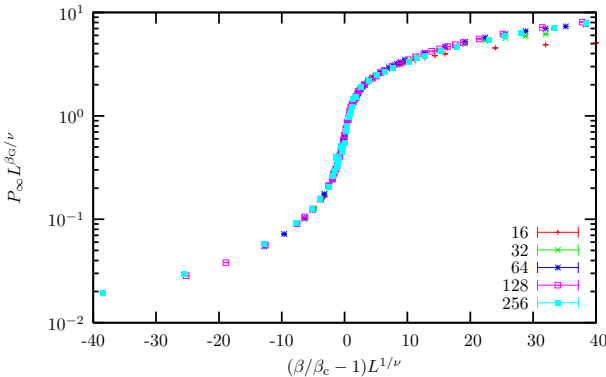


Fig. 14. Rescaled raw data of Fig. 12 plotted as a function of $(\beta/\beta_c - 1)L^{1/\nu}$, with the Ising choice $\nu = 1$, and $\beta_G = 0.626$. The data collapse is satisfactory in the critical region as well as in the entire high-temperature phase $\beta < \beta_c$. The flaring out of the data points for $\beta > \beta_c$ marks the end of the critical region.

We numerically arrived at the estimates³⁰ $\beta_G = 0.626(7)$, $\gamma_G = 0.740(4)$, leading to $\sigma = 0.732(6)$, $\tau = 2.458(5)$ in perfect agreement with the exact values $\sigma = 8/11 = 0.7273\dots$, $\tau = 27/11 = 2.4546\dots$, and the predicted fractal dimension⁵² $D = 11/8$ of the high-temperature graphs. The data were fitted over the range $L = 16 - 128$, using the least-squares Marquardt-Levenberg algorithm. With the obtained value for β_G , a satisfactory collapse of the percolation data is achieved (see Fig. 14). The collapse of the average graph size data is less satisfactory. This is not untypical for this type of observable. A similar bad data collapse we observed for the average size of geometrical (as opposed to Fortuin-Kasteleyn) spin clusters in the two-dimensional Ising model.

4.3. Summary

The case study of the Ising model on a square lattice in the high-temperature representation showed that the fractal structure of the high-temperature graphs indeed encodes the thermal critical behaviour. This representation therefore provides a purely geometric and equivalent description of the original spin formulation of the model.

5. Further Applications

The loop gas approach is by no means limited to the $O(N)$ theory. The formalism is general and can be applied to a host of other phase transitions,

not necessarily involving the proliferation of line objects. Phase transitions involving the proliferation of surfaces and hypersurfaces can be treated similarly. In this section, a few further applications are briefly discussed.

5.1. Higgs Model

A straightforward extension of the $O(N)$ theory follows by considering electrically charged particles. The continuum action describing the charged system reads

$$S = \int d^d x \left[-\frac{1}{2} |(\partial_\mu - ieA_\mu)\varphi|^2 + \frac{m^2}{2} |\varphi|^2 + \frac{g}{4!} |\varphi|^4 + \frac{1}{4} F_{\mu\nu}^2 + \frac{1}{2\alpha} (\partial_\mu A_\mu)^2 \right] \quad (132)$$

where $F_{\mu\nu} = \partial_\mu A_\nu - \partial_\nu A_\mu$ is the electromagnetic field strength, with A_μ the vector potential in d spacetime dimensions. The scalar field φ is now complex with $N/2$ complex, i.e., N real components, where N is even. The action is obtained from the neutral theory by minimal coupling the scalar field to the gauge field A_μ , with e the electric charge. The Maxwell term provides the standard kinetic term for the gauge field, while the last term with parameter α fixes a Lorentz-invariant gauge. The theory (132) is known as the Abelian Higgs model in high energy and as the Ginzburg-Landau theory in condensed matter physics. The partition function, whose general definition is given in Eq. (1), of the charged theory involves in addition to the functional integral over the scalar field also one over the gauge field, i.e.,

$$\text{Tr} = \int D\varphi DA_\mu, \quad (133)$$

where the functional measure $\int D\varphi$ is the continuum limit of the discrete measure (4) defined on the spacetime lattice, with an analogous definition for $\int DA_\mu$.

To arrive at the spacetime description of this theory, we concentrate on the coupling to the gauge field by considering only the first two terms in the action,

$$S_0 = \int d^d x \left[-\frac{1}{2} |(\partial_\mu - ieA_\mu)\varphi|^2 + \frac{m^2}{2} |\varphi|^2 \right]. \quad (134)$$

This action describes otherwise free particles coupled to an electromagnetic background field, specified by the gauge field A_μ . The corresponding partition function

$$\ln Z_0 = \ln \text{Det}^{-N/2} \left[-(\partial_\mu - ieA_\mu)^2 + m^2 \right] \quad (135)$$

is readily written as a path integral by interpreting the operator $(\partial_\mu - ieA_\mu)^2 + m^2$ as the Hamiltonian operator of a nonrelativistic charged particle of mass $M = \frac{1}{2}$ moving in a constant potential $V = m^2$ in d dimensions in the presence of an electromagnetic background field. The corresponding classical action is

$$W_0 = \int_0^s ds' \left\{ \frac{1}{4} \dot{x}^2(s') - ie \dot{x}_\mu A_\mu[x(s')] + m^2 \right\}. \quad (136)$$

According to the mnemonics discussed below Eq. (60), the spacetime representation of the partition function (135) is given in terms of this action as

$$\ln Z_0 = \frac{N}{2} \Omega \int_0^\infty \frac{ds}{s} \oint Dx(s') e^{-W_0}. \quad (137)$$

Since N is even here, the simplest Higgs model corresponds to the value $N = 2$, which in the context of condensed matter physics provides an effective description of ordinary superconductivity.

It follows from Eq. (137) that a particle trajectory Γ picks up an extra phase factor

$$U(\Gamma) = e^{ie \int_0^s ds' \dot{x}_\mu A_\mu[x(s')]} = e^{ie \int_\Gamma dx_\mu A_\mu(x)}. \quad (138)$$

This phase factor results in a Biot-Savart type of interaction between two line elements dx_μ , dy_ν of charged loops¹⁶ as can be illustrated by considering the average of the phase factor (138)

$$\begin{aligned} \langle U(\Gamma) \rangle &\equiv \int DA_\mu U(\Gamma) \exp \left\{ - \int d^d x \left[\frac{1}{4} F_{\mu\nu}^2 + \frac{1}{2\alpha} (\partial_\mu A_\mu)^2 \right] \right\} \\ &= \exp \left[-\frac{e^2}{2} \int_\Gamma dx_\mu dy_\nu D_{\mu\nu}(x-y) \right], \end{aligned} \quad (139)$$

where $D_{\mu\nu}$ is the correlation function of the gauge field

$$D_{\mu\nu}(x) = \int \frac{d^d k}{(2\pi)^d} \frac{1}{k^2} \left[\delta_{\mu\nu} - (1-\alpha) \frac{k_\mu k_\nu}{k^2} \right] e^{ik \cdot x}, \quad (140)$$

as can be read off from the action (132). This long range Biot-Savart interaction between line elements of charged loops sets the Higgs model apart from the neutral $O(N)$ theory, where the loops experience only a steric repulsion.

The $|\varphi|^4$ term in the action (132) can be treated as in the $O(N)$ theory, leading to a steric repulsion for charged loops. Pasting the pieces together,

one arrives at the spacetime representation of the partition function of the Higgs model^{18–20}

$$Z = \int \mathrm{D}A_\mu \exp \left\{ - \int \mathrm{d}^d x \left[\frac{1}{4} F_{\mu\nu}^2 + \frac{1}{2\alpha} (\partial_\mu A_\mu)^2 \right] \right\} \\ \times \sum_{l=0}^{\infty} \frac{1}{l!} \left(\frac{N}{2} \right)^l \prod_{r=1}^l \left[\Omega \int_0^\infty \frac{\mathrm{d}s_r}{s_r} \oint \mathrm{D}x_r(s'_r) \right] e^{-W^{(l)}}, \quad (141)$$

with the l -particle action

$$W^{(l)} = \sum_{r=1}^l \int_0^{s_r} \mathrm{d}s'_r \left\{ \frac{1}{4} \dot{x}_r^2(s'_r) + m^2 + i e \dot{x}_{r,\mu}(s'_r) \cdot A_\mu[x_r(s'_r)] \right\} \\ + \frac{g}{6} \sum_{r,r'=1}^l \int_0^{s_r} \mathrm{d}s'_r \int_0^{s_{r'}} \mathrm{d}s'_{r'} \delta[x_r(s'_r) - x_{r'}(s'_{r'})]. \quad (142)$$

The partition function (141) represents a grand canonical ensemble of fluctuating closed worldlines of arbitrary length and shape traced out by electrically charged point particles. Since the matter field φ is complex, the worldlines have an orientation now.

From this spacetime representation it follows that the logarithm of the partition function can again be cast in the general form (87), with the loop distribution now describing charged loops. Because of the additional long range Biot-Savart interaction, the fractal structure of these loops will be different from those featuring in the neutral theory, which experience just a steric repulsion. The physical picture remains unchanged, however. As in the neutral theory, only a few small loops are present in the normal phase due to the finite line tension θ . On entering the Higgs phase, characterized by a sign change in the mass term of the Higgs model, the line tension vanishes, and the charged loops proliferate as they can become arbitrary long at no cost. The vacuum becomes filled with “a spaghetti of tangled loops”.¹⁸

5.2. Bose-Einstein Condensation

The spacetime approach was originally formulated to describe nonrelativistic quantum mechanics,¹ which fundamentally differs from its relativistic counterpart. A relativistic quantum particle roams the space dimensions as well as the time dimension, so that its worldlines are random walks in *space-time*. Such particle trajectories are parameterized by the Schwinger proper time parameter, i.e., by their arc length. A nonrelativistic particle, on the

other hand, executes a random walk in space only. Its time coordinate is given by absolute Newtonian time, which elapses uniformly forward. In a nonrelativistic ensemble, all the particles execute a random walk in space synchronously in time, with all the worldlines parameterized by Newtonian time. That is, the Schwinger proper time parameter gets replaced by New-

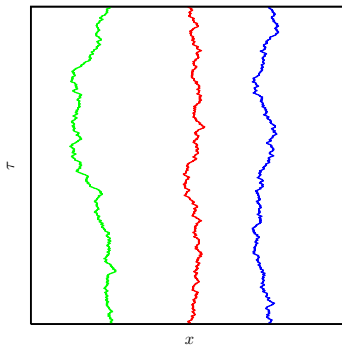


Fig. 15. Worldlines of three nonrelativistic particles on a square lattice, representing one space and the imaginary time dimension, moving synchronously from the bottom to the top of the lattice. The particles execute a Brownian random walk in x -direction. Periodic boundary conditions are chosen in the imaginary time direction.

tonian time in the nonrelativistic limit. At the technical level, this can be seen by taking the nonrelativistic limit $c \rightarrow \infty$ in, for example, the correlation function (37) of the relativistic theory. The integral over s can in this limit be approximated by the saddle point⁶¹

$$s = \tau/2m, \quad (143)$$

showing that the arc length parameter s of relativistic worldlines indeed becomes replaced by Newtonian time τ . This difference has profound implications. Because Newtonian time always elapses forward, nonrelativistic worldlines can no longer form simple loops on an infinite lattice. As a result, the number of particles present in the system is fixed. On a finite lattice, worldlines still have the possibility to close by wrapping around the lattice.

Figure 15 shows an example of the motion in imaginary time of three particles in one space dimension. Up to now, the finite lattice sizes were considered a mere approximation to systems of infinite extent, in space as well as in time. In this subsection, we instead assume that the imaginary time dimension is finite. With the time variable τ restricted to the interval

$0 \leq \tau \leq \hbar\beta$, and the inverse temperature $\beta = 1/k_B T$, one describes the system at finite temperature. The zero-temperature limit is recovered by letting the imaginary time dimension become infinite. For bosons, periodic boundary conditions are to be imposed in the imaginary time dimension, implying that the configurations of an ensemble of nonrelativistic bosons at imaginary time 0 and at $\hbar\beta$ are identical. (In contrast to the rest of the paper, we explicitly display factors of \hbar in this subsection.)

The partition function Z_l of such an ensemble of l identical nonrelativistic bosons can be expressed in terms of the probability amplitude $G[\mathbf{x}(0), \mathbf{x}(\tau)]$ for a particle to move from $\mathbf{x}(0)$ to $\mathbf{x}(\tau)$ in imaginary time τ as:⁶²

$$Z_l = \sum_P \int \prod_{r=1}^l d^d \mathbf{x}_r G [\mathbf{x}_1(0), \mathbf{x}_{P(1)}(\hbar\beta)] \cdots G [\mathbf{x}_l(0), \mathbf{x}_{P(l)}(\hbar\beta)], \quad (144)$$

where the final configuration $\{\mathbf{x}_{P(r)}(\hbar\beta)\}$ at $\tau = \hbar\beta$ is a permutation P of the initial configuration $\{\mathbf{x}_r(0)\}$ at $\tau = 0$. In contrast to the convention used up to now, here, d denotes the number of *spatial* dimensions. All possible permutations of the starting points are included as indicated by the sum \sum_P . In Feynman's spacetime approach, the amplitude $G[\mathbf{x}(0), \mathbf{x}(\tau)]$ is written as a sum over all possible particle trajectories connecting the two spatial endpoints¹

$$G[\mathbf{x}(0), \mathbf{x}(\hbar\beta)] = \int D\mathbf{x}(\tau) \exp \left(-\frac{1}{\hbar} \int_0^{\hbar\beta} d\tau \left\{ \frac{m}{2} \dot{\mathbf{x}}^2(\tau) + V[\mathbf{x}(\tau)] \right\} \right), \quad (145)$$

where $V[\mathbf{x}(\tau)]$ is the potential experienced by the particle along its worldline $\mathbf{x}(\tau)$. Expressed as a path integral, the partition function thus reads¹⁵

$$Z_l = \sum_P \int \prod_{r=1}^l D\mathbf{x}_r(\tau) \exp \left(-\frac{1}{\hbar} \int_0^{\hbar\beta} d\tau L^{(l)} \right) \quad (146)$$

with the l -particle nonrelativistic Lagrangian

$$L^{(l)} = \sum_{r=1}^l \frac{m}{2} \dot{\mathbf{x}}_r^2(\tau) + \frac{1}{2} \sum_{r \neq r'=1}^l V[|\mathbf{x}_r(\tau) - \mathbf{x}_{r'}(\tau)|] \quad (147)$$

and pair potential $V(\mathbf{x}_r, \mathbf{x}_{r'}) = V(|\mathbf{x}_r - \mathbf{x}_{r'}|)$. Figure 15 gives an example of a configuration contributing to Z_3 . Since $\mathbf{x}_{P(1)}(\hbar\beta) = \mathbf{x}_1(0)$, $\mathbf{x}_{P(2)}(\hbar\beta) = \mathbf{x}_2(0)$, and $\mathbf{x}_{P(3)}(\hbar\beta) = \mathbf{x}_3(0)$, the three particle trajectories form three separate loops around the time axis. This is typical for the high-temperature phase of a nonrelativistic ensemble of bosons, where most particles execute

a random walk in space during the time interval $0 \leq \tau \leq \hbar\beta$ that returns to its initial position. It means that the particles, being distinguishable, behave classically.

By mapping Feynman's spacetime approach onto the problem in classical statistical mechanics of chains of beads connected by springs⁶³ to numerically evaluate the path integral with the help of the Metropolis Monte Carlo method, Ceperley and Pollock,⁶⁴ and others showed that a powerful computational tool emerges that can even accurately describe a strongly interacting system like superfluid ^4He (for reviews, see Refs. [65,66]).

Bose-Einstein condensation manifests itself in Feynman's spacetime approach by the formation of so-called *cooperative exchange rings*, where individual particle trajectories hook up to form longer loops.¹⁵ An exam-

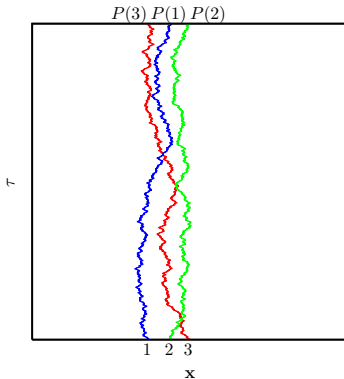


Fig. 16. Worldlines of three nonrelativistic particles on a hypercubic lattice. The vertical direction stands for the imaginary time dimension, while the horizontal direction stands for all the space dimensions. The particles move synchronously from the bottom to the top of the lattice, executing a Brownian random walk in *space*. Periodic boundary conditions are chosen in the time direction. After traversing the lattice, the particles are cyclically permuted $1 \rightarrow 2 \rightarrow 3 \rightarrow 1$.

ple is given in Fig. 16. Since $\mathbf{x}_{P(1)}(\hbar\beta) = \mathbf{x}_2(0)$, $\mathbf{x}_{P(2)}(\hbar\beta) = \mathbf{x}_3(0)$, and $\mathbf{x}_{P(3)}(\hbar\beta) = \mathbf{x}_1(0)$, the three particle trajectories now form a single loop, wrapping the time axis three times. Generally, a particle in a composite exchange ring moves in imaginary time along a trajectory that does not end at its own starting position, but at that of another particle. Whence, although the initial and final configurations are identical, the particles in a composite ring are cyclically permuted. They thereby loose their identity and become indistinguishable. This is the essence of Bose-Einstein conden-

sation, which at finite temperature can occur in space dimensions larger than two.

The connections between geometrical properties and critical exponents spelled out in these notes apply equally well to Bose-Einstein condensation.^{27,29} Specifically, the logarithm of the partition function (144) takes close to the condensation temperature again the form (87), with the worldline loop distribution ℓ_b now denoting the number density of worldlines wrapping around the time axis b times. In the high-temperature phase, the loops have a finite line tension, so that only small loops winding around the imaginary time axis only once or at most a few times exist. Upon approaching the condensation temperature from above, the line tension vanishes and loops with arbitrary large winding numbers appear.^{27,67} Since the winding number of a given loop corresponds to the number of cyclically permuted particles in an exchange ring in Feynman's theory, arbitrary large rings appear. The particles contained in large rings (long loops) are part of the condensate.

For a free Bose gas in $2 < d < 4$ space dimensions, $\vartheta = 0$ and the fractal dimension of the particle trajectories is that of a Brownian random walk, $D = 2$, so that $\tau = d/2 + 1$, while $\sigma = (d - 2)/2$.²⁹ Being related to the thermal critical exponents as before (see Sec. 3.3), these exponents yield

$$\alpha = \frac{d - 4}{d - 2}, \quad \beta = \frac{1}{2}, \quad \gamma = \frac{2}{d - 2}, \quad \nu = \frac{1}{d - 2}, \quad \eta = 0, \quad (148)$$

which are precisely the critical exponents of the spherical model in d space dimensions. This model corresponds to taking the limit $N \rightarrow \infty$ in the $O(N)$ spin model.^{68,69} Despite being noninteracting, a free Bose gas is not in the universality class of the Gaussian model. The nontrivial exponents (148) derive from the constraint that the total number of particles is fixed. Without this constraint, which is relevant when considering Bose-Einstein condensation in a free Bose gas at constant pressure, Gaussian exponents follow.^{68,69} In four space dimensions, corresponding to the upper critical dimension and above, i.e., $d \geq 4$, the exponents of the spherical and Gaussian models coincide.

The critical properties of Bose-Einstein condensation in an *interacting* nonrelativistic Bose gas are given by the $N = 2$, φ^4 universality class. To state this more concretely, the equilibrium thermal critical properties of Bose-Einstein condensation in such an interacting system in three space dimensions, say, can be computed from the theory (3) with $d = 3$, now considered a *classical theory* in three space dimensions. The connection between the nonrelativistic quantum theory and the classical $O(2)$ model

is as follows.

Consider the square end-to-end vector $[\mathbf{x}_r(\tau) - \mathbf{x}_r(0)]^2$ of the r th particle. For a free Bose gas, with the partition function (146), its average is readily calculated with the result in d space dimensions

$$\langle [\mathbf{x}_r(\tau) - \mathbf{x}_r(0)]^2 \rangle = d \frac{\hbar}{m} \tau. \quad (149)$$

This expression shows that the worldlines of free nonrelativistic particles can be interpreted as trajectories traced out in *space* by a random walker taking steps of typical size

$$a = \sqrt{\frac{d}{2\pi}} \lambda_T \quad (150)$$

during each imaginary time interval $\tau = \hbar\beta$. Here, λ_T is the de Broglie thermal wavelength

$$\lambda_T \equiv \sqrt{\frac{2\pi\hbar^2\beta}{m}}. \quad (151)$$

The step size of the coarse-grained random walk is small when the thermal wavelength is small, i.e., at high temperatures (β small) and for large particle masses. These conditions correspond to the classical limit. Bose-Einstein condensation sets in when the step size becomes on the order of the interparticle distance $1/n^{1/d}$. Setting $a = 1/n^{1/d}$ leads to an estimate of the condensation temperature of a free Bose gas

$$k_B T_0 = \frac{2\pi\hbar^2}{m} \left(\frac{n}{\zeta(d/2)} \right)^{2/d}, \quad (152)$$

with ζ the Riemann zeta function

$$\zeta(s) = \sum_{l=1}^{\infty} \frac{1}{l^s}, \quad (153)$$

and where the particle number density n is assumed to be given. If this density is small or if the mass of the particles is large, the condensation temperature is low.

The inclusion of a self-interaction in the free (3+1)-dimensional nonrelativistic quantum field theory changes the fractal structure of the world-lines, as they acquire a steric repulsion now, but leaves the basic picture unchanged. Consider a grand canonical nonrelativistic ensemble

$$Z = \sum_{l=0}^{\infty} \frac{1}{l!} e^{\beta\mu l} Z_l, \quad (154)$$

with μ the chemical potential and Z_l given in Eq. (146). The coarse-grained random walks of the interacting theory in three-dimensional space can be identified with the high-temperature graphs of the three-dimensional O(2) spin model. Each set bond corresponds to a particle wrapping the time axis once. On a cubic lattice, the smallest closed graph involves four bonds, so that translated back to the nonrelativistic quantum theory, exchange rings smaller than four are not visible in the spin model. In the high-temperature phase of the spin model, only a few small high-temperature graphs are present. This reflects the fact that in the nonrelativistic quantum theory most worldlines wrap the imaginary time axis only once and that very few larger exchange rings are present at high temperatures. A large single closed high-temperature graph of b bonds amounts in the nonrelativistic quantum theory to a large exchange ring involving b particles. The proliferation of high-temperature graphs in the spin model corresponds in the nonrelativistic quantum theory to the proliferation of worldlines, wrapping arbitrary many times around the imaginary time axis, and signals the onset of Bose-Einstein condensation.

5.3. Summary

The formalism developed in these notes is shown to be easily adapted to describe charged systems as well as Bose-Einstein condensation.

6. Dual Theories

As was first pointed out by Helfrich and Müller,⁷⁰ the high-temperature graphs of O(N) spin models describe in addition to the particle trajectories at the same time a second set of *physical* lines. In this section, we briefly discuss examples in $d = 2, 3$ and 4, respectively.

6.1. Peierls Domain Walls

Consider the Ising, i.e., the O(1) model on a square lattice. According to the famous Kramers-Wannier duality,⁷¹ the high-temperature graphs of the model form line-like Peierls *domain walls*,⁷² separating geometrical spin clusters of opposite orientation on the dual lattice. Each bond in a high-temperature graph cuts a nearest neighbour pair of anti-parallel spins on the dual lattice in two. The link connecting the two anti-parallel spins on the dual lattice is perpendicular to the high-temperature bond on the original lattice. On an infinite lattice, the Kramers-Wannier duality implies that

observables calculated at an inverse temperature β in the original Ising model can be transcribed to those of the dual model at an inverse temperature $\tilde{\beta}$. The duality map interchanges the low-temperature and high-temperature phases. The relation between the two temperatures is readily established by noting that an occupied high-temperature bond represents a factor $K = \tanh \beta$. The anti-parallel spin pair on the dual lattice, that is cut by the high-temperature bond, carries a Boltzmann weight $\exp(-2\tilde{\beta})$, so that⁷¹

$$\tanh \beta = e^{-2\tilde{\beta}}, \quad (155)$$

or $\sinh 2\beta = 1 / \sinh 2\tilde{\beta}$. The critical temperature β_c follows from this relation by setting $\beta = \tilde{\beta}$, with the result

$$\beta_c = \ln(1 + \sqrt{2})/2 = 0.44068679 \dots \quad (156)$$

By the Kramers-Wannier duality, the fractal dimension of the line-like Peierls domain walls at criticality coincides with the one of the high-temperature graphs, i.e., $D = \frac{11}{8}$.

6.2. Vortex Lines

We next consider the three-dimensional O(2) model. The fractal dimension of the corresponding high-temperature graphs has been estimated in a recent Monte Carlo study⁴⁹ as $D = 1.7655(20)$ at the critical point. By a duality map,^{16–18} these high-temperature graphs describe at the same time the magnetic vortex lines of the three-dimensional Higgs model (132). Vortices constitute the topological defects of the Higgs model and are line-like in three dimensions. The duality map again interchanges the low-temperature and high-temperature phases of the two models. Given the values⁷³ $\eta = 0.0380(4)$ and $\nu = 0.67155(27)$ of the O(2) model obtained through Monte Carlo simulations, the relations (107) and (103) lead to the values

$$\tau = 6.2965(60), \quad \vartheta = 0.1965(20), \quad \sigma = 0.8434(13), \quad (157)$$

for the configurational entropy exponents of closed and open magnetic vortices, τ and ϑ , respectively, and for the exponent σ , characterizing the vanishing of the line tension when the critical point is approached. The estimate for ϑ was first given in Ref. [49].

From the perspective of vortices, the phase diagram of the three-dimensional Higgs model is as follows. For convenience, we take the model

as effective theory of ordinary type-II superconductors in three space dimensions. Whereas in the superconducting phase only a few small vortex loops are present, the density and size of the loops increase when the temperature rises. Loops of all sizes appear at the critical point, and the vacuum becomes filled with vortex loops. The disordering effect of the proliferating vortices destroys the superconducting phase and drives the phase transition to the normal phase. Because of the Meissner effect, the magnetic interaction is screened in the superconducting phase and vortex line elements experience only a short range interaction which is well approximated by a steric repulsion. This is precisely the type of interaction experienced by the high-temperature graphs of the O(2) model.

The three-dimensional O(2) model also possesses vortex lines as topological solutions. In contrast to those in a superconductor, the vortices in a superfluid experience a long range interaction, mediated by the gapless Goldstone mode associated with the spontaneous breaking of the O(2) symmetry in the $|\varphi|^4$ theory. The model whose high-temperature graphs describe these vortices is the Higgs model, as follows again from the duality map.^{16–18} The long range interaction experienced by the high-temperature graphs of the Higgs model is the Biot-Savart interaction discussed in Sec. 5.1. The duality between the O(2) and the Higgs models implies that the particle trajectories of one model appear as vortex lines in the other.¹⁸

It was first suggested by Onsager⁷⁴ that proliferating vortex loops drive the superfluid phase transition in liquid ^4He . He envisaged that as the critical temperature is approached from below, the vortex loops proliferate and thereby disorder the superfluid state, causing the system to revert to the normal state. The precise nature of the three-dimensional superfluid phase transition was investigated from this perspective in a recent high-precision Monte Carlo study.⁷⁵ One of the observables considered is the total vortex line density v . By means of standard finite-size scaling analysis of the corresponding susceptibility

$$\chi = L^3(\langle v^2 \rangle - \langle v \rangle^2), \quad (158)$$

the inverse critical temperature β_c was estimated and shown to be consistent with the estimate of a previous study directly in terms of the field variables.⁷⁶ However, when percolation observables were considered, such as the probability for the presence of a vortex loop spanning the lattice, slight but statistically significant deviations from β_c were found. For all observables considered, the vortex proliferation threshold β_p is larger than β_c . That is, from these observables one would conclude that the vortices

proliferate too early at a temperature below the critical one. From the duality map alluded to above, the vortex proliferation threshold is expected to coincide with the critical point. It is not clear at the moment, whether this discrepancy is physical, or an artifact of the percolation observables used. With the percolation threshold taken as an adjustable parameter, reasonable estimates were obtained from percolation observables for the critical exponents ν and β , consistent with those of the XY model.⁷⁵

Even in systems without a thermodynamic phase transition, the notion of vortex proliferation can be useful in understanding the phase structure. An example is provided by the three-dimensional Abelian Higgs lattice model with *compact* gauge field (see below).⁷⁷ In addition to vortices, the compact model also features magnetic monopoles as topological defects, which are point-like in three dimensions. In the presence of monopoles, vortex lines no longer need to be closed as they can originate at a monopole and terminate at an antimonopole. When the vortex line tension is finite, monopoles and antimonopoles are tightly bound in pairs. The part of phase diagram where this is the case is called the Higgs region, which corresponds to the superconducting phase in the noncompact theory. When the vortex line tension vanishes, monopoles and antimonopoles are no longer bound in pairs, and instead form a plasma. In the part of the phase diagram where this is the case, the system exhibits charge confinement. It is well established that one can move from the Higgs region into the confining region without encountering thermodynamic singularities.⁷⁸ The susceptibility data for various observables define, however, a precisely located phase boundary. More specifically, for sufficiently large lattices, the maxima of the susceptibilities at the phase boundary do not show any finite-size scaling, and the susceptibility data obtained on different lattice sizes collapse onto single curves without rescaling, indicating that the infinite-volume limit is reached. In Ref. [77], it was argued that this phase boundary marks the vortex proliferation threshold. A well-defined and precisely located phase boundary across which geometrical objects proliferate, yet thermodynamic quantities remain nonsingular has become known as a *Kertész line*. Such a line was first introduced in the context of the Ising model in the presence of an applied magnetic field.⁷⁹

6.3. Monopole Loops

As a last example, we consider the four-dimensional *pure compact* U(1) lattice gauge theory described by the Wilson action⁸⁰

$$S_g = \beta \sum_{x,\mu<\nu} [1 - \cos \theta_{x,\mu\nu}]. \quad (159)$$

Here, β is the inverse gauge coupling, the sum extends over all lattice sites x and lattice directions μ , and $\theta_{x,\mu\nu}$ denotes the plaquette variable

$$\theta_{x,\mu\nu} \equiv \Delta_\mu \theta_{x,\nu} - \Delta_\nu \theta_{x,\mu}, \quad (160)$$

with the lattice difference operator $\Delta_\nu \theta_{x,\mu} \equiv \theta_{x+a\hat{\nu},\mu} - \theta_{x,\mu}$ and the compact variable $\theta_{x,\mu} \in [-\pi, \pi]$, living on the link connecting the lattice site x with $x + a\hat{\mu}$. The link variable is related to the continuum gauge field $A_\mu(x)$ via

$$\theta_{x,\mu} = eaA_\mu(x). \quad (161)$$

The lattice action (159) reduces to the ordinary Maxwell action in the continuum limit $a \rightarrow 0$, provided one sets

$$\beta = \frac{1}{a^{4-d} e^2}. \quad (162)$$

As for the compact Higgs model, the pure compact gauge theory possesses point-like monopoles in three dimensions. In four dimensions, these defects become line-like.⁸¹ The monopole loops experience in addition to a steric repulsion also a long range Biot-Savart interaction. The field theory in which these monopole lines appear as particle trajectories (high-temperature graphs) is the four-dimensional noncompact Higgs model (132).^{16,17,19} That is, the pure compact U(1) lattice gauge theory is dual to the noncompact Higgs model. These models possess two phases. The pure compact U(1) theory has a confining phase at strong coupling (small β), corresponding to the superconducting phase of the Higgs model, and a Coulomb phase at weak coupling (large β) characterized by a massless photon. Monte Carlo simulations⁸² show that in the Coulomb phase only a few small monopole loops are present. With increasing coupling constant (decreasing β), the density and size of the loops increase. At the critical point very close to $\beta_c = 1.0$, the monopole loops proliferate and thereby disorder the system.^{83,84} The Coulomb phase gives way to the strong-coupling confining phase, where the vacuum is filled with a spaghetti of tangled monopole loops. It is worth emphasizing that the monopole loops drive the phase transition, i.e., the monopole loops proliferate right at the confinement phase transition.^{83,84} In showing this, percolation observables of the type discussed here have

been used.²⁴ The order of the phase transition is not an established fact. In case it is continuous, the relations between the fractal structure of loops and the critical exponents laid out in these notes also apply here.

6.4. Summary

Besides picturing the worldlines of the particles described by the field theory under consideration, the high-temperature graphs can have a second interpretation as topological line defects, such as Peierls domains walls ($d = 2$), vortices ($d = 3$), or monopole lines ($d = 4$). The field theory in which such line-like configurations appear as topological defects is said to be dual to the original one. Both field theories describe the same physical lines, once interpreted as particle trajectories, once as line defects.

Acknowledgements

One of us (A.S.) kindly thanks Prof. Y. Holovatch for the invitation to present one of the Ising Lectures-2004 at the Institute for Condensed Matter Physics of the National Academy of Sciences, Lviv, Ukraine. He gratefully acknowledges the hospitality and financial support provided by the Institute.

This work is partially supported by the DFG grant No. JA 483/17-3 and by the German-Israel Foundation (GIF) under grant No. I-653-181.14/1999.

References

1. R. P. Feynman, Rev. Mod. Phys. **20**, 367 (1948).
2. H. Kleinert, *Path Integrals in Quantum Mechanics, Statistics, Polymer Physics, and Financial Markets* (World Scientific, Singapore, 2004) 4th edition.
3. R. P. Feynman, Phys. Rev. **80**, 440 (1950).
4. J. Schwinger, Phys. Rev. **82**, 664 (1951).
5. L. Alvarez-Gaumé and E. Witten in: *Current Algebra and Anomalies*, edited by S. B. Treiman, R. Jackiw, B. Zumino, and E. Witten (World Scientific, Singapore, 1985).
6. A. M. Polyakov, *Gauge Fields and Strings* (Harwood, New York, 1987).
7. M. J. Strassler, Nucl. Phys. B **385**, 145 (1992).
8. C. Schubert, Phys. Rept. **355**, 73 (2001).
9. M. E. Fisher, Rev. Mod. Phys. **70**, 653 (1998).
10. D. J. Amit, *Field Theory, the Renormalization Group and Critical Phenomena* (World Scientific, Singapore, 1984) 2nd edition.
11. D. I. Uzunov, *Introduction to the Theory of Critical Phenomena: Mean Field, Fluctuations and Renormalization* (World Scientific, Singapore, 1993).

12. H. Kleinert and V. Schulte-Frohlinde, *Critical Properties of ϕ^4 -Theories* (World Scientific, Singapore, 2001).
13. H. E. Stanley, *Introduction to Phase Transitions and Critical Phenomena* (Clarendon Press, Oxford, 1971).
14. P. G. de Gennes, Phys. Lett. A **38**, 339 (1972).
15. R. P. Feynman, Phys. Rev. **90**, 1116 (1953); *ibid* **91**, 1291 (1953); *Statistical Mechanics* (Benjamin, Reading, 1972).
16. T. Banks, B. Meyerson, and J. Kogut, Nucl. Phys. B **129**, 493 (1977).
17. M. Peskin, Ann. Phys. **113**, 122 (1978).
18. P. R. Thomas and M. Stone, Nucl. Phys. B **144**, 513 (1978).
19. M. Stone and P. R. Thomas, Phys. Rev. Lett. **41**, 351 (1978).
20. S. Samuel, Nucl. Phys. B **154**, 62 (1979).
21. E. J. Copeland, D. Haws, R. Rivers and S. Holbraad, Physica A **158**, 460 (1989).
22. E. Copeland, D. Haws, S. Holbraad, and R. Rivers, in: *The Formation and Evolution of Cosmic Strings*, edited by G. W. Gibbons, S. W. Hawking, and T. Vachaspati (Cambridge University Press, Cambridge, 1990).
23. A. Patel, Nucl. Phys. B **243**, 411 (1984).
24. S. Hands and R. Wensley, Phys. Rev. Lett. **63**, 2169 (1989).
25. N. D. Antunes, L. M. A. Bettencourt, and M. Hindmarsh, Phys. Rev. Lett. **80**, 908 (1998); N. D. Antunes and L. M. A. Bettencourt, Phys. Rev. Lett. **81**, 3083 (1998).
26. A. K. Nguyen and A. Sudbø, Phys. Rev. B **60**, 15307 (1999).
27. S. Bund and A. M. J. Schakel, Mod. Phys. Lett. B **13**, 349 (1999).
28. J. Hove, S. Mo, and A. Sudbø, Phys. Rev. Lett. **85**, 2368 (2000).
29. A. M. J. Schakel, Phys. Rev. E **63**, 026115 (2001).
30. W. Janke and A. M. J. Schakel, Nucl. Phys. B **700**, 385 (2004).
31. W. Janke and A. M. J. Schakel, Phys. Rev. Lett. **95**, 135702 (2005).
32. W. Janke and A. M. J. Schakel, *Anomalous Scaling and Fractal Dimensions*, cond-mat/0508734 (2005).
33. J. Smit, *Introduction to Quantum Fields on a Lattice* (Cambridge University Press, Cambridge, 2002).
34. H. Kleinert, *Gauge Fields in Condensed Matter* (World Scientific, Singapore, 1989) Vol. 1.
35. J. Ambjørn, Fortschr. Phys. **36**, 595 (1988).
36. K. Symanzik, in: *Euclidean Quantum Field Theory*, edited by R. Jost (Academic, New York, 1969).
37. R. Balian and G. Toulouse, Phys. Rev. Lett. **30**, 544 (1973).
38. B. Nienhuis, in: *Phase Transitions and Critical Phenomena*, edited by C. Domb and J. L. Lebowitz (Academic, London, 1987), Vol. 11, p. 1.
39. T. H. Berlin and M. Kac, Phys. Rev. **86**, 821 (1952).
40. L. Chayes, L. P. Pryadko, and K. Shtengel, Nucl. Phys. B **570**, 590 (2000).
41. P. R. Gerber and M. E. Fisher, Phys. Rev. B **10**, 4697 (1974).
42. J. L. Jacobsen, N. Read, and H Saleur, Phys. Rev. Lett. **90**, 090601 (2003).
43. D. Stauffer and A. Aharony, *Introduction to Percolation Theory*, 2nd edition (Taylor & Francis, London, 1994).

44. R. P. Feynman, in: *Progress in Low Temperature Physics*, edited by C. J. Gorter (North-Holland, Amsterdam, 1955), Vol. 1, p. 17.
45. R. H. Swendsen and J. S. Wang, Phys. Rev. Lett. **58**, 86 (1987).
46. U. Wolff, Phys. Rev. Lett. **62**, 361 (1989).
47. K. Binder, Z. Phys. B **43**, 119 (1981).
48. D. S. McKenzie and M. A. Moore, J. Phys. A **4**, L82 (1971).
49. N. Prokof'ev and B. Svistunov, Phys. Rev. Lett. **96**, 219701 (2006).
50. I. Jensen, J. Phys. A **36**, 5731 (2003).
51. I. Jensen, J. Phys. A **37**, 5503 (2004).
52. B. Duplantier and H. Saleur, Phys. Rev. Lett. **61**, 1521 (1988).
53. C. M. Fortuin and P. W. Kasteleyn, Physica **57**, 536 (1972).
54. A. Coniglio, Phys. Rev. Lett. **62**, 3054 (1989).
55. B. Duplantier, Phys. Rev. Lett. **84**, 1363 (2000).
56. V. L. Berezinskii, Sov. Phys. JETP **34**, 610 (1972).
57. J. M. Kosterlitz and D. J. Thouless, J. Phys. **C6**, 1181 (1973).
58. W. Janke and A. M. J. Schakel, Comp. Phys. Comm. **169**, 222 (2005).
59. H.-M. Erkinger, *A new cluster algorithm for the Ising model*, Diplomarbeit, Technische Universität Graz (2000).
60. K. Binder and D. W. Heermann, *Monte Carlo Simulation in Statistical Physics* (Springer, Berlin, 1997).
61. C. R. Stephens, Ann. Phys. (NY) **181**, 120 (1988).
62. T. Matsubara, Prog. Theor. Phys. **6**, 714 (1951).
63. D. Chandler and P. G. Wolynes, J. Chem. Phys. **74**, 4078 (1981).
64. D. M. Ceperley and E. L. Pollock, Phys. Rev. Lett. **56**, 351 (1986).
65. W. Smith and K. Singer, CCP5 Information Quarterly **25**, 18 (1987).
66. D. M. Ceperley, Rev. Mod. Phys. **67**, 279 (1995).
67. M. Stone, Int. J. Mod. Phys. B **4**, 1465 (1990).
68. J. D. Gunton and M. J. Buckingham, Phys. Rev. **166**, 152 (1968); see also the textbook: R. K. Pathria, *Statistical Mechanics*, 2nd edition (Butterworth-Heinemann, Oxford, 1996), sec. 12.5.
69. D. V. Shopova and D. I. Uzunov, Phys. Rep. **379**, 1 (2003).
70. W. Helfrich and W. Müller, in *Continuum Models of Discrete Systems* (University of Waterloo Press, Waterloo, Ontario, Canada, 1980) p. 753.
71. H. A. Kramers and G. H. Wannier, Phys. Rev. **60**, 252 (1941).
72. R. Peierls, Proc. Camb. Phil. Soc. **32**, 477 (1936).
73. M. Campostrini, M. Hasenbusch, A. Pelissetto P. Rossi, and E. Vicari, Phys. Rev. B **63**, 214503 (2001).
74. L. Onsager, Nuovo Cimento Suppl. **6**, 249 (1949).
75. E. Bittner, A. Krinner, and W. Janke, Phys. Rev. B **72**, 094511 (2005).
76. E. Bittner and W. Janke, Phys. Rev. Lett. **89**, 130201 (2002); Phys. Rev. B **71**, 024512 (2005).
77. S. Wenzel, E. Bittner, W. Janke, A. M. J. Schakel, and A. Schiller, Phys. Rev. Lett. **95**, 051601 (2005).
78. E. Fradkin and S. H. Shenker, Phys. Rev. D **19**, 3682 (1979).
79. J. Kertész, Physica A **161**, 58 (1989).
80. K. G. Wilson, Phys. Rev. D **10**, 2445 (1974).

81. A. M. Polyakov, Phys. Lett. B **59**, 82 (1975).
82. T. A. DeGrand and D. Toussaint, Phys. Rev. D **22**, 2478 (1980).
83. R. Gupta, M. A. Novotny, and R. Cordery, Phys. Lett. B **172**, 86 (1986).
84. M. Baig, H. Fort, and J. B. Kogut, Phys. Rev. D **50**, 5920 (1994).

CHAPTER 4

REPRESENTATIONS OF SELF-ORGANIZED CRITICALITY

Alexander Olemskoi^a and Dmytro Kharchenko^b

Sumy State University,

2 Rimskii-Korsakov Str., UA-40007 Sumy, Ukraine

E-mail: a) alex@ufn.ru, b) dikh@sumdu.edu.ua

We represent general approach allowing one to produce a complex self-similar behaviour inherent in a system, being in critical state that appeared as a result of self-organization. A synergetic concept of self-organized criticality for a sandpile automata is developed where both one-avalanche system and ensemble of avalanches are discussed within the framework of theory of noise induced phenomena. In the spirit of Edwards paradigm, an effective thermodynamics is introduced to determine the distribution over an avalanche ensemble, characterized by the effective temperature. Steady-state behaviour of the moving grains number, as well as nonextensive values of their complexity and energy are studied in detail. The power law distribution over the avalanche sizes is described within a stochastic fractional Lorenz system, where the energy noise plays a crucial role. Dynamics of the system is studied in the framework of Euclidean field theory. The distribution is shown to be a solution of both fractional and nonlinear Fokker–Planck equations. We find relations between the exponent of the size distribution, fractal dimension of phase space, characteristic exponent of multiplicative noise, number of governing equations, dynamical exponents and nonextensivity parameter.

Contents

1	Introduction	182
2	Brief Overview of Approaches for Self-Organized Criticality	184
3	Synergetic Concept	186
3.1	Self-Consistent Approach	187
3.2	Self-Similarity of the Avalanche Ensemble	201
4	Euclidean Field Approach and Optimal Trajectories	208
4.1	Variational Principle	209
4.2	Dynamics of the System Exhibiting SOC	212

5 Scaling Properties of the System with SOC	220
Appendix . Fractional Integral and Derivative	227
References	228

1. Introduction

The self-organized critical state
with all its fluctuations is not
the best possible state,
but it is the best state
that is dynamically achievable.
Per Bak, "How Nature Works"

Self-organized criticality (SOC) is the general mechanism allowing to produce a complex self-similar behaviour inherent in a system being in critical state. The evolution into the critical state occurs in absence of designed scheme accompanied with small perturbations leading to catastrophic events known as avalanches. Usually, to identify the complexity of the system behaviour the following criteria are used: (i) a fractal geometry of the evolving system; (ii) an anomalous time evolution with $1/f$ spectrum (one-over- f noise at which there is intermittency of rapid and slow regimes); (iii) catastrophes or avalanches; (iv) a power-law distribution over avalanche sizes.¹ Above critical state is established solely due to self-organization processes that means large “many-body” systems in a stable equilibrium do not exhibit complex behaviour, i.e. if such a system is disturbed, then nothing, except relaxation, happens. The complex state is understood as a border between predictable behaviour and unpredictable chaos. The complexity of chaotic as equilibrium systems occurs only at a special point of the control parameters. In systems with SOC above characteristics of complexity are independent on a special selection of tuning parameter such as temperature, pressure and so on.

The SOC behaviour appears in vast variety of systems such as a real sandpile (ensemble of grains of sand moving along increasingly tilted surface),^{2–5} intermittency in biological evolution,^{6–11} earthquakes, forest-fires, depinning transitions in random medium, and so on.¹² A simplest example of a complex process with SOC is a biological evolution where each species change their fitness to mutate in each time instant according to a behaviour of coupled species. Such evolution is out of balance where periods of stasis (no mutations) and avalanche-like mutations occur. In these systems all above characteristics of complexity are observed. Another example of SOC system is the sand or rice pile. If the pile is formed, then addition of the one grain onto the top can produce sand or rice slides named as

avalanches. The dynamics of the avalanches depends on the behaviour of all grains involved in such a process. These systems are out of balance and are complex. A sandpile exhibits a special type of behaviour where periods of stasis are interrupted by avalanches being caused by a domino effect, when large catastrophic avalanches occur as a result of the same dynamics that produces small events. A toy model of the sandpile can describe snow avalanches, earthquakes and other catastrophic events in which the system accumulates an energy during long time period (process of self-organization) and releases it in burst-like avalanches during short life-time. In such a way, one should consider SOC as a justification of catastrophism and abandon ideas of long-term predictability.

A main feature of the systems displaying SOC is their self-similarity that leads to a power-law distribution over avalanche sizes. Respectively, in most cases, SOC models are studied by making use of the scaling-type arguments supplemented by extensive computer simulations.^{13,14} In contrast, the present effort is an attempt to put forward analytical approach, which is able to describe both the process of a single avalanche formation and the behaviour of a whole avalanche ensemble in a phenomenological manner within the framework of standard Langevin dynamics with anomalous type processes and generalized statistics.

In Section 2 we represent the most important results for the system with SOC. Section 3 contains the self-consistent theory of the flux steady state. It enables us to treat the problem of a single avalanche formation on the basis of the unified analytical approach that is relevant for the case of fixed energy in Ref. [15]. Here we take into account additive noises of the sand velocity components and sandpile slope. By this, an increase of the noise intensities causes avalanche emergence even in non-driven systems, where the control parameter noise plays a crucial role. A corresponding fluctuational regime of this type corresponds to a distribution of the order parameter in an algebraic form with an integer exponent. In order not to being restricted to such a particular case we introduce a unified system with a fractional feedback. This assumption allows us to describe a subcritical regime of the avalanche formation in natural manner. The above generalization puts forward to consider the avalanche ensemble. Following famous Edwards paradigm,^{16,17} an effective scheme addressed to non-extensive thermodynamics¹⁸ is proposed to determine a time-dependent distribution over energies of moving sand grains. To generalize the Edwards scheme to non-stationary non-extensive systems, we use the fractional Lorenz system, where the avalanche size plays a role of the order parameter, non-extensive complexity is reduced to the

conjugate field and the non-conserved energy of the moving grains is the control parameter. Within the framework of this approach, the phase diagram is calculated to define the different domains of system behaviour as a function of noise intensities of the above values. As a result, we arrive at a natural conclusion that the power-law distribution over avalanche sizes inherent in the SOC regime is caused by noise of the energy.

Discussion of the dynamics of the avalanches is performed in Section 4. Here we use the Euclidean field theory and investigate optimal trajectories of the system evolution in terms of most probable values of the avalanche size and its conjugate momentum. We investigate the difference between influence of white and coloured noise of the energy of moving grains. It will be shown that the anomalous behaviour can be observed when the system passes to the domain of small avalanche size. Considering stationary picture we will show that the stationary avalanches are realized at small values of the autocorrelation time of the energy noise.

In Section 5 we show that the corresponding distribution is the solution of both nonlinear Fokker-Planck equation, that appears in the description of non-extensive systems,¹⁸ and fractional Fokker-Planck equation inherent in Levy-type processes characterized by a dynamical exponent.¹⁹ As a result, we obtain relations between the exponent of the distribution over avalanche sizes, fractal dimension of phase space, characteristic exponent of multiplicative noise, a number of governing equations needed to present self-consistent behaviour in SOC regime, dynamical exponent and Tsallis nonextensivity parameter. In the Appendix we collect information needed to use fractional derivatives and integrals.

2. Brief Overview of Approaches for Self-Organized Criticality

Historically, SOC was introduced with a help of computer simulation procedure on sand or rice piles that gives all above mentioned properties of complex system.^{1,20–23} Later, another scenario of SOC was introduced by simulation of biological species evolution.^{6–11} These simplest models with updated algorithms show a complex behaviour that allows to describe a real picture of avalanches formation, mutations of species, earthquakes, formation of river net, processes of urbanization, financial bursts et cetera (see Refs. [1,24] and citation therein).

Among the above models the sandpile is the simplest and both analytically in Refs. [25–30] and numerically in Refs. [20,31–38] most widely

studied. In analytical treatment a variety of field theory approaches should be noticed. Among them, the field scheme,³⁹ based on a nonlinear diffusion equation that has failed to account for the main feature of self-organizing systems – the self-consistent character of avalanche dynamics. An obvious reason is that the one-parameter approach does not take into account a feedback between open subsystem and environment, that are related to order and control parameters, respectively^{27,40} (see criticism in Refs. [3,4] also). A much more substantial picture is given within two-parameter approaches (Refs. [3-5,41]) that use both fundamental fields: gauge ones related to hydrodynamic modes as a sandpile height and material fields as a number of moving sand grains (avalanche size). The mean-field approximation shows that the self-similar regime of the sandpile dynamics is relevant for subcritical behaviour, where a characteristic time for the variation of the order parameter is much larger than that of the control parameter. Moreover, the latter follows the former adiabatically. Adiabatic behaviour of this type is inherent in the usual regime of system evolving in course of phase transitions⁴² and jammed motion of vehicles,⁴³ so that an adiabatic approach will be taken as basis of our consideration.

Perfect treatment of the SOC has been achieved within three-parameter approach based on the Reggeon field theory that uses the density of active sites ρ_a as order parameter and the conserved field of the energy density ζ as the control parameter.^{15,30} Along this line, SOC regime appears as a result of competition between a rate of the energy input $h > 0$ and a dissipation rate ϵ . The considered system behaves in quite different manner when, on the one hand, $h = \epsilon = 0$ and total energy is conserved, and, on the other hand, for a driven sandpile when $h \rightarrow 0^+$, $\epsilon \rightarrow 0$ under the stationarity condition $\epsilon > h$. The first case can be reduced to the picture of supercritical regime, where a non-homogeneity of initial energy distribution results in a non-Markovian term and space-dependent parameters. At dimensions above critical value $d_c = 4$, this case is found to be identical to the simplest Landau picture with $\rho_a \sim \zeta - \zeta_c$ in the active stationary state ($\zeta > \zeta_c$) and $\rho_a = 0$ in the absorbing configuration ($\zeta < \zeta_c$). A fundamentally different picture appears in the case of driven sandpile, where due to external input $h \rightarrow 0^+$, the energy density is no longer an independent field that can be reduced to the critical value ζ_c . In this case, the average magnitude of the density of active sites is equal to $\langle \rho_a \rangle = h/\epsilon$, so that the susceptibility $\chi \equiv \langle \partial_h \rho_a \rangle$ turns out to be $\chi = \epsilon^{-1}$. As a consequence, a response function behaves as $\chi(r) \sim r^{2-d} e^{-r/\xi}$ at large distances r , where d is a space dimension and $\xi \sim \epsilon^{-1/2}$ is a correlation length that is a scale for the system size $L \sim \epsilon^{-1/\mu}$.

It is remarkable that such a mean-field-type behaviour is caused solely by a stationary condition and a translational invariance.¹⁵ Respectively a set of basic critical exponents governing the scaling avalanche formation reads:³⁰ $\beta = \gamma = \delta = 1$, $\mu = 2$, $\nu = 1/2$ and $\eta = 0$. On the other hand, scaling relations accompanied by the equality of the susceptibility and the mean size of avalanche lead to the following expressions

$$\tau = 1 + \frac{z}{D}, \quad \tau = 2 \left(1 - \frac{1}{D} \right); \quad D = \frac{\mu}{\sigma} \quad (1)$$

for the exponents of the avalanche size distribution

$$P(s, \epsilon) = s^{-\tau} \mathcal{P}(x); \quad x \equiv s/s_c, \quad s_c \sim \epsilon^{-1/\sigma}, \quad (2)$$

where a critical size s_c is connected with system size $L \sim \xi$ and a characteristic time $t_c \sim L^z$ as follows: $s_c \sim L^D \sim t_c^{D/z}$ (exponents $D = \mu/\sigma$ and z are the fractal dimension and the dynamical exponent related to a critical avalanche). According to Ref. [30], the mean-field values of the above exponents are given by: $\tau = 3/2$, $\sigma = 1/2$, $D = 4$, and $z = 2$.

Despite the mentioned theories allows one to investigate the critical behaviour they do not incorporate the fluctuational mechanisms of avalanches formation. Therefore, in next sections we propose a self-consistent scheme to show how avalanches can be formed due to the influence of stochastic environment. We generalize the synergetic model introducing a fractional feedback to take into account properties of the self-similarity.

3. Synergetic Concept

In this Section, we present the analytical description of the sandpile model as a self-consistent system.⁴⁴ Along the standard approach,⁴⁵ we will use both gauge and material fields. The former are reduced to velocity components and sandpile slope considered while studying a single avalanche formation (Sec. 3.1), whereas the latter are reduced to a number of moving sand grains at examination of a distribution over avalanche sizes (Sec. 3.2). We consider the self-consistent theory of the flux steady state and introduce fluctuations of all modes to investigate the distributions of the system states. To identify the self-similar properties of the avalanche ensemble we modify the standard approach through the introduction of fractional feedback.

3.1. Self-Consistent Approach

In this section we treat the problem of a single avalanche formation on the basis of the unified analytical approach (Sec. 3.1.1) related to the case of fixed energy.¹⁵ Section 3.1.2 deals with taking into account the additive noises of the sand velocity components and sandpile slope. In Sec. 3.1.3 we examine a behaviour of a self-similar system.

3.1.1. Mechanistic Model of the Sandpile

Within framework of the simplest model of a real sandpile, its surface at given time t is defined by the dependence $y = y(t, x)$. The flow of sand locally can be described in terms of three quantities: the horizontal and vertical components of the sand velocity, $\dot{x} = \partial_t x$, $\dot{y} = \partial_t y$, and the surface slope $y' = \partial_x y$. The key point of our approach is that the above degrees of freedom are assumed to be of a dissipative type, so that, when they are not coupled, their relaxation to the steady state is governed by the Debye-type equations:

$$\frac{d\dot{x}}{dt} = -\frac{\dot{x}}{\tau_x}, \quad (3)$$

$$\frac{d\dot{y}}{dt} = -\frac{\dot{y}}{\tau_y^{(0)}}, \quad (4)$$

$$\frac{dy'}{dt} = \frac{y'_0 - y'}{\tau_S}, \quad (5)$$

where τ_x , $\tau_y^{(0)}$ and τ_S are the relaxation times of the velocity components and the slope, respectively. Eqs. (3) – (5) imply that the sand rests in the stationary state $\dot{x} = \dot{y} = 0$ and the equilibrium slope $y' = y'_0 \neq 0$ plays the role of a control parameter.

Since the motion of a sand grain along different directions is not independent, Eq. (3) should be changed by adding the term $f = \dot{y}/\gamma$, that describes a liquid friction force along the y -axis (γ is the kinetic coefficient). Then, we have

$$\tau_x \ddot{x} = -\dot{x} + a^{-1} \dot{y}, \quad (6)$$

where $a \equiv \gamma/\tau_x$. Note that, owing to the diffusion equation $\dot{y} = Dy''$ (D is the diffusion coefficient), the friction force seems to be driven by the curvature of the sandpile surface

$$f = (D/\gamma)y''. \quad (7)$$

In the stationary state, when $\ddot{x} = 0$, the solution of Eq. (6) defines the tangent line $y = ax + \text{const}$, so that the friction force $f = \tau_x^{-1}\dot{x}$ is proportional to the horizontal component of the sand velocity. Taking into consideration the relation (7) and using the chain rule $dy'/dt = \dot{y}' + y''\dot{x}$, Eq. (5) leads to the equation of motion for the slope

$$\tau_S \dot{y}' = (y'_0 - y') - (\tau_S/D) \dot{y} \dot{x}. \quad (8)$$

In a similar manner, the equation for the vertical component of the velocity can be deduced

$$\tau_y \ddot{y} = -\dot{y} + \frac{\tau_y}{\tau_x} y' \dot{x}, \quad \frac{1}{\tau_y} \equiv \frac{1}{\tau_y^{(0)}} \left(1 + \frac{y'_0}{a} \frac{\tau_y^{(0)}}{\tau_x} \right). \quad (9)$$

Note that the higher order terms are disregarded in Eq. (9) and the renormalized relaxation time τ_y depending on the stationary slope y'_0 is introduced.

Equations (6), (8) and (9) constitute the basis for self-consistent description of the sand flow on the surface with the slope y' driven by the control parameter y'_0 . The distinguishing feature of these equations is that nonlinear terms, that enter Eqs. (8) and (9), are of opposite signs, while Eq. (6) is linear. Physically, the latter means that on the early stage the avalanche begins to move along the tangent $y = ax + \text{const}$. The negative sign of the last term in Eq. (8) can be regarded as a manifestation of Le Chatelier principle, i.e., since the slope increase results in the formation of an avalanche, the velocity components \dot{x} and \dot{y} tend to impede the growth of the slope. The positive feedback of \dot{x} and y' on \dot{y} in Eq. (9) plays a fundamental role in the problem. As we will show later, it is precisely the reason for the self-organization that causes the avalanche generation.

After suitable rescaling, Eqs. (6), (8) and (9) can be rewritten in the form of the well-known Lorenz system:

$$\dot{u} = -u + v, \quad (10)$$

$$\epsilon \dot{v} = -v + uS, \quad (11)$$

$$\delta \dot{S} = (S_0 - S) - uv, \quad (12)$$

where $u \equiv (\frac{\tau_y}{\tau_x})^{1/2} (\frac{\tau_S}{D})^{1/2} \dot{x}$, $v \equiv (\frac{\tau_y}{\tau_x})^{1/2} (\frac{\tau_S}{D})^{1/2} \dot{y}/a$ and $S \equiv (\frac{\tau_y}{\tau_x}) y'/a$ are the dimensionless velocity components and the slope, respectively; $\epsilon \equiv \tau_y/\tau_x$, $\delta \equiv \tau_S/\tau_x$ and the dot now stands for the derivative with respect to the dimensionless time t/τ_x . In the general case, the system (10)–(12) cannot be solved analytically, but in the simplest case, where $\epsilon \ll 1$ and $\delta \ll 1$, the vertical velocity v and the slope S can be eliminated by making use of the adiabatic

approximation that implies neglecting of the left hand side of Eqs. (11) and (12). As a result, the dependencies of S and v on the horizontal velocity u are given by

$$S = \frac{S_0}{1 + u^2}, \quad v = \frac{S_0 u}{1 + u^2}. \quad (13)$$

Note that, under assumption that u is within the physically meaningful range between 0 and 1, the slope S is a monotonically decreasing function of u , whereas the velocity v increases with u (at $u > 1$ we have $dv/du < 0$ and the flow of the sand becomes unstable).

Substitution of the second Eq. (13) into Eq. (10) yields the Landau-Khalatnikov equation

$$\dot{u} = -\partial_u E \quad (14)$$

with the kinetic energy

$$E = \frac{1}{2}u^2 - \frac{1}{2}S_0 \ln(1 + u^2). \quad (15)$$

For $S_0 < 1$, E is a monotonically increasing function of u and the only stationary value of u equals zero, $u_0 = 0$, so that there are no avalanches in this case. Obviously, such a steady state is relevant for an absorbing configuration.¹⁵ If the slope S_0 exceeds the critical value, $S_c = 1$, the kinetic energy takes its minimum with the non-zero steady state velocity components $u_e = v_e = (S_0 - 1)^{1/2}$ and the slope $S_e = 1$.

The above scenario represents a supercritical regime of an avalanche formation and is related to a second-order phase transition.⁴¹ The latter can be easily seen from the expansion of the kinetic energy (15) in a power series of $u^2 \ll 1$. So, the critical exponents γ , δ , ν are identical to those obtained within the framework of the mean-field theory.³⁰ However, the value $\beta = 1/2$ is twice smaller because our order parameter (the velocity) is not reduced to the same (the number of active sites) in theory.³⁰

It is a drawback of the outlined approach that it fails to account for the subcritical regime of the self-organization. That is the reason for the appearance of avalanches and analogous to the first-order phase transition rather than the second-order one. So, one has to modify the above theory by assuming that the effective relaxation time $\tau_x(u)$ increases with the velocity u from value $\tau_x(1 + m)^{-1}$, $m > 0$ to τ_x .⁴² The simplest two-parameter approximation is

$$\frac{\tau_x}{\tau_x(u)} = 1 + \frac{m}{1 + (u/u_0)^2}, \quad (16)$$

where $0 < u_0 < 1$. The expression for the kinetic energy (15) then changes by adding the term

$$\Delta E = \frac{m}{2} u_0^2 \ln \left[1 + \left(\frac{u}{u_0} \right)^2 \right] \quad (17)$$

and the stationary values of u read:

$$u_e^m = u_{00} \left\{ 1 \mp \left[1 + u_0^2 u_{00}^{-4} (S_0 - S_c) \right]^{1/2} \right\}^{1/2}, \quad (18)$$

$$2u_{00}^2 \equiv (S_0 - 1) + S_c u_0^2, \quad S_c \equiv 1 + m.$$

The upper sign in the right hand side of Eq. (18) meets the value of the unstable state u^m , where the kinetic energy $E + \Delta E$ has the maximum, the lower one corresponds to the stable state u_e . The corresponding values of the stationary slope are equal

$$S^\pm = \frac{1 + u_{00}^2 \pm \sqrt{(1 + u_{00}^2)^2 - (1 - u_0^2) S_0}}{1 - u_0^2}. \quad (19)$$

The larger value S^+ meets the unstable state and smoothly increases from the quantity

$$S_m = 1 + u_0 \sqrt{m/(1 - u_0^2)} \quad (20)$$

at the parameter $S_0 = S_{c0}$ with

$$S_{c0} = (1 - u_0^2) S_m^2 \quad (21)$$

to the marginal value $S_c = 1 + m$ at $S_0 = S_c$. The S_0 -dependencies of u_e , u^m , and S_e are presented in Fig. 1. As is shown in Fig. 1a, under the adiabatic condition $\tau_S \ll \tau_x$, the parameter S_0 slowly increases being below S_c ($S_0 \leq S_c$), therefore no avalanches can form. At the point $S_0 = S_c$ the velocity u_e jumps upward to the value $\sqrt{2}u_{00}$ and its further smooth increase is determined by Eq. (18). If the parameter S_0 then decreases the velocity u_e continuously decreases to the point, where $S_0 = S_{c0}$ and $u_e = u_{00}$. At this point the velocity instantaneously falls to zero. Referring to Fig. 1b, the stationary slope S_e shows a linear increase from 0 to S_c with the parameter S_0 being in the same interval and, after the jump down to the value $(1 - u_0^2)^{-1}$ at $S_0 = S_c$, S_e smoothly decays to 1 at $S_0 \gg S_c$. When the parameter S_0 decreases from S_c down to S_{c0} , the slope grows. When the point S_{c0} , (21) is reached, the avalanche stops, so that the slope undergoes the jump from S_m , (20) up to S_{c0} . For $S_0 < S_{c0}$, again the

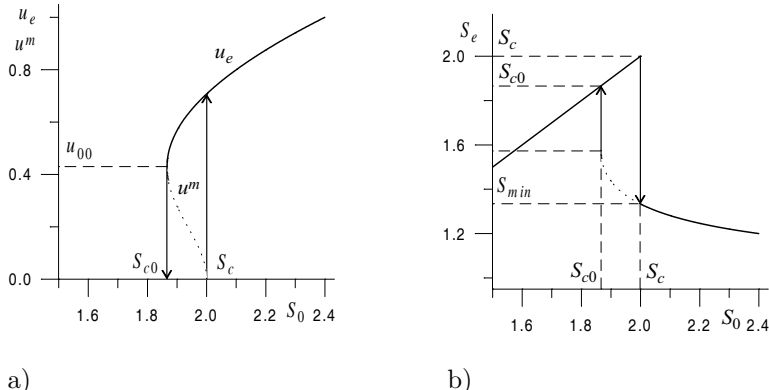


Fig. 1. The S_0 -dependencies of (a) the velocities u_e , u^m , and (b) the equilibrium slope S_e . The arrows indicate the hysteresis loops.

parameter S_e does not differ from S_0 . Note that this subcritical regime is realized provided the parameter m , that enters the dispersion law (16), is greater than

$$m_{\min} = \frac{u_0^2}{1 - u_0^2}. \quad (22)$$

According to the picture described, the avalanche generation is characterized by the well pronounced hysteresis, when the grains of sand initially being at rest begin to move downhill only if the slope of the surface exceeded its limiting value $S_c = 1 + m$, whereas the slope S_{c0} needed to stop the avalanche is less than S_c (see Eqs. (20), (21)). This is the case in the limit $\tau_S/\tau_x \rightarrow 0$ and the hysteresis loop shrinks with the growth of the adiabaticity parameter $\delta \equiv \tau_S/\tau_x$. In addition to the smallness of δ , the adiabatic approximation implies also, that the ratio $\tau_y/\tau_x \equiv \epsilon$ is small. In contrast to the former assumption, the latter does not seem to be realistic for the considered system, where in general $\tau_y \approx \tau_x$. Thus, it is of interest to study to what extent the finite value of ϵ could change the results.

Owing to the condition $\delta \ll 1$, Eq. (12) is still algebraic and S can be expressed in terms of u and v . As a result, we derive a system of two differential equations that can be studied within the phase portrait method. The phase portraits for various values of ϵ are displayed in Fig. 2, where the knot point O represents the stationary state and the saddle point S is related to the maximum of the kinetic energy. As is obvious from the Fig.

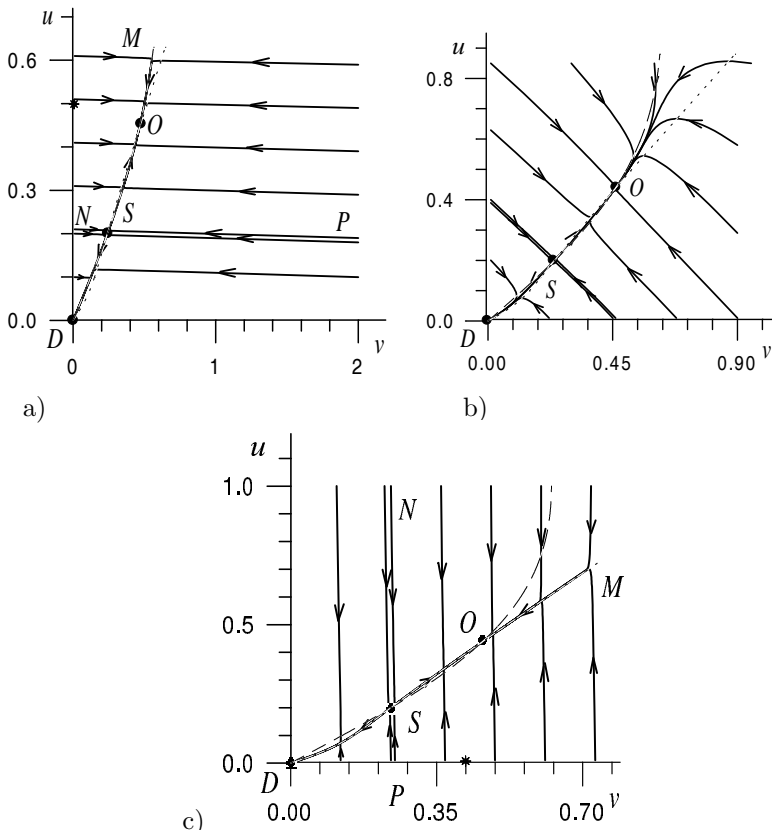


Fig. 2. Phase portraits in the v - u plane at $m = 1, u_0 = 0.1, S_0 = 1.25S_c$ for (a) $\epsilon = 10^{-2}$; (b) $\epsilon = 1$; (c) $\epsilon = 10^2$.

2, independent of ϵ , there is the universal region that attracts all phase trajectories and its structure seems to be almost insensitive to changes in ϵ . An analysis of time dependencies $v(t)$ and $u(t)$ reveals that the velocity components slow down appreciably in this region in comparison to the remaining parts of trajectories that are almost rectilinear (it is not difficult to see that this effect is caused by the smallness of the parameter δ). Since most of the time the system is in vicinity of this universal region, we arrive at the conclusion that finite values of ϵ qualitatively do not affect the results obtained in the adiabatic approximation.

3.1.2. Noise Influence on Avalanche Formation

We now focus on the effect of additive noises of the velocity components u , v , and the slope S . To this end, we add to right-hand parts of Eqs. (10) – (12) the stochastic terms $I_u^{1/2}\xi$, $I_v^{1/2}\xi$, $I_S^{1/2}\xi$, respectively [here the white noise intensities I_u , I_v , I_S are measured in units $(\tau_x/\tau_y)(D/\tau_S)$, $a^2(\tau_x/\tau_y)(D/\tau_S)$, $a^2(\tau_x/\tau_y)$, correspondingly, and $\xi(t)$ is δ -correlated stochastic function].⁴⁶ Then, within the adiabatic approximation, equations (11), (12) are reduced to the time-dependencies

$$v(t) = \bar{v} + \tilde{v}\xi(t), \quad S(t) = \bar{S} + \tilde{S}\xi(t); \quad (23)$$

$$\begin{aligned} \bar{v} &\equiv S_0 u d(u), & \tilde{v} &\equiv \sqrt{I_v + I_S u^2} d(u), \\ \bar{S} &\equiv S_0 d(u), & \tilde{S} &\equiv \sqrt{I_S + I_v u^2} d(u), & d(u) &\equiv (1 + u^2)^{-1}. \end{aligned} \quad (24)$$

Here deterministic components are reduced to Eq. (13), whereas fluctuational ones follow from the known property of additivity of variance of independent Gaussian random quantities.⁴⁶ Thus, an application of the slaving principle inherent in synergetics⁴⁷ transforms noises of both vertical velocity component v and slope S , which are additive initially, to multiplicative form. As a result, a combination of Eqs. (10), (23), (24) leads to the Langevin equation

$$\dot{u} = f(u) + \sqrt{I(u)} \xi(t), \quad f \equiv -\partial_u E, \quad (25)$$

where the force f is related to the energy E determined by Eq. (15) and expression for the effective noise intensity

$$I(u) \equiv I_u + (I_v + I_S u^2) d^2(u) \quad (26)$$

is obtained in accordance with above mentioned property of noise variances additivity.

To continue in the usual way,⁴⁶ let us write the Fokker–Planck equation related to the Langevin one (25):

$$\partial_t P(u, t) = \partial_u \{ -f(u)P(u, t) + \partial_u [I(u)P(u, t)] \} \quad (27)$$

At steady state, that will be the only case we consider, the probability distribution $P(u, t)$ becomes a time-independent function $P(u)$ and under the usual condition, that the expression in braces of the right-hand part in Eq. (27) is equal to zero, this leads to a stationary distribution

$$P(u) = Z^{-1} \exp\{-U(u)\}, \quad (28)$$

where Z is a normalization constant. The effective energy

$$U(u) = \ln I(u) - \int_0^u \frac{f(u')}{I(u')} du', \quad f \equiv -\partial_u E, \quad (29)$$

is determined by the bare energy E , Eq. (15), the noise intensity $I(u)$ and Eq. (26) (see Ref. [48]). Combining these expressions, we can find the explicit form of $U(u)$, which is too cumbersome to be reproduced here. The equation which defines the locations of the maxima of distribution function $P(u)$

$$x^3 - S_0 x^2 - 2I_S x + 4(I_S - I_v) = 0, \quad x \equiv 1 + u^2, \quad (30)$$

is much simpler. According to Eq. (30), maxima are insensitive to changes in the intensity of the noise I_u of the velocity component u , but they are determined by the value S_0 of the sandpile slope and the intensities I_v , I_S of the noises of the vertical velocity component v and the slope S which acquire the multiplicative character in Eq. (26). Hence, for simplicity I_u can be set equal to 0 and Eqs. (15), (29) and (26) give the following expression for the effective energy:

$$U(u) = \frac{1}{2} \left[\frac{u^4}{2} + (2 - S_0 - i)u^2 + (1 - i)(1 - S_0 - i) \ln(i + u^2) \right] + I_S \ln[g_S^2(u) + ig_v^2(u)], \quad i \equiv I_v/I_S. \quad (31)$$

According to Eq. (30), the effective energy (31) has a minimum at $u = 0$ if the stationary slope S_0 does not exceed the critical level

$$S_c = 1 + 2I_S - 4I_v \quad (32)$$

whose value increases at increasing intensity of the noise of the sandpile slope, but decreases with one of the vertical velocities. Here, sand grains do not move. In the simple case $I_v = 0$, the avalanche creation is related to solutions

$$u_{\pm}^2 = \frac{1}{2} \left[S_0 - 3 + \sqrt{(3 - S_0)^2 + 4(2S_0 - 3 + 2I_S)} \right] \quad (33)$$

which are obtained from Eq. (30) after elimination of the root $u^2 = 0$. The magnitude of this solution has its minimum

$$u_c^2 = \frac{1}{2} \left[(S_0 - 3) - \sqrt{(S_0 + 7)(S_0 - 1)} \right] \quad (34)$$

on the line defined by expression (32) with $I_v = 0$. At $S_0 < 4/3$ the roots $\pm u_c$ are complex, starting from $S_0 = 4/3$ they become zero and at $S_0 > 4/3$

one has real values $u_+ = -u_-$. In this way, the tricritical point

$$S_0 = 4/3, \quad I_S = 1/6 \quad (35)$$

addresses to the appearance of roots $u_{\pm} \neq 0$ of Eq. (30) that means avalanche creation. If condition (32) is satisfied, the root $u = 0$ corresponds to the minimum of the effective energy (31) at $S_0 < 4/3$, whereas at $S_0 > 4/3$ this root corresponds to the maximum, and the roots u_{\pm} – to symmetrical minima.

Now, we find another condition of stability of the roots u_{\pm} . Setting the discriminant of Eq. (30) equal to zero, we get the equations

$$I_S = 0, \quad I_S^2 - I_S \left[\frac{27}{2} \left(1 - \frac{S_0}{3} \right) - \frac{S_0^2}{8} \right] + \frac{S_0^3}{2} = 0, \quad (36)$$

the second of which gives

$$2I_S = \left[\frac{27}{2} \left(1 - \frac{S_0}{3} \right) - \frac{S_0^2}{8} \right] \pm \left\{ \left[\frac{27}{2} \left(1 - \frac{S_0}{3} \right) - \frac{S_0^2}{8} \right]^2 - 2S_0^3 \right\}^{1/2}. \quad (37)$$

This equation defines a bell-shaped curve $S_0(I_S)$, which intersects the horizontal axis at the points $I_S = 0$ and $I_S = 27/2$, and has a maximum $S_0 = 2$ at

$$I_S = 2. \quad (38)$$

It is easy to see that for $I_v = 0$ this line touches the curve (32) at point (35).

Let us now consider the more general case of two multiplicative noises $I_v, I_S \neq 0$. Introducing the parameter $a = 1 - i$, $i = I_v/I_S$ and the renormalized variables $\tilde{I} \equiv I_S/a^2$, $\tilde{S}_0 \equiv S_0/a$, $\tilde{u}^2 = (1 + u^2)/a - 1$, at $i < 1$ we reproduce all above expressions with the generalized energy \tilde{U}/\tilde{I} in Eq. (31). Thus, the action of the noise of the vertical velocity component v is reduced to the renormalization of the extremum value of the horizontal one by the quantity $(a^{-1} - 1)^{1/2}$. As a result, the region of divergence $\tilde{u} \approx 0$ becomes inaccessible.

The condition of extremum of the generalized energy (31) splits into two equations, one of which is simply $u = 0$, and the other one is given by Eq. (30). As mentioned above, the analysis of the latter indicates that the line of existence of the zero solution is defined by expression (32). The tricritical point has the coordinates

$$S_0 = \frac{4}{3}(1 - I_v), \quad I_S = \frac{1}{6}(1 + 8I_v). \quad (39)$$

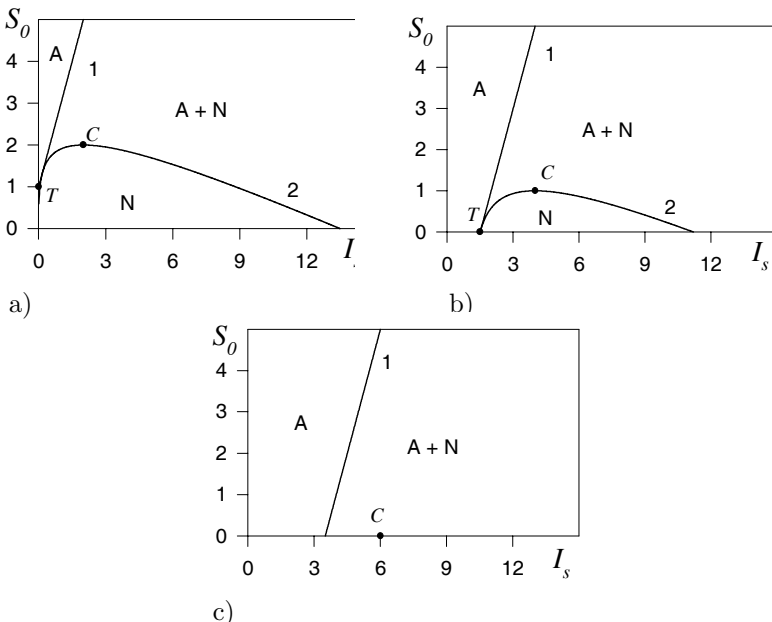


Fig. 3. Phase diagrams for fixed values I_v of the noise intensities of the vertical velocity component: (a) $I_v = 0$; (b) $I_v = 1$; (c) $I_v = 2$. Curves 1 and 2 define the boundary of stability of avalanche and avalanche-free phases (A: a flux phase; N: a non-flux phase).

The phase diagram for the fixed intensities I_v is shown in Fig. 3. Here the curves 1, 2 define the thresholds of absolute loss of stability for the fluxless and flux steady states, respectively. Above line 1 the system is in a stable flux state, below curve 2 it is in fluxless one, and between these lines the two-phase domain is realized. For $I_v < 1/4$ the situation is generally the same as in the simple case $I_v = 0$ (see Fig. 3a). At $I_v > 1/4$ even for small intensities I_S of the slope noise (Fig. 3b) the avalanches formation is possible. According to (39) the tricritical point lies on the I_S axis at $I_v = 1$, and if the noise intensity I_v is larger than the critical value $I_v = 2$ the stable fluxless state disappears (see Fig. 3c).

To conclude, the above consideration shows that the dissipative dynamics of grains flow in a real sandpile can be represented within the framework of the Lorenz model where the horizontal and vertical velocity components play the role of the order parameter and its conjugate field, respectively, and the sandpile slope is the control parameter. In Section 3.1.1, the noiseless case is examined to show that an avalanche is created if the externally

driven sandpile slope y'_c is larger than the critical magnitude

$$y'_c = (\tau_x \tau_y)^{-1/2} \gamma. \quad (40)$$

In this sense, the systems with small values of the kinetic coefficient γ and large relaxation times τ_x, τ_y of the velocity components are preferred. However, the sand flow appears as usual phase transition because the avalanche creation in the noiseless case is only possible due to the externally driven growth of the sandpile slope.

A consideration of the additive noises of the above degrees of freedom shows that the stochasticity influence is non-essential for the horizontal velocity component and that it is crucial for both the vertical velocity component and the sandpile slope. The boundary of the domain of avalanche formation is set by the equality for the dimensionless noise intensities

$$I_S = -\frac{1}{2} + 2I_v, \quad (41)$$

following from Eq. (30) at conditions $x = 1$ ($u = 0$) and $S_0 = 0$. According to Eq. (41), in absence of the sandpile slope noise the avalanche is created if the intensity of vertical velocity component exceeds the value

$$I_{v0} = \frac{1}{4} \frac{D\gamma^2}{\tau_x \tau_y \tau_S}, \quad (42)$$

corresponding to the point O in Fig. 4. An increase of both the vertical velocity and the sandpile slope noises causes the avalanche formation if its intensities are bounded by the condition (41). The domain of the mixed state appears with further increase of these intensities above the values

$$I_{v1} = \frac{D\gamma^2}{\tau_x \tau_y \tau_S}, \quad I_{S1} = \frac{3}{2} \frac{\gamma^2}{\tau_x \tau_y}, \quad (43)$$

at the point T in Fig. 4. If the noise intensity of the vertical velocity exceeds the larger value

$$I_{v2} = 2 \frac{D\gamma^2}{\tau_x \tau_y \tau_S}, \quad (44)$$

corresponding to the sandpile slope noise $I_{S2} = 6\gamma^2/\tau_x \tau_y$ (the point C in Fig. 4), the fluxless steady state disappears at all.

Physically, we have to take into consideration that the SOC regime is not relevant to a flux-type state itself, but rather to an intermittent regime of avalanche formation corresponding to the domains in the phase diagrams in Figs. 3, 4, where a mixture of both phases A and N (avalanche and avalanche-free) exists. According to the above analysis, such an intermittent

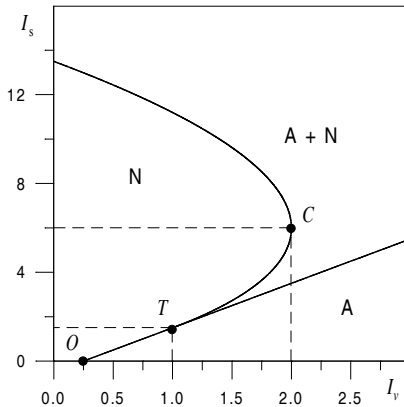


Fig. 4. Phase diagram of a system with the noises of the slope I_s and the vertical velocity component I_v (the slope $S_0 = 0$; D : disordered point, T : tricritical point, C : critical point).

behaviour may be realized within the region located above line (41) and outside the curve that is determined by

$$I_v = I_S \left[1 - \left(\frac{2}{27} \right)^{1/2} \sqrt{I_S} \right] \quad (45)$$

with the dimensionless values I_v , I_S . The corresponding phase diagram is depicted in Fig. 4 to show a very non-trivial form (especially, within the domain $I_{v1} \leq I_v \leq I_{v2}$).

3.1.3. Generalized Model

To proceed, let us examine an explicit form of the probability (28) determined, for different regimes, by the effective energy (29). In the case $I_u, I_v \ll I_S$, we obtain a distribution

$$P(u) \approx I_v^{-1} (1 + u^2)^2 \exp \left\{ I_v^{-1} \int f(u) (1 + u^2)^2 du \right\}, \quad (46)$$

$$f(u) \equiv -u + S_0 u / (1 + u^2)$$

that differs from the power dependence inherent in self-similar systems. Contrary, at intermittent behaviour, when $I_u, I_v \ll I_S$, the supercritical

values of the slope noise intensity I_S cause the following distribution form

$$P(u) \approx I_S^{-1} \left(\frac{1+u^2}{u} \right)^2 \exp \left\{ I_S^{-1} \int \frac{f(u)(1+u^2)^2}{u^2} du \right\} \sim u^{-2}. \quad (47)$$

Thus, the case $I_u, I_v \ll I_S$ addresses to the power-law distribution inherent in self-similar behaviour. However, in general case, the obtained exponent should not be reduced to the integer 2, but to fractional one.⁴⁸

To get rid off such a restriction, the multiplier u in the nonlinear terms of Eqs. (10) – (12) is supposed to be replaced by power term u^a , with an exponent $0 \leq a \leq 1$. Taking into account the stochastic additions, one obtains the basic equations in dimensionless form

$$\begin{aligned} \dot{u} &= -u + v + \sqrt{I_u} \xi(t), \\ \epsilon \dot{v} &= -v + u^a S + \sqrt{I_v} \xi(t), \\ \delta \dot{S} &= (S_0 - S) - u^a v + \sqrt{I_S} \xi(t). \end{aligned} \quad (48)$$

It appeared that the agreement of the Lorenz self-organization scheme with the SOC concept, related to self-similar systems, is achieved, if one assumes that both positive and negative feedbacks are fractional. Within such an assumption, the adiabatic approximation $\epsilon, \delta \ll 1$ leads to the Langevin equation (cf. Eq. (25))

$$\dot{u} = f_a(u) + \sqrt{I_a(u)} \xi(t), \quad (49)$$

where the force $f_a(u)$ and the noise intensity $I_a(u)$ are as follows:

$$\begin{aligned} f_a(u) &\equiv -u + S_0 u^a d_a(u), \\ I_a(u) &\equiv I_u + (I_v + I_S u^{2a}) d_a^2(u), \quad d_a(u) \equiv (1 + u^{2a})^{-1}. \end{aligned} \quad (50)$$

The corresponding distribution (cf. Eqs. (28), (29))

$$P_a(u) = \frac{Z^{-1}}{I_a(u)} \exp \{-E_a(u)\}, \quad (51)$$

where Z is the partition function, determined by an effective potential

$$E_a(u) \equiv - \int_0^u \frac{f_a(u')}{I_a(u')} du'. \quad (52)$$

The extremum points of this distribution are determined by the equation

$$2aI_S u^{2a} + (1 + u^{2a})^2 u^{1-a} [S_0 - u^{1-a} (1 + u^{2a})] = 2a(I_S - 2I_v), \quad (53)$$

according to which the boundary of the flux state

$$I_S = 2I_v, \quad (54)$$

relates to the condition $u = 0$. Critical values of state parameters are fixed by the condition $|\frac{du}{dS_0}| = \infty$ leading to an additional equation

$$\begin{aligned} & u^{2(1-a)} (1 + u^{2a})^2 [(2 + a^{-1}) + (a^{-1} - 1) u^{-2a}] \\ & - \frac{1}{2} S_0 u^{1-a} (1 + u^{2a}) [(3 + a^{-1}) + (a^{-1} - 1) u^{-2a}] = 2aI_S. \end{aligned} \quad (55)$$

Expressions (53) – (55) generalize the simple equalities (30), (41) and (45) related to the case $a = 1$.

Above expressions show that qualitative results of Sec. 3.1.2 obtained for the particular case $a = 1$ remain valid passing to the general case $0 \leq a \leq 1$. Indeed, the most essential difference is observed for the noiseless case, namely the steady-state velocity u becomes nonzero within the whole interval of the driven slope S_0 (see Fig. 5). An increase of the vertical

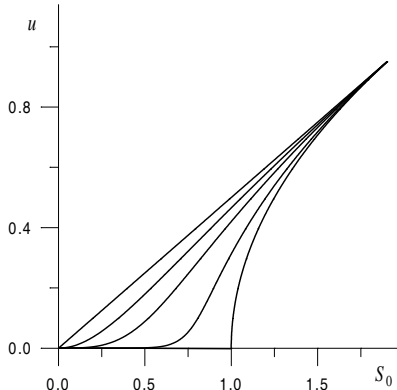


Fig. 5. The S_0 -dependence of the steady-state velocity u at various values of $a = 0, 0.5, 0.7, 0.9, 1.0$ from left to right.

velocity noise I_v causes monotonic u -growth, whereas I_S -increase leads to an effective barrier formation near the point $u = 0$, so that the dependence $u(S_0)$ becomes non-monotonic at the values of I_S above the straight line (54) (see Figs. 6). Here, by analogy with noiseless case (see Fig. 1), lower branches of curves correspond to unstable values of the order parameter, while the upper ones correspond to the stable ones. According to Fig. 7, the domain, where avalanches can not be created, is located near intermediate values of the state parameters S_0, I_v, I_S . The phase diagram related to the

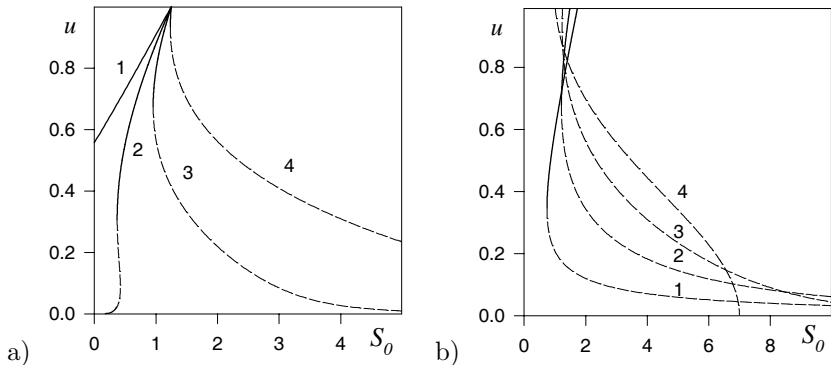


Fig. 6. The S_0 -dependence of the steady-state velocity u : a) at various values of noise intensity of the slope I_S ($a = 0.75$, $I_v = 1$) 1: $I_S = 1$; 2: $I_S = 2$; 3: $I_S = 3$; 4: $I_S = 5$; b) at various values of a ($I_v = 1$, $I_S = 5$) 1: $a = 0.25$; 2: $a = 0.5$; 3: $a = 0.75$; 4: $a = 1.0$.

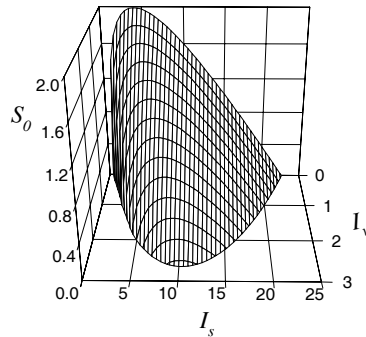


Fig. 7. Three-dimensional phase diagram (avalanche-free domain is located under surface).

avalanche formation reveals the same form as for the simplest case $a = 1$, but the straight line (41) shifts abruptly to (54) with escaping the point $a = 1$ (compare Fig. 8a with Fig. 4). According to Fig. 9, an increase of the vertical velocity noise I_v increases the domain of the avalanche formation.

3.2. Self-Similarity of the Avalanche Ensemble

In contrast to the previous discussion, when the process of a single avalanche formation has been considered, in this section we will study analytically the self-similar size distribution over avalanche ensemble. This means that,

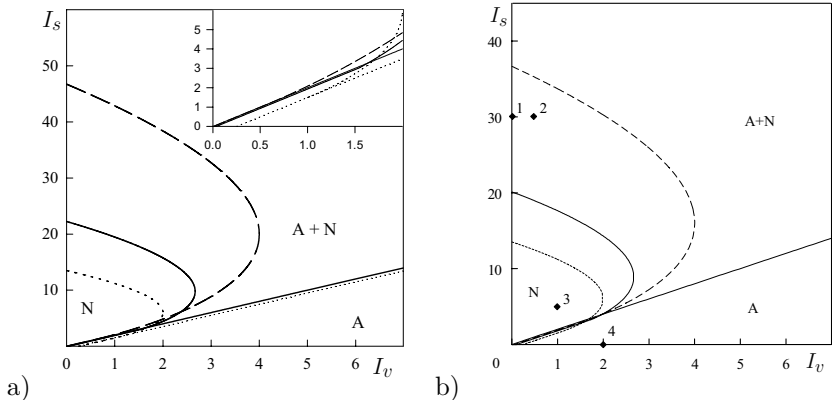


Fig. 8. Phase diagrams of a system with the noises of the slope I_S and the vertical velocity component I_v ($S_0 = 0$): a) model (48) with $a = 0.5, 0.75, 1.0$; b) model (58) with $\tau/2 = 0.5, 0.75, 1.0$ (pointed, solid and dashed curves, respectively). Diamonds correspond to curves 1 – 4 in Fig. 11.

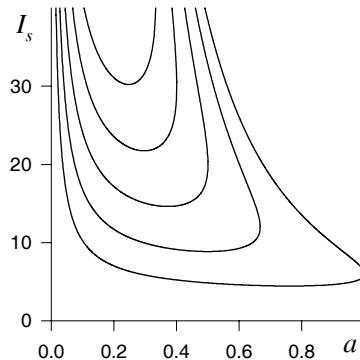


Fig. 9. Phase diagram in the $I_S - a$ plane at various values of noise intensity of the vertical velocity component: $I_v = 2, 3, 4, 5, 6$ from bottom to top (avalanche-free domain is located inside the curves).

along lines of Sec. 3.1.2 we will account for noises of a complete set of degrees of freedom, as well as the fractional feedback type introduced in Sec. 3.1.3. Therefore, the Lorenz system unified in the above manner is the basis of our examination. However, instead of visible geometric-and-mechanic characteristics of a 'real' sandpile, the system under consider-

ation is now parameterized by a set of pseudo-thermodynamic variables, that describe the avalanche ensemble in the spirit of the famous Edwards paradigm^{16,17} generalized to nonstationary system. Within the framework of the usual synergetic approach, these degrees of freedom play the role of order parameter, conjugate field and control parameter.

It is principally important that the use of the slaving principle of both synergetic and the fractional nature of the system feedback is shown to stipulate multiplicative character of noise. It will be shown, that this causes a nonextensivity of the applied thermodynamical scheme, so that we have to use q -weighted averages instead of usual ones. So, energy of moving sand grains is defined by expression

$$\zeta_q \equiv \sum_i \zeta_i p_i^q, \quad (56)$$

where p_i is a probability to move grain i with energy ζ_i , $q \neq 1$ is a positive parameter that is a measure of the system's nonextensivity determined below. Nonextensive complexity of moving sand grains is an analog to Tsallis entropy¹⁸ that is determined as follows:

$$\Sigma_q \equiv -\frac{\sum_i p_i^q - 1}{q - 1}. \quad (57)$$

The three-parameter set of the standard synergetic scheme⁴⁷ is completed by the avalanche size s .

Following the above elaborated line, we postulate that a self-consistent behaviour of the considered system is presented adequately by a set of pointed out quantities governed by the Lorenz-type equations (cf. Eqs. (48))

$$\begin{aligned} \tau_s \dot{s} &= -s^{\tau/2} + a_s \Sigma_q + \sqrt{I_s} \xi(t), \\ \tau_\Sigma \dot{\Sigma}_q &= -\Sigma_q + a_\Sigma s^{\tau/2} \zeta_q + \sqrt{I_\Sigma} \xi(t), \\ \tau_\zeta \dot{\zeta}_q &= (\zeta^0 - \zeta_q) - a_\zeta s^{\tau/2} \Sigma_q + \sqrt{I_\zeta} \xi(t). \end{aligned} \quad (58)$$

Here τ_s , τ_Σ , τ_ζ denote relaxation times of corresponding values, a_s , a_Σ , a_ζ are related feedback parameters, I_s , I_Σ , I_ζ are respective white noise intensities, τ is a positive exponent and ζ^0 is the externally driven energy of the sand motion. The particular feature of the first of these equations is that in a noiseless case genuine characteristics s , Σ_q are linearly connected. On the other hand, the two last equations (58) show that the connection of values ζ_q , Σ_q , that are of a thermodynamic type, with the avalanche size s is nonlinear. Physically, this means a nonlinear relation between the complexity and the avalanche size energy near steady states. Moving away leads to negative feedback of the avalanche size and the complexity on

the energy that, in accordance with Le Chatelier principle, results in the energy decrease. Moreover, positive feedback appears of the avalanche size and the energy on the complexity, which causes complexity increase that is the reason of the avalanche ensemble's self-organization.

To analyse the system (58), it is convenient to measure the time t in unit τ_s and introduce the scales for variables s , Σ_q , ζ_q , I_s , I_Σ and I_ζ as follows:

$$t^{sc} \equiv t_s(a_\Sigma a_\zeta)^{\frac{1}{2}-\frac{1}{\tau}}, \quad s^{sc} \equiv (a_\Sigma a_\zeta)^{-\frac{1}{\tau}}, \quad \Sigma_q^{sc} \equiv a_s^{-1}(a_\Sigma a_\zeta)^{-\frac{1}{2}}, \\ \zeta_q^{sc} \equiv (a_s a_\Sigma)^{-1}; \quad I_s^{sc} \equiv (a_\Sigma a_\zeta)^{-\frac{2}{\tau}}, \quad I_\Sigma^{sc} \equiv a_s^{-2}(a_\Sigma a_\zeta)^{-1}, \quad I_\zeta^{sc} \equiv (a_s a_\Sigma)^{-2}.$$

Then, the scaled Lorenz system (58) takes the simple form

$$\begin{aligned} \dot{s} &= -s^{\tau/2} + \Sigma_q + \sqrt{I_s} \xi(t), \\ \vartheta \dot{\Sigma}_q &= -\Sigma_q + s^{\tau/2} \zeta_q + \sqrt{I_\Sigma} \xi(t), \\ \theta \dot{\zeta}_q &= (\zeta^0 - \zeta_q) - s^{\tau/2} \Sigma_q + \sqrt{I_\zeta} \xi(t), \end{aligned} \quad (59)$$

with the ratios of relaxation times

$$\vartheta \equiv \tau_\Sigma / \tau_s, \quad \theta \equiv \tau_\zeta / \tau_s. \quad (60)$$

It is worth to notice that system (59) gets the form of Eqs. (48) if the values s , Σ_q , ζ_q , $\tau/2$, ϑ and θ are replaced by u , v , S , a , ϵ and δ , respectively. The only difference is caused by replacement of s by $s^{\tau/2}$ in the first equation of the system (59).

It is well known that a complete set of SOC systems could be reduced to one of two families:³⁰ systems with deterministic dynamics extremely driven by a random environment (growing interface models, Bak-Sneppen evolution model etc.) and the stochastic dynamics family (models of earthquakes, forest-fire etc.).^a A remarkable peculiarity of the obtained system (59) is the possibility to present both mentioned families in a natural manner. The former is related to noiseless case, when $I_s, I_\Sigma, I_\zeta = 0$ but the energy relaxation time is larger than that of the complexity and avalanche size ($\tau_\zeta \geq \tau_\Sigma, \tau_s$); on the other hand, a parameter of the environment drive ζ^0 has to take a larger values than the critical one $\zeta_c = 1$ (see Ref. [42]). In such a case, system (59) describes a strange attractor⁴⁷ that might represent the behaviour the SOC systems of the first type. A proper stochastic behaviour is relevant for non-vanishing intensities $I_s, I_\Sigma, I_\zeta \neq 0$ that make possible the appearance of the SOC regime even in absence of a driven affect ($\zeta^0 = 0$).

^aIn general, we deal with much more complicated problem, see Ref. [49].

Taking into account that the problem of the Lorenz strange attractor is well known,⁴⁷ we will restrict ourselves to the treatment of the stochastic system, where the adiabatic condition $\vartheta \ll 1$, $\theta \ll 1$ are applicable. Then, the two last equations of system (59) lead to dependencies of the type of Eqs. (23)

$$\Sigma_q(t) = \bar{\Sigma}_q + \tilde{\Sigma}_q \xi(t), \quad \zeta_q(t) = \bar{\zeta}_q + \tilde{\zeta}_q \xi(t), \quad (61)$$

where the deterministic and fluctuational components are determined as follows (cf. Eqs. (24))

$$\begin{aligned} \bar{\Sigma}_q &\equiv \zeta^0 s^\tau / 2 d_\tau(s), \quad \tilde{\Sigma}_q \equiv \sqrt{I_\Sigma + I_\zeta s^\tau} d_\tau(s); \\ \bar{\zeta}_q &\equiv \zeta^0 d_\tau(s), \quad \tilde{\zeta}_q \equiv \sqrt{I_\zeta + I_\Sigma s^\tau} d_\tau(s), \quad d_\tau(s) \equiv (1 + s^\tau)^{-1}. \end{aligned} \quad (62)$$

Due to the slaving principle of synergetics, the initially adiabatic noises of the complexity and the energy are transformed to a multiplicative form. On the other hand, the relation between the complexity and energy

$$\bar{\Sigma}_q = \sqrt{\bar{\zeta}_q(\zeta^0 - \bar{\zeta}_q)}, \quad (63)$$

that can be deduced with the dependencies (62), leads to the expression

$$T = - \left(1 - \frac{\zeta^0}{2\bar{\zeta}_q} \right)^{-1} \sqrt{\frac{\zeta^0}{\bar{\zeta}_q} - 1} \quad (64)$$

for the effective temperature $T \equiv \partial_{\bar{\Sigma}_q} \bar{\zeta}_q$. As depicted in Fig. 10a, T is a monotonically increasing function of the energy with boundary values $T(\bar{\zeta}_q = 0) = 0$ and $T(\bar{\zeta}_q = \zeta^0/2) = \infty$. At the latter point the value of T changes instantaneously to $-\infty$ and then increases monotonically again to initial value $T = 0$ at $\bar{\zeta}_q = \zeta^0$. This means that in the domain $0 \leq \bar{\zeta}_q < \zeta^0/2$ the avalanche system is dissipative and behaves in a usual way; on contrast, in the domain $\zeta^0/2 < \bar{\zeta}_q \leq \zeta^0$ a self-organization process evolves, so that an energy increase leads to a complexity decrease, in accordance with a negative temperature. At steady state, where an avalanche has got a stationary size $s_0 = \sqrt{\zeta^0 - 1}$, the temperature takes the stationary value

$$T_0 = - \frac{\sqrt{\zeta^0 - 1}}{1 - \zeta^0/2} \quad (65)$$

that is negative in the supercritical domain $\zeta^0 > 1$. According to Fig. 10b, the magnitude T_0 decreases monotonically with the driven energy from value $T_0(\zeta^0 = 1) = 0$ to $T_0(\zeta^0 \rightarrow 2) \rightarrow -\infty$.

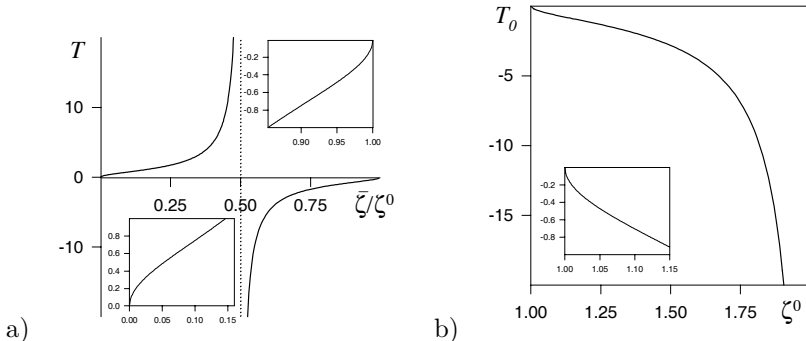


Fig. 10. The energy dependencies of the avalanche ensemble temperatures: a) nonstationary effective temperature T versus ratio $\bar{\zeta}/\zeta^0$ of nonstationary energy to external driven value; b) stationary temperature T_0 versus external driven energy ζ^0 .

The presented self-organization regime relates to externally driven systems, which are relevant for the usual phase transition but not the SOC itself. To study the latter within the above consideration, let us combine Eqs. (61) and (62) with the first of equations (59) in a way that has been used above for obtaining the Langevin equation (25). By analogy with Sec. 3.2, this leads to stochastic equation (49), where the effective force and noise intensity are given by Eqs. (50) with accuracy to the replacements mentioned after Eqs. (60): the quantities s , Σ_q , ζ_q , $\tau/2$ have to be taken instead of u , v , S , a . Then, all results obtained in Sec. 3.2 can be used immediately. Particularly, it is found that the influence of the random scattering of the avalanche size is non-essential, whereas energy and complexity noises lead to a crucial effect. The related picture is reflected in Fig. 8 given in the $I_\zeta - I_\Sigma$ plane that is formed by corresponding noise intensities of avalanche ensemble. The mixed domain A+N with respect to the intermittency regime is bounded by the straight line (54) and the bell-shaped curve of Eqs. (45). According to Fig. 9, where the exponent a has to be replaced by $\tau/2$, the random scattering growth of the complexity extends the SOC domain along the axis of the exponents τ .

Now, we will discuss the distribution of the avalanche size on basis of Eqs. (50) – (52). For arbitrary noise intensities one has

$$P(s) = \frac{Z^{-1}}{I(s)} \exp \left\{ \int_0^s \frac{f(s')}{I(s')} ds' \right\};$$

$$f(s) \equiv -s + \zeta^0 s^{\tau/2} d_\tau(s), \quad (66)$$

$$I(s) \equiv I_s + (I_\Sigma + I_\zeta s^\tau) d_\tau^2(s), \quad d_\tau(s) \equiv (1 + s^\tau)^{-1}.$$

In the SOC regime, the driven energy vanishes, $\zeta^0 = 0$, and the distribution (66) behaves as depicted in Fig. 11 for different noise intensities of both energy and complexity. It can be seen that the power-law dependence inherent in the SOC regime is observed only in the limits $s \ll 1$ and $I_s, I_\Sigma \ll I_\zeta$. In this case, the distribution (66) is reduced to the canonical form (2), where the second multiplier takes the form

$$\mathcal{P}(s) = \frac{d_\tau^{-2}(s)}{Z} \exp \left\{ -I_\zeta^{-1} \int_0^s \frac{d_\tau^{-2}(s')}{(s')^{\tau-1}} ds' \right\}, \quad d_\tau(s) \equiv (1 + s^\tau)^{-1}. \quad (67)$$

It is easy to see that deviation of this multiplier from a constant value is estimated by term $\sim s^{2-\tau}$, that increases with decrease of τ and growth of avalanche size to extremely large values $s \sim 1$, i.e., with escaping SOC domain. This is confirmed by Fig. 12, where the deviation $\delta\tau$ of the slope of dependence $P(s)$, Eqs. (66) in the linear domain from the theory parameter τ is depicted as a function of the parameter τ itself. In accordance with the above estimate, it can be seen that the deviation $\delta\tau$ takes a maximal value $\delta\tau < 10^{-1}\tau$ at non-essential values $\tau < 1$ or with noise intensity growth to enormous values $I_S \sim 10^3$.

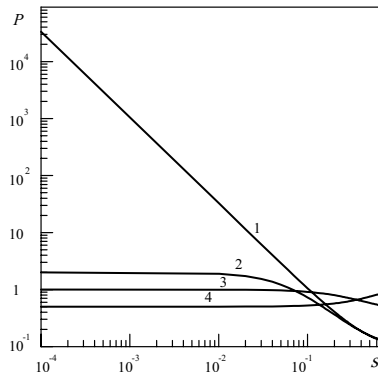


Fig. 11. The distribution function (66) at $\tau = 1.5$ at various regimes (pointed out by diamonds in Fig. 8b). 1: $I_v = 0, I_S = 50$ (SOC); 2: $I_v = 0.5, I_S = 30$ (A+N); 3: $I_v = 1, I_S = 5$ (N); 4: $I_v = 2, I_S = 0.5$ (A).

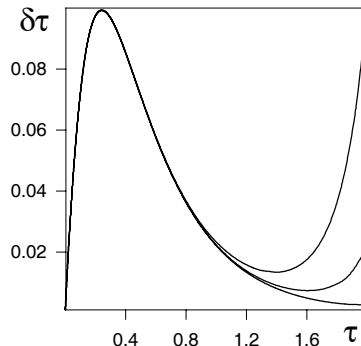


Fig. 12. Deviation $\delta\tau$ of the linear slope of curve 1 depicted in Fig. 11 from the parameter τ versus the exponent τ itself ($I_S = 10, 50, 10^3$ from bottom to top).

4. Euclidean Field Approach and Optimal Trajectories

Considering dynamics of stochastic systems one deals with behaviour of most probable values of stochastic variable or its averages. The last allows to determine the statistical picture of the systems evolution. The former shows the dynamics of maxima of the probability density function, which correspond to macrostates (phases) appeared in a course of noise induced behaviour (see Ref. [50] and references therein). Such a macrostate define new properties of the system which can not be observed in a noiseless case. Considering the problem of dynamics of stochastic systems, variational principles can be useful to determine optimal trajectories of the system evolution (see Refs. [51-55]). The mathematical tool which allows to investigate the dynamics of the system and to find probability of rare fluctuations is the path integral trajectories method. Unfortunately, in most works the quasi-classic WKB approximation is speculated being restricted by consideration of weak noise limit only and therefore it can not give a complete information about the noise influence playing a crucial role. More essential effects of the noise influence on the dynamics of the system are observed with a help of the Euclidean field theory (EFT) to account the original properties of stochastic process.⁵¹ As it appeared this theory allows to investigate the processes of an absorbing state formation.^{56,57} We apply the approach based on EFT to explore the picture of spontaneous (avalanche-type) dynamics realized in the system with SOC regime.⁵⁸

4.1. Variational Principle

Let us start with a multiplicative noise Langevin equation for a relevant macrovariable $s(t)$ in the form

$$\dot{s} = \mathcal{D}_1(s) + \sqrt{2\mathcal{D}_2(s)}\zeta(t), \quad (68)$$

where $\mathcal{D}_1(s)$ represents an effective drift coefficient, $\mathcal{D}_2(s)$ plays a role of the effective diffusion coefficient, $\zeta(t)$ indicates the white noise with zero mean and correlations given as follows:

$$\langle \zeta(t) \rangle = 0, \quad \langle \zeta(t)\zeta(t') \rangle = \delta(t - t'). \quad (69)$$

Here, Itô interpretation of Eq. (68) is used and therefore, Eq. (68) is associated with the Fokker–Planck equation in the form of Kramers–Moyal expansion⁴⁶

$$\partial_t P(s, t) = -\partial_s \mathcal{D}_1(s)P(s, t) + \partial_s^2 \mathcal{D}_2(s)P(s, t). \quad (70)$$

In order to investigate the system dynamics in the framework of the path integral approach we should construct the probability functional in the form

$$P(s; \tilde{t} \rightarrow \infty) \propto \exp(-\mathcal{S}), \quad (71)$$

where imaginary time $\tilde{t} = it$ is used. The optimal trajectories are given with a help of minimization procedure for the Euclidean action: $\delta\mathcal{S} = 0$.

To construct \mathcal{S} let us pass to a new process $y(t)$, which is associated with $s(t)$ as $ds/dy = \sqrt{2\mathcal{D}_2(s(y))}$. The new stochastic process $y(t)$ satisfies the Langevin equation

$$\dot{y} = \tilde{h}(s(y)) + \zeta(t), \quad \tilde{h} \equiv \frac{\mathcal{D}_1(s)}{\sqrt{2\mathcal{D}_2(s)}} - \frac{1}{2}\partial_s \sqrt{2\mathcal{D}_2(s)}. \quad (72)$$

The obtained equation (72) allows us to use the standard field scheme^{45,59,60} based on analysis of the generating functional. The latter has the form

$$Z\{u(t)\} = \int Z\{y(t)\} \exp\left(\int u y dt\right) Dy(t) \quad (73)$$

where

$$Z\{y(t)\} = \left\langle \prod_t \delta\left\{\dot{y} - \tilde{h} - \zeta\right\} \det\left|\frac{\delta\zeta}{\delta y}\right|\right\rangle_{\zeta}, \quad (74)$$

here Dy denotes integration over all paths starting at $y(0)$ for $t = 0$ and ending at $y(t_f)$ for $t = t_f$ (for the sake of simplicity, we return to notation of the imaginary time as t). The argument of the δ -function in Eq. (74) can

be reduced to Langevin equation (72), and the Jacobian of transformation from variables $\zeta(t)$ to $y(t)$ is equal to unity in the Itô calculus.⁴⁶

To analyse functional (74) we can take into account the identity

$$\delta \{y(t)\} = \int_{-i\infty}^{i\infty} \exp \left(- \int q y dt \right) Dq. \quad (75)$$

Averaging over the noise ζ with the help of the Gaussian distribution

$$\Pi\{\zeta\} \propto \exp \left\{ -\frac{1}{2} \int \zeta^2(t) dt \right\}, \quad (76)$$

and taking into account Eq. (75), we reduce functional Eq. (74) to the standard form

$$Z\{y(t)\} = \int e^{-S\{y(t), q(t)\}} Dq. \quad (77)$$

Here the corresponding Lagrangian is

$$\mathcal{L}(y, q) = q \left(\dot{y} - \tilde{h} \right) - q^2/2. \quad (78)$$

For the next we use the Euler equations

$$\frac{\partial \mathcal{L}}{\partial z} - \frac{d}{dt} \frac{\partial \mathcal{L}}{\partial \dot{z}} = \frac{\partial \mathcal{R}}{\partial \dot{z}}, \quad z \equiv \{y, q\}, \quad (79)$$

where the dissipative function is defined as

$$\mathcal{R}(y) = \dot{y}^2/2. \quad (80)$$

As a result, the equations for the most probable realizations of the stochastic fields $y(t)$ and $q(t)$ assume the form

$$\dot{y} = \tilde{h} + q, \quad (81)$$

$$\dot{q} = -q \left(1 + \partial_y \tilde{h} \right) - \tilde{h}. \quad (82)$$

A comparison of Eq. (81) with the stochastic equation (72), having the same form, shows that the fields $y(t)$ and $q(t)$ are the most probable values of amplitudes of the auxiliary hydrodynamic mode and fluctuation of the conjugate force. In order to return to the initial field $s(t)$, we get the Lagrangian and the dissipative function as follows:

$$\mathcal{L}(s, \phi) = \phi [\dot{s} - \mathcal{D}_1(s) + \partial_s \mathcal{D}_2(s)/2] - \mathcal{D}_2(s) \phi^2, \quad (83)$$

$$\mathcal{R}(s) = \dot{s}^2/4\mathcal{D}_2(s), \quad (84)$$

where the definition $\phi = \partial\mathcal{L}/\partial\dot{y}$ is used for the conjugate momentum, which yields to the relation $q = \sqrt{2\mathcal{D}_2(s)}\phi$. Therefore, the Euler equations (79) read

$$\dot{s} = \mathcal{D}_1(s) - \frac{1}{2}\partial_s\mathcal{D}_2(s) + 2\mathcal{D}_2(s)\phi, \quad (85)$$

$$\begin{aligned} \dot{\phi} &= -\phi \left\{ 1 + \partial_s \left[\mathcal{D}_1(s) - \frac{1}{2}\partial_s\mathcal{D}_2(s) \right] + \phi\partial_s\mathcal{D}_2(s) \right\} \\ &\quad - \frac{\mathcal{D}_1(s)}{2\mathcal{D}_2(s)} + \frac{1}{2}\partial_s \frac{\mathcal{D}_2(s)}{2\mathcal{D}_2(s)}. \end{aligned} \quad (86)$$

In the stationary case $\dot{s} = \dot{\phi} = 0$ we have

$$\phi = -\frac{\mathcal{D}_1(s)}{2\mathcal{D}_2(s)} + \frac{1}{4}\partial_s \ln \mathcal{D}_2(s), \quad (87)$$

$$\phi \left\{ \partial_s \left[\mathcal{D}_1(s) - \frac{1}{2}\partial_s\mathcal{D}_2(s) \right] + \phi\partial_s\mathcal{D}_2(s) \right\} = 0. \quad (88)$$

From Eqs. (87), (88) it follows that steady states are defined by the equations

$$\mathcal{D}_1(s) - \frac{1}{2}\partial_s\mathcal{D}_2(s) = 0, \quad (89)$$

$$\mathcal{D}_1(s) - \frac{1}{2}\partial_s\mathcal{D}_2(s) - \sqrt{\mathcal{D}_2(s)} = 0. \quad (90)$$

First of these equations gives points on the phase plane (ϕ, s) with abscissa $\phi = 0$ and the second one gives points situated off the axis $\phi = 0$. Physically, the first equation defines the bifurcation diagram for most probable values of stochastic variable s , whereas the second one allows to find a corresponding phase diagram when solutions of both equations coincide. The meaning of Eqs. (87), (88) becomes clear if we consider the additive noise limit, i.e. $\mathcal{D}_2(s) = \text{const}$. In the domain of the system parameters at which there are no solutions of Eq. (89) we have a point on the phase plane (ϕ, s) with abscissa $\phi \neq 0$ and ordinate given by solution of Eq. (90). Condition (87) indicates that the conjugate momentum ϕ has an opposite sign to the force value $\mathcal{D}_1(s)$. According to Eq. (88), the “susceptibility” $(\partial_s^2 V)^{-1} = -1/\partial_s\mathcal{D}_1(s)$ takes an infinite value. Thus, such a point on the phase plane corresponds to the stationary state of a thermodynamic system being unstable with respect to the transition into the ordered phase with $s \neq 0$. In the case of $\phi = 0$ the ordinate is given by a solution of Eq. (89). In the additive limit, this point corresponds to the state of thermodynamic

equilibrium. Of course, during the process of its evolution a real thermodynamic system tends to the equilibrium state with $\phi = 0$, but not to the unstable state where $\phi \neq 0$.

According to obtained equations we can consider the probability of realization of a phase trajectory corresponding to different initial values $s(0) \equiv s(t_0)$. The probability can be obtained from Eqs. (83), (85) integrating over the whole path $s(t)$, starting from $s(0)$. The related expression for the probability takes the form

$$P(s(0)) \propto \exp \left[- \int_{s(0)} \mathcal{D}_2(s(t)) \phi^2(t) dt \right]. \quad (91)$$

4.2. Dynamics of the System Exhibiting SOC

Here we discuss the system described by the set of pseudo-thermodynamical variables $\{s, \Sigma, \zeta\}$ under the constraint of an adiabatic approximation.⁴⁴ According to the Sec. 3.2, where the control parameter fluctuates with noise intensity I_ζ , we suppose that $I_s = I_\Sigma = 0$. Next let us assume the noise of the control parameter to be coloured: related Langevin force is characterized by $\langle \xi(t)\xi(t') \rangle = C(t, t')$.

Within the adiabatic approach we use the effective Langevin equation

$$\dot{s} = f(s) + g(s)\xi(t), \quad (92)$$

where the force $f(s)$ and the noise amplitude $g(s)$ are

$$f(s) \equiv -s^{\tau/2} + \zeta^0 s^{\tau/2} d_\tau(s), \quad g(s) = \sqrt{I_\zeta} s^{\tau/2} d_\tau(s); \quad d_\tau(s) \equiv (1 + s^\tau)^{-1}. \quad (93)$$

Considering the SOC regime in a non-driven system let us put $\zeta^0 = 0$. In order to avoid non-physical situation we should restrict ourselves by consideration of the values for avalanche size which lies in the interval $s \in (b_0, \infty)$, $b_0 = 0+$. Next we will consider only nonzero values of s , supposing a state with $s = 0$ as a nonavalanche one. As will be shown below, in the case of white (Sec.4.2.1) or coloured (Sec.4.2.2) noise the boundary b_0 can transform the kinetics of the system at $s \ll 1$.

4.2.1. Pure White Noise

The simplest situation corresponds to the case of white noise, where correlation function has the form

$$C(t, t') = \delta(t - t'). \quad (94)$$

This is rather mathematical than physical model but it gives results which can be treated to set a general properties of the system. In such a case, the drift and diffusion coefficients are

$$\mathcal{D}_1 = f(s), \quad \mathcal{D}_2 = g^2(s)/2. \quad (95)$$

Then, the equations (85), (86) read

$$\dot{s} = f(s) - \frac{1}{2}g(s)\partial_s g(s) + g^2(s)\phi, \quad (96)$$

$$\dot{\phi} = -\phi \left[\partial_s \left(f(s) - \frac{1}{2}g(s)\partial_s g(s) \right) + \phi g(s)\partial_s g(s) \right] - \frac{\dot{s}}{g^2(s)}. \quad (97)$$

In the stationary case the avalanche size is given by Fig. 13. Here, solid

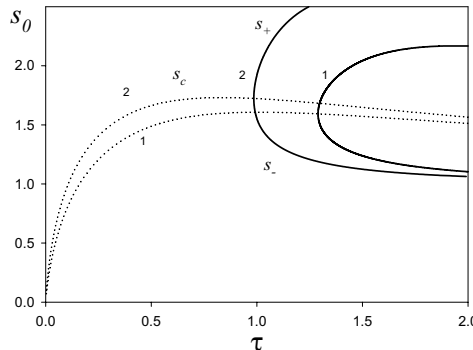


Fig. 13. Stationary value of the avalanche size s_0 vs. exponent τ at $I_\zeta = 100, 150$ (curves 1 and 2, correspondingly).

lines (denoted as s_- , s_+) correspond to the solution of the stationary equation (96) at $\phi = 0$, the dotted lines mean the solutions of (97) at $\phi \neq 0$. Making use of the analysis of the stationary solutions in the case of additive noise, we conclude that solutions s_- , s_+ situated on the axis $\phi = 0$ define the equilibrium states. Because in stationary case Eq. (96) has always a trivial solution $s_0 = 0$, one should conclude that the stable equilibrium states are characterized by the two points on the phase plane (ϕ, s) with coordinates $(0, 0)$ and $(0, s_+)$. The stationary solution denoted as dotted line s_c corresponds to the state with coordinate $(\phi_0 \neq 0, s_c)$. According to the phase diagram in Fig. 14 and related dependencies in Fig. 13 we see

that an increase in the noise intensity I_ζ leads to formation of the stationary avalanche at small values of the exponent τ . Deviation of the exponent τ from the specific value 2 corresponds to an increase in the nonlinearity of main functions that define the avalanches formation. The domains denoted as N and A+N in Fig. 14 determine values of I_ζ , τ at which there are no avalanche $s_0 = 0$ (N) and both the noise induced state with $s_0 \neq 0$ and avalanche-free state of $s_0 = 0$ coexist (A+N).

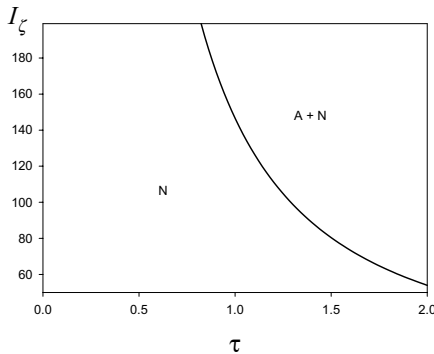


Fig. 14. Phase diagram of stationary avalanche formation (N and A+N denote domains of avalanche-free and mixing states, respectively).

To investigate the system dynamics we plot corresponding phase portraits (see Fig. 15) at different noise autocorrelation times. The general picture of phase portraits shown in Fig. 15a is characterized by the presence of a separatrix QS_cF . It divides the phase plane into two isolated domains, corresponding to large and small values of s . The domain of large values is characterized by an infinite increase of the most probable value of avalanche size s and its conjugate momentum ϕ at $t \rightarrow \infty$. Above the separatrix QS_cF phase trajectories do not give essential contribution to the stationary distribution (91). The formation of the domain corresponding to values $s \ll 1$ is associated with the multiplicative nature of the noise. In this domain, $s(t)$ tends to the attractive point O with coordinates $s = \phi = 0$. It will be shown below that in this domain the small values of avalanche size s and its conjugate momentum ϕ correspond to maximal values of the probability (91) in the limit $t \rightarrow \infty$. Comparing Fig. 15a, Fig. 15b, we see that they differ by the location of the attraction node on the axis $\phi = 0$ when one moves through the critical value $\tau = 1$. The general property

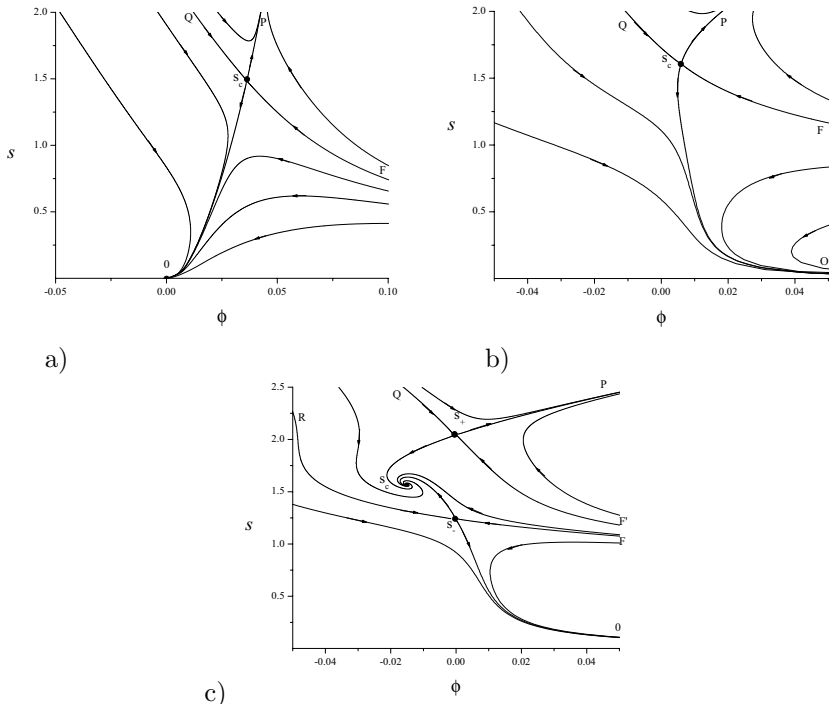


Fig. 15. Phase portraits of the system with white noise at $I_\zeta = 100$: a) $\tau = 0.5$; b) $\tau = 1.2$; c) $\tau = 1.5$.

of the phase portrait shown in Fig. 15c is a presence of two separatrices with branches RS_-F and QS_+F' . They divide the phase plane into three isolated domains, corresponding to large, intermediate and small values of s . The first domain is characterized by an infinite increase of the quantities s and ϕ at $t \rightarrow \infty$. The domain of intermediate values of s , in which the system passes into the stationary ordered state with a nonzero value of avalanche size is of interest. This domain determines the noise induced transition kinetics.

Let us analyse the behaviour of the system in each of these domains. To this end we consider the probability of realization of a phase trajectory corresponding to different initial values $s(0) \equiv s(t = 0)$. The dependence $P(s(0))$ obtained for the index $\tau < 1$ is shown in Fig. 16 (curve 1). It is seen that apart from the trivial increase of $P(s(0))$ the probability jumps near separatrix of the phase portraits. Outside the region restricted by the

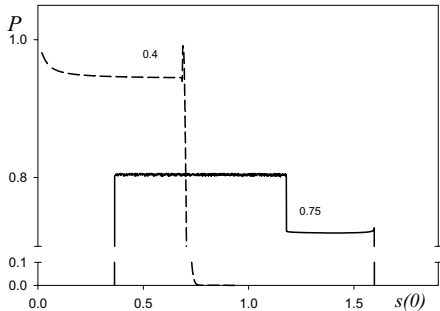


Fig. 16. Dependence of the probability P of realization of different trajectories on the initial value of the avalanche size $s(0)$ at $I_\zeta = 100$. Dashed and solid curves correspond to $\tau = 0.8, 1.5$. The initial value of the conjugate momentum is $\phi(0) = 0.015$.

(outer) separatrix, we have $P = 0$, because $s(t), \phi(t) \rightarrow \pm\infty$ at $t \rightarrow \infty$. Such a behaviour of the probability $P(s(0))$ can be explained by the form of the time dependencies $s(t)$ and $\phi(t)$ during relaxation of the initial value (see Fig. 17) for various values of the index τ . To this end we put $\dot{\phi} = 0$ in

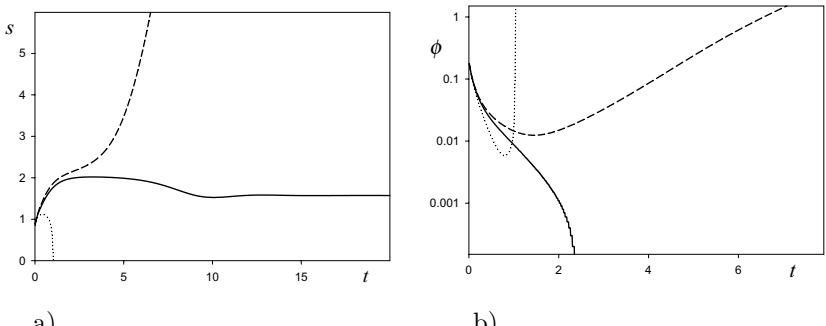


Fig. 17. A typical picture of the temporal behaviour for the avalanche size (a) and the conjugate momentum (b) at $\tau = 3/2$, $I_\zeta = 100$. Solid curves correspond to the trajectories inside the domain $FS_C F'$, dashed lines correspond to trajectories above the separatrix $F'S_+$, dotted curves correspond to domain of small values $s(0)$.

Euler equations. The obtained equation gives stationary values of conjugate momentum in the limit $s \rightarrow 0$:

$$\phi \propto \begin{cases} \frac{1}{4}(1-\tau)s^{1-\tau}, & \tau < 1; \\ \frac{1}{2}(\tau-1)s^{-1}, & \tau > 1. \end{cases} \quad (98)$$

Thus, at $\tau < 1$ the system tends in the course of time to the origin $s = \phi =$

0. At $\tau \geq 1$, the attraction node jumps to infinity ($s = 0, \phi \rightarrow \infty$). The corresponding integrand in the distribution (91) reads

$$g^2(s)\phi^2 \propto \begin{cases} (1-\tau)^{-2} s^{2(1-\tau/2)}, & \tau < 1; \\ \frac{1}{4}(\tau-1)^2 s^{-2(1-\tau/2)}, & \tau > 1. \end{cases} \quad (99)$$

It is characterized by the inversion of the sign of the exponent when the critical value $\tau = 1$ is exceeded. Substituting Eq. (98) at $\tau < 1$ into Euler equations and retaining the leading term in it, we obtain

$$s \propto (t_0 - t)^H, \quad t < t_0, \quad H^{-1} = 2 - \tau, \quad (100)$$

where t_0 is a constant, which characterizes the time during which the point moves towards the axis $s = 0$. Inserting Eq. (100) into Eq. (99) and the obtained expression into Eq. (91) we receive the probability $P(s(0))$ which differs from zero in the domain $s \ll 1$. Physically, it means that if the fluctuations excite the system then its behaviour tends to suppress such an excitation. In other words, the state $s(0) \neq 0$ relaxes to $s(t \rightarrow \infty) \rightarrow 0$ along optimal trajectories that are realized with non zero probability.

A completely different situation is observed at $\tau > 1$. In this case, $g^2\phi^2$ acquires an exponent with an opposite sign in accordance with Eq. (99). As a result, the probability (91) vanishes at $s \ll 1$. The physical reason behind such a behaviour is that the system moves towards the axis $s = 0$ for a finite time interval $t_0 < \infty$. It ensures an infinite value of the conjugate momentum $\phi \propto t^{-1/(2-\tau)}$. This can be visualized as the rise of the absorbing state (the precipitation of a condensate of configuration points from the phase portrait domain $s \ll 1$ onto the abscissa when $\phi \rightarrow \infty$). Note that the condition $t_0 < \infty$ is fulfilled only below the separatrix branch RS_O in Figs. 15b,c, while in the region bounded by separatrices RS_F and QS_F' we have $t_0 \rightarrow \infty$, and the divergence of the integrand in Eq. (91) is not manifested. Consequently, the equality $P = 0$ holds only below the line RS_F .

4.2.2. Coloured Noise

In the simplest form, the problem of coloured noise can be introduced considering the effects of the auto-correlation of the Langevin force $\zeta(t)$ in Eq. (92). Next we assume a specific form for the noise ζ : we choose Ornstein–Uhlenbeck noise, i.e. Gaussian-distributed stochastic variable with zero mean and exponentially decaying correlator

$$\langle \zeta(t)\zeta(t') \rangle = \frac{1}{2\tau_\zeta} \exp\left(-\frac{|t-t'|}{\tau_\zeta}\right). \quad (101)$$

They arise as solutions of Langevin equation

$$\tau_\zeta \dot{\zeta} = -\zeta + \xi(t), \quad (102)$$

where $\xi(t)$ is a white noise, namely, with zero mean and δ -correlated: $\langle \xi(t)\xi(t') \rangle = \delta(t-t')$. In such a representation the system given by Eqs. (92), (101) is a non-Markovian in its properties. To pass to the Markovian process $s(t)$ the unified coloured noise approximation⁶¹ can be used.

If we take a time derivative of Eq. (92), expressing first $\dot{\zeta}$ in terms of ζ and ξ from Eq. (102) and then ζ in terms of \dot{s} and s from Eq. (92), we obtain the following non-Markovian stochastic differential equation

$$\tau_\zeta \left(\ddot{s} - \dot{s}^2 \frac{\partial_s g(s)}{g(s)} \right) = -\lambda(s) \dot{s} + f(s) + g(s) \xi(t), \quad (103)$$

where

$$\lambda(s) = 1 - \tau_\zeta f(s) \partial_s \ln \left[\frac{f(s)}{g(s)} \right]. \quad (104)$$

Here, following unified coloured noise approximation, we can recover a Markovian stochastic differential equation. It needs to use adiabatic elimination (neglecting \ddot{s}) and neglect \dot{s}^2 so that the system's dynamics is governed by a Fokker–Planck equation. Using Itô differential rule, the resulting equation is linear in \dot{s} and takes the form

$$\lambda(s) \dot{s} = f(s) + g(s) \xi(t). \quad (105)$$

An expression in the left hand side of Eq. (105) defines a time derivative for a new variable z . The relation between z and s is $dz = \lambda(s)ds$. An evolution equation for $s(t)$ can be written down as Eq. (68) with drift and diffusion coefficients

$$\begin{aligned} \mathcal{D}_1(s) &= \frac{f(s)}{\lambda(s)} - \frac{1}{2} g^2(s) \partial_s \ln \lambda(s), \\ \mathcal{D}_2(s) &= \frac{1}{2} \left(\frac{g(s)}{\lambda(s)} \right)^2. \end{aligned} \quad (106)$$

Therefore, related Euler equations read

$$\dot{s} = \frac{f(s)}{\lambda(s)} - \frac{1}{2} \frac{g(s)}{\lambda(s)} \partial_s \ln \lambda(s) - \frac{1}{2} \partial_s \ln \left(\frac{g(s)}{\lambda(s)} \right) + \left(\frac{g(s)}{\lambda(s)} \right)^2 \phi, \quad (107)$$

$$\begin{aligned} \dot{\phi} &= -\phi \left\{ \partial_s \left[\frac{f(s)}{\lambda(s)} - \frac{1}{2} \frac{g(s)}{\lambda(s)} \partial_s \ln \lambda(s) - \frac{1}{2} \partial_s \ln \left(\frac{g(s)}{\lambda(s)} \right) \right] \right. \\ &\quad \left. + \phi \frac{g(s)}{\lambda(s)} \partial_s \frac{g(s)}{\lambda(s)} \right\} - \frac{\dot{s} \lambda^2(s)}{g^2(s)}. \end{aligned} \quad (108)$$

In the stationary case $\dot{s} = \dot{\phi} = 0$ we have

$$\phi = -\frac{\lambda(s)f(s)}{g^2(s)} + \frac{1}{2}\partial_s \ln g(s), \quad (109)$$

$$\phi \left\{ \frac{\lambda(s)f(s)}{g^2(s)} \partial_s \ln \left[\frac{f(s)}{g(s)} \right] + \frac{1}{2} [\partial_s \ln \lambda(s)] \partial_s \ln g(s) - \frac{\partial_s^2 g(s)}{2g(s)} \right\} = 0. \quad (110)$$

From obtained formulas and the phase diagram shown in Fig. 18a it follows that in the limit $\tau \rightarrow 0$ we pass to the white noise system discussed in the previous section. An influence of coloured nature of the multiplicative

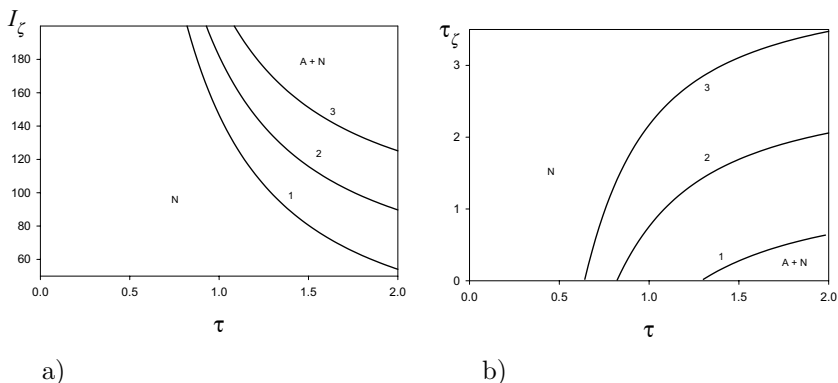


Fig. 18. Phase diagrams for the system with coloured noise: a) I_ζ vs. τ , curves 1, 2, 3 correspond to $\tau_\zeta = 0.001, 0.5, 1$; b) τ_ζ vs. τ at $I_\zeta = 100, 200, 300$ (curves 1, 2, 3, respectively).

noise is reduced to the following: (i) an increase in the noise auto-correlation time τ_ζ increases the critical values of the noise intensity I_ζ when the system passes to the domain of stationary avalanches (see Fig. 18a); (ii) Fig. 18b shows that an increase in τ_ζ produces transition from the ordered state to the disordered (avalanche-free) state. The picture of stationary solutions is shown in Fig. 19. It is seen that the formation of the stationary avalanche occurs in a discontinuous manner inherent to the first order transitions. Here at large τ_ζ the phase portrait of the system is characterized by one stable point with coordinate $(0, 0)$ and one saddle point, situated on the axis s . The form of the phase portrait in the considered case is the same as in Fig. 15. If we pass to the low-frequency fluctuations with $\tau_\zeta \ll 1$, the stationary avalanche is formed and two steady state points appear in the phase portrait with coordinates determined by the condition $\phi = 0$ and

specified by the coordinates s_{\mp} as solutions of the steady-state equation (110).

Considering the time dependencies, it should be noted that the form of $s(t)$, $\phi(t)$ and $g(s)\phi(s)$ does not change essentially comparing with the white noise case. Therefore, for the considered case the asymptotics given by Eqs. (98), (99) are the same. The exponent τ does not change its critical value 1 at which the absorbing configuration is formed. Indicated features mean that the coloured nature of the noise can not change the universality class of the system behaviour. Therefore, an influence of the coloured fluctuations is reduced to control of a process of the stationary avalanches formation through the spectral quantity τ_ζ .

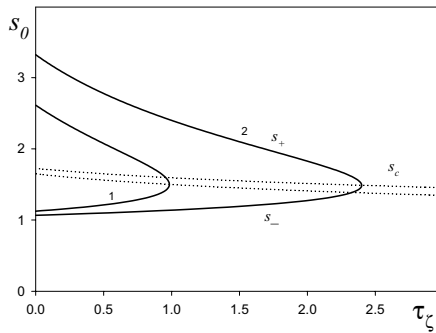


Fig. 19. Stationary solutions for the system with coloured noise. 1: $I_\zeta = 150$, $\tau = 1.5$; 2: $I_\zeta = 200$, $\tau = 1.5$.

5. Scaling Properties of the System with SOC

A remarkable peculiarity of expression (67) is that, within the limits $s \ll 1$, $I_s, I_\Sigma \ll I_\zeta$ inherent in the SOC regime, it can be expressed in the terms of standard form Gamma-function $\Gamma(x)$ and fractional integral $\mathcal{I}_{-s}^{2-\tau}$ of order $2 - \tau$ (see the Appendix and, for details, Ref. [62])

$$\mathcal{P}(s) = \frac{d_\tau^{-2}(s)}{Z} \exp \left\{ - \frac{\Gamma(2 - \tau)}{I_\zeta} \mathcal{I}_{-s}^{2-\tau} d_\tau^{-2}(s) \right\}. \quad (111)$$

On the other hand, it is well-known¹⁹ that expressions of this kind appear as a solution of the fractional Fokker–Planck equation

$$\partial_t^\omega \mathcal{P}(s, t) = \partial_{-s}^\varpi \left\{ s \mathcal{P}(s, t) + \frac{I_\zeta}{\Gamma(\varpi)} \partial_{-s}^\varpi [d_\tau^2 \mathcal{P}(s, t)] \right\}, \quad (112)$$

where the fractional derivative ∂_x^ϖ (see (A.141)) is used to be inverted to the fractional integral (A.140). Multiplying equation (112) by term $s^{2\varpi}$ and averaging over s according to the definition

$$\langle s^z \rangle \equiv \int_{-\infty}^{\infty} s^z \mathcal{P}(s, t) ds, \quad (113)$$

one obtains at $\alpha \equiv 2\varpi$

$$\langle s^z \rangle \sim t, \quad z = \frac{2\varpi}{\omega}, \quad (114)$$

where z is a dynamical exponent. This relation corresponds to the large time limit, where only the diffusive contribution is essential. Combining expressions (111), (114) and (A.140) leads to the relations $2 - \tau = \varpi = z\omega/2$, that yield

$$\tau = 2 - \frac{z\omega}{2}. \quad (115)$$

Comparing this equation with the second of the known relations (1), one obtains

$$\omega z = \frac{4}{D}. \quad (116)$$

The mean-field values $\omega = 1$ and $D = 4$ are related to the dynamical exponent $z = 1$ that, in accordance with definition (114), is related to unusual ballistic limit of SOC regime. On the other hand, the fractional Fokker–Planck equation (112) leads to the usual diffusive regime with $z = 2$ only in artificial case, when the time-derivative exponent is assumed to be $\omega = 1/2$.

The obvious reason of such discrepancy in the non-consistent application of the usual field relations (1) to the Lorenz system (59). In this system, the stochastic degrees of freedom s , Σ_q and ζ_q , whose number is $n = 3$, serve as the different space directions. However, the stochastic process evolves for any of these variables in a plane spanned by the given variable itself and its conjugated momentum. Moreover, the multiplicative character of noise, which is determined by the exponent a in expressions (50), reduces the fractal dimension of every plane to the value $2(1 - a)$.^{48,63} Thus, the

resulting fractal dimension of phase space, where the stochastic system evolves, is as follows:

$$D = 2n(1 - a), \quad (117)$$

where $n = 3$ for the exploited here Lorenz system. Inserting this dimension into expression (116) leads to $\omega z = 2$, which, in contrast to the relation $\omega z = 1$ obtained above, is correct in the simplest case $\omega = 1$, $z = 2$ [the latter is relevant to a single stochastic degree of freedom ($n = 1$) with additive noise ($a = 0$)]. In the general case, equations (115) – (117) yield the final result

$$\tau = 2 \left[1 - \frac{1}{2n(1 - a)} \right]. \quad (118)$$

The respective dependencies are depicted in Fig. 20a,b to show that the exponent τ increases monotonically from its minimum value $\tau = 1$ at the critical number $(1 - a)^{-1}$ to the upper value $\tau = 2$ in the limit $n \rightarrow \infty$; thereby, an a -growth shifts the dependence $\tau(n)$ to large values of n , i.e., decreases the exponent τ .

It is easy to see that relation (118) reproduces known results of different approaches for the dimension D (see Ref. [64]). In the case related to mean-field theory, one has $\tau = 3/2$ and equation (118) expresses the number of self-consistent stochastic equations needed for treating the SOC behaviour as a function of the exponent of the corresponding multiplicative noise:

$$n = \frac{2}{1 - a}. \quad (119)$$

In accordance with Fig. 20c, a self-consistent mean-field treatment is possible if the number of relevant equations is larger than the minimum magnitude $n_c = 2$. Approaches of Refs. [3,14,30,41,65] represent examples of such considerations, where noise is supposed to have additive character ($a = 0$). Switching the multiplicative noise leads to an a -growth and non-contradicting representation of the SOC demands an increase in the number of self-consistent equations: for example, within the field scheme¹⁵ related to directed percolation ($a = 1/2$), the mean-field approximation is applicable for dimensions larger than the critical magnitude $d_c = 4$; here and in Refs. [42,43] the Lorenz scheme ($n = 3$) with multiplicative noise is characterized by the exponent $a = 1/3$ (see below).

Let us now focus on the relation of the above exponents to the nonextensivity parameter q related to Tsallis definitions (56), (57).¹⁸ The relevant

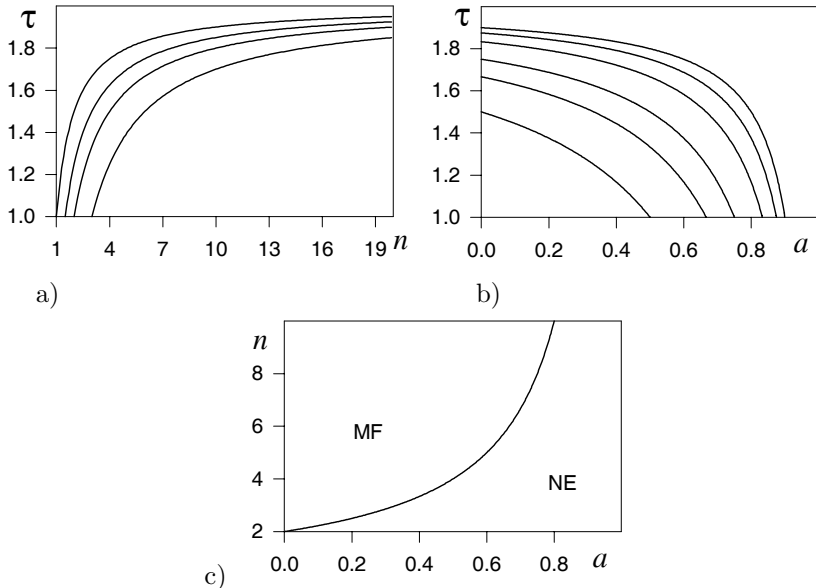


Fig. 20. Dependencies of exponent τ of avalanche size distribution: a) on number n of representing equations ($a = 0, \frac{1}{3}, \frac{1}{2}, \frac{2}{3}$ from top to bottom); b) on exponent a of multiplicative noise ($n = 2, 3, 4$ from bottom to top); (c) phase diagram displaying mean-field domain.

kinetic behaviour could be described by the nonlinear Fokker–Planck equation

$$\partial_t^\beta P(s, t) = \partial_{-s}^2 P^q(s, t), \quad (120)$$

where ∂_t^β is the fractional derivative and the measure units are chosen in such a way that the effective diffusion coefficient disappears ($\beta > 0$, $q > 0$ are the relevant exponents^{66,67}). Supposing a normalized distribution function in a self-similar form

$$P(s, t) = s_c^{-1} \mathcal{P}(x); \quad s_c \equiv s_c(t), \quad x \equiv s/s_c, \quad (121)$$

we obtain

$$s_c^{1+q} \sim t^\beta, \quad \mathcal{P}^{q-1} \sim x^2. \quad (122)$$

On the other hand, we could use the fractional Fokker–Planck equation of the type of Eq. (112):

$$\partial_t^\beta P(s, t) = \partial_{-s}^\alpha P(s, t). \quad (123)$$

Inserting the solution (121), one finds the dependencies

$$s_c^\alpha \sim t^\beta, \quad \mathcal{P} \sim x^{\alpha-1}, \quad x \rightarrow 0 \quad (124)$$

whose comparison with Eqs. (122) yields

$$1 + q = \alpha. \quad (125)$$

Because the average $|s|$ in Eq. (113) is reduced to the scale s_c in the case of self-similar systems, the relevant dependencies (114), (122), and (124) give

$$1 + q = z\beta. \quad (126)$$

Combining this equality with Eqs. (116), (117) leads to the resulting expression for the nonextensivity parameter of the considered system:

$$1 + q = \frac{2}{n(1-a)}. \quad (127)$$

The minimal value $q = 2/n - 1$ is related to systems with additive noise ($a = 0$), which is relevant to the mean-field picture at a number of governing equations $n < 2$ ($n = 1$). Switching the multiplicative noise with increasing exponent $a > 0$ leads to a q -growth and the self-organizing system gets a nonextensive character ($q \geq 1$) in the limit $n \leq 1/(1-a)$. In accordance with the above estimation the fractional Lorenz system is nonextensive, essentially if the exponent $a > 2/3$.

It is worth to remember that above we have assumed the superdiffusion process only to be related to Lévy flights at discrete time instant with arbitrary displacements, including infinite ones.⁶⁸ Related to the Fokker–Planck equation (112), such processes are characterized by the exponents $\beta = 1$ and $\alpha < 2$, the first of which is constant, whereas the second one characterizes the fractal time-sequence of the Lévy flights and leads to the dynamical exponent $z \equiv \alpha/\beta < 2$ (see the last of equations (114)). The probability distribution of the displacement \mathbf{x} , that is dependent on microscopic conditions, reads

$$p(\mathbf{x}) \sim x^{-(D+\gamma)} \quad (128)$$

and is characterized by the fractal dimension D and the microscopic step exponent γ . It is obvious that in the case of rare events, when $\gamma < 2$, the dynamical exponent z is reduced to the microscopic step exponent ($z = \gamma < 2$), whereas at $\gamma \geq 2$ one has $z = 2$.⁶⁹

In the opposite case of subdiffusion processes, a microscopic ingredient is the random Lévy walks instead of the discrete Lévy flights. This process evolves continuously in course of the time over discrete placed traps, so that

the exponents $\beta < 1$ describes fractal properties of this space that depend on microscopic conditions. These properties generate the transformation of the usual Boltzmann-Gibbs statistics in a nonextensive manner.¹⁸ The subdiffusion process is presented by the Tsallis-type distribution⁷⁰

$$p(\mathbf{x}) \propto [1 + \beta(q - 1)x^2]^{-\frac{1}{q-1}}, \quad \beta = \text{const} > 0, \quad (129)$$

where the deviation $q - 1$ of the nonextensive parameter is caused by the fractal nature of the system phase space that is connected to the step exponent γ as follows:

$$q = 1 + \frac{2}{D + \gamma}. \quad (130)$$

A formal advantage of the distribution (129) is that the corresponding q -weighted average

$$\langle \mathbf{x}^2 \rangle_q \equiv \int \mathbf{x}^2 p^q(\mathbf{x}) d^D x, \quad (131)$$

where the integrand varies as $x^{-(1+\gamma)}$, converges for arbitrary step exponents $\gamma > 0$. As a result, the equation of motion of the random Lévy walker is given by

$$\langle \mathbf{x}^2 \rangle_q \sim t^\beta, \quad \beta = \begin{cases} q - 1 & \text{at } \gamma, q < 2, \\ 1 - (q - 1)\frac{D}{2} & \text{at } \gamma \geq 2, q > 1. \end{cases} \quad (132)$$

In contrast to Eq. (124), where the exponents $\alpha < 2$, $\beta = 1$ are relevant for the superdiffusion, one has here the inverted relations $\alpha = 2$, $\beta < 1$. Thus, in accordance with the subdiffusion nature, the last equality (114) yields the dynamical exponent $z > 2$.

In the general case $\alpha/2, \beta \neq 1$, inserting Eqs. (132) into the relation (126) leads to the result

$$z = \begin{cases} \frac{q+1}{1 - \frac{D}{2}(q-1)} & \text{at } 1 < q \leq q_D, \\ \frac{q+1}{q-1} & \text{at } q_D \leq q \leq 2, \end{cases} \quad (133)$$

where the boundary value of the nonextensivity parameter is introduced:

$$q_D \equiv \frac{4 + D}{2 + D}. \quad (134)$$

To avoid misunderstanding, let us emphasize that in contrast to equalities $\tau = 1 + z/D$, $\tau = 2(1 - 1/D)$, $D = \mu/\sigma$, (115), (116), which could be related both to the real phase space and to the configurational one (the latter is spanned by variables of governing equations), the above-obtained relations (132) – (134) are relevant for the real phase space only. This is

reflected by attributing in the former case the fractal dimension D to the real coordinate space only, whereas in the latter case it is reduced to the effective value (117). According to our treatment, a central role is played by the relation (117) since, in analogy with a renormalization group, we have considered the properties of the configurational space but not real diffusion process.

Finally, let us answer the questions, why the Lorenz system is used and not the Rössler one or some other? The reason can be recognized within a supersymmetry field approach, whose use shows that the Lorenz system could be generated by the Langevin equation for an order parameter that is relevant for a standard stochastic system.⁷¹ Moreover, it is easy to see with microscopic consideration that the Lorenz system is related to the simplest Hamiltonian of a boson-fermion system.⁷² Here, the bosons are described by creation and annihilation operators b_l^+, b_l , satisfying the usual commutation relation: $[b_l, b_m^+] = \delta_{lm}$, where l, m are the site numbers. The two-level Fermion subsystem is described by operators $a_{l\alpha}^+, a_{l\alpha}$, $\alpha = 1, 2$, that fulfill the anti-commutation relation $\{a_{l\alpha}, a_{m\beta}^+\} = \delta_{lm}\delta_{\alpha\beta}$. The occupation numbers $b_{\mathbf{k}}^+ b_{\mathbf{k}}$ determine the Boson distribution in \mathbf{k} -representation that corresponds to the Fourier transform of lattice sites l . To represent the Fermi subsystem we introduce the operator $d_l \equiv a_{l1}^+ a_{l2}$ determining the polarization with respect to the saturation over levels $\alpha = 1, 2$, as well as the occupation numbers $n_{l\alpha} \equiv a_{l\alpha}^+ a_{l\alpha}$. The behaviour of the system is defined by the Dicke Hamiltonian

$$H = \sum_{\mathbf{k}} \left\{ (E_1 n_{\mathbf{k}1} + E_2 n_{\mathbf{k}2}) + \omega_{\mathbf{k}} b_{\mathbf{k}}^+ b_{\mathbf{k}} + \frac{i}{2} w (b_{\mathbf{k}}^+ d_{\mathbf{k}} - d_{\mathbf{k}}^+ b_{\mathbf{k}}) \right\}, \quad (135)$$

where $E_{1,2}$ are Fermi energies, $\omega_{\mathbf{k}}$ is the Boson dispersion law, the imaginary unit before the interaction w reflects the Hermitian property.

The Heisenberg equations of motion are

$$\dot{b}_{\mathbf{k}} = -i\omega_{\mathbf{k}} b_{\mathbf{k}} + \frac{w}{2} d_{\mathbf{k}}; \quad (136)$$

$$\dot{d}_{\mathbf{k}} = -i\Delta d_{\mathbf{k}} + \frac{w}{2} b_{\mathbf{k}} (n_{\mathbf{k}2} - n_{\mathbf{k}1}), \quad \Delta \equiv E_2 - E_1; \quad (137)$$

$$\dot{n}_{\mathbf{k}1} = \frac{w}{2} (b_{\mathbf{k}}^+ d_{\mathbf{k}} + d_{\mathbf{k}}^+ b_{\mathbf{k}}), \quad \dot{n}_{\mathbf{k}2} = -\frac{w}{2} (b_{\mathbf{k}}^+ d_{\mathbf{k}} + d_{\mathbf{k}}^+ b_{\mathbf{k}}). \quad (138)$$

At the resonance, the first terms in the right-hand sides of equations (137), (138) containing frequencies $\omega_{\mathbf{k}}$ and Δ may be suppressed by introducing factors $\exp(-i\omega_{\mathbf{k}}t)$ and $\exp(-i\Delta t)$ for the time dependencies $b_{\mathbf{k}}(t)$, $d_{\mathbf{k}}(t)$, respectively. To take the dissipation into account, these frequencies

acquire additional imaginary terms $-i/\tau_x$, $-i/\tau_y$ characterized by the relaxation times τ_x , τ_y (here the conditions $\text{Im } \omega_{\mathbf{k}} < 0$, $\text{Im } \Delta < 0$ reflect the causality principle). As a result, equations (137), (138) get the dissipative terms $-b_{\mathbf{k}}/\tau_x$, $-d_{\mathbf{k}}/\tau_y$, where τ_x is the relaxation time of Boson distribution and τ_y is the Fermion polarization time. Obviously, one can suppose that the dissipation also influences the Fermi occupancy levels $n_{\mathbf{k}\alpha}(t)$. However, since the stationary values are $n_{\mathbf{k}\alpha}^0 \neq 0$ (in the case of external drive $n_{\mathbf{k}2}^0 > n_{\mathbf{k}1}^0$), the dissipative terms in Eqs. (138) take much more complicated form $-(n_{\mathbf{k}\alpha} - n_{\mathbf{k}\alpha}^0)/\tau_S$, where τ_S is the relaxation time of the Fermion distribution over levels $\alpha = 1, 2$.

Now, let us introduce the macroscopic quantities

$$\begin{aligned} u_{\mathbf{k}} &\equiv \langle b_{\mathbf{k}}^+ \rangle = \langle b_{\mathbf{k}} \rangle, & v_{\mathbf{k}} &\equiv \langle d_{\mathbf{k}} \rangle = \langle d_{\mathbf{k}}^+ \rangle, \\ S_{\mathbf{k}} &\equiv \langle n_{\mathbf{k}2} - n_{\mathbf{k}1} \rangle, & S_{\mathbf{k}}^0 &\equiv \langle n_{\mathbf{k}2}^0 - n_{\mathbf{k}1}^0 \rangle, \end{aligned} \quad (139)$$

where the angular brackets denote thermodynamical averaging. Then, neglecting the correlation in particles distribution over quantum states and omitting the dependence on the wave vector \mathbf{k} , the Heisenberg equations (137) – (138) result in the initial Lorenz system (6), (8) and (9), whose parameters $a = 1$, $\tau_x = 2/w$, $D = (2w)^{-1}$. The dimensionless variables in the system (10) – (12) are as follows: $u \equiv w(\tau_y \tau_S)^{1/2} \dot{x}$, $v \equiv w(\tau_y \tau_S)^{1/2} \dot{y}$ and $S \equiv (w \tau_y / 2) y'$.

Appendix . Fractional Integral and Derivative

Here the basic properties of fractional integral and derivative are given. The integral of fractional order ϖ is defined by the equality

$$\mathcal{I}_x^{\varpi} f(x) \equiv \frac{1}{\Gamma(\varpi)} \int_0^x \frac{f(x')}{(x - x')^{1-\varpi}} dx', \quad \varpi > 0, \quad (\text{A.140})$$

where $f(x)$ is arbitrary function, $\Gamma(x)$ is Euler Gamma-function. Related derivative $\partial_x^{\varpi} \equiv \mathcal{I}_x^{-\varpi}$ of order $\varpi > 0$ is determined as follows:

$$\partial_x^{\varpi} f(x) \equiv \frac{1}{\Gamma(-\varpi)} \int_0^x \frac{f(x')}{(x - x')^{1+\varpi}} dx'. \quad (\text{A.141})$$

At $0 < \varpi < 1$ it is convenient to use equation

$$\partial_x^{\varpi} f(x) \equiv \frac{\varpi}{\Gamma(1-\varpi)} \int_0^x \frac{f(x) - f(x')}{(x - x')^{1+\varpi}} dx', \quad (\text{A.142})$$

where we take into account known equality $x\Gamma(x) = \Gamma(x + 1)$ for $x \equiv -\varpi$.

References

1. P. Bak, *How Nature Works* (Oxford Univ.Press., Oxford, 1997).
2. S. F. Edwards and D. R. Wilkinson, Proc. Roy. Soc. A **381**, 17 (1982).
3. A. Mehta and G. C. Barker, Rep. Prog. Phys. **57**, 383 (1994).
4. J.-P. Bouchaud, M. E. Cates, J. R. Prakash, and S. F. Edwards, J. Phys. I (France) **4**, 1383 (1994).
5. K. P. Hadeler and C. Kuttler, Granular Matter **2**, 9 (1999).
6. P. Bak and K. Sneppen, Phys. Rev. Lett. **71**, 4083 (1993).
7. T. S. Ray and N. Jan, Phys. Rev. Lett. **72**, 4045 (1994).
8. B. Jovanovic, S. V. Buldyrev, S. Halvin, and H. E. Stanley, Phys. Rev. E **50**, 2403 (1994).
9. S. Maslov, M. Parzuski, and P. Bak, Phys. Rev. Lett. **73**, 2162 (1994).
10. P. Grassberger, Phys. Lett. A **200**, 277 (1995).
11. K. Ito, Phys. Rev. E **52**, 3232 (1995).
12. T. Halpin-Healy and Y.-C. Zhang, Phys. Rep. **254**, 215 (1995).
13. M. Parzuski, S. Maslov, and P. Bak, Europhys. Lett. **27**, 97 (1994).
14. M. Parzuski, S. Maslov, and P. Bak, Phys. Rev. E **53**, 414 (1996).
15. A. Vespignani, R. Dickman, M.A. Muñoz, and S. Zapperi, Phys. Rev. Lett. **81**, 5676 (1998); Phys. Rev. E **62**, 4564 (2000).
16. S. F. Edwards and R. B. S. Oakeshott, Physica A **157**, 1080 (1989).
17. S. F. Edwards, in: *Granular Matter: An Interdisciplinary Approach*, edited by A. Metha (Springer-Verlag, New-York, 1994).
18. C. Tsallis, in: *Lecture Notes in Physics*, edited by S. Abe and Y. Okamoto (Springer-Verlag, Heidelberg, 2001).
19. G. M. Zaslavsky, Chaos **4**, 25 (1994); Physica D **76**, 110 (1994); A. I. Saichev and G. M. Zaslavsky, Chaos **7**, 753 (1997).
20. P. Bak, C. Tang, and K. Wiesenfeld, Phys. Rev. Lett. **59**, 381 (1987).
21. C. Tang and P. Bak, Phys. Rev. Lett. **60**, 2347 (1988).
22. K. Wiesenfeld, C. Tang, and P. Bak, J. Stat. Phys. **54**, 1441 (1989).
23. Z. Olami, H. J. S. Feder, and K. Christensen, Phys. Rev. Lett. **68**, 1244 (1992).
24. H. J. Jensen, *Self-Organized Criticality* (Cambridge Univ. Press., Cambridge, 1998).
25. D. Dhar and R. Ramaswamy, Phys. Rev. Lett. **63**, 1659 (1989); D. Dhar, Phys. Rev. Lett. **64**, 1613, (1990); D. Dhar and S. N. Majumdar, J. Phys. A: Math.Gen. **23**, 4333 (1990).
26. L. Pietronero, A. Vespignani, and S. Zapperi, Phys. Rev. Lett. **72**, 1690 (1994); Phys. Rev. E **51**, 1711 (1995).
27. A. Diaz-Guilera, Europhys. Lett. **26**, 177 (1994).
28. H. Flyvbjerg, K. Sneppen, and P. Bak, Phys. Rev. Lett. **71**, 4087 (1993).
29. M. Vergeles, A. Maritan, and J. R. Banavar, Phys. Rev. E **55**, 1998 (1997).
30. A. Vespignani and S. Zapperi, Phys. Rev. Lett. **78**, 4793 (1997); Phys. Rev. E **57**, 6345 (1998).
31. L. P. Kadanoff, S. R. Nagel, L. Wu, and S. Zhu, Phys. Rev. A **39**, 6524 (1989).
32. P. Grassberger and S. S. Manna, J. Phys. (France) **51**, 1077 (1990).

33. H. M. Jaeger, C.-H. Liu, and S. R. Nagel, Phys. Rev. Lett. **62**, 40 (1989); H. M. Jaeger, C.-H. Liu, and S. R. Nagel, Science **255**, 1523 (1992).
34. M. Bretz, J. B. Cunningham, P. L. Kurczynski, and F. Nori, Phys. Rev. Lett. **69**, 2431 (1992).
35. V. Frette, K. Christensen, A. Malthe-Sorensen, J. Feder, T. Josssang, and T. Meakin, Nature **379**, 49 (1996).
36. S. Field, J. Witt, and F. Nori, Phys. Rev. Lett. **74**, 1206 (1995).
37. K. Chrinstensen, H. Fogedby, and H. J. Jensen, J. Stat. Phys. **63**, 653 (1991).
38. H. J. Jensen, K. Christensen, and H. C. Fogedby, Phys. Rev. B **40**, 7425 (1989).
39. T. Hwa and M. Kadar, Phys. Rev. A **45**, 7002 (1992).
40. Y.-C. Zhang, Phys. Rev. Lett. **63**, 470 (1989).
41. L. Gil and D. Sornette, Phys. Rev. Lett. **76**, 3991 (1996).
42. A. I. Olemskoi and A. V. Khomenko, JETP **83**, 1180 (1996).
43. A. I. Olemskoi and A. V. Khomenko, Phys. Rev. E **63**, 036116 (2001).
44. A. I. Olemskoi, A. V. Khomenko, and D. O. Kharchenko, Physica A **323**, 263 (2003).
45. J. Zinn-Justin, *Quantum Field Theory and Critical Phenomena* (Clarendon Press, Oxford, 1993).
46. H. Risken, *The Fokker-Planck Equation* (Springer, Berlin, 1989).
47. H. Haken, *Synergetics, an Introduction* (Springer, Berlin, 1983).
48. A. I. Olemskoi, Physics-Uspekhi **41**, 269 (1998).
49. M. Cencini, M. Falcioni, E. Olbrich, H. Kantz, and A. Vulpiani, Phys. Rev. E **62**, 427 (2000).
50. W. Horsthemke and R. Lefever, *Noise Induced Transitions. Theory and Application in Physics, Chemistry, and Biology* (Springer, Heidelberg, 1984).
51. P. C. Martin, E. D. Siggia, and H. A. Rose, Phys. Rev. A **8**, 423 (1973).
52. R. Graham, in: *Lecture Notes in Physics*, **84** (Springer, Berlin, 1978).
53. H. K. Jensen, Z. Phys. B **23**, 377 (1976).
54. A. S. Mikhailov and A. S. Loskutov, *Foundations of Synergetics* (Springer, Berlin, 1996).
55. P. Hänggi, in: *Noise in Nonlinear Dynamical Systems: Theory, Experiment, Simulations*, edited by F. Moss and P.V.E. McClintock (Cambridge Univ. Press, Cambridge, 1989), p.307.
56. A. I. Olemskoi and D. O. Kharchenko, Phys. Solid State **42**, 532 (2000).
57. D. O. Kharchenko, Physica A **308**, 101 (2002).
58. A. I. Olemskoi and D. O. Kharchenko, in: *Variational and Extremum Principles in Macroscopic Systems*, edited by S. Sieniutycz and H. Farkas (Elsevier, Amsterdam, 2005), p.695.
59. F. Langouche, D. Roekaerts, and E. Tirapegui, *Functional Integral and Semi-classical Expansions* (Reidel, Dordrecht, 1982).
60. M. Freidlin, *Functional Integration and Partial Differentail Equations* (Princeton Univ. Press, Princeton, 1985).
61. F. Castro, H. S. Wio, and G. Abramson, Phys. Rev. E, **52**, 159 (1995).
62. S. G. Samko, A. A. Kilbas, and O. I. Marichev, *Fractional Integrals and Derivatives – Theory and Applications* (Gordon and Breach, New-York, 1993).

63. D. O. Kharchenko, Fluct. Noise Lett. **2**, L273 (2002).
64. A. Chessa, E. Marinari, A. Vespignani, and S. Zapperi, Phys. Rev. E **57**, R6241 (1998).
65. K. P. Hadeler and C. Kuttler, Granular Matter **2**, 9 (1999).
66. A. I. Olemskoi, JETP Lett. **71**, 285 (2000).
67. A. I. Olemskoi and D. O. Kharchenko, Physica A **293**, 178 (2001).
68. J.-P. Bouchaud and A. Georges, Phys. Rep. **195**, 127 (1991).
69. H. C. Fogedby, Phys. Rev. E **58**, 1690 (1998).
70. D. H. Zanette and P. A. Alemany, Phys. Rev. Lett. **75**, 366 (1995).
71. A. I. Olemskoi and A. V. Khomenko, *preprint cond-mat/0008121* (2000).
72. A. I. Olemskoi, *Theory of Structure Transformations in Non-Equilibrium Condensed Matter* (NOVA Science, New-York, 1999).

CHAPTER 5

PHASE TRANSITIONS IN THE PSEUDOSPIN-ELECTRON MODEL

Ihor Stasyuk

*Institute for Condensed Matter Physics
of the National Academy of Science of Ukraine,
1 Svientsitskii Str., UA-79011 Lviv, Ukraine
E-mail: ista@icmp.lviv.ua*

A review of the present state of investigations of the pseudospin-electron model (PEM), which is used in the theory of strongly correlated electron systems, is given. The model is used to describe the systems with the locally anharmonic elements of structure represented in the model by pseudospins. The consideration is based on the dynamical mean field theory approach and the generalized random phase approximation. Electron spectrum and thermodynamics of the model are investigated; the cases of the simplified model, the model with strong interaction and the two-sublattice model are studied more in detail. The phase transitions into other uniform or modulated states as well as superconducting phases are described; the criteria of their realization are established. Based on this, the description of structural and dielectric (ferroelectric type) instabilities, phase separation and bistability phenomena is given. A comparison is made with the thermodynamics of the Falicov-Kimball model (which can be considered as a particular case of PEM). The possibility of applying the PEM to the analysis of thermodynamics of the real HTSC systems is discussed. Attention is paid to the unsolved problems in the study of PEM.

Contents

1	Introduction	232
2	Thermodynamics of Simplified PEM in Dynamical Mean Field Theory	235
3	Simplified PEM in Generalized Random Phase Approximation	243
3.1	Strong Coupling Case; $U = 0$, $\Omega = 0$	243
3.2	Weak Coupling Case; $U = 0$	256
3.3	Superconductivity in the PEM	269
4	Thermodynamics of PEM at Finite U Values; the $U \rightarrow \infty$ Limit	272
5	Two-Sublattice Pseudospin-Electron Model	279

6 Conclusions	285
Acknowledgements	288
References	288

1. Introduction

Much attention is paid in recent years to the investigation of systems with strong electron correlations, such as crystalline compounds with the transition and rare-earth ions (transition metals, transition metal oxides, mixed valent compounds, heavy fermion systems, high temperature superconductors, etc.). Their specific electronic, magnetic and conducting properties as well as the presence of a variety of phase transitions and the phenomena that are connected with this property are caused to a great extent by the splitting and reconstruction of energy spectrum due to correlation effects. The theory of such systems is based on the Hubbard model and on its generalizations, where the crucial idea is the one concerning the decisive role of the strong short-range interaction of particles (electrons). At the presence of additional (i.e., vibrational) degrees of freedom, one can mention, among others, the pseudospin-electron model (PEM). The model appeared recently in connection with the investigation of the high- T_c superconductors. It was introduced to describe the contribution of locally-anharmonic elements of the crystal structure to their electronic properties.

Electron system in PEM is described by the Hubbard Hamiltonian while the anharmonic vibrational modes are treated using the pseudospin formalism. The model Hamiltonian is as follows

$$H = \sum_i [U n_{i,\uparrow} n_{i,\downarrow} + (g S_i^z - \mu)(n_{i,\uparrow} + n_{i,\downarrow}) - h S_i^z - \Omega S_i^x] + \sum_{i,j,\sigma} t_{ij} a_{i,\sigma}^+ a_{j,\sigma}. \quad (1)$$

Here $a_{i,\sigma}$, $a_{i,\sigma}^+$ are electron annihilation and creation operators, $n_{i,\sigma}$ is an electron occupation number; besides the electron correlation (U -term), the single-site part includes the interaction with pseudospin (g -term) and the energy of the tunnelling-like splitting of vibrational levels (Ω -term); the field h describes the asymmetry of local potential. The electron transfer (t -term) is included as well.

The pseudospin-electron Hamiltonian (in form (1) with inclusion only of the g -interaction) was used by Müller with the aim of describing the anharmonic vibrations in the oxygen subsystem of the high- T_c superconducting crystals of the YBaCuO type.¹ The $\text{YBa}_2\text{Cu}_3\text{O}_{7-\delta}$ crystal is a typical and most studied example of such objects. The unit cell contains, besides two superconducting planes, the chain (at the $\delta \ll 1$ composition)

elements Cu₁-O₁, connected by Cu₁-O₄-Cu₂ bridges with Cu₂-O₂ plains through the apical oxygen ions O₄. The vibrations of these ions along the *c*-axis (perpendicularly to the plains) exhibit a strong anharmonicity. Much evidence exists in support of this concept. One can mention the EXAFS data,^{2,3} Raman scattering and dielectric measurements,^{4–9} local polaron phenomena,^{10,11} bistabilities in the normal phase region¹² as well as neutron scattering investigations¹³ or the results of the first principle LAPW calculations.¹⁴ Despite a certain ambiguity in the data, the conclusions were made about the existence of two different equilibrium positions of the O₄ ion. The local double-well picture as an approximate simplified model was supported by the oxygen O₄ vacancy effect on the positions of apical ions observed in Ref. [15].

Moreover, a connection between positions of O₄ ions and electron states in Cu₂-O₂ plains plays an important role in YBa₂Cu₃O_{7- δ} crystals. The data given in Ref. [16] point to the existence of a significant correlation between the occupancy of electron states of the Cu₂ ion and the R_{O₄-Cu₂} distance as well as to the decrease of this distance at the transition from the metallic orthorombic phase to the semiconducting one (that takes place at $\delta > \delta^* = 0.55$). These and other similar facts suggest the presence of a large electron-vibrational coupling. In the pseudospin representation, when the pseudospin variable $S_i^z = \pm 1/2$ defines the positions of O₄ ions, it is described by the $gS_i^z n_{i\sigma}$ term.

Consideration based on the PEM was applied to the HTSC systems starting from Refs. [1,17–20]. Hamiltonian similar to (1) was used by Hirsch and Tang in the study of electron states in the framework of cluster calculations. In the context of the idea concerning the effect of anharmonicity on the superconducting transition temperature,^{17–19,21} the possible connection between superconducting pairing and the lattice anharmonicity was considered by Frick et al.²² (the quantum Monte-Carlo calculations). In what follows, the investigations of the PEM were devoted to the analysis of the electron spectrum,²³ the pseudospin and collective dynamics,^{24,25} the charge and pseudospin pair correlations and the behaviour of dielectric susceptibility.²⁶

In subsequent investigations, the main attention was paid to the thermodynamics of the model in special cases and simplifications: (i) a model with the infinitely large correlation ($U \rightarrow \infty$) when the double occupation of electron states on the site is excluded; (ii) simplified PEM with $U = 0$ and $\Omega = 0$; (iii) simplified model ($U = 0$) with the tunnelling-like dynamics ($\Omega \neq 0$); (iv) two-sublattice PEM for the layered structures

of the YBaCuO-type; (v) the cluster PEM of ferroelectric-superconductor heterostructures.^{27,28}

There was performed a study of phase transitions between the states with different electron concentrations and with different orientations of pseudospins (in the regime of the fixed chemical potential, $\mu = \text{const}$), and the phase separation effects at a given concentration of electrons ($n = \text{const}$).^{29,30} The possibility of the appearance of a doubly modulated (so-called chessboard) phase or an incommensurate phase (in the case of weak coupling) was established;^{31–33} the superconducting instability in PEM was analysed.³⁴ In the case of two-sublattice PEM the structural instabilities of the ferroelectric type as well as the bistability phenomena were revealed and analysed.^{35–38} The study of the PEM thermodynamics was performed mainly within the generalized random phase approximation (GRPA).³⁹ A method of dynamical mean field theory (DMFT) was used in the case of simplified PEM,²⁹ when the analytic formulation of the theory is possible.

As was shown, the PEM also possesses an interesting collective dynamics of pseudospins. The corresponding spectrum changes its form depending on the electron concentration and temperature;^{24,25} the spectrum is different at high or small values of g and its shape also depends on the h and Ω parameters. In Refs. [40–42], the contributions into Raman scattering intensity, connected with the mentioned collective pseudospin excitations (that correspond to the phonon-like vibrations of anharmonic subsystems in the YBaCuO structures) and electron intraband and interband transitions, were considered.

The PEM is closely related to the Falicov-Kimball (FK) model intensively studied in recent years (see, for example, Ref. [43]), in which the interaction between the localized and itinerant particles (electrons) is responsible for the similar phase transitions (between states with different concentrations of particles and with/without spatial modulation). The simplified version of PEM corresponds to the FK model in case there is no tunnelling-like splitting in the PEM and when the localized and the moving particles in FK model have different chemical potentials (one can pass to FK model putting $S_i^z = w_i - 1/2$ and $h = \tilde{\mu}$, where w_i and $\tilde{\mu}$ are occupation number and chemical potential of localized particles, respectively). The regimes of thermodynamic averaging are usually different for both models (a fixed concentration of the localized particles for FK model and a given value of the field h for the PEM).

It should be mentioned that for the recent few years the PEM has found

application in describing the charge transfer in molecular and crystalline systems with hydrogen bonds.⁴⁴ The model is also very promising in investigating the thermodynamics of processes connected with ionic intercalation in the layered structures (see Ref. [45]), where different separated positions exist in the unit cell for the intercalating ion, and the hopping between them is possible (intercalation of Li^+ ions in the TiO_2 matrix provides an example of such a situation⁴⁶). A specific version of PEM was recently used⁴⁷ in modelling the electronic properties and the field effect in the $\text{CuO}_2/\text{SrTiO}_3$ interfaces in HTSC/STO heterostructures.

This paper presents a review of the main results concerning the thermodynamics and energy spectrum of the PEM in the above-mentioned cases and approximations. The case of the simplified PEM ($U = 0$; $\Omega = 0$ or $\Omega \neq 0$) is considered more in detail. Dynamic properties of PEM are not considered here. Attention is paid to the possible application of the PEM to the description of inhomogeneous states, structural instabilities and bistability phenomena as well as transitions into the phases with the charge modulation in the high T_c superconductors and other systems to which the model can be applied.

2. Thermodynamics of Simplified PEM in Dynamical Mean Field Theory

The dynamical mean field theory approach proposed by Metzner and Vollhardt⁴⁸ for the Hubbard model (see also Ref. [49] and references therein) is a nonperturbative scheme which is exact in the limit of the infinite space dimension ($d \rightarrow \infty$). The method is very successful in considering the systems with strong electron correlations and is used with advantage in solving a variety of problems and models. Within the framework of DMFT, investigations of the single-particle spectrum and the thermodynamics of the simplified PEM were performed for a strong coupling case ($g \gg W$, where W is the half-width of the initial electron band).²⁹ The Fourier-transform $G_\sigma(\omega_n, \mathbf{k})$ of the electron Green's function

$$G_{ij}^\sigma(\tau - \tau') = -\langle T a_{i\sigma}(\tau) a_{j\sigma}^+(\tau') \rangle_0 / \langle \sigma(\beta) \rangle_0, \quad (2)$$

(where T denotes the τ - ordering procedure) with the scattering matrix

$$\sigma(\beta) = T \exp \left\{ - \int_0^\beta d\tau \sum_{ij\sigma} t_{ij} a_{i\sigma}^+(\tau) a_{j\sigma}(\tau) \right\} \quad (3)$$

and the averaging with the single-site part $H_0 = \sum_i H_i$ of the Hamiltonian (1), is expressed as a series in terms of the electron hopping parameter t_{ij} . The Larkin's equation

$$G_{ij}^\sigma(\tau - \tau') = \Xi_{ij}^\sigma(\tau - \tau') + \Xi_{il}^\sigma(\tau - \tau'') t_{lm} G_{mj}^\sigma(\tau'' - \tau') \quad (4)$$

separates the total irreducible (with respect to t_{ij}) part Ξ^σ ; formally

$$G_\sigma(\omega_n, \mathbf{k}) = \frac{1}{\Xi_\sigma^{-1}(\omega_n, \mathbf{k}) - t_{\mathbf{k}}}. \quad (5)$$

In the case of high dimensions ($d \rightarrow \infty$), when the hopping integral is scaled ($t_{ij} \rightarrow t_{ij}/\sqrt{d}$), only single-site contributions survive in the expression for Ξ_σ :⁵⁰

$$\Xi_{ij}^\sigma(\tau - \tau') = \delta_{ij} \Xi_\sigma(\tau - \tau'); \quad \Xi_\sigma(\omega_n, \mathbf{k}) = \Xi_\sigma(\omega_n). \quad (6)$$

Such a site-diagonal function, as it was shown by Brandt and Mielsch,⁵¹ can be calculated by mapping the infinite-dimensional lattice problem on the atomic model

$$\begin{aligned} e^{-\beta H} \rightarrow e^{-\beta H_{\text{eff}}} &= e^{-\beta H_0} \\ &\times T \exp \left\{ - \int_0^\beta d\tau \int_0^\beta d\tau' \sum_\sigma J_\sigma(\tau - \tau') a_\sigma^+(\tau) a_\sigma(\tau') \right\} \end{aligned} \quad (7)$$

with auxiliary Kadanoff–Baym field $J_\sigma(\tau - \tau')$ ⁵² which should be selfconsistently determined from the condition that the same function Ξ_σ defines the Green's functions for lattice (5) and atomic limit

$$G_\sigma^{(a)}(\omega_n) = \frac{1}{\Xi_\sigma^{-1}(\omega_n) - J_\sigma(\omega_n)}. \quad (8)$$

“Dynamical” mean field $J_\sigma(\tau - \tau')$ (so-called coherent potential) describes the hopping (transfer) of electron from atom into environment at the moment τ , and propagation in environment without stray into atom until moment τ' . The connection between this “dynamical” mean field of atomic problem and Green's function of the lattice can be obtained using standard coherent potential approximation (CPA):⁴⁹

$$J_\sigma(\omega_n) = \Xi_\sigma^{-1}(\omega_n) - G_\sigma^{-1}(\omega_n), \quad (9)$$

where

$$G_\sigma^{(a)}(\omega_n) = G_\sigma(\omega_n) = \int_{-\infty}^{+\infty} dt \frac{\rho(t)}{\Xi_\sigma^{-1}(\omega_n) - t} \quad (10)$$

is a single-site Green's function both for atomic limit and lattice. Here summation over wave vector was changed by the integration with the density of states (DOS) $\rho(t)$ (the Gaussian one for the hypercubic lattice $\rho(\varepsilon) = \frac{1}{W\sqrt{\pi}}e^{-\varepsilon^2/W^2}$ and semi-elliptic DOS for the Bethe lattice $\rho(\varepsilon) = \frac{2}{\pi W^2}\sqrt{W^2 - \varepsilon^2}$, see Ref. [49]).

In order to find expression for Green's function in the atomic limit, one can use the fact that the statistical operator of the single-site problem (7) can be expressed in the form²⁹

$$e^{-\beta H_{\text{eff}}} = P^+ e^{-\beta H_+} + P^- e^{-\beta H_-} \quad (11)$$

because the atomic space of states splits into two independent subspaces.

As a result, the single-electron Green's function is a sum of Green's functions in subspaces and is equal to

$$G_{\sigma}^{(a)}(\omega_n) = \frac{\langle P^+ \rangle}{i\omega_n + \mu - J_{\sigma}(\omega_n) - \frac{g}{2}} + \frac{\langle P^- \rangle}{i\omega_n + \mu - J_{\sigma}(\omega_n) + \frac{g}{2}}. \quad (12)$$

Here $\langle \dots \rangle$ is the statistical averaging with the effective Hamiltonian (7). Partition functions in subspaces are

$$\begin{aligned} Z_{\pm} &= S p e^{-\beta H_{\pm}} = e^{\pm \frac{\beta h}{2} - Q_{\pm}} \\ &= e^{\pm \frac{\beta h}{2}} \prod_{\sigma} \left(1 + e^{-\beta(\mu \mp \frac{g}{2})} \right) \prod_n \left(1 - \frac{J_{\sigma}(\omega_n)}{i\omega_n + \mu \mp \frac{g}{2}} \right). \end{aligned} \quad (13)$$

Pseudospin mean value is determined by the equation

$$\langle S^z \rangle = \frac{1}{2} \frac{Z_+ - Z_-}{Z_+ + Z_-} = \frac{1}{2} \tanh \frac{1}{2} (\beta h - (Q_+[\langle S^z \rangle] - Q_-[\langle S^z \rangle])). \quad (14)$$

Electron concentration mean value is determined by

$$\langle n \rangle = \frac{1}{\beta} \sum_{m\sigma} G_{\sigma}(\omega_m) \quad (15)$$

and the functional of the grand canonical potential can be derived in the standard way for DMFT

$$\frac{\Phi}{N} = \Phi_{(a)} - \frac{1}{\beta} \sum_{n\sigma} \left\{ \ln G_{\sigma}^{(a)}(\omega_n) - \frac{1}{N} \sum_{\mathbf{k}} \ln G_{\sigma}(\omega_n, \mathbf{k}) \right\}, \quad (16)$$

where

$$\Phi_{(a)} = -\frac{1}{\beta} \ln(Z_+ + Z_-) \quad (17)$$

is a thermodynamic potential for atomic problem.

The solution of the above given set of equations and the calculation of thermodynamic potential were performed for the case of semi-elliptic DOS. The field $J_\sigma(\omega_n)$ is determined by the simple cubic equation

$$J_\sigma(\omega_n) = \frac{W^2}{4} \left\{ \frac{\langle P^+ \rangle}{i\omega_n + \mu - J_\sigma(\omega_n) - \frac{g}{2}} + \frac{\langle P^- \rangle}{i\omega_n + \mu - J_\sigma(\omega_n) + \frac{g}{2}} \right\}. \quad (18)$$

The solutions with $\Im m J_\sigma(\omega) > 0$ are considered; the condition $\Im m J_\sigma(\omega) \rightarrow 0$ determines the band boundaries. Their dependence on coupling constant at the fixed value of $\langle S^z \rangle$ is shown in Fig. 1. It can be seen that there exists

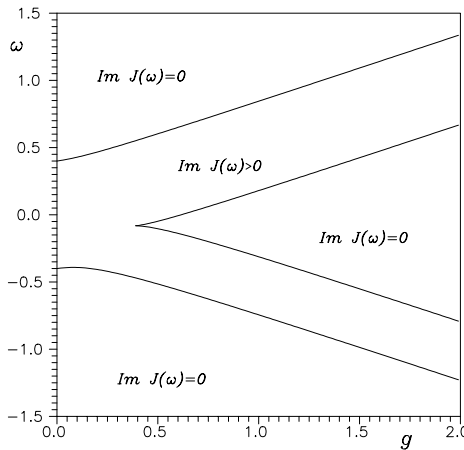


Fig. 1. Electron bands boundaries (semi-elliptic DOS, $W = 0.4$, $\langle S^z \rangle = 0.2$).

a critical value of $g \sim 0.5W$ when a gap in spectrum appears and we have an analogue of the Mott transition. In the case when the single-electron Green's function is calculated in Hubbard-I approximation (the scattering processes via coherent potential are not taken into account, $J_\sigma(\omega) = 0$ and $\Xi_\sigma(\omega_n) = \langle P^+ \rangle / (i\omega_n + \mu - g/2) + \langle P^- \rangle / (i\omega_n + \mu + g/2)$), the electron subbands are always split and the gap in spectrum exists at any values of g (see below). From this point of view, the Hubbard-I approximation is insufficient; even in the case of strong coupling ($g \gg W$) it only qualitatively describes the dependence of the subband half-widths on $\langle S^z \rangle$.²⁶

The expressions presented above allow us to investigate in the DMFT approach the thermodynamics of the simplified PEM. It was done in Ref. [26] in the $\mu = \text{const}$ and $n = \text{const}$ regimes.

In the first case, the thermodynamically stable states are determined from the minimum of the thermodynamic potential (16). Analysis of solutions of CPA equations for $J_\sigma(\omega_n)$ together with the equation (14) for $\langle S^z \rangle$ shows that in this regime the first order phase transitions with the jumps of the pseudospin mean value and electron concentration can take place. Such transitions are realized when the μ and h values correspond to the split subbands in an electron spectrum (see the phase diagram ($\mu - h$) at $T = 0$ in Fig. 2). The field dependencies of $\langle S^z \rangle$ and grand canonical

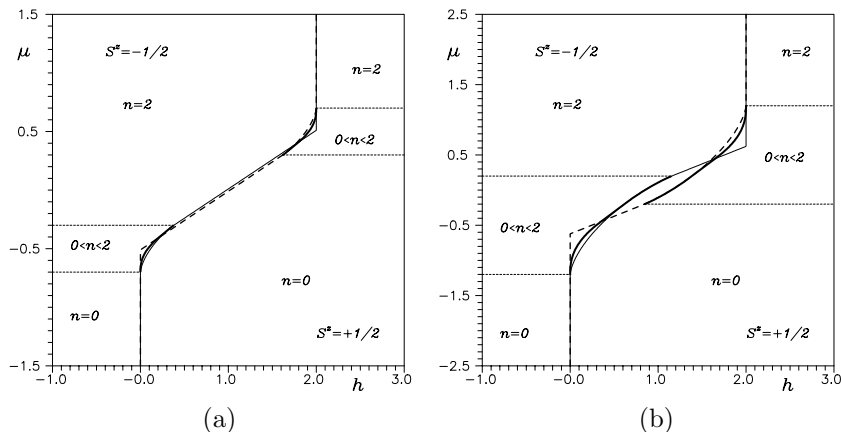


Fig. 2. Phase diagram ($\mu - h$). Dashed and thin solid lines surround regions with $S^z = \pm \frac{1}{2}$, respectively. The lines of the first order phase transition are shown in bold. a) $g = 1$, $W = 0.2$; b) $g = 1$, $W = 0.7$.

potential Φ in the region of the phase transition point are shown in Fig. 3. Since the band structure is determined by the pseudospin mean value, the change of the latter is accompanied by the corresponding reconstruction of the electron spectrum. With the temperature increase the region of the phase coexistence narrows. The corresponding phase diagram ($T_c - h$) is shown in Fig. 4. One can see that with respect to the Ising model the phase coexistence curve is shifted in the field and deviates from the vertical line. Hence, the possibility of the first order phase transition with the temperature change exists in the pseudospin-electron model for the narrow range of h values.

When the electron concentration is fixed (regime $n = \text{const}$), the first order phase transition transforms into the phase separation. The regions appear where the derivative $\partial\mu/\partial n$ is negative, Figs. 5 and 6. The corre-

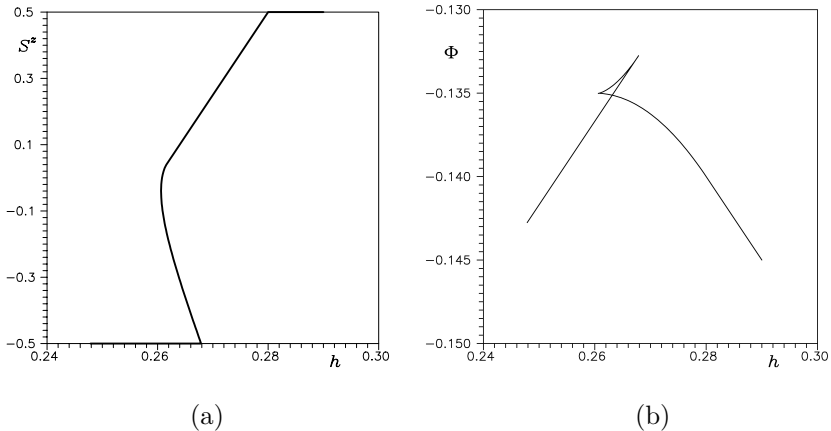


Fig. 3. Field dependencies of $\langle S_z \rangle$ (a) and grand canonical potential (b) for $\mu = \text{const}$ regime when chemical potential is placed in the lower subband $\mu = -0.37$ ($W = 0.2$, $g = 1$, $T = 0$).

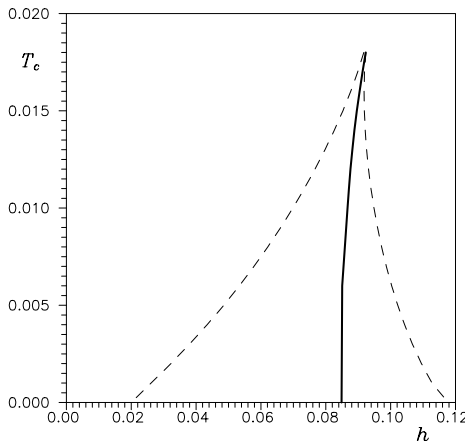


Fig. 4. Phase diagram ($T_c - h$): solid and dashed lines indicate the first order phase transition line and boundaries of the phase stability region, respectively ($g = 1$, $W = 0.2$, $\mu = -0.5$)

sponding phase diagram ($T - n$) is built (Fig. 7, see also Ref. [26]) with the use of the “Maxwell rule” which follows in this case from the replacement of the original free energy in its concavity region by the tangent line. The diagram describes the separation to the states with the large and small electron concentrations (and with the $\langle S^z \rangle \approx -1/2$ and $\langle S^z \rangle \approx +1/2$ pseudospin

averages at low temperatures, respectively).

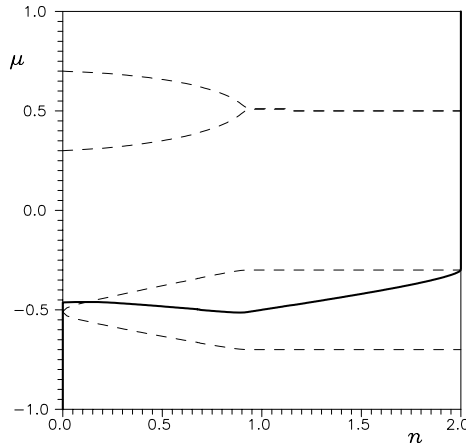


Fig. 5. Dependence of the chemical potential μ and electron bands boundaries (dashed lines) on the electron concentration n ($T = 0.001$, $g = 1$, $W = 0.2$, $h = 0.1$).

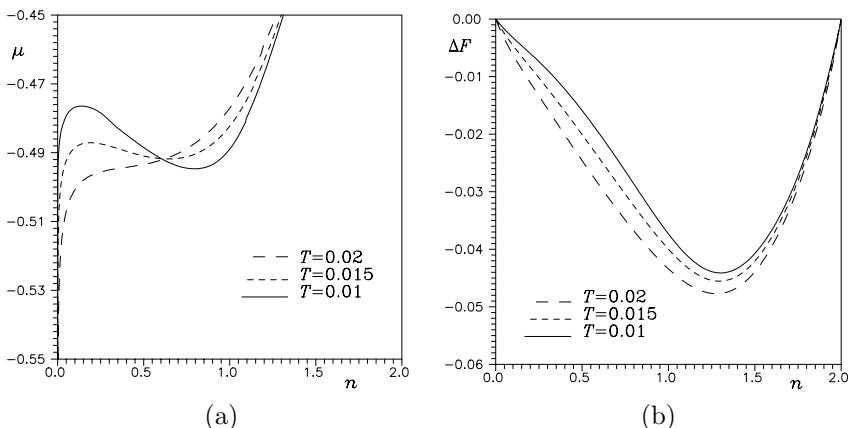


Fig. 6. Dependence of the chemical potential μ (a) and the deviation of free energy from linear dependence $\Delta F = F(n) - \frac{n}{2}F(2) - (1 - \frac{n}{2})F(0)$ (b) on the electron concentration n for different temperatures T ($g = 1$, $W = 0.2$, $h = 0.1$).

It should be noted that the problem of phase separation in strongly correlated systems is not new (see Ref. [53] and references therein). It was

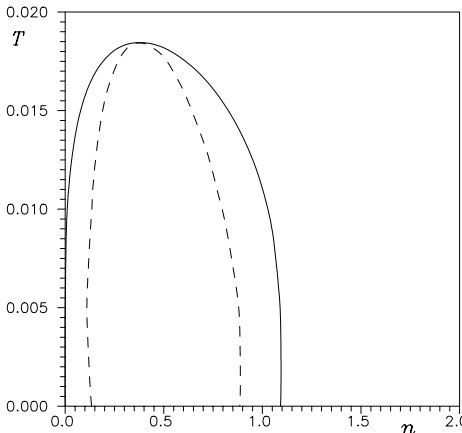


Fig. 7. Phase diagram ($T - n$) for phase separated state. Solid line: binodal, dashed line: spinodal ($g = 1$, $W = 0.2$, $h = 0.1$).

shown for Hubbard and $t - J$ models⁵⁴ that for some values of the parameters, the system separates into hole-rich and hole-poor regions with paramagnetic and antiferromagnetic orders, respectively. In our case of PEM without electron correlations, the system separates into regions with electron spectrum that contains both wide empty electron band and occupied localized states (at $n \sim 0$) and partially filled wide electron band and empty localized states (at $n \sim 1$), see Fig. 5; their weights are determined by the electron concentration. Localized states of such a type (polarons) result from the strong electron-pseudospin coupling (strong interaction of electrons with the out of plane apical oxygen vibrations) in the case of YBaCuO-type structures, and it can be supposed that the hopping between such polarons manifests itself in the carrier relaxation.⁵⁵

For the first time the possibility of phase separation in PEM was mentioned in Ref. [56] where it was considered within GRPA in the limit of strong correlation $U \rightarrow \infty$ (see below, Sec. 4). Here it is obtained for the opposite case of $U = 0$. As a whole, such a picture of phase transitions into a new uniform phase is in agreement with the known results for the FK model in the case of strong coupling (see Ref. [43]). But, as is evident from the phase diagram obtained in Ref. [57] for this model, in the region of large but finite values of g the phase with double modulation can appear. In order to detect instabilities associated with the wave vector $\mathbf{k} \neq \mathbf{0}$ one

should calculate the susceptibility functions and analyse their temperature and \mathbf{k} - dependencies. Such an investigation was performed for PEM in the framework of GRPA (see below, Secs. 3.1.2 and 3.2.2).

3. Simplified PEM in Generalized Random Phase Approximation

A more complete investigation of the PEM was performed in the framework of the generalized random phase approximation (GRPA). Such an approach was formulated by Izyumov and Letfulov³⁹ for the calculation of the pair correlation functions and magnetic susceptibility of the Hubbard and $t - J$ models. It is based on the expansions in terms of electron transfer and consists in the summation of the diagrams having a structure of sequences of the electron loops (created by the electron Green's functions) joined by vertices of various types appearing due to short-range interactions.^{26,39}

Thermodynamics of PEM was studied in the GRPA for $U = 0$, $\Omega = 0$ (simplified model) in the cases of strong ($g \gg W$) and weak ($g < W$) coupling as well as in the limit of the infinitely large on-site electron repulsion ($U \rightarrow \infty$). Let us first consider the results obtained for simplified model.

3.1. Strong Coupling Case; $U = 0$, $\Omega = 0$

3.1.1. Thermodynamics of the Uniform State

First we consider the case of strong coupling. Here the single-site states can be used as the basic ones and the formalism of electron annihilation (creation) operators $a_{i\sigma} = b_{i\sigma}P_i^+$, $\tilde{a}_{i\sigma} = b_{i\sigma}P_i^-$ ($P_i^\pm = 1/2 \pm S_i^z$) acting at a site with certain pseudospin orientation was introduced.³⁰ Using this representation we can write the model Hamiltonian in the form

$$\begin{aligned} H &= H_0 + H_{\text{int}}, \\ H_0 &= \sum_i \{ \varepsilon(n_{i\uparrow} + n_{i\downarrow}) + \tilde{\varepsilon}(\tilde{n}_{i\uparrow} + \tilde{n}_{i\downarrow}) - hS_i^z \}, \\ H_{\text{int}} &= \sum_{ij\sigma} t_{ij} (a_{i\sigma}^+ a_{j\sigma} + a_{i\sigma}^+ \tilde{a}_{j\sigma} + \tilde{a}_{i\sigma}^+ a_{j\sigma} + \tilde{a}_{i\sigma}^+ \tilde{a}_{j\sigma}). \end{aligned} \quad (19)$$

Here, $\varepsilon = -\mu + g/2$ and $\tilde{\varepsilon} = -\mu - g/2$ are the energies of single-site states.

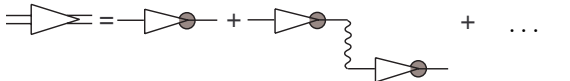
Expansion of the calculated quantities in terms of electron transfer leads to the infinite series of terms containing the averages of the T -products of the $a_{i\sigma}$, $\tilde{a}_{i\sigma}$ operators. The evaluation of such averages is made using the corresponding Wick's theorem.^{30,58} The results are expressed in terms of

the products of nonperturbed Green's functions and averages of a certain number of the projection operators P_i^\pm which are calculated by means of the semi-invariant expansion.³⁰

Nonperturbed electron Green's function is equal to

$$g(\omega_n) = \langle g_i(\omega_n) \rangle; \quad g_i(\omega_n) = \frac{P_i^+}{i\omega_n - \varepsilon} + \frac{P_i^-}{i\omega_n - \tilde{\varepsilon}}. \quad (20)$$

In the diagrammatic representation it has the meaning of the simplest irreducible Larkin part in the series for the free single-electron Green's function $G_{\mathbf{k}}(\omega_n)$. In the Hubbard-I type approximation (see previous section) $G_{\mathbf{k}}(\omega_n)$ can be written as a sum of the following chain diagrams



$$+ \dots, \quad (21)$$

or

$$G_{\mathbf{k}}(\omega_n) = [g^{-1}(\omega_n) - t_{\mathbf{k}}]^{-1}, \quad (22)$$

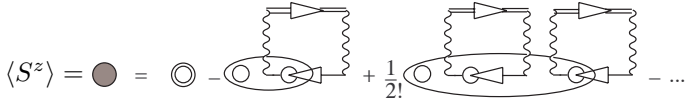
and its poles (after analytic continuation $i\omega_n \rightarrow \omega + i\delta$) determine the electron spectrum

$$\varepsilon_{I,II}(t_{\mathbf{k}}) = \frac{t_{\mathbf{k}}}{2} - \mu \pm \frac{1}{2} \sqrt{g^2 + 4t_{\mathbf{k}}\langle S^z \rangle g + t_{\mathbf{k}}^2}. \quad (23)$$

The electron subbands are divided by a gap which tends to zero only at $g \rightarrow 0$.

There are used here (and below) the following diagrammatic notations: $\bigcirc = S_i^z$, $\text{---} \bigcirc \text{---} = g_i(\omega_n)$, wavy line is the electron intersite hopping t_{ij} . Semi-invariants are represented by ovals and contain the δ -symbols on the site indices.

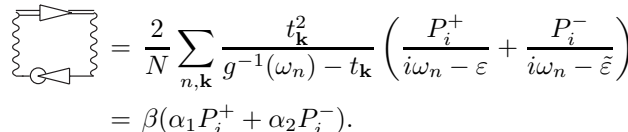
In the adopted approximation the diagrammatic series for the pseudospin mean value can be presented in the form



$$\langle S^z \rangle = \bigcirc = \bigcirc - \text{oval} + \frac{1}{2!} \text{oval} - \dots. \quad (24)$$

In the spirit of the traditional mean field approach⁵⁹ the renormalization of the basic semi-invariant by the insertion of independent loop fragments is taken into account in (24).

The analytical expression for the loop is as follows:



$$\begin{aligned} \text{loop diagram} &= \frac{2}{N} \sum_{n,\mathbf{k}} \frac{t_{\mathbf{k}}^2}{g^{-1}(\omega_n) - t_{\mathbf{k}}} \left(\frac{P_i^+}{i\omega_n - \varepsilon} + \frac{P_i^-}{i\omega_n - \tilde{\varepsilon}} \right) \\ &= \beta(\alpha_1 P_i^+ + \alpha_2 P_i^-). \end{aligned} \quad (25)$$

Similarly, the diagrammatic series for the electron concentration mean value is as follows:

$$\langle n_i \rangle = \square - \left(\square - \frac{1}{2!} \right) + \dots \quad (26)$$

$$+ \sum_{\alpha} ,$$

$$\text{where } \square = n_i, \quad \square_{\alpha} = \frac{1}{i\omega_n - \varepsilon^{\alpha}}, \quad \square_{\alpha}^{\alpha} = \frac{\langle P_i^{\alpha} \rangle}{i\omega_n - \varepsilon^{\alpha}}, \quad \varepsilon^{\alpha} = (\varepsilon, \tilde{\varepsilon}),$$

$$P_i^{\alpha} = (P_i^+, P_i^-).$$

The grand canonical potential Φ and pair correlation functions ($\langle S_i^z S_j^z \rangle$, $\langle S_i^z n_j \rangle$, $\langle n_i n_j \rangle$) are calculated according to self-consistent scheme of the GRPA: in sequences of loop diagrams in the expressions for Φ and correlators the connections between any two loops by more than one semi-invariant are omitted. We have, respectively

$$\Delta\Phi = \frac{1}{2} \left(\square - \frac{1}{3} \right) + \dots \quad (27)$$

$$\langle S_i^z S_j^z \rangle = \square_{\alpha}^{\alpha} = \square_{\alpha}^{\alpha} - \quad (28)$$

$$\square_{\alpha} = P_i^{\alpha}, \quad \square_{\alpha}^{\alpha} = - \square_{\alpha} + = \square_{\alpha}^{\alpha} . \quad (29)$$

The first term in equation (28) takes into account a direct action of the

internal effective self-consistent field on pseudospins:

$$\begin{aligned}
 \text{Diagram: } &= \text{Diagram: } - \text{Diagram: } + \\
 &+ \frac{1}{2!} \text{Diagram: } - \dots .
 \end{aligned} \tag{30}$$

leading to the renormalization of the second-order semi-invariant due to the inclusion of “single-tail” loop-like parts. Second term in equation (28) describes an interaction between pseudospins which is mediated by electron hopping. From (24) and (25), the equation for the pseudospin mean value follows:

$$\langle S^z \rangle = \frac{1}{2} \tanh \left\{ \frac{\beta}{2} (h + \alpha_2 - \alpha_1) + \ln \frac{1 + e^{-\beta\varepsilon}}{1 + e^{-\beta\tilde{\varepsilon}}} \right\}, \tag{31}$$

where

$$\alpha_2 - \alpha_1 = \frac{2}{N} \sum_{\mathbf{k}} t_{\mathbf{k}} \frac{\varepsilon - \tilde{\varepsilon}}{\varepsilon_I(t_{\mathbf{k}}) - \varepsilon_{II}(t_{\mathbf{k}})} [n(\varepsilon_{II}(t_{\mathbf{k}})) - n(\varepsilon_I(t_{\mathbf{k}}))]. \tag{32}$$

The grand canonical potential in the considered approximation has the form:

$$\begin{aligned}
 \Delta\Phi = \Phi - \Phi \Big|_{t=0} = & -\frac{2}{N\beta} \sum_{\mathbf{k}} \ln \frac{(\cosh \frac{\beta}{2}\varepsilon_I(t_{\mathbf{k}}))(\cosh \frac{\beta}{2}\varepsilon_{II}(t_{\mathbf{k}}))}{(\cosh \frac{\beta}{2}\varepsilon)(\cosh \frac{\beta}{2}\tilde{\varepsilon})} \\
 & + \langle S^z \rangle (\alpha_2 - \alpha_1) - \frac{1}{\beta} \ln \cosh \left\{ \frac{\beta}{2} (h + \alpha_2 - \alpha_1) + \ln \frac{1 + e^{-\beta\varepsilon}}{1 + e^{-\beta\tilde{\varepsilon}}} \right\} \\
 & + \frac{1}{\beta} \ln \cosh \left\{ \frac{\beta}{2} h + \ln \frac{1 + e^{-\beta\varepsilon}}{1 + e^{-\beta\tilde{\varepsilon}}} \right\}.
 \end{aligned}$$

With respect to the initial GRPA scheme,^{26,39} the action of the internal effective self-consistent field on pseudospins is taken into account by including the mean field type contributions into the expressions for all thermodynamic quantities. The electron concentration and pseudospin mean values as well as correlation functions are calculated consistently with the thermodynamics functions. It can be checked explicitly^{30,31} using the relations

$$\frac{d\Phi}{d(-\mu)} = \langle n \rangle; \quad \frac{d\Phi}{d(-h)} = \langle S^z \rangle; \quad \frac{dS^z}{d(-\beta h)} = \langle S^z S^z \rangle_{q=0}. \tag{33}$$

At high temperatures, equation (31) possesses only a uniform solution $\langle S_i^z \rangle = \langle S^z \rangle$. However, there exists a possibility of phase transition between different uniform phases with the different pseudospin mean values.

For the first time the possibility of such a transition, which leads to the structural (dielectric) instability, was considered for the PEM in the limit of the strong electron correlation ($U \rightarrow \infty$) in Refs. [25,26] (this issue is analysed below, see Sec. 4). A relatively complete description of this transition was also given in Ref. [60] for the PEM with a direct interaction between pseudospins (in the $t_{ij} = 0$ limit).

Within the GRPA scheme presented here, the uniform-uniform phase transition in the simplified PEM was analysed in Ref. [30]. The solutions of the set of equations (33) which correspond to the absolute minimum values of $\Delta\Phi$ were determined and analysed. The calculations were numerically performed for the square lattice with the nearest-neighbour hopping ($d = 2$ DOS with the bandwidth $2W$). The obtained picture of the phase transition in the $\mu = \text{const}$ and $n = \text{const}$ regimes is very similar to the case of DMFT approach. When the chemical potential is fixed, there exist jumps of the pseudospin mean value and electron concentration on the phase transition line (Fig. 8). The $(h - \mu)$ and $(T_c - h)$ phase diagrams are nearly the same by their shape as in the DMFT case despite the fact that electron energy spectrum in GRPA is split at any values of g , see Figs. 9, 10. The same conclusion can be made when we compare the $(T - n)$ phase diagrams obtained in the $n = \text{const}$ regime; the corresponding phase separation areas are shown in Fig. 11. The difference in positions of critical points in the (h, T) plane calculated in the DMFT and GRPA approaches is also small (see Figs. 4 and 10b).

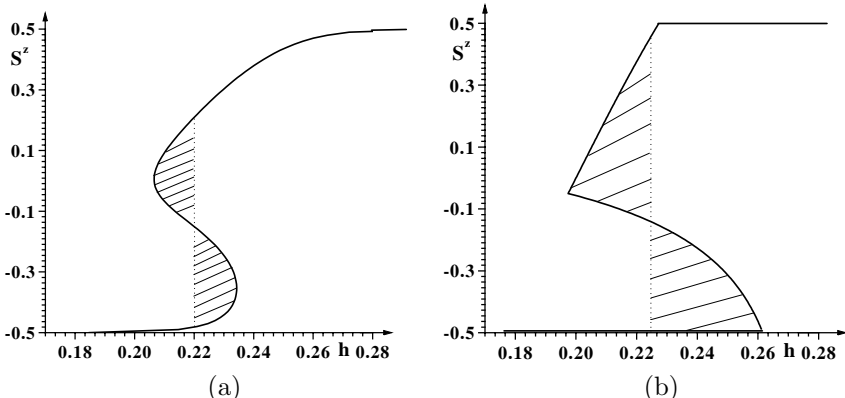


Fig. 8. Field dependence of $\langle S^z \rangle$ ($W = 0.2$, $\mu = -0.4$, $g = 1.0$) for $\mu = \text{const}$ regime; $T = 0.01$ and $T = 0$.

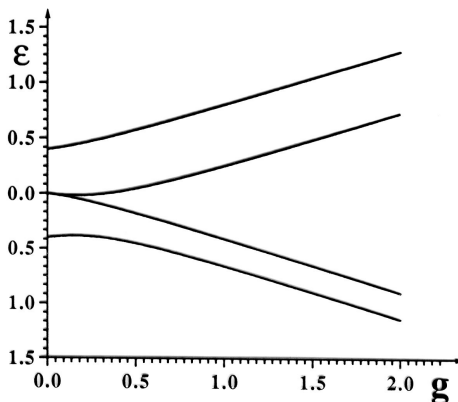


Fig. 9. Electron bands boundaries ($t_0 = 0.4$, $\langle S^z \rangle = 0.2$).

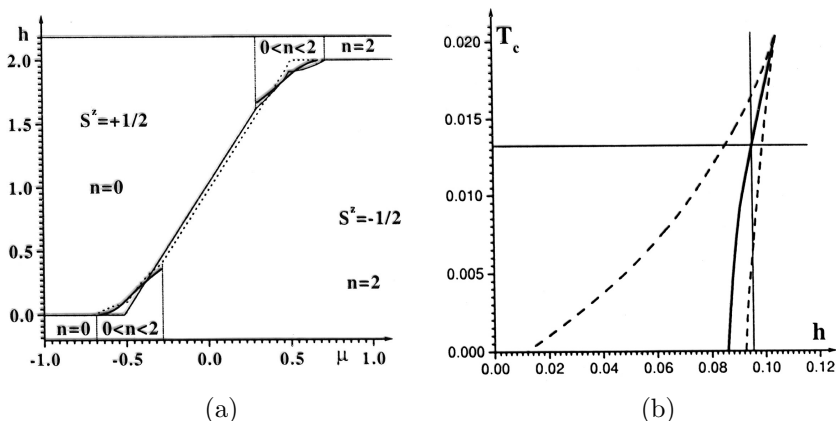


Fig. 10. (a): $(h-\mu)$ phase diagram ($T = 0$, $t_0 = 0.2$, $g = 1$). (b): (T_c-h) phase diagram ($g = 1$, $t_0 = 0.2$, $\mu = -0.5$).

In figures discussed above, the case is presented when the chemical potential is placed in the lower energy subband. If μ is placed in the upper subband, the results are transformed according to the internal symmetry of the Hamiltonian and the following replacements should be made

$$\mu \rightarrow -\mu, \quad h \rightarrow 2g - h, \quad n \rightarrow 2 - n, \quad S^z \rightarrow -S^z. \quad (34)$$

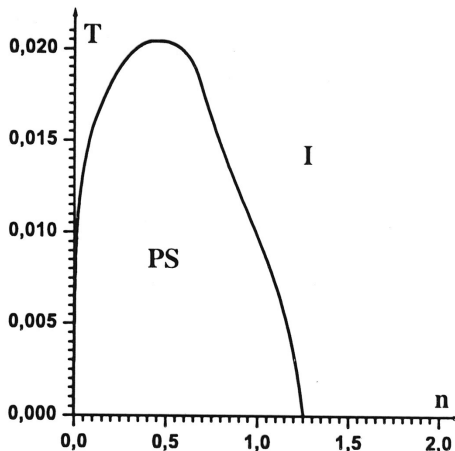


Fig. 11. $(T - n)$ phase diagram ($h = 0.1$, $t_{k=0} = 0.2$, $g = 1$).

Summing up, we can conclude that the generalization of GRPA scheme,^{30,31} which takes into account the mean-field loop-like contributions to the semi-invariant averages, makes it possible to calculate the thermodynamic functions and to investigate the first order phase transitions between different uniform phases. At the transitions, there always remains a gap (in the strong coupling case, $g \gg W$) in the electron spectrum. With the change of the mean value of the pseudospin a reconstruction of the electron spectrum takes place, at which the widths of the electron subbands change which results in the jump-like change of electron concentration (at the given chemical potential μ , it corresponds to a charge transfer from /to the electron reservoir).

The phase coexistence curve in the (h, T) plane is tilted from the vertical line; therefore, there is a possibility of the first order phase transition with the temperature change (in the narrow interval of the field h values). It should be noted that the existence of the shifted and tilted coexistence curve (as the result of the local pseudospin-electron interaction) was obtained for the first time in Ref. [60] for a PEM with the direct interaction between pseudospins. In the case considered here, such a direct interaction is not included, but due to electron transfer there appears an indirect one (the latter is formed by the loop-like contributions $\langle \Pi_q \rangle$). The relative role of the direct and indirect interactions between pseudospins is analysed more

in detail in Sec. 5, on the example of the two-sublattice PEM.

Herein below, considering the $\langle S^z S^z \rangle_{\mathbf{q}}$ pair correlation function, we shall look at the possibility of the spatially modulated charge (charge density wave, CDW) and pseudospin orderings in the PEM with $U = 0$, $\Omega = 0$ in the strong coupling case.

3.1.2. The Chess-Board Phase

The analysis of the $\langle S^z S^z \rangle_{\mathbf{q}}$ correlator temperature behaviour shows that for certain values of model parameters, the high temperature phase may be unstable with respect to fluctuations with $\mathbf{q} \neq \mathbf{0}$.³¹ Solution of Eq. (28) for pseudospin correlator has the form

$$\langle S^z S^z \rangle_{\mathbf{q}} = \frac{1/4 - \langle S^z \rangle^2}{1 + [\Pi]_{\mathbf{q}} (\frac{1}{4} - \langle S^z \rangle^2)}, \quad (35)$$

where $[\Pi]_{\mathbf{q}}$ characterizes an interaction between pseudospins via electron subsystem:

$$[\Pi]_{\mathbf{q}} = \sum_{\alpha, \beta} (-1)^{\alpha + \beta} \text{Diagram}, \quad (36)$$

and its singularities

$$1 + [\Pi]_{\mathbf{q}} (\frac{1}{4} - \langle S^z \rangle^2) = 0$$

give the instability points of uniform phase.

It follows from calculations³¹ that for some model parameter values, the uniform phase becomes unstable with respect to fluctuations with $\mathbf{q} = (\pi, \pi)$ (the chess-board phase).

To consider the thermodynamics of the chess-board phase analytically, we take into account the modulation of the pseudospin and electron distribution, introducing two kinds of sites: $\langle S_1^z \rangle$ and n_1 correspond to one sublattice and $\langle S_2^z \rangle$ and n_2 to the other one. In this case the single-electron Green's function for the l sublattice is equal to:

$$G_l(\mathbf{k}, \omega_n) = \frac{g_l(\omega_n)}{1 - t_{\mathbf{k}}^2 g_1(\omega_n) g_2(\omega_n)}, \quad (37)$$

where $g_l(\omega_n)$ ($l = 1, 2$) is the nonperturbated Green's function for sublattice l . The single-electron spectrum is determined from the equation

$$x^4 - (g^2/2 + t_{\mathbf{k}}^2)x^2 - g t_{\mathbf{k}}^2 (\langle S_1^z \rangle + \langle S_2^z \rangle)x + g^4/16 - g^2 t_{\mathbf{k}}^2 \langle S_1^z \rangle \langle S_2^z \rangle = 0. \quad (38)$$

The roots $\varepsilon_1(t_{\mathbf{k}}) \geq \varepsilon_2(t_{\mathbf{k}}) \geq \varepsilon_3(t_{\mathbf{k}}) \geq \varepsilon_4(t_{\mathbf{k}})$ of the equation (38) form four subbands. The widths of subbands depend on the mean values of pseudospins.

The branches $\varepsilon_1(t_{\mathbf{k}}), \varepsilon_2(t_{\mathbf{k}})$, on the one side, and $\varepsilon_3(t_{\mathbf{k}}), \varepsilon_4(t_{\mathbf{k}})$ on the other side, form two pairs of bands which are always separated by a gap. The equation for pseudospin mean values (31) can be now written in the form:

$$\langle S_l^z \rangle = \frac{1}{2} \tanh \left\{ \frac{\beta}{2} (h + \alpha_2^l - \alpha_1^l) + \ln \frac{1+e^{-\beta\varepsilon}}{1+e^{-\beta\tilde{\varepsilon}}} \right\}, \quad l = 1, 2 \quad (39)$$

where expressions for the effective self-consistent fields are

$$\alpha_2^l - \alpha_1^l = \frac{2}{N} \sum_{\mathbf{k}} t_{\mathbf{k}}^2 (\varepsilon - \tilde{\varepsilon}) \sum_{i=1}^4 A_i^l n[\varepsilon_i(t_{\mathbf{k}}) - \mu], \quad (40)$$

$$A_i^l = \frac{\varepsilon_i(t_{\mathbf{k}}) + g \langle S_{l'}^z \rangle}{(\varepsilon_i(t_{\mathbf{k}}) - \varepsilon_j(t_{\mathbf{k}}))(\varepsilon_i(t_{\mathbf{k}}) - \varepsilon_p(t_{\mathbf{k}}))(\varepsilon_i(t_{\mathbf{k}}) - \varepsilon_m(t_{\mathbf{k}}))}, \quad i \neq j, p, m, \quad l \neq l'.$$

Expression for the electron mean number follows from (33):

$$\begin{aligned} \langle n_1 + n_2 \rangle &= \frac{2}{N} \sum_{\mathbf{k}} \sum_{i=1}^4 n[\varepsilon_i(t_{\mathbf{k}}) - \mu] \\ &\quad - 2 \left[(\langle P_1^+ \rangle + \langle P_2^+ \rangle) n(\tilde{\varepsilon}) + (\langle P_1^- \rangle + \langle P_2^- \rangle) n(\varepsilon) \right], \end{aligned} \quad (41)$$

and the grand canonical potential (27) can be written for the two-sublattice case in the following analytic form:

$$\begin{aligned} \Delta\Phi &= -\frac{2}{N\beta} \sum_{\mathbf{k}} \ln \frac{\prod_{i=1}^4 \cosh \left[\frac{\beta}{2} (\varepsilon_i(t_{\mathbf{k}}) - \mu) \right]}{(\cosh \frac{\beta}{2}\varepsilon)^2 (\cosh \frac{\beta}{2}\tilde{\varepsilon})^2} + \sum_{l=1,2} \langle S_l^z \rangle (\alpha_2^l - \alpha_1^l) \\ &\quad + \sum_{l=1,2} \left[-\frac{1}{\beta} \ln \cosh \left\{ \frac{\beta}{2} (h + \alpha_2^l - \alpha_1^l) + \ln \frac{1+e^{-\beta\varepsilon}}{1+e^{-\beta\tilde{\varepsilon}}} \right\} \right. \\ &\quad \left. + \frac{1}{\beta} \ln \cosh \left\{ \frac{\beta}{2} h + \ln \frac{1+e^{-\beta\varepsilon}}{1+e^{-\beta\tilde{\varepsilon}}} \right\} \right]. \end{aligned} \quad (42)$$

As previously in the investigation of equilibrium conditions, we consider two different thermodynamic regimes.

a) The $\mu = \text{const}$ regime.

The equilibrium is defined by the minimum condition of Φ (42). Numerical analysis of solutions of equations (39)-(41) which satisfy this criterion, was performed in Ref. [31]. The examples of the calculated field dependencies of

$\langle S_1^z - S_2^z \rangle$ (the order parameter for the chess-board phase) and grand canonical potential are presented in Fig. 12 for low temperatures (the case $g \gg W$ is considered). It is seen from comparison of the Φ values for the uniform and the chess-board phases that the modulated phase is thermodynamically stable at intermediate values of the h field in the region between points a and b . These points correspond to the first and second order phase transi-

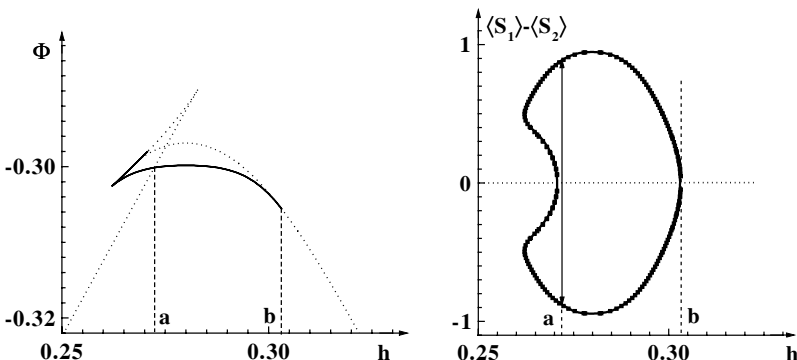


Fig. 12. Field dependence of the grand canonical potential and order parameter ($T = 0.005$, $\mu = -0.36$, $W = 0.2$, $g = 1$). Dotted and solid lines correspond to the uniform and the chess-board phases, respectively. See the text for a whole description.

tions, respectively. In the first case, the jump-like change of order parameter is accompanied by characteristically similar changes of the subband widths and, as a result, by changes of the electron concentration.

The resulting phase diagram ($h - \mu$) at low temperatures is shown in Fig. 13. The chess-board phase exists as an intermediate phase between the uniform phases with different $\langle S^z \rangle$ and n values. Transitions between the uniform and modulated phases are of the first or second order and can be realized in the case when μ is placed in ε_2 or ε_3 subbands or between them. Transitions between different uniform phases (described in the previous section), which are of the first order, take place when the chemical potential is placed within the ε_1 , ε_4 and partially within ε_2 , ε_3 subbands.

The shape of the ($T - h$) phase diagram strongly depends on the μ value. In the case when μ is placed in the ε_3 subband, such a diagram is shown in Fig. 14a. With the temperature increase, the first order phase transition between the uniform and the chess-board phases transforms into the first order phase transition between uniform phases and, finally, disappears in the critical point θ_c . The diagram shows the possibility of the first order

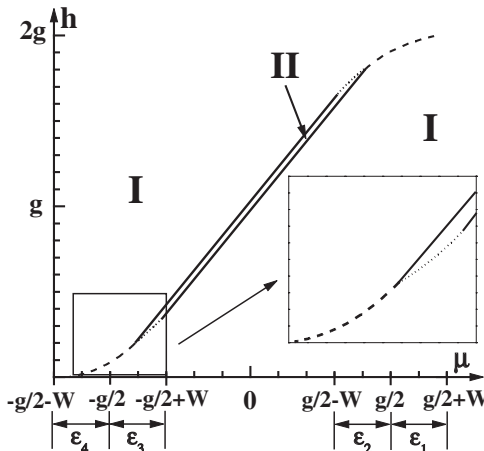


Fig. 13. $(h - \mu)$ phase diagram ($T = 0.005$, $W = 0.2$, $g = 1$). I: uniform phase, II: chess-board phase. Dashed lines: first order phase transitions between the uniform phases with different pseudospin mean values. Dotted lines: first order phase transitions between the uniform and the chess-board phases. Solid lines: second order phase transitions.

phase transitions between uniform phases and either first or second order ones between the uniform and the chess-board phases at the change of temperature.

In the case when chemical potential lies between the ε_1 , ε_2 and ε_3 , ε_4 subbands, the transitions between phases I (uniform) and II (chess-board) are of the second order; the corresponding $(T - h)$ diagram is shown in Fig. 14b.

b) The $n = \text{const}$ regime.

In this regime, the equilibrium is defined by a minimum of the free energy $F = \Phi + \mu N$. This condition forms a set of equations (39) and (41) for the pseudospin mean values and chemical potential. The obtained dependencies of F and μ on the electron concentration are presented in Fig. 15.

One can see the regions with $d\mu/dn \leq 0$ where the phase separation into regions with different phases (the uniform and the chess-board phases in this case) and with different electron concentrations and pseudospin mean values take place.

Based on the obtained results, the phase diagram ($n - h$) was constructed (Fig. 16). The phase separation into regions with the uniform and the chess-board phases takes place when the chemical potential is placed within the

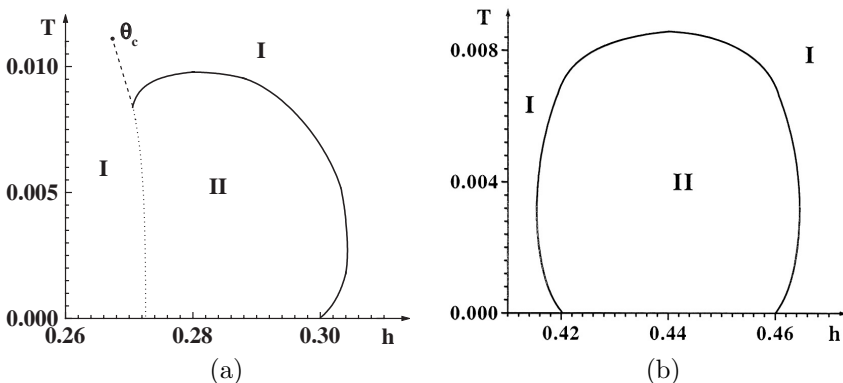


Fig. 14. (a): Phase diagram ($T - h$) ($\mu = -0.36$, $W = 0.2$, $g = 1$). I: uniform phase, II: chess-board phase. Dashed lines: first order phase transitions between different uniform phases (bistability). Dotted line: first order phase transitions between the uniform and the chess-board phases. Solid lines: second order phase transitions. (b): Phase diagram ($T - h$) ($\mu = -0.28$, $t_{k=0} = 0.2$, $g = 1$).

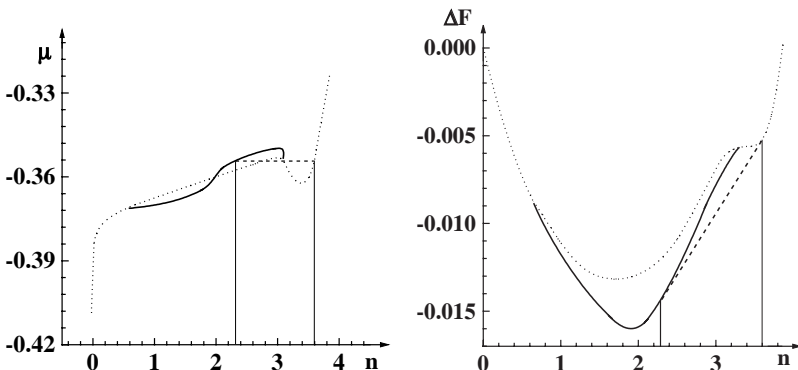


Fig. 15. Dependence of the chemical potential μ on the electron concentration n and deviation of the free energy from linear dependence ($T = 0.005$, $h = 0.28$, $W = 0.2$, $g = 1$). Dashed line: phase separation area. Dotted line: uniform phase. Solid line: chess-board phase.

subbands ε_2 , ε_3 . That agrees with the results obtained in the $\mu = \text{const}$ case when within this area we had the first order phase transition between the corresponding phases.

The phase separated and the chess-board phase regions narrow with the temperature increase, but thick solid lines in Fig. 16 approach faster

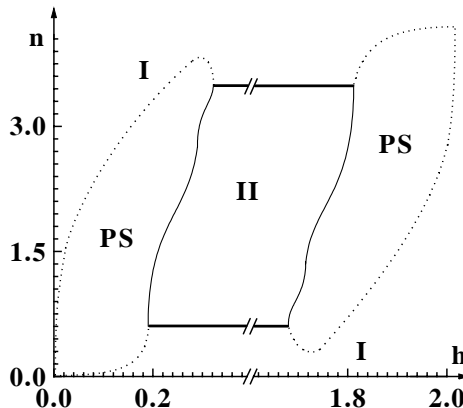


Fig. 16. Phase diagram ($n - h$) ($T = 0.005$, $W = 0.2$, $g = 1$). I: uniform phase, II: chess-board phase, PS: phase separation area.

one another and, for high enough temperatures, we have only the phase separation into the regions with uniform phases.

The fact of the existence of doubly-modulated (chess-board) phase in the PEM as intermediate one between segregated phases (at low temperatures) is similar to the results obtained in DMFT for the Falicov-Kimball model by Freericks and Lemansky.⁶¹ Investigation of temperature T_c of instability of the high-temperature phase of the FK model as a function of the ordering wave vector (determined by the divergence of the relevant susceptibility) showed that near half-filling ($\rho_e = 0.5$) the chess-board phase is stable, while the segregated phase exists at the occupations near electron band edges. The region of modulated phase narrows at the increase of g and disappears at $g \rightarrow \infty$.⁵⁷ In this limit the thermodynamically stable states were analyzed⁶² based on the calculations of the grand canonical potential and the phase separation diagrams (where besides the spinodal lines the lines of the first order transition temperatures were shown) were built; the cases of different electron concentrations ρ_e were considered.

Nevertheless, one cannot claim the one-to-one correspondence. The calculations of Freericks and Lemansky were performed in another thermodynamic regime: the concentration of heavy particles ρ_i was fixed (that would correspond to the given value of $\langle S^z \rangle$ for PEM). The closest to our case are the results obtained by Brandt and Mielsch.⁶³ They constructed the ($T - \rho_i$) diagrams at the finite g values for the FK model. The obtained sequence of phases (segregated-modulated-segregated) when ρ_i increases (from $\rho_i = 0$

up to $\rho_i = 1$) is the same as for PEM at the increase of the field h .

3.2. Weak Coupling Case; $U = 0$

Now let us consider the case of weak coupling ($g < W$). We can base on the perturbation theory approach taking the mean field Hamiltonian as the zero-order one.³² We use the approximation

$$gn_i S_i^z \rightarrow gn_i \langle S_i^z \rangle + g \langle n_i \rangle S_i^z - g \langle n_i \rangle \langle S_i^z \rangle \quad (43)$$

in this case, based on the arguments that for the simplified PEM with $U = 0$ the interaction constant g plays the role which is similar to that of U in the Hubbard model, and at the decrease of g below the critical value ($g \sim W$) the system should pass to the mean field regime of the Hartree-Fock type.

Having in mind the possibility that the system can be in the uniform or modulated state, we shall consider, as above, two different cases. The first one corresponds to the homogeneous pseudospin ordering and spatially uniform mean distribution of electrons. The second one is the case of modulation with doubling of the lattice period (chess-board phase).

3.2.1. Uniform Phase

The Hamiltonian of PEM in the mean-field approximation (MFA) reads

$$H = H_{el} + H_s + U, \quad (44)$$

$$H_{el} = \sum_{i,\sigma} (g\eta - \mu) n_{i,\sigma} + \sum_{i,j,\sigma} t_{i,j} a_{i,\sigma}^+ a_{j,\sigma},$$

$$H_s = \sum_i [(gn - h) S_i^z + \Omega S_i^x], \quad (45)$$

$$U = -g \sum_i n\eta = -Ngn\eta.$$

The parameters $\langle n_i \rangle = n$ and $\langle S_i^z \rangle = \eta$ are determined from the set of equations

$$n = \frac{1}{N} \sum_{\mathbf{k}\sigma} (e^{\beta(g\eta + t_{\mathbf{k}} - \mu)} + 1)^{-1} \equiv \frac{1}{N} \sum_{\mathbf{k}\sigma} f(g\eta + t_{\mathbf{k}}), \quad (46)$$

$$\eta = \frac{h - gn}{2\lambda} \tanh\left(\frac{\beta\lambda}{2}\right); \quad \lambda = \sqrt{(gn - h)^2 + \Omega^2}.$$

The grand canonical potential in the MFA is given by the expression

$$\frac{\Phi}{N} = -\frac{T}{N} \sum_{\mathbf{k},\sigma} \ln(1 + e^{\frac{\mu - t_{\mathbf{k}} - gn}{T}}) - T \ln(2 \cosh \frac{\beta\lambda}{2}) - gnn \quad (47)$$

where $\lambda = \sqrt{(gn - h)^2 + \Omega^2}$.

Similarly to the strong coupling case, we can distinguish the regimes of the constant electron chemical potential $\mu = \text{const}$ (where the stable states can be found from the minimum Φ condition) and the given electron concentration $n = \text{const}$ (when one should find the minimum of the free energy $F = \mu n + \Phi$).

a) Thermodynamics in the $\mu = \text{const}$ regime.

We consider at first the simplest case $\mu = 0, h = g$. Here the solution $\eta = 0, n = 1$ of the set of equations (46) exists at any temperature and describes a disordered phase. Furthermore, at low temperatures there appears a non-zero solution $\eta \neq 0, n \neq 1$. A critical temperature T_c is determined from the equation

$$1 + \frac{g^2}{2\Omega} \tanh \frac{\beta\Omega}{2} \Pi_0 = 0, \quad (48)$$

which in the case $\Omega \rightarrow 0$ reduces to the form

$$1 + \frac{\beta}{4} g^2 \Pi_0 = 0, \quad (49)$$

Here

$$\Pi_0 = \frac{2}{N} \sum_{\mathbf{k}} f'(t_{\mathbf{k}}) = 2 \int_{-W}^W dt \rho(t) f'(t). \quad (50)$$

In the low temperature limit we have $T_c = \frac{g^2}{2} \rho(0)$ (when the DOS at the Fermi level $\rho(\mu)|_{\mu=0}$ is finite). In the case $\Omega \neq 0$ there exists such a critical value $\Omega_{cr} = g^2 \rho(0)$ ($\Omega_{cr} = \frac{g^2}{2W}$ for the rectangular DOS), above which (at $\Omega > \Omega_{cr}$) the phase transition to ordered phase disappears. This is equivalent to the existence of a critical value of g : at given Ω the phase transition is possible when $g > g_{cr} = \sqrt{\frac{\Omega}{\rho(0)}}$. In the case of the DOS with logarithmic singularity, the critical temperature exists at any values of the tunneling splitting parameter Ω and at $\frac{\Omega}{g} \gg \frac{g}{W}$ we have an asymptotic expression:

$$T_c \approx 2eW \exp\left(-\frac{\Omega W \pi^2}{2g^2}\right). \quad (51)$$

The physical nature of the phase transition considered here at $h = g, \mu = 0$ (the fixed μ regime) is as follows: the appearance of an ordered phase is connected with its stabilization due to the shift of the electron band down to the low energy values under the effect of the internal field; this ensures the corresponding gain in the electron energy (it should be mentioned that

the electron band spectrum in this case remains unsplit in the uniform phase; only the shift of the band as a whole can take place).

This mechanism remains the main reason of the phase transition when the initial electron band is not half-filled. In this case (when $\mu \neq 0$) we performed the investigation using the numerical calculations when the set of equations (46) is solved and using the expression (47) for the grand canonical potential Φ . The selection of solutions was carried out using the condition of the absolute minimum of Φ .

As can be seen,³² below T_c the system undergoes the first order phase transition with jumps of the mean values of the electron concentration and pseudospin at the change of the field h ; the phase transition point is determined using the Maxwell rule. The similar transition takes place at the change of the chemical potential at fixed h . The presence of the tunneling-like splitting decreases the temperature of the phase transition at the fixed values of μ and h .

The regions of coexistence of phases with different values of the electron concentration and pseudospin are shown in the plane (μ, h) at $\Omega = 0$ and $\Omega \neq 0$ in Figs. 17.

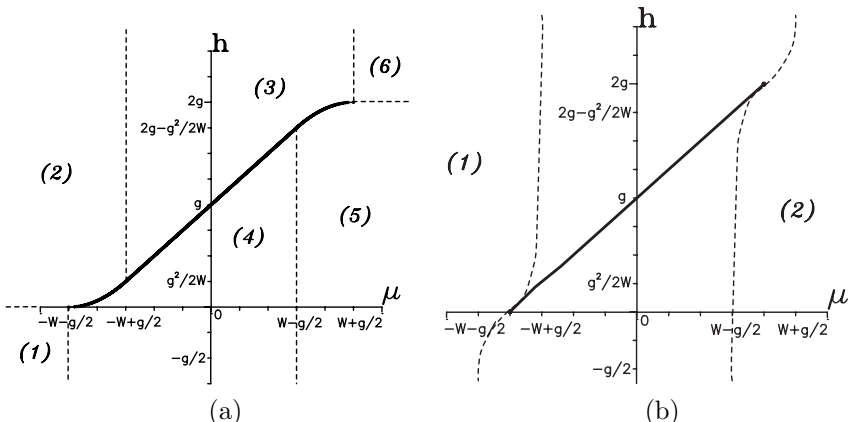


Fig. 17. (a): The ground state diagram ($T = 0, \Omega = 0$). Regions with different n, η values are separated by dashed lines and a solid line (the phase transition line); (1) $n = 0, \eta = -1/2$; (2) $n = 0, \eta = 1/2$; (3) $\eta = 1/2, n = 1 + \frac{\mu}{W} - \frac{g}{2W}$; (4) $\eta = -1/2, n = 1 + \frac{\mu}{W} + \frac{g}{2W}$; (5) $n = 2, \eta = -1/2$; (6) $n = 2, \eta = 1/2$. (b): The $(h - \mu)$ phase diagram ($T = 0.004, \Omega = 0.12$). Regions with different n, η values are separated by dashed lines and a solid line (the phase transition line): (1) $n \approx 0, \eta \approx \frac{1}{2} \frac{h}{\sqrt{h^2 + \Omega^2}}$; (2) $n \approx 2, \eta \approx \frac{1}{2} \frac{h - 2g}{\sqrt{(h - 2g)^2 + \Omega^2}}$.

Phase transition lines in the plane (T, h) at different values of μ are shown in Fig. 18. Such a line is vertical for the case $\mu = 0$ only; for the case $\mu \neq 0$, the line is bent. This makes the first order phase transition possible at the change of temperature (with the jumps of the parameters η, n). The slopes of the phase equilibrium curves are opposite for $\mu > 0$ and $\mu < 0$. The lines of the critical points are shown for the cases $\Omega = 0, \Omega \neq 0$; the calculations are carried out using rectangular density of states. Similar phase diagrams are obtained using direct momentum summation for square lattice (Fig. 19). As in the case of rectangular DOS, the maximum T_c is achieved at $\mu = 0$ but the critical temperature line has a more pronounced peak.

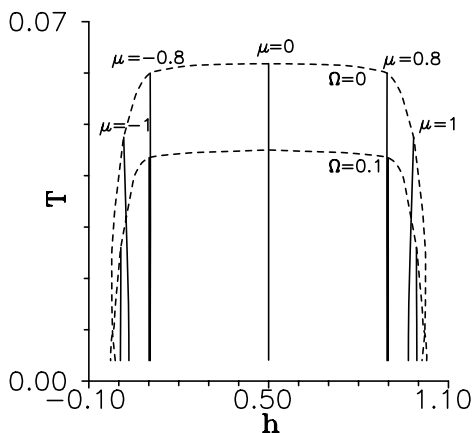


Fig. 18. The critical temperature lines (dashed lines) and the phase transition lines (solid lines) for $\Omega = 0$ and $\Omega = 0.1$ (the case of the rectangular DOS).

b) Thermodynamics in the $n = \text{const}$ regime.

The values n_1, n_2 and η_1, η_2 between which the jumps of the electron concentration and pseudospin mean value take place at the phase transitions in the $\mu = \text{const}$ case, correspond to the phases which coexist in the phase transition points. In the regime $n = \text{const}$, there is a phase separation on the phases with the above mentioned values of n and μ . For example, at the parameter value $\Omega = 0$, $h = 0.7$, $T = 0.008$, the system is unstable with respect to the phase separation in the region $n_1 = 1.149 < n < n_2 = 1.645$.³²

Phase separation regions are shown in Fig. 20 at different temperatures

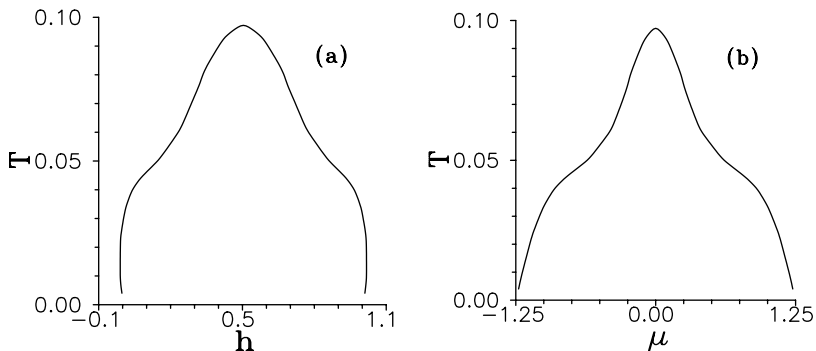


Fig. 19. The critical temperature lines on the a) (h, T) and b) (μ, T) planes for $\Omega = 0$ (direct momentum summation is used).

(the calculations were carried out for square lattice using direct momentum summation when solving the set of equations (46)). At the increase of temperature the separation region narrows and at $T > T_c$ it disappears. The presence of the tunneling-like splitting leads to the decrease of the area of phase separation region and to the lowering of T_c .

It can be noted that at weak coupling, when only uniform states are considered, we have one phase separation region in the (h, n) plane while in the strong coupling case ($g \gg W$) there exist two such regions at the distance of order g along h axis; the modulated phase is placed between them³¹ (see also Sec. 3.1.2).

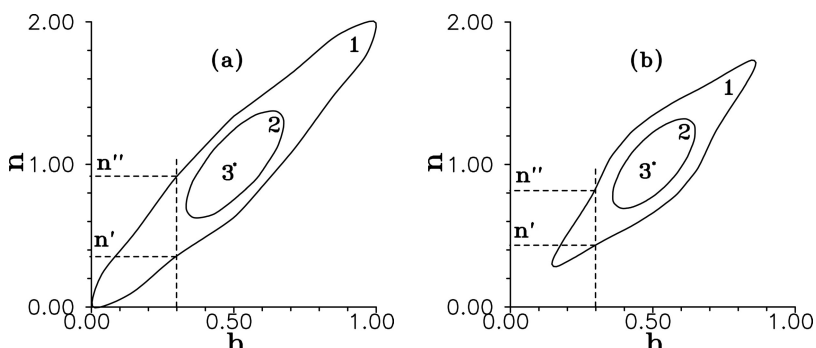


Fig. 20. $(n - h)$ -phase diagram in the cases a) $\Omega = 0$; b) $\Omega = 0.1$. Phase separation regions for different temperatures are shown. a) 1: $T = 0.008$, 2: $T = 0.08$, 3: $T = 0.0972$; b) 1: $T = 0.008$, 2: $T = 0.075$, 3: $T = 0.0903$.

3.2.2. Phase with Double Modulation

Let us consider now the thermodynamics of the simplified PEM in the case of doubly modulated phase. The possibility for such a phase was shown at a strong coupling ($g \gg W$); the necessary condition was the location of the chemical potential between the split electron subbands. Now (at $g < W$) the band is unsplit and in such a situation there must be another mechanism of stabilizing the lattice modulation.

At the double modulation the crystal can be divided into two sublattices ($\alpha = 1, 2$), and the parameters $\eta_\alpha = \langle S_{i\alpha}^z \rangle$, $n_\alpha = \sum_\sigma \langle n_{i\alpha\sigma} \rangle$ can be introduced (i is an unit cell index). Similarly to the homogeneous phase, the mean field approximation is used. The modulation leads to the splitting in the electron spectrum due to difference between the internal field acting in sublattices

$$\lambda_{\mathbf{k}\alpha} = g \frac{\eta_1 + \eta_2}{2} + (-1)^\alpha \sqrt{(g \frac{\eta_1 - \eta_2}{2})^2 + t_{\mathbf{k}}^2} \quad (52)$$

(the similar effect takes place in the FK model⁶⁴). The initial band is divided into two subbands separated by the gap $\Delta = g|\eta_1 - \eta_2|$ (see Fig. 21).

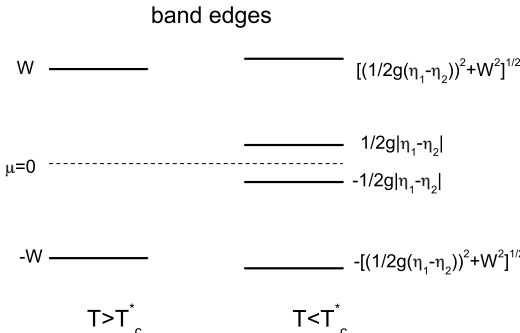


Fig. 21. The band edges for the cases $T > T_c^*$ (homogeneous phase) and $T < T_c^*$ (the double modulation case); $\mu = 0, h = g$.

Contributions from both sublattices are present in the equation for the electron concentration in sublattices

$$n_\alpha = \frac{1}{N} \sum_{\mathbf{k}\sigma} \left(\frac{1 + \cos 2\phi}{2} (e^{\beta(\lambda_{\mathbf{k}\alpha} - \mu)} + 1)^{-1} + \frac{1 - \cos 2\phi}{2} (e^{\beta(\lambda_{\mathbf{k}\beta} - \mu)} + 1)^{-1} \right), \quad (53)$$

where

$$\cos 2\phi = \frac{-g \frac{\eta_1 - \eta_2}{2}}{\sqrt{(g \frac{\eta_1 - \eta_2}{2})^2 + t_{\mathbf{k}}^2}}$$

can be obtained diagonalizing the mean-field two-sublattice Hamiltonian of the model.³² Another equation which appears as a result of the averaging of the operator $S_{i\alpha}^z$ has the form

$$\eta_{\alpha} = \frac{h - gn_{\alpha}}{2\tilde{\lambda}_{\alpha}} \tanh\left(\frac{\beta\tilde{\lambda}_{\alpha}}{2}\right). \quad (54)$$

Here

$$\tilde{\lambda}_{\alpha} = \sqrt{(gn_{\alpha} - h)^2 + \Omega^2}. \quad (55)$$

In the mean field approximation, the grand canonical potential for the double modulation case has the form

$$\begin{aligned} \frac{2\Phi}{N} = & -\frac{T}{N} \sum_{\mathbf{k},\sigma} \ln((1 + e^{-\frac{\lambda_{\mathbf{k}1}-\mu}{T}})(1 + e^{-\frac{\lambda_{\mathbf{k}2}-\mu}{T}})) \\ & - T \ln(4 \cosh \frac{\beta\tilde{\lambda}_1}{2} \cosh \frac{\beta\tilde{\lambda}_2}{2}) - g(n_1\eta_1 + n_2\eta_2). \end{aligned} \quad (56)$$

The solution of the set of equations for the n_{α} and η_{α} parameters and the investigations of thermodynamically stable states were carried out numerically.³² It was established that phase transitions from the uniform to the low temperature modulated phase are of the second or first order. This is illustrated in Fig. 22, where the phase transition lines at $\mu = 0$ are shown for $\Omega = 0$ and $\Omega \neq 0$ (here a direct momentum summation is used in calculations); the tricritical points are also present here.

The difference $\delta n = n_1 - n_2$ (as well as the difference $\delta\eta = \eta_1 - \eta_2$) can play a role of the order parameter for the modulated phase. Coming from the equations for δn and $\delta\eta$ we obtain the following condition of the appearance of nonzero solutions

$$\begin{aligned} 1 = & \frac{g}{N} \sum_{\mathbf{k}\sigma} \frac{1}{t_{\mathbf{k}}} \left(e^{\beta(g\eta - t_{\mathbf{k}} - \mu)} + 1 \right)^{-1} \\ & \times \left[\beta g \frac{(h - gn)^2}{\lambda^2} \left(\frac{1}{4} - \langle \sigma^z \rangle^2 \right) + g \langle \sigma^z \rangle \frac{\Omega^2}{\lambda^3} \right]. \end{aligned} \quad (57)$$

Proceeding from this equation, we can find a critical temperature T_c^* as the maximum temperature (among the set of temperatures which are obtained for different h values) which fulfills this equation at a fixed value of the

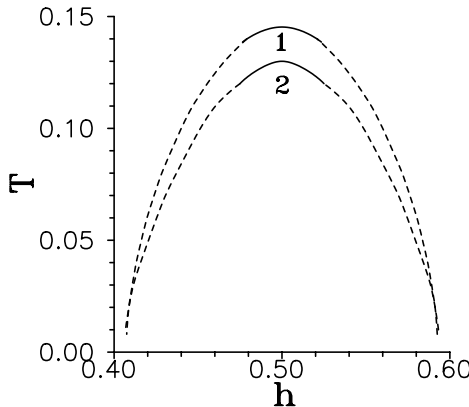


Fig. 22. The phase transition lines (solid and dashed lines are the lines of the second and of the first order phase transitions, respectively) from the uniform phase to the phase with double modulation (1 : $\Omega = 0$; 2 : $\Omega = 0.2$).

chemical potential. This temperature is the point of the second order phase transition to modulated phase at the corresponding value of the field h .

In the symmetric case, when $\mu = 0$, $h = g$ and in the high-temperature phase $n = 1$, $\eta = 0$, the equation (57) reduces to the form

$$1 = -\frac{g^2}{\Omega} \tanh \frac{\beta \Omega}{2} \frac{1}{N} \sum_{\mathbf{k}} \frac{1}{t_{\mathbf{k}}} f(t_{\mathbf{k}}). \quad (58)$$

The critical temperatures T_c^* , obtained in the cases of rectangular DOS and DOS with logarithmic singularity, are, respectively,

$$T_c^* \approx \frac{eW}{2} \exp \left(-\frac{2\Omega W}{g^2} \right) \quad (59)$$

and

$$T_c^* \approx 2eW \exp \left(-\frac{\pi \sqrt{\Omega W}}{g} \right). \quad (60)$$

In both cases, they are higher than the corresponding temperatures T_c for transitions between uniform phases and remain finite at high Ω values.

It can be seen that $T_c^* > T_c$ also at $\mu \neq 0$, but for the μ values, which are less than the certain ($|\mu| < \mu_0$) value. The typical dependencies of T_c^* and T_c on μ are shown in Fig. 23 in the cases $\Omega = 0$ and $\Omega \neq 0$. One can conclude that in the case of the electron band occupation close to the half-filling, the transition to modulated phase should be realized. The transition

between two different uniform phases is possible only when μ is placed near the band edges.

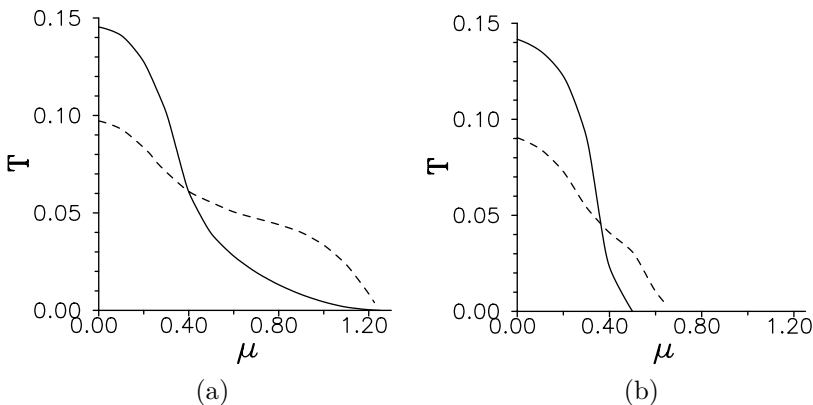


Fig. 23. The dependence of the critical temperature on the chemical potential; a) $\Omega = 0$ b) $\Omega = 0.1$. Solid line refers to the case of the phase with double modulation, dashed line refers to the transition into the homogeneous phase.

The existence of the first order phase transitions between uniform and doubly modulated phases, shows the possibility of a separation into these two phases. This takes place at certain values of the electron concentration. The corresponding $(n - h)$ diagrams are shown in Fig. 24. The borders of the separation regions were obtained from the convexity condition of the free energy defined as $F/N = \Phi/N + n\mu$. As temperature increases, the separation area narrows, but in the middle of it there appears a region of the chess-board phase existence. This is an additional feature which supplements the picture of separation shown in Fig. 20. At high enough temperatures, only the second order phase transition into the doubly modulated state remains and the phase separation region disappears.

3.2.3. Pair Correlation Function and Susceptibilities

The analysis of thermodynamically stable equilibrium states of the PEM in the case of weak coupling can be supplemented by an investigation of temperature and wave vector dependencies of the pseudospin, electron density and mixed pair correlation function. The corresponding Green's functions were calculated in Ref. [33] within the GRPA scheme. The cases of isother-

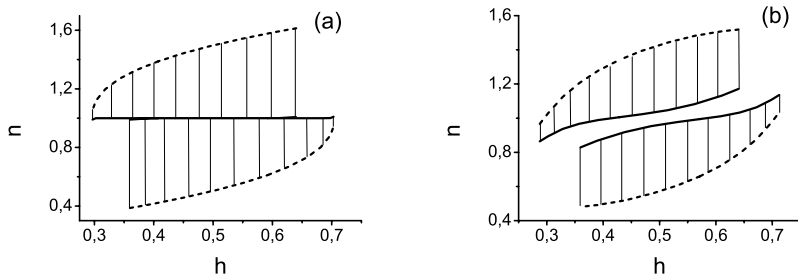


Fig. 24. $(n - h)$ phase diagram, $\Omega = 0$. Phase separation regions are shown for different temperatures: a) $T = 0.008$, b) $T = 0.08$. Dashed lines denote the borders of the uniform phase, thick solid lines denote the borders of the phase with doubly modulated lattice period.

mal response were considered, where the isothermal susceptibility

$$\chi_T(\mathbf{q}, \omega_n) = \int_0^\beta \langle T_\tau M(0)M(\tau) \rangle_{\mathbf{q}} e^{i\omega_n \tau} d\tau - \beta \langle M \rangle^2 \delta(\omega_n) \quad (61)$$

is expressed in terms of the Matsubara Green's function and the so-called "isolated" response, which is described by means of the two-time Zubarev Green's function

$$\chi_I(\mathbf{q}, \omega) \sim \langle \langle M | M \rangle \rangle_{\mathbf{q}\omega}. \quad (62)$$

The dipole moment M_i of the unit cell was taken in the form: $M_i = d_e n_i + d_s S_i^z$; here the electron contribution due to nonhomeopolarity of occupancy of the electron orbitals was taken into account besides the pseudospin contribution.

Such an expression for dipole moment comes from the form of transverse component of polarization in the case of the YBaCuO structure. The electron component corresponds to the charge transfer in a perpendicular direction from/to the Cu_2O_2 layers (with the participation of the Cu-O chains), while the pseudospin component is connected with the redistribution of the ionic charges when O_4 ion moves from one equilibrium position to another.^{26,65}

Similarly to the above considered strong coupling case, the simple sequences of loop diagrams are taken into account in the diagrammatic representation for Matsubara's correlators. The connections between loops are accomplished by semi-invariants or by the boson (pseudospin) Green's

functions. The contribution that corresponds to the separate link is (see Ref. [33])

$$\Sigma_{\mathbf{q}}(\omega) = \frac{1}{2} \sin^2 \vartheta [K_{\mathbf{q}}^0(\omega_n) + K_{\mathbf{q}}^0(-\omega_n)] \langle \sigma^z \rangle_0 - M_{\mathbf{q}}(\omega_n). \quad (63)$$

Here

$$\begin{aligned} K_{\mathbf{q}}^0(\omega_n) &= \frac{1}{i\omega_n - \lambda}; \quad M_{\mathbf{q}}(\omega_n) = \beta b' \cos^2 \vartheta \delta(\omega_n), \\ \sin \vartheta &= \Omega/\lambda; \quad \langle \sigma^z \rangle_0 = b = \frac{1}{2} \tanh \frac{\beta \lambda}{2}; \quad b' = \frac{\partial b}{\partial(\beta \lambda)}. \end{aligned} \quad (64)$$

The pseudospin Green's function $K_{\mathbf{q}}^0(\omega_n)$ is constructed of operators of the transverse pseudospin components acting in the rotated reference system ($K_{\mathbf{q}}^0 \sim \langle T\sigma^+\sigma^- \rangle$; $\sigma_i^z = S_i^z \cos \vartheta - S_i^x \sin \vartheta$; $\sigma_i^x = S_i^x \cos \vartheta + S_i^z \sin \vartheta$) and has a pole at λ (the pseudospin reversal energy). The semi-invariant $M_{\mathbf{q}}(\omega_n)$, describing the correlation of longitudinal pseudospin components ($\sim T\langle \sigma^z \sigma^z \rangle^c$), is proportional to $\delta(\omega)$. There is no such contribution in $\Sigma_{\mathbf{q}}(\omega)$ when the Green's functions are calculated using the equation of motion and the decoupling procedure for Zubarev's functions. Thus, the isothermal (χ_T) and isolated (χ_I) susceptibilities do not coincide for PEM.³³ It should be mentioned that a similar result is also obtained in the cases $U \rightarrow \infty^{26}$ and $t_{ij} \rightarrow 0^{25}$

In the GRPA scheme, the summation of loop sequences leads to the expression for pseudospin correlator

$$\langle TS^z S^z \rangle_{\mathbf{q},\omega} = -\frac{\Sigma_{\mathbf{q}}(\omega)}{1 - g^2 \Sigma_{\mathbf{q}}(\omega) \Pi_{\mathbf{q}}(\omega)}, \quad (65)$$

where

$$\Pi_{\mathbf{q}}(\omega) = \frac{2}{N} \sum_{\mathbf{k}} \frac{n(t_{\mathbf{k}}) - n(t_{\mathbf{k}-\mathbf{q}})}{\omega + t_{\mathbf{k}} - t_{\mathbf{k}-\mathbf{q}}} \quad (66)$$

is the standard electron loop contribution.

The condition $\langle TS^z S^z \rangle_{\mathbf{q},\omega=0} \rightarrow \infty$ (which corresponds to divergence of isothermal susceptibility χ_T) indicates an instability with respect to transition into modulated (at $q \neq 0$) or another uniform (at $q = 0$) phase. The thermodynamic parameter values, at which $\chi_T \rightarrow \infty$, determine the spinodal points.

The equation

$$\lambda^2 + g^2 \sin^2 \theta \lambda \langle \sigma^z \rangle_0 \Pi_{\mathbf{q}} + \lambda^2 g^2 \beta b' \cos^2 \theta \Pi_{\mathbf{q}} = 0 \quad (67)$$

was solved together with equation (46) for the mean values η and n written in MFA. The function $\Pi_{\mathbf{q}}$ was calculated numerically by the direct momentum summation for square lattice.

At fixed values of chemical potential, the critical point can be defined as an upper point of spinodal (on the (T, h) plane) with the highest temperature depending on the wave vector \mathbf{q} value. Fig. 25 shows the dependencies of the critical temperature and the corresponding wave vector on the chemical potential in the case $\Omega = 0$ (only positive values of the chemical potential are shown; at $h = g$, the picture is symmetrical with respect to the point $\mu = 0$ which coincides with the centre of the energy band). We can see that the case $\mathbf{q} = (\pi, \pi)$ is realized when $|\mu| \lesssim 0.25$ at chosen parameter values, which means that the system can pass into the phase with doubly modulated lattice period. The case $\mathbf{q} = 0$ (transition into the uniform phase) is realized when $0.85 \lesssim |\mu| \leq 1.25$.^a The system undergoes transition to the incommensurate phase at intermediate values of the chemical potential. The presence of tunneling splitting narrows the interval of values of μ at which the above mentioned transitions take place; at high enough values of Ω , the transition into the chess-board phase occurs only.

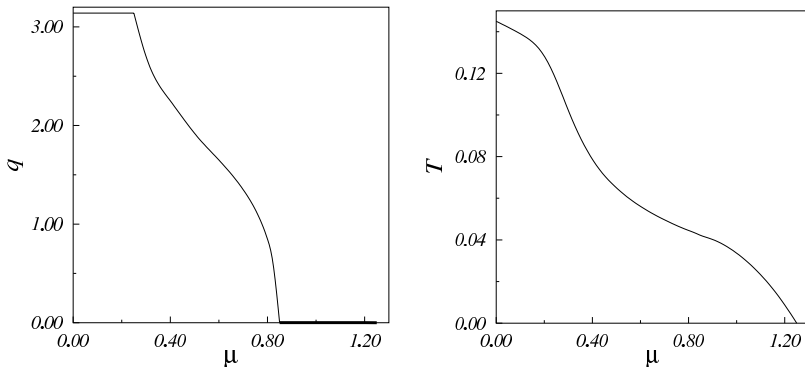


Fig. 25. The dependence of the modulation wave vector $\mathbf{q}=(q,q)$ and the temperature of absolute instability of high-temperature phase on the chemical potential, $\Omega = 0$, $g = 0.5$.

The given results at $\Omega = 0$ generally correspond to the picture of phase transitions in the FK model obtained in DMFT in the case of weak coupling.^{57,63,66} It was shown for FK model that at small values of n the

^a $1.25 = W + g/2$; this value corresponds to the upper edge of the band when $\langle S^z \rangle = \frac{1}{2}$.

phase separation can be realized, while near half-filling of the band the chess-board phase is preferable and, finally, at intermediate values of n the appearance of phase with an incommensurate modulation is possible. The transitions into one or another phase were observed by the divergences of corresponding susceptibilities. It should be mentioned that such a procedure did not enable the authors to reveal the thermodynamically stable states in the regions where the instabilities of the both types (at $\mathbf{q} = 0$ and $\mathbf{q} = (\pi/a, \pi/a, \dots)$) are superimposed; this problem can be solved based on the analysis of the behaviour of the grand canonical potential.

The GRPA scheme used here to investigate the PEM is advantageous in interpreting the dielectric susceptibility divergences due to the explicit dependence of the $\chi_T(\mathbf{q}, 0)$ function on the wave vector. In the DMFT approach at $d \rightarrow \infty$ such a dependence enters only through the function $X(\mathbf{q}) = \frac{1}{d} \sum_{j=1}^d \cos q_j$ that leads to some difficulties in considering the incommensurate ordering. Besides, in Refs. [57,63,66] there was used a regime of a fixed concentration of localized particles; in the PEM this corresponds to the regime $\langle S^z \rangle = \text{const}$. In this case, the authors came to a conclusion that the transition to the chess-board phase at $g < W$ is always continuous and spinodals are the lines of phase transitions.⁶¹ In such a situation the separation into the uniform and modulated phases would be impossible. Contrary to that, by analysing the behaviour of the grand canonical potential we showed that the transition to the chess-board phase can be both of the second order (the spinodals are the phase transition lines) and of the first order (spinodals do not coincide with phase transition lines). Due to the first order phase transition to the chess-board phase, the possibility of the phase separation into the uniform and the chess-board phases in the case of weak coupling was demonstrated. Such a possibility, as was shown in Ref. [64], see also Sec. 3.1.2, exists in the case of large values of coupling constant. It should be mentioned that in Ref. [61] only the possibility of phase separation into different uniform phases was investigated.

Though the phase transitions in the PEM at weak coupling are similar to the transitions revealed in this model in the case of strong interaction, $g \gg W$,^{30,31} the physical mechanisms of transitions are to a greater extent distinct. In the case of strong coupling, the electron spectrum is always split due to the one-site interaction. The mechanism which ensures the advantage of the transition is connected with the different character of the electron spectrum reconstruction in the subbands and with the corresponding redistribution of the electron density of states. At weak coupling, a new phase,

which appears at the transition between uniform phases, is stabilized due to the shift of the electron band as a whole. The phase with a double modulation appears due to energy gain at the splitting of the initial band at the Fermi level (the effect is similar to the Peierls instability at the interaction with phonons). Besides that, the dependencies of the critical temperatures on the coupling constant g are different in the both cases: T_c (or T_c^*) is proportional to g^2 at $g \ll W$, while at $g \gg W$ the critical temperatures decrease ($\sim \frac{1}{g}$) when g increases (such a type of behaviour of T_c^* for the FK model was obtained in Refs. [51,63]).

3.3. Superconductivity in the PEM

Due to the presence of intrinsic dynamics, the PEM at $\Omega \neq 0$ also possesses an instability with respect to transition into superconducting (SC) state. Under certain conditions the transition to SC state will compete with the transition to modulated phase (CDW). Among others, close attention to this problem for an electron system interacting with anharmonic structure units was paid in Ref. [67]. It was shown that, when there is no electron correlation, the transition temperature to CDW, T_p , is higher than that to SC, T_c . The authors, however, considered only the case where the local potential is symmetric and the electron filling is close to a half. The question concerning the appearance of superconductivity for a wider range of the model parameters and electron concentrations has not been examined. It was just the point of investigation performed in Ref. [34] within the GRPA. To examine the possibility of the appearance of SC phase we calculated the static susceptibility χ^{SC} in the superconducting channel. Taking into account the diagrams which correspond to ladder approximation (with the parallel directions of lines of the fermion Green's functions), we obtained the Bethe-Salpeter equation for the superconducting vertex part $\Gamma_{\omega_1, \omega_2}(\mathbf{k}_1, \mathbf{k}_2)$ ³⁴

$$\Gamma = \Gamma^0 + T \sum_{\mathbf{k}_3, \omega_3} \Gamma^0 \chi^0 \Gamma, \quad (68)$$

where $\chi_{\omega_1}^0(\mathbf{k}_1) = \frac{1}{N} G_{\mathbf{k}_1}^0(\omega_1) G_{-\mathbf{k}_1}^0(-\omega_1)$; $\Gamma^0 = g^2 \langle TS^z S^z \rangle_{\mathbf{k}_2 - \mathbf{k}_1, \omega_1 - \omega_2}$ is given by the expression (65). The susceptibility

$$\chi^{SC} = \frac{1}{N} \sum_{\mathbf{k}, \mathbf{q}} \int_0^\beta \langle T_\tau a_{\downarrow \mathbf{k}}(\tau) a_{\uparrow -\mathbf{k}}(\tau) a_{\uparrow -\mathbf{q}}^+ a_{\downarrow \mathbf{q}}^+ \rangle e^{i\omega_n \tau} d\tau \quad (69)$$

is connected with the vertex part Γ in the following way

$$\frac{1}{T}\chi^{SC} = \sum_{\omega, \mathbf{k}} \chi_{\omega}^0(\mathbf{k}) + T \sum_{\mathbf{k}_1, \mathbf{k}_2, \omega_1, \omega_2} \chi_{\omega_1}^0(\mathbf{k}_1) \Gamma_{\omega_1, \omega_2}(\mathbf{k}_1, \mathbf{k}_2) \chi_{\omega_2}^0(\mathbf{k}_2). \quad (70)$$

Both approximations, the ladder one for the $\Gamma_{\omega_1, \omega_2}(\mathbf{k}_1, \mathbf{k}_2)$ vertex construction and the chain (GRPA) one for the construction of $\Gamma_{\omega_1, \omega_2}^0(\mathbf{k}_1, \mathbf{k}_2)$, were employed by analogy with what was done in the $t - J$ model for the SC description.⁶⁸ The mentioned approximations correspond to the known Migdal-Eliashberg (ME) one, which is usually used in considering the electron-phonon systems, particularly in the Holstein model. Considering the phonon frequencies to be small in comparison with the transfer integral,⁶⁹ one gets results in qualitative agreement with the quantum Monte Carlo simulations.²² Since the PEM is similar to the Holstein model, and may be considered as a double-level approximation of the latter one, the ME approximation is expected to be satisfactory in the limits of non-half filling, low temperatures, and small Ω .

A way to find the SC transition temperature is to determine a temperature, at which the susceptibility in the superconducting channel diverges. It corresponds to the condition when the scattering matrix

$$T_{\omega_1 \omega_2}(\mathbf{k}_1, \mathbf{k}_2) = T \chi_{\omega_1}^0(\mathbf{k}_1) \Gamma_{\omega_1 \omega_2}^0(\mathbf{k}_1, \mathbf{k}_2) \quad (71)$$

has an eigenvalue which is equal to unity.^{69,70} In calculations performed in Ref. [34], the approximation $\Gamma^0 \approx -g^2 \Sigma$, similar to the non-renormalized ME approximation in the Holstein model,⁶⁹ was used. This can be done in the high-temperature phase, when the system has not still passed to the CDW state. In such a case the unperturbed vertex part does not depend on the wave vector and thus the unit eigenvalue of the matrix

$$\tilde{T}_{\omega_1 \omega_2} = T \sum_{\mathbf{k}_1} \chi_{\omega_2}^0(\mathbf{k}_1) \Gamma_{\omega_1 \omega_2}^0 \quad (72)$$

should be found at first. Of all the temperatures within the (T, h) plane which satisfy this condition, the highest one is chosen as the critical SC transition temperature.

Numerical calculations performed in Ref. [34] show that the SC transition in the simplified PEM is possible (in the weak coupling case) at the electron concentrations away from half-filling (when the chemical potential is placed near the electron band edges) and outside the region of the above described transitions with the modulation of the electron and pseudospin density (see Fig. 26). Such a picture is similar to that obtained within the DMFT for the Holstein model⁶⁹ (but, in the latter case, the incommensurate

phase does not appear at the intermediate values of μ). This is also consistent with the results obtained by quantum Monte-Carlo simulations.^{22,71} These papers just established that SC could appear at low temperatures; the transition to incommensurate CDW was not studied.

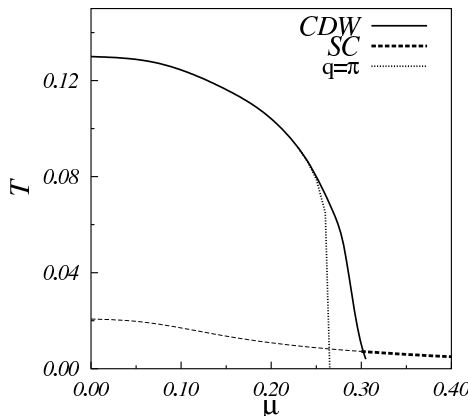


Fig. 26. The temperature of the absolute instability of the high-temperature phase with respect to the transitions to CDW (solid line) and SC (bold dashed line) as functions of the chemical potential, for $\Omega = 0.2$ and $g = 0.5$. Dotted line shows the temperature of the transition to the phase with the modulation wave vector $\mathbf{q} = (\pi, \pi)$.

The estimates performed in Ref. [34] show that at $W \approx 0.5$ eV and $g \approx 0.25$ eV, the maximum value of the SC transition temperature is $T_{max}^{SC} \approx 10 - 40$ K. This agrees with the conclusions obtained for PEM in Ref. [67], where calculations were performed by analogy with the scheme used for the Eliashberg equations in the limit of a weak electron-phonon interaction, provided that the renormalization of the pseudospin excitation energy is neglected. According to the estimations carried out in Ref. [72], if there were no CDW, the SC transition temperature would be $T^{SC} \approx 40$ K at the band filling close to a half.

The question of what occurs in the systems as the tunneling splitting frequency grows further is also of great interest. It was shown in Ref. [32] that, at $\mu = 0$, the critical temperature of transition to the phase with double lattice period modulation, T_c^{CDW} , decreases with the increase in Ω according to the exponential law: $T_c^{CDW} \sim \exp\left(-\frac{\pi\sqrt{\Omega W}}{g}\right)$, see (60). It follows from the analysis of the behaviour of the $\tilde{T}_{\omega_1\omega_2}$ matrix elements³⁴ that the SC transition temperature, T_c^{SC} , changes with Ω in a similar way. In this

case, for $\mu = 0$, $T_c^{\text{SC}}(\Omega \rightarrow \infty) \approx T_c^{\text{CDW}}(\Omega \rightarrow \infty)$. As is seen from Fig. 26, with the increase in $|\mu|$, the CDW transition temperature falls more rapidly than the SC one. Thus, for the non-zero values of the chemical potential, provided that Ω is sufficiently large, the SC transition temperature is expected to be higher than the CDW one, and there will only be the transition to SC. However, as was noted above, to make the correct analysis of the competition between these transitions, the renormalized Γ^0 vertex should be used when solving Eq. (71) and determining T_{SC} . Moreover, when Ω values are sufficiently large, the applicability of the approximation in deriving this equation turns out to be unjustified.

The mechanism that leads in the PEM to SC, which we have considered here, as well as the traditional phonon one, does not result in high values of T_c , and apparently it does not explain the HTSC phenomenon.

4. Thermodynamics of PEM at Finite U Values; the $U \rightarrow \infty$ Limit

The analysis similar to the one given above was performed in Refs. [24–26,73–76] for the PEM with $U \neq 0$. The presence of the electron-electron on-site interaction leads to some differences in the behaviour of the model with respect to the case of FK model (even if $\Omega = 0$). The consideration was based on expansions in terms of electron transfer t_{ij} , as in the strong coupling limit $g \gg W$.

The single-site Hamiltonian

$$H_i = Un_{i\uparrow}n_{i\downarrow} - \mu(n_{i\uparrow} + n_{i\downarrow}) + g(n_{i\uparrow} + n_{i\downarrow})S_i^z - hS_i^z - \Omega S_i^x \quad (73)$$

that includes the U -term can be reduced to the diagonal form using the rotation transformation $|R\rangle = \alpha_{Rr}^{(\varphi_r)}|r\rangle$,^{26,73} where $|R\rangle = |n_{i\uparrow}, n_{i\downarrow}, S_i^z\rangle$ is the single-site basis of states

$$\begin{aligned} |1\rangle &= |0, 0, 1/2\rangle & |\tilde{1}\rangle &= |0, 0, -1/2\rangle \\ |2\rangle &= |1, 1, 1/2\rangle & |\tilde{2}\rangle &= |1, 1, -1/2\rangle \\ |3\rangle &= |0, 1, 1/2\rangle & |\tilde{3}\rangle &= |0, 1, -1/2\rangle \\ |4\rangle &= |1, 0, 1/2\rangle & |\tilde{4}\rangle &= |1, 0, -1/2\rangle, \end{aligned} \quad (74)$$

and

$$\cos \varphi_r = \frac{n_r g - h}{\sqrt{(n_r g - h)^2 + \Omega^2}}. \quad (75)$$

In terms of Hubbard operators $X^{rs} = |r\rangle\langle s|$, acting on the new basis, the transformed Hamiltonian of the model is

$$H = \sum_{ir} \lambda_r X_i^{rr} + \sum_{ij\sigma} t_{ij} a_{i\sigma}^+ a_{j\sigma} \quad (76)$$

with

$$\lambda_{r_i\tilde{r}} = U\delta_{r,r} + E_0 n_r \pm \frac{1}{2}\sqrt{(n_r g - h)^2 + \Omega^2}$$

and

$$a_{i\sigma}^+ = \sum_{mn} A_{mn}^\sigma X_i^{mn}, \quad a_{i\sigma} = \sum_{mn} A_{mn}^\sigma X_i^{nm}. \quad (77)$$

Here $n_1 = 0$, $n_2 = 2$, $n_3 = n_4 = 1$ ($n_{\tilde{r}} = n_r$); expressions for A_{mn}^σ are given in Ref. [26].

The detailed consideration of single-electron spectrum of model (1) at $U \neq 0$ was performed in Refs. [23,74] in the Hubbard-I approximation. The interaction with the anharmonic (pseudospin) mode splits the energy levels of ordinary Hubbard model 0, E_0 and $2E_0 + U$ into sublevels $\lambda_{r,\tilde{r}}$. As a result, each Hubbard single-electron band splits into four subbands. In the independent subband approximation

$$\varepsilon_{rs}(\mathbf{q}) = \lambda_r - \lambda_s + t_{\mathbf{q}} (A_{rs}^\sigma)^2 \langle X^{rr} + X^{ss} \rangle, \quad (78)$$

where $(rs) = (41), (\tilde{4}\tilde{1}), (\tilde{4}1), (4\tilde{1}), (23), (\tilde{2}\tilde{3}), (\tilde{2}3), (2\tilde{3})$ for $\sigma = \uparrow$ and substitution $4 \leftrightarrow 3$ should be done for $\sigma = \downarrow$. The widths and statistical weights of the subbands are determined by parameters A_{rs}^σ . The four lower and four higher bands correspond to the hole and electron pair motion, respectively. Their positions depend on the value of the asymmetry field h (see Fig. 27, where the band edges as functions of h are shown at the fixed value of μ).

Thermodynamics and dielectric properties of PEM with $U \neq 0$ were studied in Refs. [26,75]. Being interested in the problem of lattice instabilities in high- T_c superconductors of YBaCuO - type we calculated the transverse dielectric susceptibility (corresponding to the ε_{zz} component for YBaCuO - structure), using, as above (see Sec. 3.2.3), the expression $P_i = d_s S_i^z + d_e n_i$ for local dipole moment. We can respectively separate ion, electron and mixed components in the total susceptibility

$$\begin{aligned} \chi_{\perp}(\mathbf{q}, \omega_n) &= d_S^2 \chi^{SS}(\mathbf{q}, \omega_n) + d_e^2 \chi^{nn}(\mathbf{q}, \omega_n) \\ &+ d_S d_e (\chi^{Sn}(\mathbf{q}, \omega_n) + \chi^{nS}(\mathbf{q}, \omega_n)), \end{aligned} \quad (79)$$

where $\chi^{AA'} = K^{AA'}$ in the regime $\mu = \text{const}$ (when we fix the value of the chemical potential and permit the charge redistribution between conducting

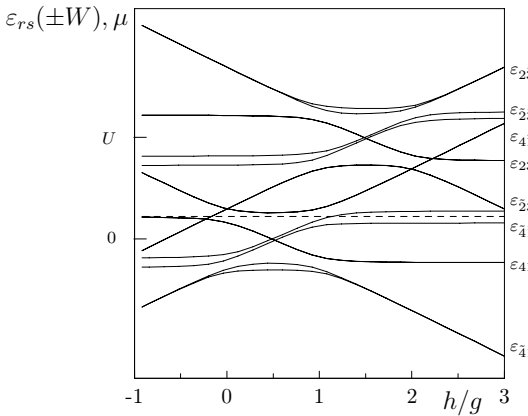


Fig. 27. Single-electron spectrum depending on h/g in the $\mu = \text{const}$ regime; $U = 2.2$, $g = 1$, $h = 0.7$, $\Omega = 0.3$, $W = 0.2$, $\mu = 0.5$.

sheets Cu_2O_2 and other structural elements, having in mind an application of the model to the YBaCuO -type crystals) and

$$\chi^{AA'} = K^{AA'} - \frac{K^{An} K^{nA'}}{K^{nn}} \quad (80)$$

in the regime $n = \text{const}$ (when we fix the electron concentration n in the conducting sheets Cu_2O_2).²⁶ Here $K^{AA'}(\mathbf{q}, \omega_n)$ are Fourier-transforms of semi-invariant Matsubara's Green's functions

$$K_{lm}^{AA'}(\tau - \tau') = \langle T \tilde{A}(\tau) \tilde{A}'_m(\tau') \rangle^c \quad (81)$$

constructed of the operators S_i^z , n_i .

In the case of zero hopping ($t_{ij} = 0$) the exact expressions for correlation functions $\chi^{ss}(\omega_n)$, $\chi^{nn}(\omega_n)$, $\chi^{ns}(\omega_n)$ can be easily obtained.²⁵

For $n = \text{const}$ regime the main contribution into susceptibility is produced by the pseudospin subsystem. The susceptibility

$$X^{ss} \cong \frac{ds^r}{vc} \sum_{r=1}^4 \frac{\Omega^2}{[(n_r g - h)^2 + \Omega^2]^{3/2}} \langle X^{\tilde{r}\tilde{r}} - X^{rr} \rangle \quad (82)$$

as a function of h generally possesses three peaks. The maxima at $h = 0$, g and $2g$ correspond to the points of possible dielectric instabilities (that can appear due to the proximity of corresponding energy subbands). The

intensities of peaks are redistributed with the change of n ; this is illustrated in Fig. 28a for the case $U/W \gg 1$ ($\Omega = 0.3g$, $0 < n < 1$), when only two peaks are present; the first peak disappears at $n \rightarrow 1$ and the second one disappears at $n \rightarrow 0$. The effect remains the same at $t_{ij} \rightarrow 0$.

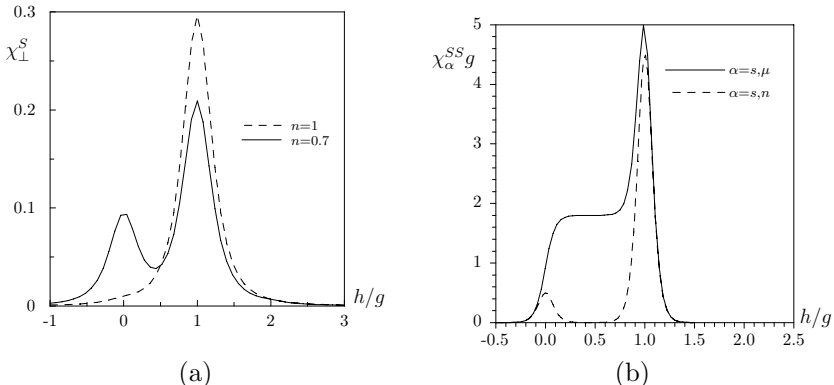


Fig. 28. (a): Dielectric susceptibility as a function of h/g at different electron concentrations; $U = 2.2$, $g = 1$, $h = 0.7$, $\Omega = 0.3$, $W = 0.2$, $d_S = 0.6$. (b): Pseudospin component of susceptibility $\chi_{\alpha}^{ss} g$ vs h/g for $\Omega = 0$ ($\omega_n = 0$, $n = 0.9$, $T/g = 0.05$).

In the $\mu = \text{const}$ regime there are three regions of h values ($h < 0$, $0 < h < g$ and $h > g$) with different field and temperature behaviour of susceptibility (see Fig. 28b). This is a result of the difference in the direction and value of the total effective field $h - n_i g$ acting on the pseudospin at site i when electron occupation on this site changes ($n_i = 0$ or 1), which testifies to a strong correlation between electron and pseudospin subsystem.

The behaviour of transverse dielectric susceptibility χ^{ss} as a function of the field h and temperature becomes more complicated when we take into account the electron transfer. The calculations of components of susceptibility (79) were performed^{25,26} at $t_{ij} \neq 0$ in the particular case of no tunneling splitting in anharmonic potential well ($\Omega = 0$).

Green's functions (81), constructed of the operators

$$n_{i\sigma} = \sum_{r=1}^4 n_r (X_i^{rr} + X_i^{\tilde{r}\tilde{r}}), \quad S_i^z = \frac{1}{2} \sum_{r=1}^4 n_r (X_i^{rr} - X_i^{\tilde{r}\tilde{r}}), \quad (83)$$

can be expressed in terms of functions

$$K_{lm}^{(pq)}(\tau - \tau') = \langle T X_l^{pp}(\tau) X_m^{qq}(\tau') \hat{\sigma}(\beta) \rangle_{oc}. \quad (84)$$

The perturbation theory with respect to electron hopping term t_{ij} and the corresponding diagrammatic technique for Hubbard operators⁵⁸ were used to calculate these functions. The diagrammatic series were summed up in the GRPA, where the sequences of electron “loops” connected by semiinvariants (similarly to the case of the simplified PEM, see Sec. 3.1.1) or by vertices with the three fermion lines (such vertices appear only at $U \neq 0$) are taken into account.

The Fourier transforms $K^{(pr)}(\mathbf{q}, \omega_n)$ of functions (81) can be presented in the form^{25,26}

$$\begin{aligned} K^{pp'}(\omega_n, \mathbf{q}) = & \beta \left\{ \bar{\bar{b}}_{pp'}(\mathbf{q}) + \left[' \Pi(0, \mathbf{q}) \bar{\bar{b}}(\mathbf{q}) \right]_{pp'} + \left[\bar{\bar{b}}(\mathbf{q}) \Pi'(0, \mathbf{q}) \right]_{pp'} \right. \\ & \left. + \left[' \Pi(0, \mathbf{q}) \bar{\bar{b}}(\mathbf{q}) \Pi'(0, \mathbf{q}) \right]_{pp'} \right\} \delta(\omega_n) + \Pi''_{pp'}(\omega_n, \mathbf{q}). \end{aligned} \quad (85)$$

The first term in the right hand side of (85) is the “full” semi-invariant of the second order that satisfies the Dyson-type equation

$$\bar{\bar{b}}_{pq} = \tilde{b}_{pq} + \left(\tilde{b} \Pi \bar{\bar{b}} \right)_{pq}. \quad (86)$$

Here $\tilde{b}_{pq} = \langle X^{pp} X^{qq} \rangle_{0c}$ is the second-order semi-invariant calculated in mean-field approximation and the full “loop” contributions Π , Π' , $'\Pi$, Π'' are determined from the Bethe-Salpeter type equations

$$\begin{aligned} \Pi'' &= \Pi''_0 + \Pi''_0 \Pi' + ' \Pi_0 \Pi'', \\ \Pi' &= \Pi'_0 + \Pi'_0 \Pi' + \Pi_0 \Pi'', \\ ' \Pi &= ' \Pi_0 + ' \Pi_0 ' \Pi + \Pi_0 \Pi'', \\ \Pi &= \Pi_0 + \Pi_0 ' \Pi + \Pi'_0 \Pi. \end{aligned} \quad (87)$$

Zero-order polarization loops Π_0 , Π'_0 , $'\Pi_0$, Π''_0 are constructed of the single-electron Green’s functions which are calculated in the Hubbard-I approximation (corresponding to the summation of chain fragments of diagrams).^{25,26} Loops Π'_0 , $'\Pi_0$, Π''_0 are determined only by intraband transitions whereas loop Π_0 is determined by the interband transitions as well

$$\Pi_0(mr, np) = \frac{1}{N} \sum_{\mathbf{k}} t_{\mathbf{k}} t_{\mathbf{k}+\mathbf{q}} \frac{n_+[\varepsilon_{mr}(\mathbf{k})] - n_+[\varepsilon_{np}(\mathbf{k}+\mathbf{q})]}{i\omega_n + \varepsilon_{mr}(\mathbf{k}) - \varepsilon_{np}(\mathbf{k}+\mathbf{q})}. \quad (88)$$

where $\varepsilon_{mr}(\mathbf{k})$ are determined in (78) and $n_+(\lambda)$ is Fermi distribution.

Numerical calculations of the static dielectric susceptibility $\chi_{\perp}(\mathbf{q}, 0)$ performed in Refs. [25,75] along the $(0, 0) \div (\pi, \pi)$ line in the 2D Brilloine zone, revealed that, similarly to the above considered case $U = 0$, the essential

feature of the model is the presence of divergences on the temperature dependencies of functions χ_n^{ss} and χ_μ^{ss} (Fig. 29). They appear in a certain range of the model parameter values. For $h > 0$ and $h < g$ such divergen-

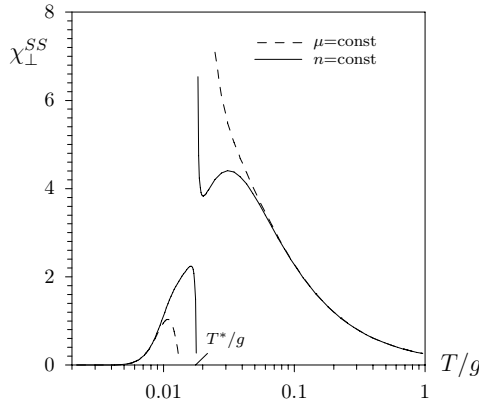


Fig. 29. Temperature dependence of χ^{ss} at $n = 0.95$ and $\mathbf{q} = 0$ ($U \rightarrow \infty$, $h/g = 1.05$, $W/g = 0.2$).

cies exist only at $\mathbf{q} = 0$ (Γ -point) and can be treated as the manifestation of the dielectric type instabilities which appear in the pseudospin subsystem (i.e., the system of anharmonic oscillators) under the influence of the effective interactions. As in the case of a simplified model, it means that the system can transform to another uniform phase. The corresponding phase diagram T^* vs n is shown in Fig. 30(a), where the lines limiting the stability region are plotted. For $0 < h < g$, besides the dielectric instability at Γ -point at $n \gtrsim 0$, the instability at $\mathbf{q} = (\frac{\pi}{a}, \frac{\pi}{a})$ (M -point) with respect to the charge ordering (double modulation) occurs (Fig. 30(b)). Such an instability is realized when the electron band (that corresponds to the lower Hubbard subband at $U \rightarrow \infty$) is nearly fully occupied.

The above mentioned divergences on the temperature dependencies and an increase of the dielectric susceptibility which takes place in the vicinity of $h = 0$ and $h = g$ values (for $U \rightarrow \infty$, $n < 1$) are connected, first of all, with the polarization contributions Π_0 from the electron transitions between hole subbands ($\tilde{4}\tilde{1}$) and ($\tilde{4}1$) (or ($\tilde{4}\tilde{1}$) and ($4\tilde{1}$)). Just for $h \sim 0$ and $h \sim g$ these subbands come nearer to each other.

It should be noted that the results presented here for dielectric response

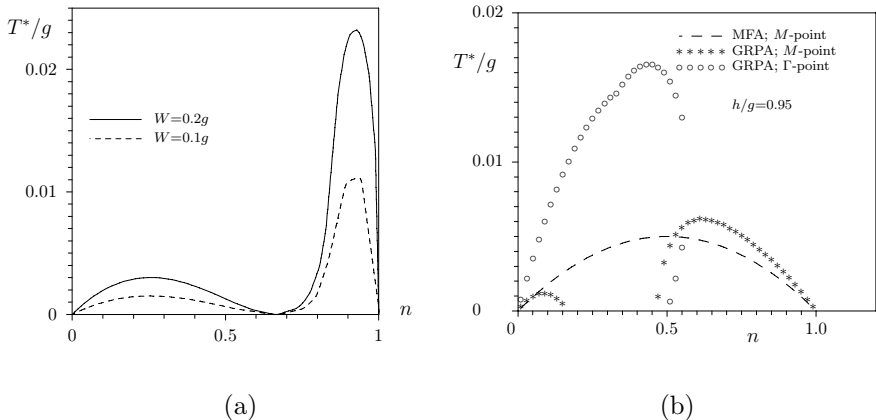


Fig. 30. Dependence of the instability temperature T^* on the electron concentration n in the cases $h > g$ and $0 < h < g$. (a) $U \rightarrow \infty$, $\Omega = 0$, $n/g = 1.05$ (dielectric instability, $\mathbf{q} = 0$). (b) $U \rightarrow \infty$, $\Omega = 0$, $n/g = 0.95$ ($\circ \circ \circ$ —dielectric instability, $\mathbf{q} = 0$; $\ast \ast \ast$ —instability with respect to CDW ordering, $\mathbf{q} = (\pi, \pi)$; dashed line shows the MFA results).

of PEM in the $U \rightarrow \infty$ limit were used in Ref. [25] in describing the dielectric anomalies which have been observed in the high- T_c superconductors of the YBaCuO type at an early stage of investigations. In particular, the temperature dependence of χ_n^{ss} given in Fig. 29 was related to the one obtained experimentally for $\text{YBa}_2\text{Cu}_3\text{O}_{7-\delta}$ ⁹ where the similar behaviour of dielectric permittivity ε_c was found at the temperature near (and above) the point of the superconducting phase transition.

An interesting feature of the model at large values of U is the possibility of change of the electron concentration n under the influence of h . Such an effect can take place in the $\mu = \text{const}$ regime; this becomes possible when the chemical potential leaves (or enters) the energy subband²⁴ (Figs. 27 and 31(a)). The change of n is accompanied by the corresponding change of the pseudospin mean value (Fig. 31(b)). In the case of YBaCuO structure, this means that if μ moves inside the subband with the change of e.g. external electric field, then the electron concentration (average occupancy of states) in Cu_2O_2 layers changes. This causes a redistribution of O_4 ions in their equilibrium positions. All this may correspond to the so-called electric-field effect observed in HTSC compounds (see, for example, Ref. [77]).

The obtained results show that in the $U \rightarrow \infty$ limit the PEM also exhibits a tendency to transform into another uniform or doubly modulated phase at low temperatures. It resembles the behaviour of the FK model in

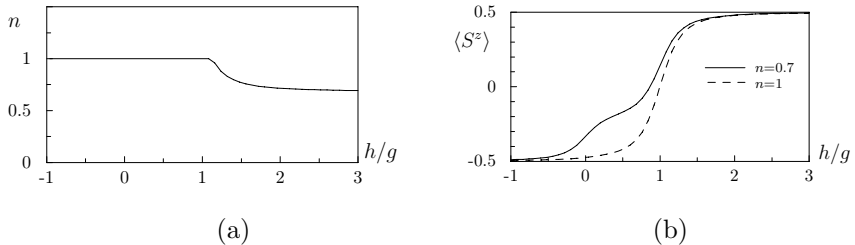


Fig. 31. Mean electron concentration n (a) and pseudospin mean value (b) as a function of h/g in the $\mu = \text{const}$ regime.

the strong coupling case.⁵⁷ The plots in Fig. 30 are given without the effect of phase separation. When the segregation on the regions with different n values takes place, the corresponding uniform phases or both the uniform and the modulated ones will coexist.

5. Two-Sublattice Pseudospin-Electron Model

Two-sublattice PEM^{35–38,76} appeared as a generalization of the usual PEM with the aim of more realistic description of the anharmonic subsystem of the apex oxygen ions in the YBaCaO type structures. In this case the pseudospin energy in the internal field is of the form $h \sum_i (S_{i1}^z - S_{i2}^z)$ that is the reflection of the mirror symmetry of the problem. Hamiltonian of the model is of the form³⁵

$$\begin{aligned}
 \hat{H} &= H_e + H_s + h_{l-s} + H_{s-s}, \\
 H &= H_e + H_s + H_{e-s} + H_{s-s}, \\
 H_e &= -\mu \sum_{n,s} (n_{n1}^s + n_{n2}^s) + U \sum_n (n_{n1}^\uparrow n_{n1}^\downarrow + n_{n2}^\uparrow n_{n2}^\downarrow) \\
 &\quad + \sum_{ij} \sum_{s\alpha} t_{ij} a_{is\alpha}^+ a_{js\alpha}, \\
 H_s &= -h \sum_n (S_{n1}^z - S_{n2}^z) - \Omega \sum_n (S_{n1}^x + S_{n2}^x), \\
 H_{e-s} &= g \sum_{n,s} (n_{n1}^s S_{n1}^z - n_{n2}^s S_{n2}^z), \\
 H_{s-s} &= -J \sum_n S_{n1}^z S_{n2}^z - \frac{1}{2} \sum_{n,n'} \sum_{\alpha,\beta} J_{nn'}^{\alpha\beta} S_{n\alpha}^z S_{n\beta}^z.
 \end{aligned} \tag{89}$$

Here, $n_{n\alpha}^s$ and $S_{n\alpha}^z$ are operators of the electron occupation number ($S = \uparrow, \downarrow$) and pseudospin, respectively, in the n -th unit cell ($\alpha=1,2$ cor-

responds to the two apex oxygen O₄ in the cell). Additionally to the term H_{e-s} describing the interaction between electrons and pseudospins, the direct interaction H_{s-s} between pseudospins is included; the $JS_{n1}^z S_{n2}^z$ interaction within the one-cell clusters is separated. Hamiltonian (89) is invariant with respect to the particle-hole transformation: $n_{n\alpha}^s \rightarrow 1 - n_{n\alpha}^s$, $h \rightarrow 2g - h$, $\mu \rightarrow -\mu - U$.

Thermodynamics of the system described by Hamiltonian (89) without a term related to the electron transfer was studied in Refs. [35,36]. The mean-field approximation combined with the exact treatment of interactions within the one-cell clusters was used. For this purpose the single-clusters basis of states $|R_i\rangle \equiv |n_{i1}^\uparrow, n_{i1}^\downarrow, n_{i2}^\uparrow, n_{i2}^\downarrow\rangle \oplus |S_{i1}^z, S_{i2}^z\rangle$, which consist of sixty-four state vectors, was introduced. In such a way the grand canonical potential Φ_{MF} and the mean values $\langle S_\alpha^z \rangle$ and $\sum_s \sum_{\alpha=1}^2 \langle n_{n\alpha}^s \rangle = n$ were calculated.³⁵

Instead of the $\langle S_\alpha^z \rangle$ parameters, we can use their linear combinations: $\eta = \langle S_1^z + S_2^z \rangle$ (the order parameter for the ordered ferroelectric-like phase) and $\xi = \langle S_1^z - S_2^z \rangle$ (the parameter which is responsible for the in-phase reorientation of both pseudospins in the unit cell). In the regime $\mu = \text{const}$ we obtain the equations for η and ξ from the condition of the minimum of the grand canonical potential Φ_{MF}

$$\begin{cases} \left(\frac{\partial \Phi_{MF}}{\partial \eta} \right)_\mu = 0, \\ \left(\frac{\partial \Phi_{MF}}{\partial \xi} \right)_\mu = 0. \end{cases} \quad (90)$$

$$\begin{aligned} \Phi_{MF} = & \frac{1}{4} \{ (J_{11} + J_{12})\eta^2 + (J_{11} - J_{12})\xi^2 \} \\ & - T \ln \left[2 \left\{ e^{\beta \frac{J}{4}} \cosh \beta \frac{(J_{11} + J_{12})\eta}{2} + e^{-\beta \frac{J}{4}} \cosh \beta \left(h + \frac{(J_{11} - J_{12})\xi}{2} \right) \right\} \right. \\ & + 8e^{\beta\mu} \left\{ e^{\beta \frac{J}{4}} \cosh \beta \frac{(J_{11} + J_{12})\eta}{2} \cosh \beta \frac{g}{2} + e^{-\beta \frac{J}{4}} \cosh \beta \left(h \right. \right. \\ & \left. \left. + \frac{(J_{11} - J_{12})\xi}{2} - \frac{g}{2} \right) \right\} + 8e^{2\beta\mu} \left\{ e^{\beta \frac{J}{4}} \cosh \beta \frac{(J_{11} + J_{12})\eta}{2} \right. \\ & \left. \left. + e^{-\beta \frac{J}{4}} \cosh \beta \left(h + \frac{(J_{11} - J_{12})\xi}{2} - g \right) \right\} \right]. \end{aligned} \quad (91)$$

In the case $n = \text{const}$ the condition of the minimum value of the free energy $F_{MF} = \Phi_{MF} + \mu n$, supplemented by the equation for chemical potential

$$-\frac{\partial \Phi_{MF}}{\partial \mu} = n,$$

was used to determine the thermodynamically stable equilibrium states.

When the set of equations (90) has a non-zero solution for η and the corresponding thermodynamic potential has a minimum, then our system is in the polar (ferroelectric) phase. The obtained phase diagrams in the $\mu = \text{const}$ case^{35,36} are shown in Fig. 32 (all parameters are normalized here by $J_{11} + J_{12} > 0$). One can see that at $\frac{J_{11}-J_{12}}{J_{11}+J_{12}} = -1$ (the case of pseudospin-pseudospin interaction between different sublattices only) the phase transition into ferroelectric phase is of the second order. The presence of the intra-sublattice interaction leads to the possibility of change of the phase transition order and the appearance of tricritical points. An increase of the $\frac{J_{11}-J_{12}}{J_{11}+J_{12}}$ parameter causes the narrowing of the ferroelectric region; its width is also proportional to J . At $J = 0$, $J_{12} = 0$ the model transforms into the one-sublattice PEM; the ferroelectric phase disappears and we have the first-order phase transition with zero value of the order parameter η and a sharp change of parameter $\xi = \langle S_1^z - S_2^z \rangle$.

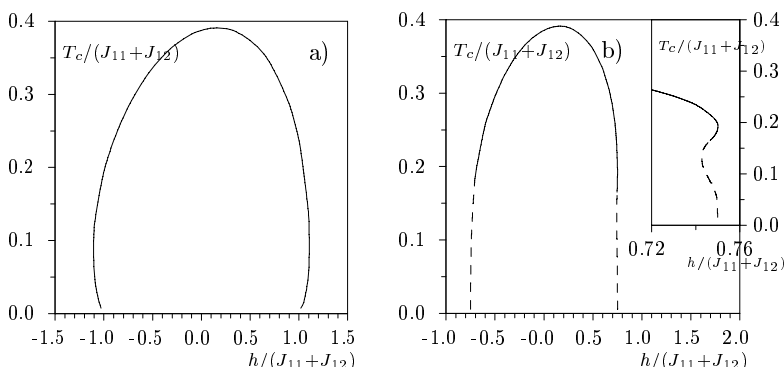


Fig. 32. $(T_c - h)$ phase diagrams at different values of parameter $J_{11} - J_{12}$ in the regime $\mu = \text{const}$: a) $\frac{J_{11}-J_{12}}{J_{11}+J_{12}} = -1$, b) $\frac{J_{11}-J_{12}}{J_{11}+J_{12}} = 0$. Other parameters: $J/(J_{11} + J_{12}) = -1$, $g/(J_{11} + J_{12}) = 1$, $\mu/(J_{11} + J_{12}) = -1$. The phase transitions can be of the second (solid lines) or of the first order (dotted lines).

In the $n = \text{const}$ regime, the region of h values at which the ferroelectric phase exists becomes broader. The corresponding phase diagrams are shown in Fig. 33 at different values of long range interaction $J_{\alpha\beta} = \sum_{n'} J_{nn'}^{\alpha\beta}$ and fixed concentration $n = 0.4$.

For comparison, there are also shown the phase transition lines obtained in the so-called one loop-approximation (in which the higher order corrections to the MFA described by two-tailed diagrams³⁶ are taken into ac-

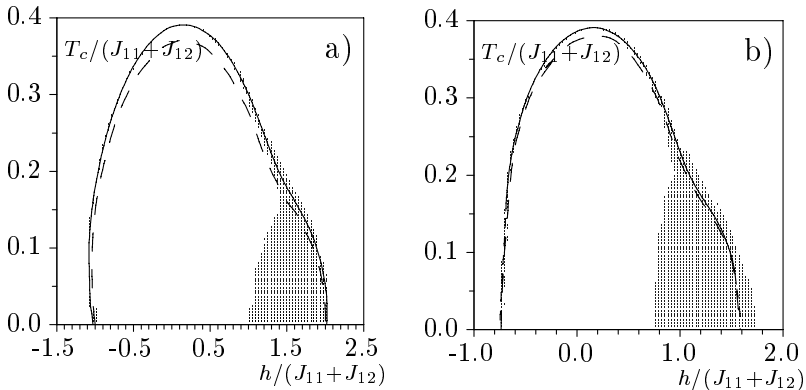


Fig. 33. The h dependence of the temperature of ferroelectric phase transition T_c at different values of parameter $J_{11} - J_{12}$ in the regime $n = \text{const}$: a) $(J_{11} - J_{12})/(J_{11} + J_{12}) = -1$, b) $(J_{11} - J_{12})/(J_{11} + J_{12}) = 0$. Other parameters: $J/(J_{11} + J_{12}) = 1$, $g/(J_{11} + J_{12}) = 1$, $n = 0.4$. Solid lines and dashed lines represent the second order and the first order phase transitions, respectively. The widely spaced dashed line corresponds to a one-loop approximation. Dots represent a separation area.

count). In the areas marked by points, the system is separated into two regions with concentrations n_1 and n_2 ($n_1 < n < n_2$). Also, one can notice that phase separation takes place near the border of stability region of two phases (the ordered phase with nonzero polarization and the disordered one). That is why the ordered phase spreads wider and extends up to the edge of the separated area. Fig. 34 illustrates such a behaviour. Here the dashed lines represent the region of ferroelectric type instabilities. These lines would separate the ferroelectric phase if there were no phase separation. Figure 34(b) also shows that at a fixed value of asymmetry parameter h at concentration $n < 0.75$ (at low temperature), the ordered phase is possible only due to the phase separation.

Now, let us focus briefly on the effect of electron transfer. As above, we restrict ourselves to the limit $U \rightarrow \infty$. The case is considered, when the chemical potential is placed in the region of energy subbands ($\alpha = 1, 2$)

$$\begin{aligned}\varepsilon_\alpha^{31}(\mathbf{k}) &= \varepsilon_\alpha^{41}(\mathbf{k}) = -(-1)^\alpha \frac{g}{2} + t_{\mathbf{k}} \langle X_\alpha^{44} + X_\alpha^{11} \rangle_0, \\ \varepsilon_\alpha^{\tilde{3}\tilde{1}}(\mathbf{k}) &= \varepsilon_\alpha^{\tilde{4}\tilde{1}}(\mathbf{k}) = (-1)^\alpha \frac{g}{2} + t_{\mathbf{k}} \langle X_\alpha^{\tilde{4}\tilde{4}} + X_\alpha^{\tilde{1}\tilde{1}} \rangle_0\end{aligned}\quad (92)$$

separated by the gap equal to g . The Hubbard-I approximation in which the expressions (92) are given here, was improved in Ref. [38] by the mean-field corrections (being of the form of the loop-like inclusions) to the elec-

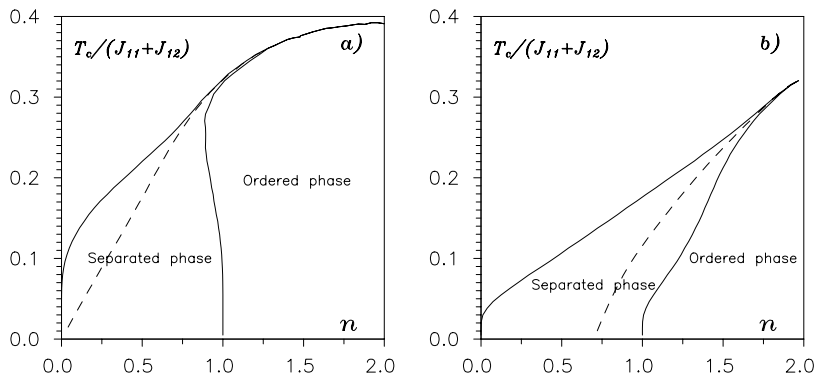


Fig. 34. Phase ($T - n$) diagram in a mean field approximation. The phase separation region is limited by solid lines. The dashed lines point to the region of ferroelectric instabilities. Parameters: $(J_{11} - J_{12})/(J_{11} + J_{12}) = 1$, $J/(J_{11} + J_{12}) = g/(J_{11} + J_{12}) = 1$; a) $h/(J_{11} + J_{12}) = 1$, b) $h/(J_{11} + J_{12}) = 1.35$.

tron Green's functions. Thus, renormalization of spectrum due to the shift of subbands dependent on electron concentration was taken into account. Besides, the mean values of Hubbard operators in (92) were determined self-consistently; the free energy of the pseudospin-electron systems was calculated in the above described GRPA approach. The pseudospin part of the two-sublattice Hamiltonian was taken in the MFA.

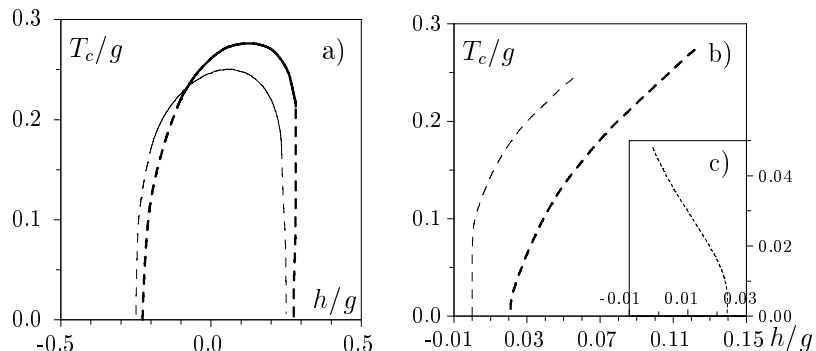


Fig. 35. Dependence of temperature of the phase transition T_c on the parameter h at different values of interaction parameters J_{11} and J_{12} in the regime $\mu = \text{const} = -g$. Thick lines correspond to the case $t_{ij}/g = 0.2$; thin lines correspond to the case $t_{ij} = 0$. a) $J_{11} = J_{12} = g/2$, b) $J_{11} = g, J_{12} = 0$. c) $J_{11} = J_{12} = 0, t_{ij}/g = 0.2$. Phase transitions are either of the second order (solid lines) or of the first order (dashed lines).

Figure 35 illustrates the effect of electron subsystems on the shape of the phase diagram. With respect to the standard Mitsui model (which corresponds to the $g = 0$ and $t_{ij} = 0$ limit), the phase boundary becomes asymmetric and the region of the ferroelectric phase existence is shifted to the higher values of h . As it has already been noted, at $J_{12} = 0$, ferroelectric phase does not exist and only a discontinuous change of ξ on the transition line takes place. Such a transition also remains in the case when $J_{11} = 0$ and only the indirect interaction via electron subsystem is present.

The changes in electron spectrum (see Refs. [37,38]) are demonstrated in Fig. 36(b). In the case shown in Fig. 36, when at $n = \text{const}$ the separation into ferroelectric and nonpolar phases takes place, the $\eta(n)$ and $\mu(n)$ dependencies indicate that the ferroelectric phase appeared before the separation. This is also supported by the presence of concavity in the free energy (dashed tangent lines in Fig. 36(c) link the points with concentration values n_1, n_2 and n_3, n_4 on which the separation takes place). Hence, there is a separation into paraelectric and ferroelectric phases at concentrations $n_1 < n < n_2$ and $n_3 < n < n_4$. The pure ferroelectric phase exists in the concentration range $n_2 < n < n_3$. The separation area in the (h, n) plane changes its shape depending on the t_{ij} value. In general, the electron transfer narrows the separation region.³⁷ The reverse effect also takes place: the electron spectrum is modified by a phase separation being sensitive to concentration value.

One can relate the phase transitions and ferroelectric type instabilities described by the herein considered two-sublattice PEM to the observed dielectric and thermodynamic properties of the YBaCuO-type superconducting crystals. In some experiments, $\text{YBa}_2\text{Cu}_3\text{O}_{7-\delta}$ was found to be both pyroelectric and piezoelectric, implying the existence of macroscopic polarization directed along the c-axis.⁷⁸ The possibility of the existence of the ferroelectric-like phase was not, nevertheless, unambiguously confirmed. In the two- sublattice PEM the ordered polar phase is present in a rather restricted region of the model parameter values, where the ground state is degenerated; for example, its width along the h -axis is determined by the interaction constant between the pseudospins (describing apical O_4 ions) within the unit cell cluster. In this connection, it should be mentioned that presence of the oxygen vacancies in the chain element of structure at $\delta > 1$ effectively influences the value of field h .⁷⁹ In its turn, instability with respect to the polar phase appearance can show up only at a certain nonstoichiometry (at certain values of parameter δ).

The phase separation in the two-sublattice case is also related to the real

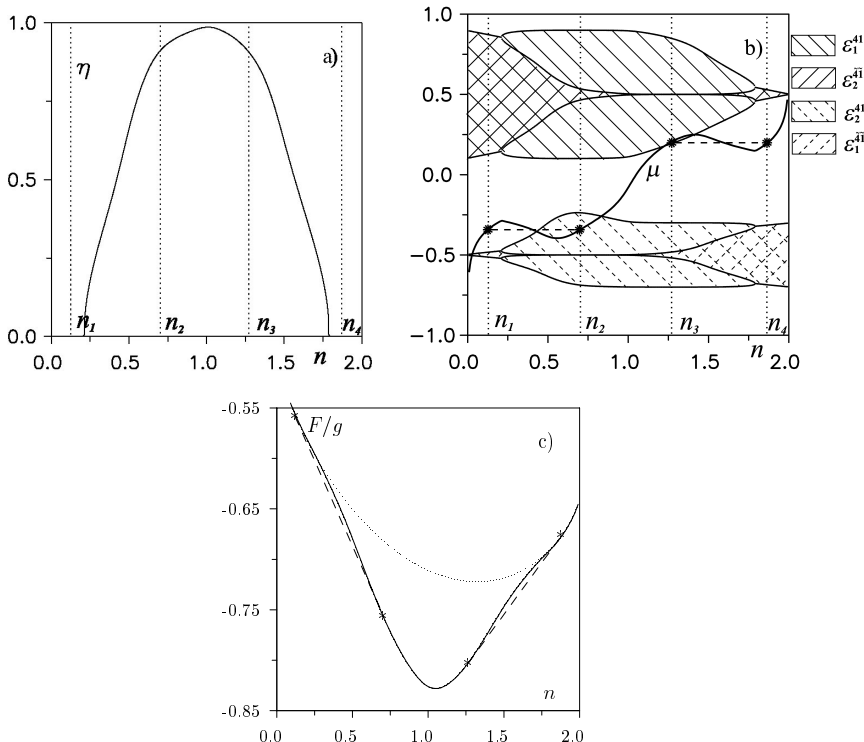


Fig. 36. Dependence of the order parameter η (a), band spectrum (b), and free energy (c) on electron concentration. The parameter values are: $J_{11} = J_{12} = g/2$, $T/g = 0.1$, $t_{ij}/g = 0.1$, $h/g = 0.5$.

structure of the $\text{YBa}_2\text{Cu}_3\text{O}_{7-\delta}$ crystal. Besides the question of microscopic nature of the so-called “stripe phases” there is a problem of the genesis of structural inhomogeneities in a single crystal of the YBaCuO type observed in the experiments using Raman spectroscopy⁶ and mesoscopic structural investigations.⁸⁰ The results obtained within the model approach show the possibility of the Mitsui - type (due to both direct and indirect, via conducting electrons, interactions between anharmonic structure units) mechanism of the mentioned instabilities.

6. Conclusions

The present investigations of thermodynamics and energy spectrum of the PEM show a variety of phases and phase transitions. Depending on the thermodynamic equilibrium regimes, they manifest themselves as (i) transi-

tions between different uniform phases, or between uniform and modulated phases, with the commensurate or incommensurate period of modulation (in the $\mu = \text{const}$ regime) or as (*ii*) transitions into phase separated states (in the $n = \text{const}$ regime). The latter takes place when at $\mu = \text{const}$, the corresponding phase transition is of the first order. Such phase transitions can be realized at the change of temperature T , field h , chemical potential μ (in the case (*i*)) and other parameters of the model. The corresponding phase diagrams are built in case of strong or weak coupling ($g \gg W$ and $g < W$, respectively).

A microscopic reason for phase transitions in standard PEM (without a direct pseudospin-pseudospin interaction) is related to the indirect effective coupling between pseudospins arising due to electron transfer and possessing a dynamic character. The form of such coupling depends on the electron concentration, temperature and the model parameter values. Consequently, the modulated phase appears at intermediate values of μ (this corresponds to the electron occupation near half-filling) both at strong and at weak coupling. However, the formation mechanisms of the effective interaction are different in these cases.

The two-sublattice PEM is a special case, close to the real HTSC systems of the YBaCuO type. The phase transitions described here, connected with the appearance of the ferroelectric state or with the jump-like change of the mutual orientation of pseudospins in sublattices, can have a relation to the segregation or bistability phenomena as well as to the development of ferroelectric-type instabilities in the mentioned systems.

The analysis carried out in the weak coupling case elucidates the role of the transverse field Ω (having a meaning of the tunneling-like splitting parameter) in the obtained picture of phase transitions. As a whole, a topology of the phase diagrams does not change at $\Omega \neq 0$ in comparison with the case $\Omega = 0$. The critical temperatures (including T_{SC}) decrease with Ω . In the case of DOS with logarithmic singularity (at dimensionality $d = 2$) a peculiar effect is revealed: the critical temperature remains finite at any large values of Ω (tending to zero at $\Omega \rightarrow \infty$, exclusively). This is the difference with respect to the behaviour of the systems with direct interaction (e.g., Ising model with transverse field). The important property is that at $\Omega \neq 0$ the superconducting phase can appear in the PEM. Such a phase competes with the modulated one and is stable at the electron occupancy near the upper (or lower) edge of the electron band.

As is seen from the results obtained in DMFT for the simplified model, the structure of electron spectrum of the PEM is different in cases $g \gg W$

and $g < W$: the split subbands due to interaction (even at $U = 0$) or a single band, respectively. The similar spectrum is obtained in the approximations, based on the Hubbard-I scheme (e.g. GRPA) in the first case or the Hartree-Fock approach in the second one. As was shown by Zeyher, Kulić, and Gehlhoff,^{81–83} GRPA keeps in a systematic way all terms of the leading order of a so-called $1/N$ expansion, where N is the local spin component number on a lattice site. Though such approximations do not adequately reproduce all the features of spectrum, the obtained phase diagrams are in a good agreement with the ones constructed in DMFT. An interesting feature of spectrum is that there exists a critical value of g : at $g > g_c$ a gap appears (in the case of simplified PEM) and a metal-insulator type transition takes place.

Pseudospin-electron model (PEM) can be considered as a generalization of the Falicov-Kimball (FK) model to the case of different thermodynamic equilibrium regimes as well as an extension of the latter model due to the inclusion of the pseudospin dynamics and the Hubbard type correlations. The PEM possesses a similar variety of phase transitions but there are differences in the conditions of their realization and in the criteria of the appearance of different phases. In the above considered cases such differences are discussed and a comparison with the results for the FK model is made.

From the point of view of theoretical studies, the investigations of the PEM are far from complete. Another interesting problem is connected with the thermodynamics of the PEM with electron transfer at $U \neq 0$ and $\Omega \neq 0$. The investigations performed revealed only the existence of instabilities connected with certain values of the wave vector \mathbf{q} but the phase diagrams determining the regions of existence of different phases have not been built so far. The intermediate coupling case ($g \sim W$), that was not adequately investigated even for the simplified PEM, calls for more detailed consideration. An important point is to complete the study of the collective excitation spectrum (connected with pseudospin reorientation, electron transitions and polaron effect) and the dynamic susceptibility. Among the possible generalizations of the model, one can note an extension to the cases with the asymmetric electron transfer (in the spirit of the asymmetric Hubbard model) and with pseudospin $S > 1/2$. They appear to be quite promising in connection with investigations of the ionic transport based on the lattice models as well as in the study of the ion intercalation processes (see e.g. Ref. 84 for a recent development in this field).

Acknowledgements

The author is grateful to A. Shvaika and T. Mysakovych for reading the manuscript and technical help.

References

1. K. A. Müller, Z. Phys. B **80**, 193 (1990).
2. S. Conradson and I. D. Raistrick, Science **243**, 1340 (1989).
3. J. Mustre de Leon, S. D. Conradson, L. Batistic, A. R. Bishop, I. D. Raistrick, M. C. Aronson, and F. H. Garzon, Phys. Rev. B **45**, 2447 (1992).
4. D. Mihajlovic and C. M. Foster, Solid State Commun. **74**, 753 (1990).
5. G. Ruani, C. Taliami, M. Muccini, K. Conder, E. Kaldis, H. Keller, D. Zech, and K. A. Müller, Physica C **226**, 101 (1994).
6. M. N. Iliev, V. G. Hadjiev, and V. G. Ivanov, Journ. Raman Spectr. **27**, 333 (1996).
7. N. Poulakis, D. Palles, E. Liarokapis, K. Conder, E. Kaldis, and K. A. Müller, Phys. Rev. B **53**, R534 (1996).
8. L. R. Testardi, W. G. Moulton, H. Matials, H. K. Ng, and C. M. Rey, Phys. Rev. B **37**, 2324 (1988).
9. V. Müller, C. Hucho, and D. Maurer, Ferroelectrics **130**, 45 (1992).
10. J. Mustre de Leon, I. Batistic, A. R. Bishop, S. D. Conradson, and S. A. Trugman, Phys. Rev. Lett. **68**, 3236 (1992).
11. J. Ranninger and U. Thibblin, Phys. Rev. B **45**, 7730 (1992).
12. A. P. Saiko and V. E. Gusakov, JETP **108**, 757 (1995).
13. P. Schweiss, W. Reichardt, M. Braden, G. Collin, G. Heger, H. Claus, and A. Erb, Phys. Rev. B **49**, 1387 (1994).
14. C. Ambrosch-Draxl and P. Knoll Physica B **194-196**, 2091 (1994).
15. J. Röhler, in: *Materials and Crystallographic Aspects of HT_c-superconductivity*, edited by E. Kaldis (Kluwer, Dordrecht, 1994), p. 353.
16. R. J. Cava and A. W. Hewat, Physica C **C165**, 419 (1990).
17. J. R. Hardy and J. W. Flocken, Phys. Rev. Lett. **60**, 2191 (1988).
18. A. Bussman-Holder, A. Simon, and H. Büttner, Phys. Rev. B **39**, 207 (1989).
19. N. M. Plakida, Physica Scripta **29**, 77 (1989).
20. J. E. Hirsch and S. Tang, Phys. Rev. B **40**, 2179 (1989).
21. N. M. Plakida and V. S. Udoenko, Mod. Phys. Lett. **B6**, 541 (1992).
22. M. Frick, W. van der Linden, I. Morgenstern, and H. Raedt, Z. Phys. B **81**, 327 (1990).
23. I. V. Stasyuk, A. M. Shvaika, and E. Schachinger, Physica C **213**, 57 (1993).
24. I. V. Stasyuk and A. M. Shvaika, Fiz. Nizk. Temp. **22**, 535 (1996).
25. I. V. Stasyuk and A. M. Shvaika, Ferroelectrics **192**, 1 (1997).
26. I. V. Stasyuk and A. M. Shvaika, Condens. Matter Phys. **3**, 134 (1994).
27. V. Koerting, Q. Yuan, P.J. Hirschfeld, T. Kopp, J. Mannhart, Phys. Rev. B **71**, 104510 (2005).
28. N. Pavlenko, T. Kopp, Phys. Rev. B **72**, 174516 (2005).
29. I. V. Stasyuk and A. M. Shvaika, Journ. Phys. Studies, **3**, 177 (1999).

30. I. V. Stasyuk, A. M. Shvaika, and K. V. Tabunshchik, Condens. Matter Phys. **2**, 109 (1999).
31. I. V. Stasyuk, A. M. Shvaika, and K. V. Tabunshchik, Ukrainian Journ. of Phys. **45**, 520 (2000).
32. I. V. Stasyuk and T. S. Mysakovich, Journ. Phys. Studies **5**, 268 (2001).
33. I. V. Stasyuk and T. S. Mysakovich, Condens. Matter Phys. **5**, 473 (2002).
34. T. S. Mysakovich and I. V. Stasyuk, Ukrainian Journ. of Phys. **49**, 607 (2004).
35. O. D. Danyliv and I. V. Stasyuk, Condens. Matter Phys. **7**, 163 (1996).
36. O. D. Danyliv, Physica C **309**, 303 (1998).
37. O. D. Danyliv and I. V. Stasyuk, Condens. Matter Phys. **5**, 523 (2002).
38. I. V. Stasyuk and O. D. Danyliv, Phys. Stat. Sol. **219**, 229 (2000).
39. Yu. A. Izumov and B. M. Letfulov, J. Phys.: Cond. Matter **2**, 8905 (1990).
40. I. V. Stasyuk and T. S. Mysakovich, Journ. Phys. Studies **3**, 344 (1999).
41. I. V. Stasyuk and T. S. Mysakovich, Physica C **341-348**, 171 (2000).
42. T. S. Mysakovich and I. V. Stasyuk, Condens. Matter Phys. **7**, 347 (2004).
43. J. K. Freericks and V. Zlatic, Rev. Mod. Phys. **75**, 1333 (2003).
44. I. V. Stasyuk, R. Ya. Stetsiv, and Yu. V. Sizonenko, Cond. Matter. Phys. **5**, 685 (2002).
45. I. V. Stasyuk and Yu. I. Dublenych, Phys. Rev. B **72**, 224209 (2005).
46. W. Wagemaker, G. J. Kearby, A. A. van Well, H. Mutka, and F. M. Mulder, J. Am. Chem. Soc. **125**, 840 (2003).
47. V. Koerting, Qingshan Yuan, P. J. Hirschfeld, T. Kopp, and J. Mannhart, Phys. Rev. B **71**, 104510 (2005).
48. W. Metzner and D. Vollhardt, Phys. Rev. Lett. **62**, 324 (1989).
49. A. Georges, G. Kotliar, W. Krauth, and M. J. Rosenberg, Rev. Mod. Phys. **68**, 13 (1996).
50. W. Metzner, Phys. Rev. B **43**, 8549 (1991).
51. U. Brandt and C. Mielsch, Z. Phys. B **75**, 365 (1989); *ibid.* **79**, 295 (1990).
52. G. Baym and L. P. Kadanoff, Phys. Rev. **124**, 287 (1961); G. Baym, Phys. Rev. **127**, 1391 (1962).
53. E. Dagotto, Rev. Mod. Phys. **66**, 763 (1994).
54. V. J. Emery and S. A. Kivelson, Physica C **209**, 597 (1993); U. Löw, V. J. Emery, K. Fabricius, and S.A. Kivelson, Phys. Rev. Lett. **72**, 1918 (1994).
55. T. Mertelj, J. Demsar, B. Podobnik, I. Poberaj, and D. Mihailovic, Phys. Rev. B **55**, 6061 (1997).
56. I. V. Stasyuk and A. M. Shvaika, Czech. J. Phys. **46**, 961 (1996).
57. J. K. Freericks, Phys. Rev. B **47**, 9263 (1993).
58. P. M. Slobodyan and I. V. Stasyuk, Theor. Math. Phys. USSR **19**, 616 (1974); (Teor. Mat. Fiz. **19**, 423 (1974)).
59. Yu. A. Izumov, F. A. Kassan-Ogly and Yu. N. Skryabin, *Field Methods in the Theory of Ferromagnetism* (Nauka, Moscow, 1974) (in Russian).
60. I. V. Stasyuk and Yu. Havrylyuk, Condens. Matter Phys. **2**, 487 (1999).
61. J. K. Freericks and R. Lemanski, Phys. Rev. B **61**, 13438 (2000).
62. J. K. Freericks, Ch. Gruber, and N. Macris, Phys. Rev. B **60**, 1617 (1999).
63. U. Brandt and C. Mielsch, Z. Phys. B **82**, 37 (1991).

64. B. M. Letfulov, Eur. Phys. J. **4**, 447 (1998); **11**, 423 (1999).
65. I. V. Stasyuk and A. M. Shvaika, Acta Phys. Polon. A **84**, 293 (1993).
66. J. K. Freericks, Phys. Rev. B **48**, 14797 (1993).
67. N. M. Plakida and V.S. Udoenko, Sverkhpr. Fiz. Khim. Tekhn. **5**, 775 (1992).
68. Yu. A. Izyumov, M. I. Katsnel'son and Yu. N. Skryabin, *Magnetism of Itinerant Electrons* (Nauka, Moscow, 1992)(in Russian).
69. J. K. Freericks, M. Jarrell, and D. J. Scalapino Phys. Rev. B **48**, 6302 (1993); *ibid.* **B50**, 403 (1994).
70. C. S. Owen and D. J. Scalapino, Physica **55**, 691 (1971).
71. W. P. Su, Phys. Rev. B **67**, 092502 (2003).
72. N. N. Bogolyubov, V. L. Aksenov, and N. M. Plakida, Teor. Mat. Fiz. **93**, 371 (1992) (in Russian).
73. I. V. Stasyuk and A. M. Shvaika, Acta Phys. Polon. A **85**, 363 (1994).
74. I. V. Stasyuk, A. M. Shvaika, and E. Schachinger, Physica B **194-196**, 1965 (1994).
75. I. V. Stasyuk and A. M. Shvaika, Physica C **235-240**, 2173 (1994).
76. I. V. Stasyuk, A. M. Shvaika, and O. D. Danyliv, Molec. Phys. Rep. **9**, 61 (1995).
77. X. X. Xi, C. Doughty, A. Walkenhorst, C. Kwon, Q. Li, and T. Venkatesan, Phys. Rev. Lett. **68**, 1240 (1992).
78. D. Mihailovic and A. J. Heeger, Solid State Comm. **75**, 319 (1990).
79. I. V. Stasyuk and O. V. Velychko, Ukrainian Journ. of Phys. **44**, 772 (1999).
80. V. M. Browning, Phys. Rev. B **65**, 2860 (1997).
81. M. L. Kulić, R. Zeyher, Phys. Rev. B **49**, 4395 (1994).
82. L. Gehlhoff, R. Zeyher, Phys. Rev. B **52**, 4635 (1995).
83. R. Zeyher, M. L. Kulić, Phys. Rev. B **53**, 2850 (1996).
84. F. Zhou, T. Maxisch, G. Ceder, Phys. Rev. Lett. **97**, 155704 (2006).

Index

- amplitude ratio, 80, 81, 119
approximation
 adiabatic, 188, 212
 coherent potential (CPA), 236
 generalized random phase (GRPA),
 243
 Hubbard-I, 238
 local potential, 45, 52
 mean-field, 6, 49, 80, 91, 222, 256
 Migdal-Eliashberg, 270
 unified coloured noise, 218
asymptotic region, 90, 113

Biot-Savart interaction, 165, 174
Bose-Einstein condensation, 125,
 166–172

charge density wave (CDW), 250
clusters, 149–155
 Fortuin-Kasteleyn, 155–163
 spin, 150, 163, 172
confinement, 125, 175, 176
correlation
 electron U , 232
 length, 80, 85
critical
 exponent, 29, 148–177, 186
 dynamical, 85, 88, 94, 186, 221
 step, 225
 opalescence, 80
 phenomena, 124–150
 point, 23, 58, 146–176, 198
 gas-liquid, 80, 85
 slowing down, 80, 89
 surface, 21
crossover, 80, 81, 91

density of states (DOS), 237
dielectric
 instability, 277
 response, 278
 susceptibility, 275
diffusion, 84, 87, 94
 subdiffusion, 224
 superdiffusion, 224
dimension
 anomalous, 28, 38, 60, 65
 critical, 80
 upper, 27, 110
 fractal, 149, 186, 222
domain walls, 172, 173, 177

Edwards paradigm, 203
effective average action, 39, 67
Einstein relation, 87, 94
equation
 Bethe-Salpeter, 269
 Fokker-Planck, 193
 fractional, 221
 nonlinear, 223
 Landau-Khalatnikov, 189
 Langevin, 193, 199
 Polchinski, 73

ferromagnet, 85, 91–93, 117
Feynman diagrams, 125–141
fractional
 derivative, 221, 227
 feedback, 186, 203
function

- β , 26, 49, 66
- Green's, 47, 235
 - Matsubara, 265
 - Zubarev, 265
- pair correlation, 245, 264
- shape, 85, 88, 117
- Goldstone mode, 62, 64, 92, 93
- Hamiltonian, 96, 97, 103
 - Dicke, 226
 - effective, 12
 - fixed point, 11
 - form-invariant, 11
 - Hubbard, 232
- high-temperature
 - expansion, 125–156
 - graphs, 125–177
 - representation, 125–163
- hopping, 128, 148
 - expansion, 129, 142
 - matrix, 128, 129
 - parameter, 135
- integral
 - fractional, 220, 227
 - functional, 140, 164
 - path, 131, 137
- Lévy
 - flight, 224
 - random walk, 224
- light scattering, 84, 97, 114
- loop
 - distribution, 125, 136
 - gas, 125, 138
 - proliferation, 150, 174, 176
- magnetic monopoles, 175, 177
- magnetization, 87, 92
- matching condition, 113–115, 117
- Mermin-Wagner theorem, 62
- mode coupling, 110–112, 115, 116
- model
 - Falicov-Kimball (FK), 234
 - Gaussian, 3
- Higgs, 164, 176
- Hubbard, 232
 - Ising, 3, 146, 147, 156, 172
 - Ising on a triangular lattice, 9
 - Lorenz, 188
 - Mitsui, 284
 - $O(N)$, 62, 127, 154, 156
 - ϕ^4 , 3, 138, 141
 - Potts, 154, 155
 - pseudospin-electron (PEM), 232
 - simplified, 243
 - two-sublattice, 279
 - sandpile, 187
 - XY, 152, 155, 173, 175
 - monopole loops, 176
 - Monte Carlo, 150, 156
- neutron scattering, 85
- noise
 - colored, 217
 - white, 193, 209, 212
- non-asymptotic region, 113, 115
- particle trajectories, 124–177
- particle-field duality, 124, 129
- phase
 - chess-board, 250
 - coexistence, 258
 - diagram, 196, 239, 265
 - ferroelectric, 281
 - Higgs, 166
 - incommensurate, 267
 - portrait, 192, 214
 - method, 191
 - separation, 239
 - transition
 - Berezinskii-Kosterlitz-Thouless, 62, 155
 - first-order, 189, 219, 239
 - Mott, 238
 - noise-induced, 208, 215
 - second-order, 21, 189
 - superfluid, 93, 125, 152, 174
 - plaquette update, 157
 - point

- fixed, 80
- spinodal, 266
- tricritical, 262, 281
- pseudospin, 232
- relaxation, 87, 89, 94
- renormalization, 94, 106, 107
 - factor, 110
- renormalization group
 - flow, 8, 21
 - equations, 107, 109, 117
 - transformation, 8, 12, 24, 32
 - fixed point, 22, 80, 106
- response
 - “isolated”, 265
 - isothermal, 265
- scaling, 31
 - finite-size, 160, 162
 - functions, 88, 90
 - relations, 23, 30, 92, 94
 - strong, 110, 112
 - weak, 110
- self-avoiding walks, 125–155
- self-organized criticality (SOC), 182, 184, 204
- self-similarity, 13, 21, 45, 201, 223
- shear viscosity, 81, 82, 117
- spacetime approach, 123–169
- spinodal, 267
- stability border line, 119
- state
 - complex, 182
 - superconducting (SC), 269
 - tricritical, 196
- superconductivity, 165–176
- superfluid, 85, 93, 118, 169, 174
- susceptibility, 85, 88, 90
- theory
 - dual, 172–177
 - dynamical mean field (DMFT), 235
 - gauge, 164–176
 - compact, 175, 176
 - Ginzburg-Landau, 164
 - lattice field, 126–148
 - mode coupling, 81, 107, 109
 - percolation, 125–176
 - Van Hove, 80, 87
- thermal conductivity, 81, 87, 118
- transport coefficients, 80, 82
- Tsallis
 - distribution, 225
 - entropy, 203
 - nonextensivity parameter, 222
- tunneling splitting, 232, 257, 271
- universality, 80–82, 86, 94, 105
 - class, 3, 23, 220
 - hypothesis, 22, 23
- vortices, 173–177
- Ward identities, 94, 110, 111
- worldlines, 124–177
- YBaCuO-type superconducting crystals, 232, 265
- \mathbb{Z}_2 -symmetry, 11